Isoenzyme Specific PFK-2/FBPase-2 Inhibition as an Anti-cancer Strategy

Jonathan Glyn Williams

Jesus College

A thesis submitted to the University of Oxford for the degree of

Doctor of Philosophy in Organic Chemistry

Supervisors: Prof. Adrian Harris and Dr Angela Russell

Trinity Term 2013

Abstract

Thesis Title:

Isoenzyme Specific PFK-2/FBPase-2 Inhibition as an Anti-cancer Strategy

Submitted for the degree of Doctor of Philosophy in Organic Chemistry by:

Jonathan Glyn Williams

Jesus College, University of Oxford

Trinity Term 2013

High aerobic glycolytic capacity is correlated with poor prognosis and increased tumour aggressiveness. 6Phosphofructo-1-kinase catalyses the first irreversible step of glycolysis, and is activated by fructose-2,6-bisphosphate, a product of the kinase activity of four bifunctional isoenzymes, 6-phosphofructo-2-kinase/fructose-2,6-biphosphatase (PFK-2/FBPase-2:PFKFB1-4). These are potential anti-tumour targets, but their individual and collective role requires further investigation.

This thesis had three aims; to validate the PFK-2/FBPase-2 isoenzymes as anti-cancer targets, to investigate the requirement for isoenzyme-specific targeting, and to initiate assay development, enabling future identification of novel inhibitors.

A panel of cancer cell lines was examined and *PFKFB3* and *PFKFB4* were confirmed to be the most strongly induced isoenzymes in hypoxia, regulated by HIF-1α. Basal and hypoxic relative *PFKFB3/PFKFB4* expression varied markedly, and three cell lines with varying expression ratios (MCF-7, U87, PC3) were selected for further study.

siRNA knockdown of each isoenzyme individually, markedly reduced 2D and 3D cell growth. The effect of PFKFB3 knockdown was consistently more pronounced, particularly in hypoxia. Double PFKFB3/PFKFB4 knockdown was significantly less effective than PFKFB3 knockdown alone. Direct antagonism of PFKFB3 and PFKFB4 on F-2,6-BP concentration was observed, with PFKFB3 exhibiting high kinase activity, as anticipated, and PFKFB4 exhibiting high bisphosphatase activity. The degree of antagonism was dependent on the relative *PFKFB3/PFKFB4* expression ratio.

Extensive efforts were made to examine the wider metabolic effect of PFKFB3/PFKFB4 on flux towards glycolysis or the pentose phosphate pathway (PPP), including using metabolite, lipid droplet, ^{13}C NMR and mass spectrometry assays. No significant change in metabolic flux was detected, the evidence presented therefore suggesting the impact of the antagonistic effects of the isoenzymes on [F-2,6-BP] extends beyond regulation of metabolic flux alone.

This study concluded that the most effective therapeutic strategy will be one that involves a PFKFB3-specific inhibitor, preferably hypoxia-targeted. Accordingly, steps were taken to validate and optimise a robust medium-throughput assay system.

Acknowledgements

My first thanks must go to Cancer Research UK for generously funding my DPhil research and also to Jesus College, Oxford for the provision of additional financial support and a Graduate Scholarship. I am indebted to my two supervisors, Prof. Adrian Harris and Dr Angela Russell for their advice and support throughout the project. Their willingness to work at the interface between different scientific disciplines has been inspiring and has also enabled me to gain exposure to a wide range of techniques that has made for an altogether more interesting project.

The support and friendship of members of the Harris group, past and present, has made my DPhil particularly enjoyable. Special mentions must go to Dr Karim Bensaad, Dr Elena Favaro, Dr Anna Ramachandran, Dr Alan McIntyre, Dr Dean Singleton, Helen Turley, Ulrike Harjes and Dr Andrew Lomas for their advice and encouragement. It has also been a pleasure to work alongside Dr Simon Wigfield, Dr Helen Sheldon, Dr Simon Lord, Dr Chris Blick, Dr Esther Bridges, Dr Rob McCormick, Dr Harriet Gee, Dr Christos Zois, Dr Leonidas Mavroeidis, Dr Dylan Jones, Ioanna Ledaki, Esther Kleibeuker and the numerous other summer and exchange students. A mention must also go to the two washroom ladies – Linda and Rose – I'll very much miss our daily chats!

I'd also like to extend my thanks to all members of the Russell group, past and present. In particular, Dr Roderick Walker, Helen Storr, Anna Nadali, Abigail Guillermo, Dr Graham Wynne, Dr Bob Westwood, Dr Carole Bataille, Dr Gu Liu, Dr Camilo Quevedo and Dr Samira Alishahi.

My project has been highly collaborative and I am extremely grateful to all those that I have worked with over the past 4 years; Dr Ramon Bartrons and Dr Anna Manzano (University of

Barcelona); Dr Nicola Sibson and Dr Sébastien Serres (Gray Institute for Radiation Oncology and Biology, University of Oxford); Dr Tim Claridge, Dr James McCullagh and Khalid Al-Qahtani (Chemistry Research Laboratory, University of Oxford).

Finally, as I bring 9 great years at Oxford to a close, I would like to thank my family for their unwavering support throughout and also all of the great friends I have made along the way. In particular, Carina, Jess, Oren and Radleigh.

Abbreviations

µM	-	Micromolar
µm	-	Micrometre(s)
μ_n	-	Sample mean (negative control)
μ_p	-	Sample mean (positive control)
2-DG	-	2-Deoxyglucose
3PO	-	3-(3-pyridinyl)-1-(4-pyridinyl)-2-propen-1-one
A	-	Adenosine
Ac	-	Acetyl
Ac_2O	-	Acetic anhydride
AcOH	-	Glacial acetic acid
ADP	-	Adenosine diphosphate
Akt	-	Protein Kinase B
AMP	-	Adenosine monophosphate
AMPK	-	5' Adenosine monophosphate-activated protein kinase
anhyd.	-	Anhydrous
ANOVA	-	Analysis of variance
APC/c	-	Anaphase promoting complex cyclosome
app.	-	Apparent
aq.	-	Aqueous
Ar	-	General aryl group
Arg	-	Arginine
ARNT	-	Aryl hydrocarbon receptor nuclear translocator protein
Asn	-	Asparagine
ATP	-	Adenosine triphosphate
b	-	Broad
B	-	Bisphosphatase activity
BCR-ABL	-	Breakpoint cluster region - Abelson
bHLH	-	Basic helix-loop-helix
BHT	-	3,5-Di-tert-4-butylhydroxytoluene
BIS-TRIS	-	Bis(2-hydroxyethyl)amino-tris(hydroxymethyl)methane
BLAST	-	Basic local alignment search tool
Bn	-	Benzyl
BODIPY	-	Boron dipyrromethene
BT20	-	Human breast adenocarcinoma cell line
BT549	-	Human breast ductal carcinoma cell line
C	-	Celsius
C	-	Cytosine
c	-	Concentration (g/mL)
cAMP	-	Cyclic adenosine monophosphate
carboxy-H_2DCFDA	-	6-Carboxy-2',7'-dichlorodihydrofluorescein diacetate
CBP	-	CREB-binding protein
Cdk-1	-	Cyclin-dependent kinase 1
cDNA	-	Complimentary deoxyribonucleic acid

Chk 1	-	Checkpoint kinase 1
cm	-	Centimetre(s)
cm^{-1}	-	Wavenumber
CML	-	Chronic myelogenous leukaemia
CoA	-	Coenzyme A
COSY	-	Correlation spectroscopy
CREB	-	cAMP response-element binding protein
CSA	-	(+)-Camphor-10-sulphonic acid
Ct	-	Threshold cycle
d	-	Doublet
d^3-MeOD	-	Deuterated methanol
d^6-DMSO	-	Deuterated dimethylsulphoxide
Da	-	Dalton(s)
DB-1	-	Human melanoma cell line
DBU	-	1,8-Diazabicyclo[5.4.0]undec-7-ene
DCA	-	Dichloroacetate
DCC	-	*N,N'*-Dicyclohexylcarbodiimide
DEAE	-	Diethylaminoethyl
DEPC	-	Diethylpyrocarbonate
DEPT	-	Distortionless Enhancement by Polarisation Transfer
DFO	-	Desferroxamine
DHAP	-	Dihydroxyacetone phosphate
DMEM	-	Dulbecco's Modified Eagle Medium
DMF	-	*N,N*-Dimethylformamide
DMOG	-	Dimethyloxaloylglycine
DMSO	-	Dimethylsulphoxide
DNA	-	Deoxyribonucleic acid
dNTP Mix	-	Deoxynucleotide solution mix
DTT	-	Dithiothreitol
DU145	-	Human prostate carcinoma cell line
EC_{50}	-	Half maximal effective concentration
EDTA	-	Ethylenediaminetetraacetic acid
eq.	-	Equivalents
ER	-	Estrogen receptor
ES	-	Electrospray
ESI	-	Electrospray Ionisation
Et	-	Ethyl
Et_2O	-	Diethyl ether
Et_3N	-	Triethylamine
EtOAc	-	Ethyl Acetate
EtOH	-	Ethanol
F-1,6-BP	-	Fructose-1,6-bisphosphate
F-1,6-BPase	-	Fructose-1,6-bisphosphatase
F-2,6-BP	-	Fructose-2,6-bisphosphate
F-6-P	-	Fructose-6-phosphate

FACS	-	Fluorescence activated cell sorting
FBS	-	Foetal bovine serum
FDG	-	Fluorodeoxyglucose
FI	-	Fluorescence intensity
Film	-	Thin film IR, using NaCl plate
FP	-	Fluorescence polarisation
F-PFK-2	-	Foetal 6-phosphofructo-2-kinase/fructose-2,6-bisphosphatase isoform
FRET	-	Fluorescence resonance energy transfer
g	-	Grams
G	-	Guanine
G1	-	Gap 1 phase (cell cycle)
G-6-P	-	Glucose-6-phosphate
GC	-	Gas chromatography
GDP	-	Guanosine diphosphate
Glu	-	Glutamic acid
GLUT	-	Glucose transporter
GSH	-	Glutathione
H	-	Hypoxia (0.1% O_2)
h	-	Hour(s)
H/H'/H''	-	Diastereotopic protons
HEK 293T	-	Human embryonic kidney cell line
HeLa	-	Human cervical carcinoma cell line
HEPES	-	4-(2-Hydroxyethyl)-1-piperazineethanesulphonic acid
hHIF	-	Human hypoxia inducible factor
HIF	-	Hypoxia inducible factor
His	-	Histidine
HIV	-	Human immunodeficiency virus
HK	-	Hexokinase
HMBC	-	Heteronuclear multiple bond coherence
HMQC	-	Heteronuclear multiple quantum coherence
HO	-	Heme oxygenase
H-PFK-2	-	Cardiac 6-phosphofructo-2-kinase/fructose-2,6-bisphosphatase isoform
HPLC	-	High Performance Liquid Chromatography
HRE	-	Hypoxia response element
HRMS	-	High resolution mass spectrometry
HRP	-	Horseradish peroxidase
HTS	-	High-throughput screen
Hz	-	Hertz
IDH	-	Isocitrate dehydrogenase
IgG	-	Immunoglobulin G
IPAS	-	Inhibitory Per/Arnt/Sim domain protein
iPFK-2	-	Inducible 6-phosphofructo-2-kinase/fructose-2,6-bisphosphatase
IR	-	Infrared spectroscopy
J	-	Coupling constant
K	-	Kinase activity
K:B	-	Kinase:bisphosphatase activity ratio

KBr	-	Potassium bromide disc (IR)
kDA	-	Kilodalton(s)
K_i	-	Dissociation constant for inhibitor binding
K_m	-	Michaelis constant
L	-	Litre(s)
LC	-	Liquid chromatography
LD	-	Lipid droplet
LDH	-	Lactate dehydrogenase
lit	-	Literature
LNCaP	-	Human prostate adenocarcinoma cell line
LOH	-	Loss of heterozygosity
LOX	-	Lysyl oxidase
L-PFK-2	-	Liver 6-phosphofructo-2-kinase/fructose-2,6-bisphosphatase isoform
Lys	-	Lysine
M	-	Molar
m	-	Multiplet
m	-	Medium
m/z	-	Atomic mass units per charge
M^+	-	Molecular ion
MAPK	-	Mitogen-activated protein kinase
MCF-10	-	Human breast epithelial cell line
MCF-7	-	Human breast adenocarcinoma cell line
MDA-MB-231	-	Human breast adenocarcinoma cell line
MDA-MB-468	-	Human breast adenocarcinoma cell line
Me	-	Methyl
MeOH	-	Methanol
mg	-	Milligram(s)
MHz	-	Megahertz
min	-	Minute(s)
mL	-	Millilitre(s)
mM	-	Millimolar
mm	-	millimetre(s)
mmol	-	Millimole(s)
mol	-	Mole(s)
mp	-	Melting point
M-PFK-2	-	Muscle 6-phosphofructo-2-kinase/fructose-2,6-bisphosphatase isoform
mRNA	-	Messenger ribonucleic acid
MS	-	Mass spectrometry
m-TBST	-	Tris-buffered saline with 0.1% Tween 20 and 5% milk powder
mTORC	-	Mammalian target of rapamycin complex
MW	-	Molecular weight
N	-	Normoxia
NAD^+	-	Nicotinamide adenine dinucleotide
NADH	-	Nicotinamide adenine dinucleotide (reduced)
$NADP^+$	-	Nicotinamide adenine dinucleotide phosphate

NADPH	-	Nicotinamide adenine dinucleotide phosphate (reduced)
ng	-	Nanogram(s)
nm	-	Nanometre(s)
NMR	-	Nuclear Magnetic Resonance spectroscopy
ns	-	Not significant
obs.	-	Obscured
ODD	-	Oxygen dependent degradation
OXPHOS	-	Oxidative phosphorylation
p	-	Chromosome region p
p300	-	Protein 300
p53	-	Protein 53
PBS	-	Phosphate buffered saline solution
PC3	-	Human prostate carcinoma cell line
PCR	-	Polymerase chain reaction
PDB	-	Protein data bank
PDH	-	Pyruvate dehydrogenase
PDK	-	Pyruvate dehydrogenase kinase
PEP	-	Phosphoenolpyruvate
PER	-	Period circadian protein
PET	-	Positron emission tomography
PFA	-	Paraformaldehyde
PFK-1	-	6-Phosphofructo-1-kinase
PFK-15	-	1-(4-Pyridinyl)-3-(2-quinolinyl)-2-propen-1-one
PFK-2/FBPase-2	-	6-Phosphofructo-2-kinase/fructose-2,6-bisphosphatase
PFKFB1-4	-	6-Phosphofructo-2-kinase/fructose-2,6-bisphosphatase isoenzymes 1-4
PFKFB4s	-	6-Phosphofructo-2-kinase/fructose-2,6-bisphosphatase-4 splice variant
PFKL	-	6-Phosphofructo-1-kinase (liver-type)
PFKM	-	6-Phosphofructo-1-kinase (muscle-type)
PFKP	-	6-Phosphofructo-1-kinase (platelet-type)
PFP	-	Pentafluorophenol
P-gp	-	Permeability glycoprotein
Ph	-	Phenyl
PHD	-	Prolyl hydroxylase domain
P_i	-	Inorganic phosphate
PI3K	-	Phosphoinositide 3-kinase
PKA	-	Protein Kinase A
PKB	-	Protein Kinase B
PKC	-	Protein Kinase C
PKM	-	Pyruvate kinase muscle isoform
pm	-	Picometre(s)
POCE	-	Proton observed carbon edited
PPi	-	Pyrophosphate
ppm	-	Parts per million
PPP	-	Pentose phosphate pathway
Pro	-	Proline
PTEN	-	Phosphate and tensin homolog

PVDF	-	Polyvinylidene fluoride
pVHL	-	von Hippel–Lindau tumour suppressor protein
py	-	Pyridine
q	-	Quartet
q	-	Chromosome region q
qRT-PCR	-	Quantitative real-time polymerase chain reaction
RFU	-	Relative fluorescence units
RIPA	-	Radioimmunoprecipitation assay
RLU	-	Relative luminescence units
RNA	-	Ribonucleic acid
ROCS	-	Rapid overlay of chemical structures
ROS	-	Reactive oxygen species
rpm	-	Rotations per minute
RPMI	-	Roswell Park Memorial Institute-1640 medium
RT	-	Room temperature
RT Buffer	-	Reverse transcriptase buffer
RWPE1	-	Human prostate epithelial cell line
s	-	Singlet
s	-	Strong
sat.	-	Saturated
Scr	-	Non-targeting scramble siRNA control
SDS-PAGE	-	Sodium dodecyl sulphate polyacrylamide gel electrophoresis
sec	-	Second(s)
SEM	-	Standard error of the mean
Ser	-	Serine
SH	-	Non-targeting scramble siRNA control (hypoxia)
shRNA	-	Small hairpin ribonucleic acid
si3	-	siPFKFB3-1 and siPFKFB3-2
si3/4	-	siPFKFB3-1, siPFKFB3-2, siPFKFB4-1 and siPFKFB4-2
si4	-	siPFKFB4-1 and siPFKFB4-2
SIM	-	Single-minded protein
SiO_2	-	Kieselgel 60 silica (Macherey-Nagel®)
siRNA	-	Small interfering ribonucleic acid
SKBR3	-	Human breast adenocarcinoma cell line
SN	-	Non-targeting scramble siRNA control (normoxia)
S_N2	-	Bimolecular nucleophilic substitution reaction
SPE	-	Solid phase extraction
SRB	-	Sulforhodamine B
str.	-	Stretch
t	-	Triplet
T	-	Thymine
$t_{1/2}$	-	Half life
T47D	-	Human ductal breast epithelial tumour cell line
TBST	-	Tris-buffered saline with 0.1% Tween 20
TCA	-	Tricarboxylic acid cycle

THF	-	Tetrahydrofuran
TIGAR	-	TP53-inducible glycolysis and apoptosis regulator
TLC	-	Thin layer chromatography
TPZ	-	Tirapazamine
TRF	-	Time resolved fluorescence
TRIS	-	Tris(hydroxymethyl)aminomethane
TS	-	Transition state
U	-	Uracil
U/Unit(s)	-	1 Unit - amount of enzyme that catalyses the conversion of 1μM substrate/min
U87	-	Human primary glioblastoma cell line
Ub	-	Ubiquitin
UBI2K	-	6-Phosphofructo-2-kinase/fructose-2,6-bisphosphatase-3 splice variant
uPFK-2	-	Ubiquitous 6-phosphofructo-2-kinase/fructose-2,6-bisphosphatase
UV	-	Ultraviolet
V	-	Volt(s)
VEGF	-	Vascular endothelial growth factor
w	-	Weak
xg	-	Times gravity
δ_C	-	Carbon (^{13}C) NMR chemical shift
δ_F	-	Fluorine (^{19}F) NMR chemical shift
δ_H	-	Proton (^{1}H) NMR chemical shift
δ_P	-	Phosphorous (^{31}P) NMR chemical shift
λ	-	Wavelength
λ_{em}	-	Emission wavelength
λ_{ex}	-	Excitation wavelength
υ_{max}	-	Infrared absorption

Table of Contents

List of Figures

List of Schemes

List of Tables

List of Equations

Chapter 1: Introduction and Aims

1.1: Cancer and its Hallmarks

The lifetime risk of developing cancer now stands at 40% for males and 37% for females in the UK, and it remains a leading cause of death worldwide (Sasieni, Shelton et al. 2011). Ageing populations, unhealthy diets, the prevalence of smoking, and other poor lifestyle choices, all mean that the number of people suffering with the disease is projected to continue increasing worldwide. This will serve to further exacerbate the social and economic burden of cancer.

Despite extensive research, we still remain heavily reliant on the surgical excision of tumours and non-selective chemo- and radio-therapies, which have limited efficacy and numerous side-effects, as a result of normal tissue damage. Identifying targetable features that distinguish cancer cells from normal cells is a major challenge, which is further compounded by the heterogenic nature of tumours (Yap, Gerlinger et al. 2012). At any one time, a tumour may consist of several colonies of cancer cells with different mutations, all striving to out-compete one other (Gerlinger, Rowan et al. 2012; Gillies, Verduzco et al. 2012; Swanton 2012). Even if chemotherapy destroys the bulk of the tumour, those resistant sub-populations that may remain have the ability to spawn new tumours.

This is further complicated by the apparent common existence of tumour-initiating cells (TICs), otherwise known as cancer stem cells (Frame and Maitland 2011). These cells are broadly defined as having the capacity to give rise to new tumours and are thought to be the driving force behind many cancers, through their capacity for self-renewal and generation of the heterogeneous cell lineages that comprise a tumour (Frank, Schatton et al. 2010; Frame and Maitland 2011). Evidence suggests that TICs are more resistant to various

chemotherapeutic agents than other tumour cells and they are thought to be responsible for the recurrence of disease in many patients who initially respond to therapy (Zhou, Zhang et al. 2009; Hanahan and Weinberg 2011). This increased resistance derives in part from their slow proliferation rates and an increased efficiency of DNA damage repair (Frame and Maitland 2011). TICs were initially assumed to be rare, but a number of studies suggest that this is not always the case and their proportional abundance seems to vary both between and within cancer types (Kelly, Dakic et al. 2007; Frame and Maitland 2011). Tumour heterogeneity and the existence of TICs both highlight the importance of combination therapies to target the entire tumour and prevent the emergence of resistant sub-clones or re-population of the tumour bulk from therapy-resistant TICs.

In general, mutations in two types of genes are linked to the on-set of cancer development; proto-oncogenes and tumour suppressor genes. Mutations in proto-oncogenes, which usually have a critical role in regulating cell growth, produce oncogenes, with dominant gain of function. For example, Ras proteins mediate signalling pathways intimately involved in cell growth, such as promoting an increase in DNA, protein and lipid synthesis, in response to growth factors. Mutation in the *ras* proto-oncogene leads to continued pro-proliferative signalling, which is linked to de-regulated cell growth and transformation (Downward 2003). If mutations occur in tumour suppressor genes, this leads to recessive loss of function (Hanahan and Weinberg 2000). Of particular importance is inactivation of the tumour suppressor protein p53. Direct inactivation through mutation of the *p53* gene is observed in over 50% of cancers, the most common genetic defect in solid tumours (Vogelstein, Lane et al. 2000). In response to cellular stress such as DNA-damage, the p53 protein plays a central role in preventing cancer development. For example, it is able to induce cell-cycle arrest or apoptotic cell death (Zuckerman, Wolyniec et al. 2009). The inactivation of the tumour-suppressive function of such proteins plays a central role in cancer pathogenesis.

Neoplastic disease is enormously complex, but Hanahan and Weinberg (Hanahan and Weinberg 2000) were able to consolidate the plethora of scientific literature into a single conceptual framework and originally proposed that there were six biological capabilities that all cancer cells acquire during the process of carcinogenesis. These were (1) self-sufficiency in growth signals, (2) insensitivity to growth-inhibitory signals, (3) evasion of apoptosis, (4) limitless replicative potential, (5) sustained angiogenesis and (6) tissue invasion and metastasis (Figure 1.1).

The Hallmarks of Cancer

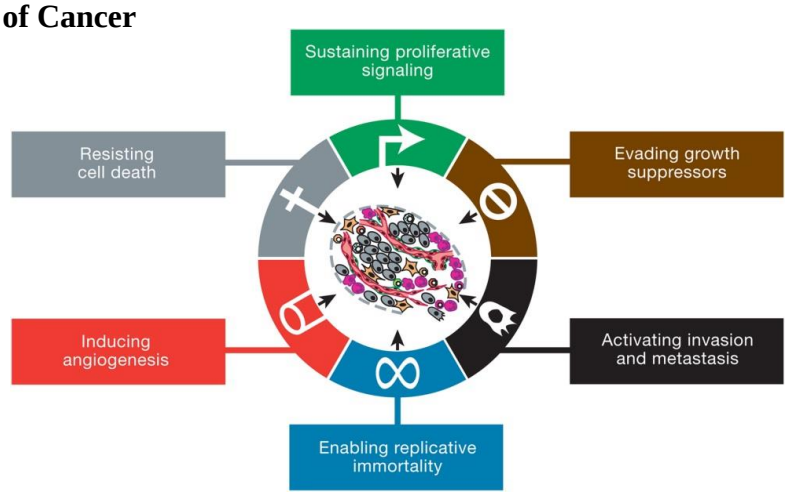

Figure 1.1: The hallmarks of cancer. Figures reproduced from (Hanahan and Weinberg 2011) with kind permission of the publishers (license number 3151300078227).

These were later refined to include two emerging hallmarks; evading immune destruction, and reprogramming of energy metabolism, to support the capacity of the cancer cell to relentlessly divide and proliferate (Figure 1.2) (Hanahan and Weinberg 2011). These hallmarks are underpinned by two "enabling characteristics"; tumour-promoting inflammation and genomic instability. The latter promotes the genetic mutations necessary for acquisition of each of the hallmarks (Figure 1.2). It follows that the most effective therapeutic strategies will likely be those that specifically target one or more of the hallmarks of cancer, or the enabling characteristics.

Emerging Hallmarks and Enabling Characteristics

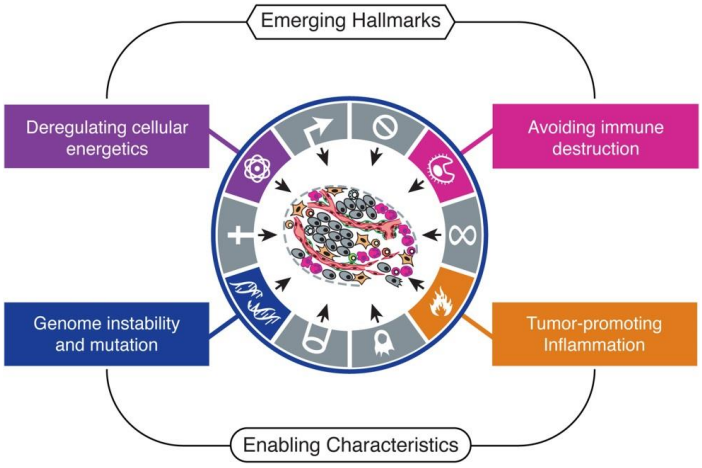

Figure 1.2: Emerging hallmarks and enabling characteristics. Figures reproduced from (Hanahan and Weinberg 2011) with kind permission of the publishers (license number 3151300078227).

These guiding concepts, as with any model, must always be considered against the backdrop of tumour heterogeneity and the tumour micro-environment. In particular, it is important to keep in mind that a solid tumour is a complex tissue consisting of multiple cell types, in addition to stromal cells recruited from normal tissues (Hanahan and Weinberg 2011). It has become increasingly apparent that the interactions between tumour cells and the stromal component can have a fundamental role in tumour progression and chemo-resistance. Much of the *in vitro* and *in vivo* work conducted to date has not taken this into account (Udagawa and Wood 2010).

1.2: Towards Targeted Chemotherapy

The development of modern chemotherapies began with the identification of the nitrogen-mustards, derivatives of former World War I chemical weapons that were found to successfully treat patients with Hodgkin's lymphoma and lymphosarcoma (Gilman and Philips 1946; Goodman, Wintrobe et al. 1946). The nitrogen mustards function via the formation of highly electrophilic intermediates, which act as non-specific alkylating agents,

binding DNA and causing inter-strand cross-linking, thereby preventing replication (Mattes, Hartley et al. 1986). In the 1940s, Sydney Farber observed folate to accelerate the progression of patients with acute lymphoblastic leukaemia (ALL) (Farber, Cutler et al. 1947; Chabner and Roberts 2005). This led to arguably the first example of rational drug design, where the folate analogue aminopterin was tested in a clinical trial and found to induce temporary remission in some patients with ALL (Farber and Diamond 1948). The folate analogue methotrexate was developed soon afterwards and was found to have an improved therapeutic index. It has shown anti-tumour activity in a wide range of solid tumours, including breast, ovarian and bladder cancer (Jaffe, Frei et al. 1974; Chabner and Roberts 2005). Both aminopterin and methotrexate were found to be potent inhibitors of the enzyme dihydrofolate reductase (DHFR), which was the first enzyme to be targeted for cancer therapy (Osborn, Freeman et al. 1958).

In the decades since, a host of other chemotherapeutic agents have been developed or identified, including the platins, such as cis-platin and carbo-platin. In common with the alkylating agents, these are highly electrophilic species and their mechanism of action involves cross-linking of DNA. Other therapeutic agents include the anti-metabolites, such as 5-fluorouracil, which inhibits nucleotide synthesis, and the taxanes and vinca alkaloids, which both act to inhibit mitosis (Lewis 2006; Morrison 2010). However, whilst many are relatively effective, they generally suffer from a lack of specificity, targeting all highly proliferative cells. This includes cells in normal tissue, leading to toxicity, i.e. a low therapeutic index. The use of these agents therefore depends on exploiting a narrow therapeutic window, maximising efficacy and minimising toxicity in non-target tissue (Masui, Gini et al. 2013).

In recent years there has been a paradigm shift in cancer treatment from such traditional chemotherapies to more specific “targeted therapies”, which are selective for a specific

molecular target with a crucial role in promoting tumour growth and advancement (Sawyers 2004; Thompson 2009). For example, selective estrogen receptor modulators (SERMs) such as tamoxifen, have been used to treat patients with invasive estrogen receptor positive breast cancer, as well as reducing occurrence when used preventatively in women with elevated risk of the disease (Jordan 2007; Cuzick, Sestak et al. 2013). SERMs are able to bind to estrogen receptors (ERs) in target tissue, specifically acting to block ERs in breast tissue and therefore also estrogen-stimulated cell growth; approximately 60-70% of tumours are ER positive (Cuzick, Sestak et al. 2013; Howell and Evans 2013).

The first major success of rational drug design targeting a specific molecular aberration in cancer cells came with the identification of Imatinib (Gleevec®) (Druker, Tamura et al. 1996; Druker, Sawyers et al. 2001). Imatinib is an ATP-competitive inhibitor of the Breakpoint cluster region – Abelson (BCR-ABL) tyrosine kinase fusion protein, which is responsible for driving cellular proliferation in Philadelphia chromosome-positive chronic myelogenous leukemia (CML) cells (Oda, Heaney et al. 1994). Through furthering understanding of such underlying molecular changes in cancer, the oncology community is making a sustained effort to identify suitable molecular targets that represent the root cause of cancer. The corresponding anti-neoplastic agents that will be developed are anticipated to be more efficacious and less toxic than their chemotherapeutic predecessors (Sawyers 2004; Thompson 2009).

Nevertheless, intrinsic or acquired resistance to such molecularly targeted therapies will likely require most to be employed in combination with other therapeutic agents. For example, most CML patients respond to Imatinib treatment initially, but relapses have been observed, particularly in those patients with more advanced disease (O'Hare, Walters et al. 2005). This relapse is primarily driven by a point mutation in the BCR-ABL kinase domain that decreases

sensitivity to Imatinib (Cowan-Jacob, Guez et al. 2004). Furthermore, the *BRAF* gene, which encodes the B-RAF protein, a key protein kinase component of the mitogen-activated protein kinase (MAPK) cell signalling pathway, is mutated in 40-50% of melanomas. This leads to constitutive pro-proliferative signalling (Gray-Schopfer, Wellbrock et al. 2007; Sullivan and Flaherty 2013). Potent inhibitors of the activated BRAF protein, such as the ATP-competitive vemurafenib, were developed as targeted agents against this specific molecular target. Such inhibitors are initially highly effective, being found to reduce tumour volume in the majority of patients in Phase III trials (Sullivan and Flaherty 2013). However, most patients, including those highly responsive to the initial therapy, experience relapse within a year (Dummer and Flaherty 2012). This is due to a variety of resistance mechanisms, including those that mediate reactivation of the MAPK pathway or up-regulation of alternative signalling pathways, such as the phosphoinositide 3-kinase (PI3K)/Akt pathway (Giroux 2013; Sullivan and Flaherty 2013). It will be important to increase understanding of mechanisms of resistance to such targeted therapies in order to develop more effective combination treatments in the future.

1.3: Tumour Hypoxia

Tumour hypoxia is a common and distinguishing characteristic of solid tumours, and is defined as a reduction in the normal oxygen tension in cells (Harris 2002). The development of new blood vessels is deregulated in tumours, leading to a structurally and functionally abnormal microvasculature, culminating in poor, irregular tumour blood flow (Harris 2002; Jain 2005). This, coupled with the rapid, uncontrolled proliferation of cancer cells, causes them to quickly outgrow their blood, and therefore their oxygen, supply (Jain 2005). Intratumoural oxygen concentration is thus highly heterogeneous and in a constant state of flux, and as the oxygen diffusion limit is around 150 μm (Helmlinger, Yuan et al. 1997), the

majority of tumours exceeding 1 mm^3 are found to contain hypoxic and necrotic regions (Dewhirst 1998; Shannon, Bouchier-Hayes et al. 2003) (Figure 1.3).

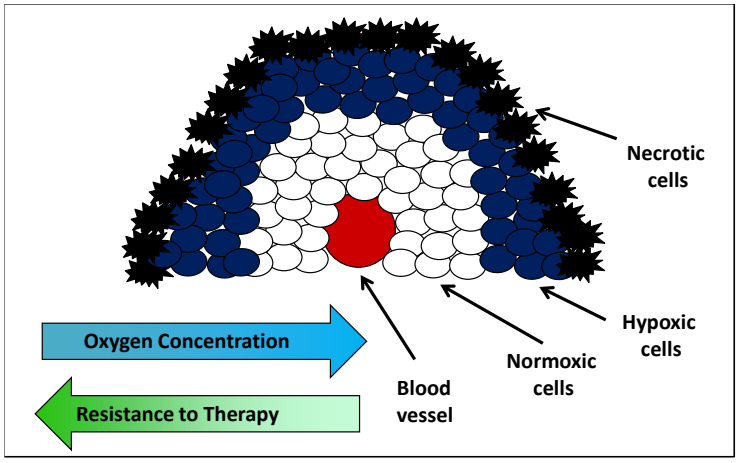

Figure 1.3: Simplified depiction of hypoxic and necrotic regions of tumour tissue with respect to the blood vessel.

Hypoxia is associated with poor prognosis as it promotes tumour progression through increased angiogenesis (Kuwai, Kitadai et al. 2003), invasiveness, metastasis (Brizel, Scully et al. 1996; Subarsky and Hill 2003) and genetic instability (Reynolds, Rockwell et al. 1996). It is also related to the up-regulation of genes encoding proteins involved in drug resistance, such as P-gp (permeability glycoprotein) (Wartenberg, Ling et al. 2003), which actively pumps many drugs out of the cell (Brown and William 2004). Hypoxia is intimately linked with changes in cancer cell metabolism (Bertout, Patel et al. 2008) and is also known to promote a more aggressive phenotype. For example, it selects for a more apoptosis-resistant clonal population that lacks functional p53, a key tumour-suppressor transcription factor (Graeber, Osmanian et al. 1996).

Hypoxic cells have been shown to have a three-fold greater resistance to radiation damage than normoxic cells, because it is the presence of oxygen in cells that enables “fixing” of radiation damage, through production of DNA-damaging oxygen free radicals (Gray, Conger et al. 1953; Overgaard and Horsman 1996). Furthermore, the “leaky”, irregular vasculature

and high interstitial pressures, coupled with large diffusion distances, mean delivery of cytotoxic agents to hypoxic areas of a tumour can be extremely inefficient (Brown and Giaccia 1998; Harris 2002; Wouters, Pauwels et al. 2007). In addition, the low oxygen, low nutrient environment reduces proliferation, leading to the presence of viable, non-cycling cells that are insensitive to those drugs targeting highly proliferative cells. The combination of these factors often promotes resistance to multiple structurally and functionally unrelated chemotherapeutic agents (multi-drug resistance) (Krishna and Mayer 2000).

1.3.1: The HIF Pathway

Hypoxia-inducible factors (HIFs) are a family of transcription factors that play a central role in both sensing and responding to changes in oxygen concentration, through inducing the expression of genes that mediate the physiologic response to hypoxia (Semenza 2007). These genes are linked with processes such as regulation of angiogenesis, e.g. vascular endothelial growth factor (VEGF), energy metabolism, e.g. lactate dehydrogenase-A (LDH-A) and pyruvate kinase-2 (PKM-2), cellular differentiation, apoptosis and tumour metastasis, among others (Williams, Telfer et al. 2005; Patiar and Harris 2006; Semenza 2007). Such pathways are integral to cancer pathogenesis.

HIF is a heterodimer, consisting of the oxygen-sensitive HIF-α subunit and the constitutively expressed aryl hydrocarbon receptor nuclear translocator subunit (ARNT, also termed HIF-1β). Both subunits are members of the basic Helix-Loop-Helix PER-ARNT-SIM (bHLH-PAS) family of transcription factors (Wang, Jiang et al. 1995). Three isoforms of HIF-α are known to exist in mammals: HIF-1α, HIF-2α and HIF-3α, each having distinct biological properties and tissue distributions.

1.3.1.1: HIF-1α

Hypoxia-inducible factor-1 (HIF-1) was first identified as a transcriptional regulator of the human erythropoietin gene (Semenza and Wang 1992; Wang, Jiang et al. 1995). The steady-state abundance of the HIF-1α subunit is dependent on oxygen concentration. Under normoxic conditions, the protein undergoes rapid degradation ($t_{1/2}$ < 5 minutes) (Huang, Arany et al. 1996), controlled by an oxygen-dependent degradation (ODD) domain (Huang, Gu et al. 1998).

Prolyl-hydroxylase domain (PHD)-containing enzymes are 2-oxogluterate-dependent oxygenases. PHDs are able to post-translationally modify HIF-1α, through hydroxylation on at least one of two proline residues (Pro-402 and Pro-564) within the ODD domain (Ivan, Kondo et al. 2001; Jaakkola, Mole et al. 2001; Masson, Willam et al. 2001; Yu, White et al. 2001). The von Hippel-Lindau tumour suppressor protein (pVHL), which is the recognition component of an E3 ubiquitin ligase complex (Iwai, Yamanaka et al. 1999), is then able to bind to the hydroxylated HIF-1α. It then mediates degradation of HIF-1α via the ubiquitin/proteasome pathway (Figure 1.4) (Maxwell, Wiesener et al. 1999; Cockman, Masson et al. 2000; Ohh, Park et al. 2000; Tanimoto, Makino et al. 2000).

The PHDs require oxygen as a co-factor and stoichiometric oxidant, to be catalytically active. Consequently, they are inhibited under hypoxic conditions, preventing HIF-1α hydroxylation and subsequent binding of pVHL (Schofield and Ratcliffe 2004). Hence, under hypoxic conditions HIF-1α is sufficiently long-lived to translocate to the nucleus, where it binds to HIF-1β, along with transcriptional co-activators such as CBP/p300 (Arany, Huang et al. 1996). This HIF-1 complex then binds to hypoxia response elements (HREs) in the promoter region of HIF-1 responsive genes, such as LDH-A and VEGF (Chilov, Camenisch et al. 1999) (Figure 1.4).

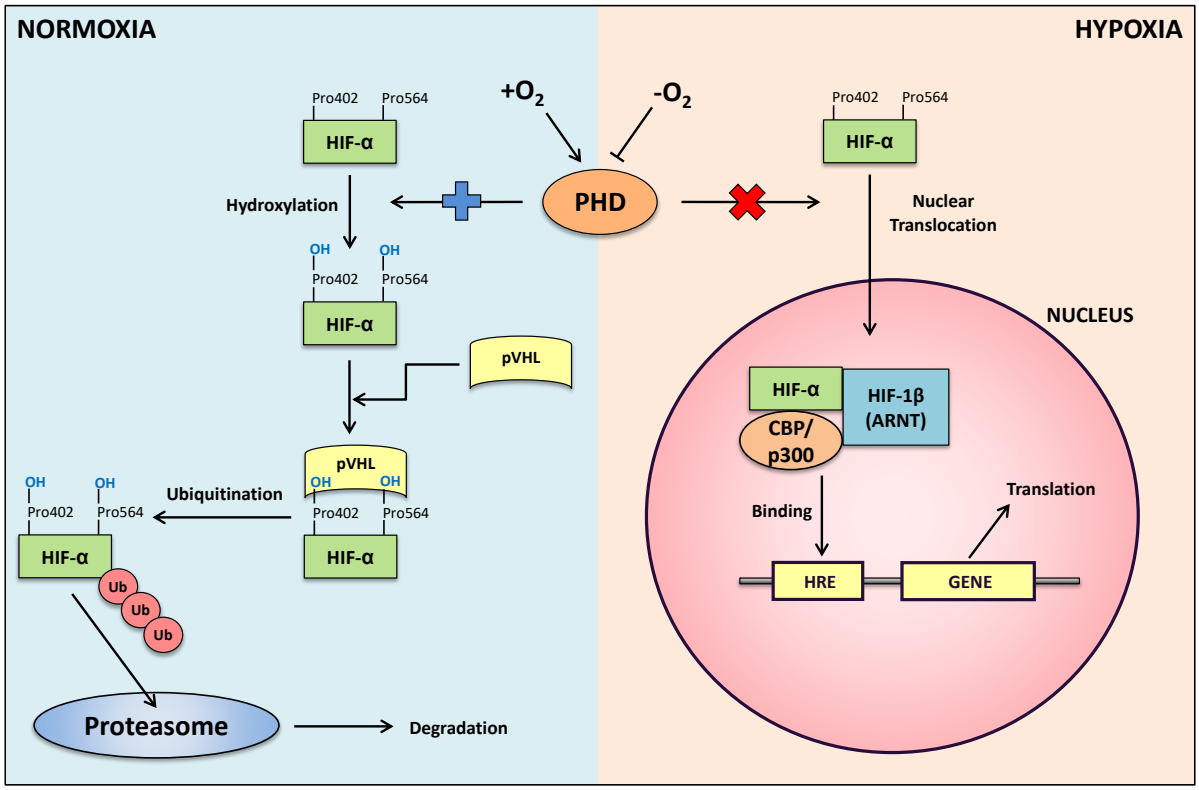

Figure 1.4: Hypoxia inducible factor (HIF) pathway under normoxic and hypoxic conditions. HIF-α is degraded under normoxic conditions via the ubiquitin/proteasome pathway. Under hypoxic conditions, HIF-α translocates to the nucleus, binds HIF-1β and mediates transcription of numerous hypoxia response genes through binding to hypoxia response elements (HREs) in their promoter regions. pVHL (von Hippel-Lindau tumour suppressor protein); Pro (proline); Ub (ubiquitin); PHD (prolyl-hydroxylase domain containing enzymes); ARNT (aryl nuclear hydrocarbon receptor nuclear translocator subunit); CBP (CREB-binding protein).

HIF-1α is ubiquitously expressed across tissue types and appears to be over-expressed in the majority of tumours, with higher prevalence in metastases than primary tumours (Zhong, De Marzo et al. 1999; Melillo 2006).

1.3.1.2: HIF-2α

HIF-2α was the second HIF factor to be discovered (Ema, Taya et al. 1997), and is structurally similar to HIF-1α, sharing approximately 48% overall amino acid sequence homology. As with HIF-1α, it is also able to bind ARNT and is regulated by pVHL. However, various studies have suggested that HIF-2α has a biological role distinct from HIF-1 (Hu, Wang et al. 2003; Carroll and Ashcroft 2006; Keith, Johnson et al. 2012). The expression of HIF-2α is far more limited than HIF-1α in normal tissue, being restricted to specific cell

types, such as cardiomyocytes, glial cells, endothelial cells, and hepatocytes (Wiesener, Jurgensen et al. 2003; Rankin and Giaccia 2008). In common with HIF-1α, HIF-2α expression is often increased in tumour tissue and elevated expression also correlates with poor patient prognosis (Rankin and Giaccia 2008).

1.3.1.3: HIF-3α

HIF-3α was first identified by Gu and colleagues (Gu, Moran et al. 1998), and shares high amino acid sequence homology with both HIF-1α and HIF-2α. However, HIF-3α has been shown to lack structures necessary for transactivation (increased gene expression), which are found to be present in the C-terminal domains of HIF-1α and HIF-2α (Hara, Hamada et al. 2001). In common with the other HIF subunits, HIF-3α is able to dimerise with ARNT, and bind HREs (Ke and Costa 2006). Additionally, six splice variants of the gene have been reported, these being human HIF-3α 1-6 (hHIF-3α1 to hHIF-3α6) (Maynard, Qi et al. 2003). The splice variant hHIF-3α2, otherwise known as inhibitory Per/Arnt/Sim domain protein (IPAS), is able to function as a dominant negative regulator of HIF-inducible gene expression. IPAS interacts with the N-terminal region of HIF-1α, rendering it unable to bind the HREs of target genes (Makino, Cao et al. 2001). Intriguingly, IPAS has itself been reported to contain an HRE, and be a HIF-1α target, thereby providing a mechanism for negative feedback regulation in response to hypoxic exposure (Makino, Uenishi et al. 2007). Relatively little research has been conducted into the function and expression pattern of HIF-3α, but current evidence suggests most HIF-dependent effects reported to date are primarily a result of HIF-1α or HIF-2α activity (Keith, Johnson et al. 2012).

1.3.2: Targeting Hypoxia

Whilst there is no doubt that hypoxia brings enormous challenges for the development of therapeutic agents, as a feature almost exclusive to solid tumour tissue, it also presents itself

as an attractive therapeutic target. Accordingly, much research has focussed on the development of hypoxia-selective agents, such as bio-reductive prodrugs, typified by tirapazamine (Brown 1993), and inhibitors of targets essential for hypoxic survival, such as HIF (Jones and Harris 2006). Hypoxia-response pathways and processes, including glycolysis and angiogenesis, have also been targeted. Effective delivery of hypoxia-targeted therapeutics to the poorly perfused hypoxic sub-fraction of the tumour requires them to have extended half-lives and/or high tissue diffusion coefficients (Saggar, Yu et al. 2013). Their use in combination with other agents designed to target the normoxic fraction of the tumour will offer the optimal therapeutic strategy (Wilson and Hay 2011). A full discussion of hypoxia-targeting is beyond the scope of this thesis, but is covered in detail in a number of literature reviews (Patiar and Harris 2006; Wilson and Hay 2011; Bailey, Wojtkowiak et al. 2012).

1.4: Cancer Metabolism and the Warburg Effect

Metabolic reprogramming is inextricably linked to each of the hallmarks of cancer. Whilst traditionally viewed as a secondary effect in response to damaged mitochondria, or reduced ATP levels, many now consider altered metabolism to be a hallmark of cancer in its own right (Kroemer and Pouyssegur 2008; Hanahan and Weinberg 2011; Ward and Thompson 2012). Altered metabolism is a feature common to cancer cells and malignancy is dependent on changes in metabolic pathways involved in glycolysis, glutaminolysis and biosynthesis of fatty acids, amino acids and nucleic acids (Ward and Thompson 2012).

A metabolic change observed almost universally in primary and metastatic cancers is a marked increase in glucose consumption, coupled with the up-regulation of glycolysis, which is the conversion of glucose to pyruvate. This change can be observed clinically through the use of ^{18}F PET imaging of 2-^{18}F-fluorodeoxyglucose (2-^{18}FDG) uptake (Gatenby and Gillies 2004). Many cancer cells sustain this up-regulation, even in the presence of oxygen, a

phenomenon first identified by Otto Warburg, now referred to as the Warburg effect (Warburg 1956) (Figure 1.5). Glycolysis uses the oxidative potential of 2 NAD^+ molecules to yield 2 pyruvate and 2 ATP molecules per molecule of glucose. In normal cells, the pyruvate is then channelled to the mitochondria, where it is oxidised via the tricarboxylic acid (TCA) cycle. This generates NADH, which fuels oxidative phosphorylation (OXPHOS) and produces a maximum 38 ATP molecules per original molecule of glucose (Figure 1.5).

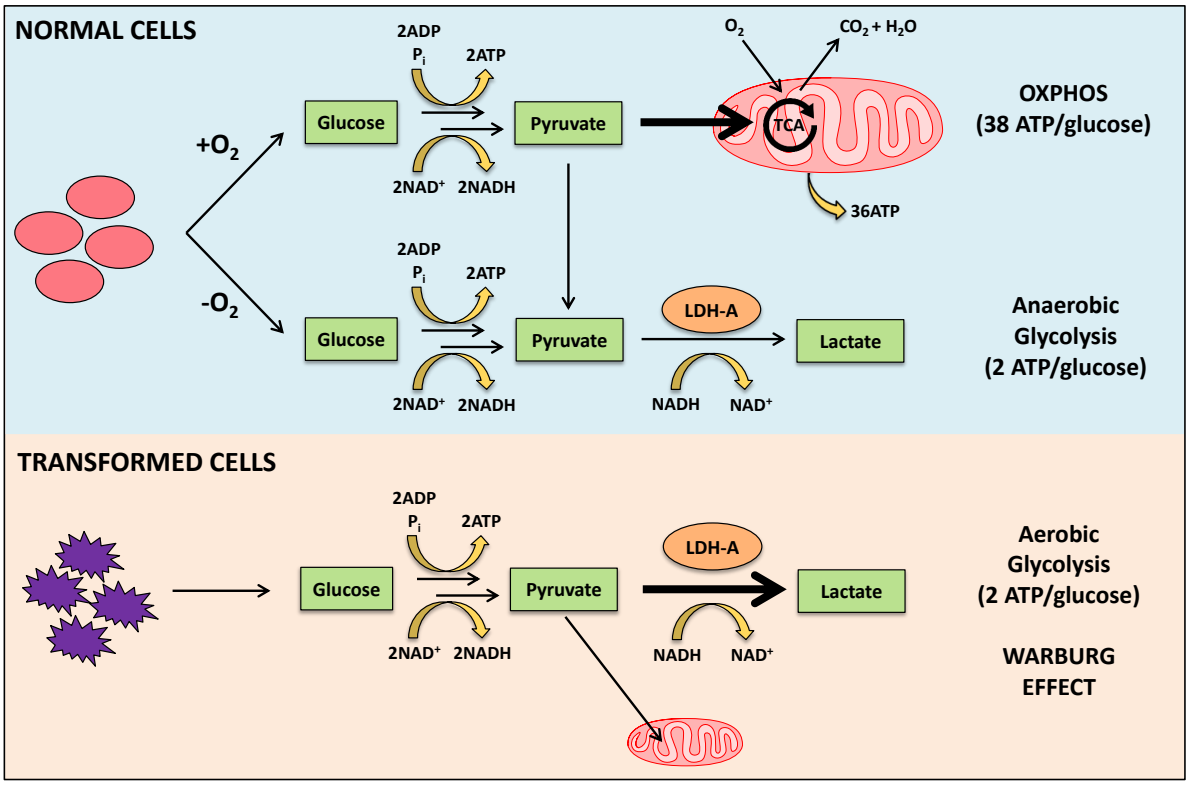

Figure 1.5: The Warburg effect. Glucose flux through glycolysis is increased under both normoxic and hypoxic conditions in transformed cells, whereas normal cells channel pyruvate to the mitochondria for full oxidative phosphorylation. ATP (adenosine triphosphate); ADP (adenosine diphosphate); LDH-A (lactate dehydrogenase A); NADH (nicotinamide adenine dinucleotide (reduced)); NAD^+ (nicotinamide adenine dinucleotide); TCA (tricarboxylic acid cycle).

It is somewhat counterintuitive then, that cancer cells would by-pass OXPHOS and switch to a form of metabolism that is over an order of magnitude less efficient in terms of ATP production. Nevertheless, numerous studies have correlated increased aerobic glycolysis with more aggressive tumour phenotypes and poor patient prognosis. Evolutionary theory dictates

that glycolysis must therefore confer a significant proliferative advantage on the cancer cells (Gillies and Gatenby 2007).

1.4.1: Why do Cancer Cells have High Aerobic Glycolysis?

Warburg originally proposed that increased aerobic glycolysis could be a direct result of dysfunctional mitochondria in cancer cells. However, many cancer cells have now been shown to have fully-functional mitochondria and active TCA cycles (Weinhouse 1976; Zu and Guppy 2004). A widely held view was that cyclical, periodic exposure to hypoxia would select for those cells able to constitutively up-regulate glycolysis, as they would better survive the periods of hypoxia (Gatenby and Gillies 2004). This theory warrants much merit, yet would only partly explain the switch to aerobic glycolysis, as some cancer cells are able to utilise glycolytic metabolism before hypoxic exposure. For example, leukemic cells are exposed to higher oxygen concentrations than most normal tissues but still undergo aerobic glycolysis (Elstrom, Bauer et al. 2004; Vander Heiden, Cantley et al. 2009). Furthermore, if this were the only explanation, one might expect Darwinian evolution to select out the inefficient glycolytic phenotype once oxygen levels increase again, such as following metastasis, yet this is not the case (Gillies, Robey et al. 2008).

Whilst glycolysis produces ATP less efficiently than OXPHOS, it produces ATP approximately 100 times faster, suggesting this energetic trade-off may be utilised in cancer cells to maximal benefit (Bartrons and Caro 2007). Accordingly, much literature has reinforced the perception that the primary purpose of increased glucose uptake by cancer cells is to facilitate an increase in ATP production through glycolysis (Pelicano, Martin et al. 2006; Gillies and Gatenby 2007). However, studies have now shown that most cancer cells produce the majority of their ATP oxidatively, with only a relatively minor fraction of their ATP deriving from glycolysis (Guppy, Leedman et al. 2002; Zu and Guppy 2004; Stubbs and

Griffiths 2010). ATP is no longer considered to be a limiting factor for cancer cell survival and proliferation (Vander Heiden, Cantley et al. 2009; Lunt and Vander Heiden 2011). In fact, it is actually the rate of consumption of ATP that may be the limiting factor, due to the inhibitory effects ATP can exert on key glycolytic enzymes, such as 6-phosphofructo-1-kinase (PFK-1) (Scholnick, Lang et al. 1973; Israelsen and Vander Heiden 2010). Researchers have therefore been forced to look beyond cellular energetics to understand the Warburg effect and two theories currently prevail (Kroemer and Pouyssegur 2008); these are related to biomass generation and an increase in extracellular acidity.

1.4.1.1: Biomass Generation

The first is the role increased glucose consumption plays in the production of the biosynthetic precursors required for growth and proliferation (anabolic synthesis). This is linked to increased production of intermediates such as Acetyl-CoA and NADPH for fatty acid production and ribose-5-phosphate (via the Pentose Phosphate Pathway (PPP)), which is required for nucleic acid production. The synthesis of these intermediates and other glycolytic intermediates used to produce non-essential amino acids, clearly imparts a proliferative advantage on the cancer cell (Vander Heiden, Cantley et al. 2009; Lunt and Vander Heiden 2011).

Furthermore, the by-product NADPH from the PPP has important anti-oxidant functions, acting as a co-factor in glutathione synthesis, which protects the cell from the effects of reactive oxygen species (ROS) (Vander Heiden, Cantley et al. 2009). Although this does in part explain the Warburg Effect, a large proportion of glucose metabolised by the cell is still exported as lactate or alanine (some studies suggest up to 90% (DeBerardinis, Mancuso et al. 2007)), which is highly carbon-inefficient. It has been speculated that this apparent

inefficiency is outweighed by the ability to rapidly up-regulate biomass production when required (Lunt and Vander Heiden 2011).

1.4.1.2: Extracellular Acidity

This leads us to the second theory, which stems from the observation that cancer cells lower the pH of their extracellular space, through the generation of lactic acid (from glycolysis) and carbonic acid (from OXPHOS). Normal physiological pH is 7.4, whereas the average extracellular pH of the tumour environment is often found to be in the range 6.2-6.7 (Paradise, Lauffenburger et al. 2011). In lowering the extracellular pH, cancer cells create a microenvironment selectively more toxic to normal tissue by promoting apoptosis in cells with functional p53 (Williams, Collard et al. 1999), as well as driving evolution of a more acid-resistant tumour phenotype (Bhujwalla, Artemov et al. 2002). This is known to facilitate tumour progression (Smallbone, Gavaghan et al. 2005), invasion via degradation of the extracellular matrix (Swietach, Vaughan-Jones et al. 2007), metastasis (Rofstad, Mathiesen et al. 2006) and suppression of the anti-cancer immune response (Fischer, Hoffmann et al. 2007). Extracellular acidification also confers a degree of drug resistance, inhibiting the intracellular accumulation of drugs that are weak bases, such as adriamycin and doxorubicin (Skovsgaard 1977; Shannon, Bouchier-Hayes et al. 2003; Hambley 2008).

It is testament to the complexity of this process that we rapidly approach the 100th anniversary of Warburg's famous observation with our understanding still incomplete. In reality, each of the causative theories previously discussed may contribute to the glycolytic switch.

1.4.2: Reprogramming and Regulation of Cell Metabolism

Metabolic regulation is extremely complex and can be controlled at multiple levels, such as through expression of different splice isoforms of metabolic enzymes, e.g. pyruvate kinase M-

2 (PKM-2) over pyruvate kinase M-1 (PKM-1), amplification or post-translational modification of metabolic enzymes, e.g. 6-phosphofructo-1-kinase (PFK-1). Furthermore, oncogenic mutations can occur in enzymes themselves, e.g. isocitrate dehydrogenase-1 (IDH-1) and isocitrate dehydrogenase-2 (IDH-2) (Mardis, Ding et al. 2009). All of these factors are known to be important drivers of altered metabolism (Ward and Thompson 2012). HIF-1 is also able to regulate metabolism through increasing the expression of numerous glycolytic enzymes, such as PFK-1 and LDH-A. Furthermore, HIF-1 also induces pyruvate dehydrogenase kinase-1 (PDK-1), which deactivates pyruvate dehydrogenase (PDH), thus restricting entry of pyruvate to the TCA cycle and therefore also suppressing OXPHOS (Kim, Tchernyshyov et al. 2006) (Figure 1.6).

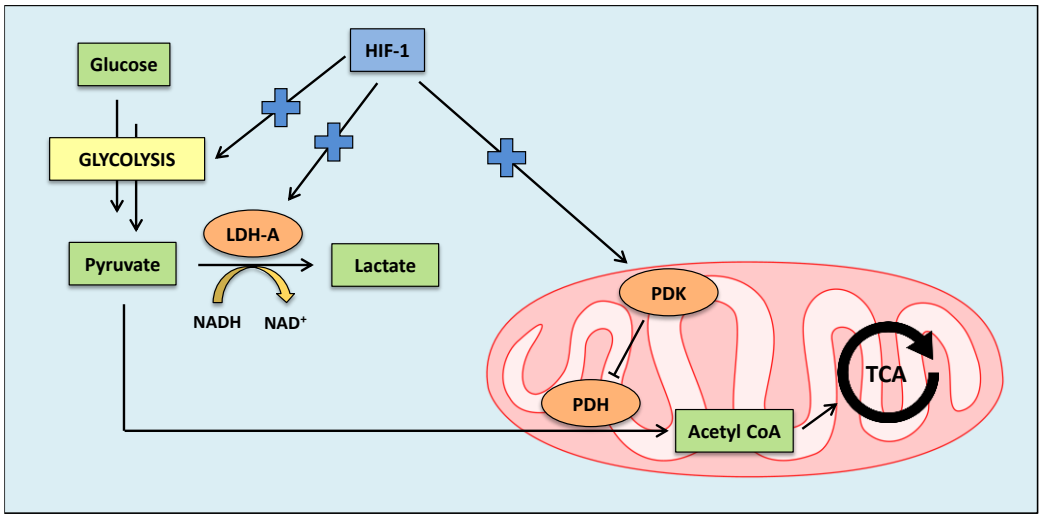

Figure 1.6: The role of hypoxia inducible factor 1 (HIF-1) in promoting glycolysis and restricting entry of pyruvate to the mitochondria. HIF-1 promotes up-regulation of glycolysis through increasing expression of glycolytic enzymes and lactate dehydrogenase A (LDH-A), and also restricts the entry of pyruvate into the tricarboxylic acid (TCA) cycle through pyruvate dehydrogenase kinase (PDK)-mediated down-regulation of pyruvate dehydrogenase (PDH) activity.

Aside from HIF-1, there are several upstream regulators of metabolic pathways. Of particular interest is the PI3K/Akt pathway, which has emerged as likely the most important and frequently activated in cancer (Robey and Hay 2009). Phosphoinositide 3-kinase (PI3K) signalling mediates activation of Protein Kinase B (Akt) via production of the phospholipid phosphatidylinositol (3,4,5)-triphosphate (PIP_3). The activation of Akt and its downstream

targets promotes cell survival, growth and proliferation, and is known to increase glucose uptake and glycolysis (Vivanco and Sawyers 2002; Elstrom, Bauer et al. 2004). Akt is therefore considered to be intimately involved in the Warburg effect (Robey and Hay 2009). Mammalian target of rapamycin complex-1 (mTORC1), downstream of PI3K/Akt, is central to enhancing protein synthesis, *de novo* lipogenesis and promoting mitochondrial biogenesis (Cunningham, Rodgers et al. 2007). Myc is also known to be important in regulating mitochondrial biogenesis, glycolysis and glutaminolysis (Li, Wang et al. 2005; Kaadige, Elgort et al. 2010).

The tumour suppressor function of p53 now appears to be closely linked to its ability to regulate metabolism, beyond its widely accepted function in controlling cell cycle arrest, apoptosis and senescence (Li, Kon et al. 2012). Indeed, loss of wild-type p53 can promote glycolysis and anabolic synthesis in cancer cells (Matoba, Kang et al. 2006). An understanding of these regulators is important, but many function through protein-protein interactions, making therapeutic targeting difficult, hence the focus on inhibiting the downstream metabolic enzyme targets of these regulators (Vander Heiden 2011).

1.4.3: Targeting Tumour Metabolism

The search for druggable metabolic targets is compounded by a number of factors. The first is an issue of selectivity akin to the limitations of chemotherapy. Many of the features of metabolic reprogramming found in cancer cells, such as aerobic glycolysis (Wang, Marquardt et al. 1976), are also shared by normal proliferative tissue. This renders many targets unsuitable due to associated side effects. The second is an issue of plasticity; cancer cells, like normal cells are often able to make use of multiple alternative biosynthetic routes to regenerate a depleted metabolite, as well as exchanging some metabolites between cells (Schulze and Harris 2012). A successful therapeutic strategy must therefore invoke a detailed

understanding of such compensatory pathways. The third is an extension of tumour heterogeneity; cancer cells within the same tumour with differing genetic mutations, or in response to differences in the microenvironment, may employ alternative metabolic reprogramming to promote their survival and proliferation (Vander Heiden 2011; Gerlinger, Rowan et al. 2012). This may necessitate the use of combination therapies to target different metabolic changes and complementary pathways.

Targeting tumour metabolism is attractive because all cancer cells rely on metabolic alterations to support their survival (Vander Heiden 2011). To date, only a small number of agents targeting metabolic pathways have been tested as potential cancer therapeutics (Vander Heiden 2011). The major challenge is to identify and exploit those metabolic differences that do exist between normal cells and cancer cells (Tennant, Duran et al. 2010). Targeting tumour-specific isoforms, or harnessing the high dependency of cancer cells on their altered metabolic pathways by suppressing, but not eliminating pathway activity, may permit selective targeting (Tennant, Duran et al. 2010). Indeed, cancer cells are thought to be more susceptible to perturbations in the activity of these pathways (Schulze and Harris 2012).

Numerous opportunities exist to target metabolic enzymes for cancer therapy, including inhibition of enzymes involved in nucleotide biosynthesis, amino acid and protein synthesis, lipid synthesis, glycolysis and TCA cycle/mitochondrial metabolism, which have been extensively reviewed elsewhere (Tennant, Duran et al. 2010; Vander Heiden 2011). Selection of suitable metabolic targets for the development of small molecule inhibitors requires a detailed understanding of the expression patterns and regulation of metabolic enzymes.

In considering potential metabolic targets, the nearly universal up-regulation of aerobic glycolysis in transformed cells and presence of hypoxia in most tumour microenvironments,

sets glycolysis apart as a particularly attractive target (Pelicano, Martin et al. 2006). Specifically targeting glycolysis in cancer cells with inhibitors would thus be expected to have broad therapeutic benefit. There are numerous strategies for targeting glycolysis, including via inhibition of glucose transporters (GLUTs), hexokinase (HK), pyruvate kinase M-2 (PKM-2) and lactate dehydrogenase A (LDH-A), which are all key proteins involved in this pathway (Pelicano, Martin et al. 2006; Porporato, Dhup et al. 2011; Zhao, Butler et al. 2013).

A number of agents targeting metabolic pathways are now in clinical trials, which are discussed in several literature reviews (Porporato, Dhup et al. 2011; Vander Heiden 2011; Schulze and Harris 2012). For example, dichloroacetate (DCA) activates PDH, by inhibiting PDK-1, which increases delivery of pyruvate to the mitochondria, thereby shifting the balance from glycolysis to mitochondrial respiration (Michelakis, Webster et al. 2008). The DCA-mediated increase in mitochondrial respiration has been found in numerous studies to increase ROS levels and induce apoptosis, whilst suppressing proliferation of cancer cells (Saed, Fletcher et al. 2011; Sanchez, McGee et al. 2013).

The glucose analogue 2-deoxyglucose (2-DG) is transported into the cell by glucose transporters (GLUTs), where it is phosphorylated by hexokinase (HK) to 2-deoxyglucose-6-phosphate. This intermediate then becomes trapped in the cell, itself inhibiting both HK and glucose-6-phosphate isomerase activity, and therefore glycolytic flux (Wick, Drury et al. 1957). Nevertheless, 2-DG activity has shown a lack of efficacy as a single agent in the clinic, but has demonstrated promise as a combination therapy. For example, it has been found to sensitise osteosarcoma and non-small cell lung cancers to adriamycin and paclitaxel in pre-clinical mouse models (Maschek, Savaraj et al. 2004). Much interest has also focussed on the anti-diabetic drug metformin. Observational studies have found metformin to provide a significant survival benefit in cancer patients with diabetes (Currie, Poole et al. 2012; Garrett,

Hassabo et al. 2012). Metformin is thought to activate AMP-activated kinase (AMPK), which induces the up-regulation of cellular processes that increase ATP production, such as glycolysis and fatty acid β-oxidation, and down-regulates ATP-consuming processes (Buzzai, Jones et al. 2007; Dowling, Goodwin et al. 2011; Schulze and Harris 2012). However, the underlying molecular mechanisms that translate this into the cancer-preventative effect of metformin remain poorly understood. Nevertheless, the potential of metformin as a cancer treatment is currently being investigated in a series of clinical studies involving patients without diabetes (Pierotti, Berrino et al. 2013).

1.5: 6-Phosphofructo-1-kinase (PFK-1) – Regulator of Glycolytic Flux

One potential therapeutic strategy that has seen much recent interest in the literature is the modulation of the enzymatic activity of 6-phosphofructo-1-kinase (PFK-1). PFK-1 is a rate-limiting enzyme, catalysing the first irreversible step of glycolysis, namely the conversion of fructose-6-phosphate (F-6-P) to fructose-1,6-bisphosphate (F-1,6-BP) (Figure 1.7).

PFK-1 is therefore an important "bottle-neck" as it signifies a metabolic commitment to the glycolytic pathway over the alternative pentose phosphate pathway (PPP), and is therefore considered to dictate the rate of glycolytic flux (Weber 1977; Pelicano, Martin et al. 2006).

PFK-1 is a tetrameric protein composed of muscle-form (PFKM), liver-form (PFKL) and/or platelet-form (PFKP) monomers, with each subunit under separate genetic control (Vora, Halper et al. 1985). Random tetramerisation of these subunits produces a range of homo- and hetero-tetrameric isoenzymes (Vora, Halper et al. 1985) and different subunit expression patterns confer distinct kinetic and regulatory properties on the PFK-1 tetramer (Moreno-Sanchez, Rodriguez-Enriquez et al. 2007).

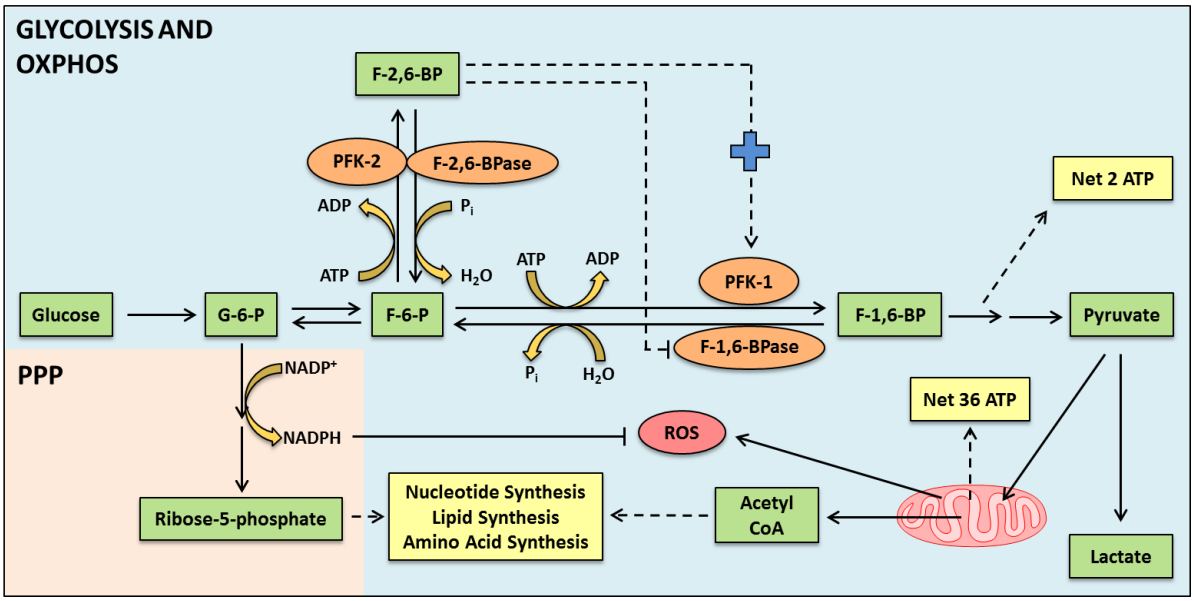

Figure 1.7: The role of 6-phosphofructo-1-kinase (PFK-1) and 6-phosphofructo-2-kinase/fructose-2,6-bisphosphatase (PFK-2/FBPase-2) in controlling flux through glycolysis and the pentose phosphate pathway (PPP). This ensures that the biosynthetic, energetic and anti-oxidant requirements of the cell are met. $NADP^+$ (nicotinamide adenine dinucleotide phosphate); NADPH (nicotinamide adenine dinucleotide phosphate (reduced)); ATP (adenosine triphosphate); ADP (adenosine diphosphate); P_i (inorganic phosphate); ROS (reactive oxygen species); G-6-P (glucose-6-phosphate); F-6-P (fructose-6-phosphate); F-1,6-BP (fructose-1,6-bisphosphate); F-1,6-BPase (fructose-1,6-bisphosphatase).

A wide range of physiological and non-physiological molecules modulate PFK activity, including metabolites, such as citrate and phosphoenolpyruvate (PEP), proteins and fatty acids (Spitz, Furtado et al. 2009). These ligands seem to act primarily by altering the position of equilibrium of the two major oligomeric conformations of the enzyme, these being the active tetrameric form and an inactive dimeric form (Leite, Da Silva et al. 2007; Zancan, Rosas et al. 2007; Zancan, Marinho-Carvalho et al. 2008). The allosteric site in PFK-1 is the site of binding of effectors including ADP and GDP (activators), and PEP, ATP and citrate (inhibitors) (Lau and Fersht 1989; Cabrera, Ambrosio et al. 2008). The net result is a feedback mechanism, which acts to maintain the steady state concentration of ATP.

PFK-1 activity is increased in transformed cells and primary tumour tissue (Hennipman, Smits et al. 1987; Hennipman, van Oirschot et al. 1988). It is interesting to note a change in subunit expression pattern during transformation, leading to the L and P subunits predominating (Sanchez-Martinez and Aragon 1997). These subunits are comparatively less

sensitive to negative feedback via citrate and ATP inhibition, and also have higher affinity for F-6-P, thereby increasing glycolytic activity (Hannemann, Jandrig et al. 2005). Indeed, Staal and colleagues showed that PFK-1 from human gliomas had elevated L subunit expression, and was less sensitive to citrate inhibition and more sensitive to activation by F-2,6-BP, compared with PFK-1 from normal brain tissue (Staal, Kalff et al. 1987). Elevated L subunit expression has also been correlated with increased aggressiveness and glycolytic efficiency (mol lactate produced per mol glucose consumed) of breast cancer cell lines (Zancan, Sola-Penna et al. 2010). Increased PFKL expression is known to mediated by HIF-1α in response to hypoxia (Semenza, Roth et al. 1994; Semenza, Agani et al. 1997).

1.5.1: Fructose-2,6-bisphosphate as an Allosteric PFK-1 Activator

Fructose-2,6-bisphosphate was identified as the most potent allosteric activator of PFK-1 (Van Schaftingen, Hue et al. 1980; Van Schaftingen, Hue et al. 1980). It is able to alleviate ATP-mediated inhibition of PFK-1 through altering the position of equilibrium, to favour the active tetrameric form of PFK-1. This permits maintenance of elevated glycolytic flux in the presence of abundant ATP (Leite, Da Silva et al. 2007; Zancan, Rosas et al. 2007; Zancan, Marinho-Carvalho et al. 2008) (Figure 1.7). Furthermore, F-2,6-BP elicits an additional pro-glycolytic effect through concomitant inhibition of fructose-1,6-bisphosphatase (F-1,6-BPase), which catalyses the conversion of F-1,6-BP to F-6-P, by directly competing with its substrate (Van Schaftingen and Hers 1981) (Figure 1.7). It is widely established that intracellular F-2,6-BP concentration is elevated in transformed cells (Hue and Rousseau 1993; Nissler, Petermann et al. 1995; Hirata, Kato et al. 1998) and various tumours (Atsumi, Chesney et al. 2002), where it is thought to be responsible for maintenance of the glycolytic phenotype. Oncogenic *ras* and *src* signalling also activate PFK-1, which is thought in part to

be mediated via an increase in F-2,6-BP concentration (Bosca, Mojena et al. 1986; Kole, Resnick et al. 1991).

Small molecule inhibition of PFK-1 would allow suppression of the glycolytic pathway, potentially reducing cancer cell survival. However, such selective inhibitors are yet to be developed (Gatenby and Gillies 2004). Additionally, ubiquitous PFK-1 expression in all cells suggests an alternative glycolytic target may be more suitable in order to reduce toxicity in normal tissue.

1.6: 6-Phosphofructo-2-kinase/fructose-2,6-bisphosphatase (PFK-2/FBPase-2)

PFK-2/FBPase-2 is a homodimeric, bifunctional enzyme. It catalyses the ATP-mediated phosphorylation of F-6-P to F-2,6-BP at its N-terminal kinase domain, whilst catalysing the degradation of F-2,6-BP to F-6-P and P_i at its C-terminal phosphatase domain. There are four isoenzymes, designated PFKFB1-4 and numerous cells and tissue types exhibit simultaneous expression of multiple isoenzymes, suggesting they may have distinct roles in regulating intracellular F-2,6-BP concentration (Calvo, Bartrons et al. 2006; Telang, Yalcin et al. 2006; Bartrons and Caro 2007). The PFK-2/FBPase-2 isoenzymes are thought to tightly control flux through the glycolytic and PPP pathways, maintaining a balance between the ATP, biosynthetic and antioxidant requirements of the cell (Herrero-Mendez, Almeida et al. 2009; Rodriguez-Rodriguez, Fernandez et al. 2012; Ros and Schulze 2013) (Figure 1.7).

The catalytic domains of each of the PFK-2/FBPase-2 isoenzymes are highly conserved (Okar, Manzano et al. 2001) and the expression pattern of the isoenzymes is regulated in a spatial and temporal manner (Gomez, Navarro-Sabate et al. 2009; Pegoraro, Maczkowiak et al. 2013). Each isoenzyme is characterised by distinct kinase: bisphosphatase activities (Table

1.1) and regulatory properties, including the degree of hypoxic induction (Minchenko, Opentanova et al. 2003; Bartrons and Caro 2007).

Isoenzyme	Chromosome	Band	MW	Reference(s)	Kinase: Bisphosphatase Activity Ratio
PFKFB1	X	q27-q28	55 kDa	(Hilliker, Darville et al. 1991) (Olson, Uyeda et al. 1989)	1.2 (bovine liver)
PFKFB2	1	q31-q32	58 kDa	(Hilliker, Darville et al. 1991) (Pape, Prokop et al. 1996)	1.8 (bovine heart)
PFKFB3	10	p14-p15	59 kDa	(Nicholl, Hamilton et al. 1997) (Manzano, Rosa et al. 1998)	> 700 (human placenta)
PFKFB4	3	p21-p22	55 kDa	(Sakata, Abe et al. 1991) (Manzano, Perez et al. 1999)	0.9 (human testes)

Table 1.1: Details of relative enzymatic activity and chromosomal location of the human PFK-2/FBPase-2 isoenzymes. Information taken from reviews by Okar and colleagues (Okar, Manzano et al. 2001) and Ros and colleagues (Ros and Schulze 2013); MW (Molecular Weight).

1.6.1: Mechanisms of the PFK-2/FBPase-2 Kinase and Bisphosphatase Reactions

Kim and colleagues employed the use of two PFKFB3 crystal structure models to study the PFK-2/FBPase-2 kinase reaction; PFKFB3 in complex with F-6-P and an unreactive ATP-analogue (β,γ-methylene-adenosine 5'-triphosphate, AMPPCP), mimicking the substrate interactions; and the product complex PFKFB3▪ADP▪F-2,6-BP (Kim, Cavalier et al. 2007). The kinase reaction is thought to be associative, proceeding via a direct S_N2 phosphoryl transfer, with no intermediate phosphoenzyme (Scheme 1.1). One of the γ phosphate oxygen atoms is proposed to serve as a base, deprotonating O(2) of F-6-P, which is followed by nucleophilic attack of the F-6-P anion on the γ phosphate group, which proceeds via a high energy pentavalent transition state (TS). The residues Lys168 and Lys47 are thought to have an important role in stabilising the TS. A redistribution of electrons then releases ADP and the product F-2,6-BP (Scheme 1.1) (Kim, Cavalier et al. 2007). Specificity of the active site for the β-anomer of F-6-P over the α-anomer is mediated through an interaction between O(1) of F-6-P and Arg189 (Kim, Cavalier et al. 2007).

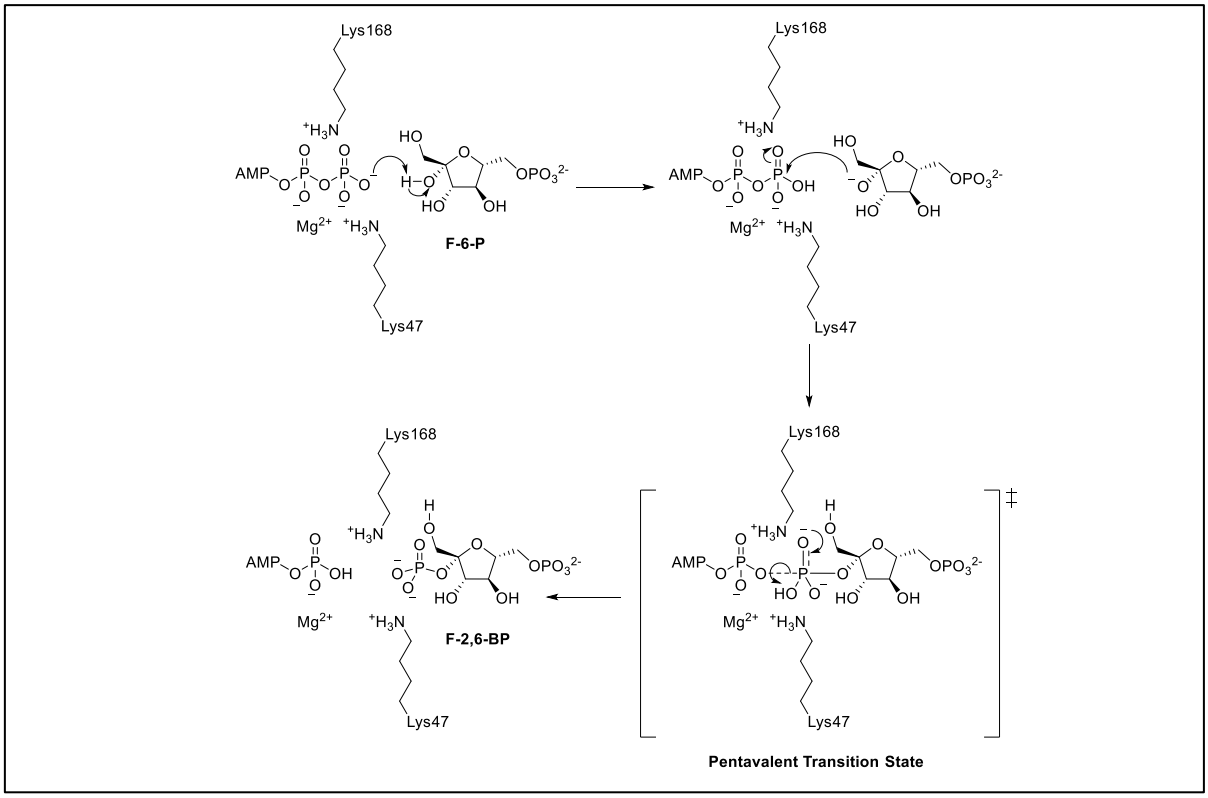

Scheme 1.1: PFK-2/FBPase-2 kinase reaction mechanism. The mechanism, proposed by Kim and colleagues (Kim, Cavalier et al. 2007), proceeds via a high-energy pentavalent transition state. AMP (adenosine monophosphate); Lys (lysine); F-6-P (fructose-6-phosphate); F-2,6-BP (fructose-2,6-bisphosphate).

A further study by the same group used three crystal structure models to examine the PFKFB3 bisphosphatase reaction; the PFKFB3 phospho-enzyme intermediate state (PFKFB3-P▪F-6-P); PFKFB3 complexed with AlF_4 at the bisphosphatase active site (PFKFB3▪AlF_4), which mimics the phosphoryl transfer transition state; and finally PFKFB3 complexed with inorganic pyrophosphate (PFKFB3▪PP_i) (Cavalier, Kim et al. 2012). These detailed the enzymatic state during substrate binding, catalysis, and product release, respectively (Cavalier, Kim et al. 2012). The group concluded that the reaction initiates through nucleophilic attack of His253 on the 2-phosphate, proceeding via a high-energy pentavalent transition state (Scheme 1.2) (Cavalier, Kim et al. 2012). Residues Asn259, Arg252 and His387 are all able to stabilise the build-up of negative charge in the transition state, through electrostatic stabilisation and hydrogen bonding. Redistribution of electrons releases the F-6-P anion, which is protonated by a Glu322 residue. This residue itself then acts as a base,

deprotonating a water molecule, which facilitates attack of a hydroxyl anion on the electrophilic phosphorous. This mediates production of inorganic phosphate and release of the histidine residue (Scheme 1.2) (Cavalier, Kim et al. 2012).

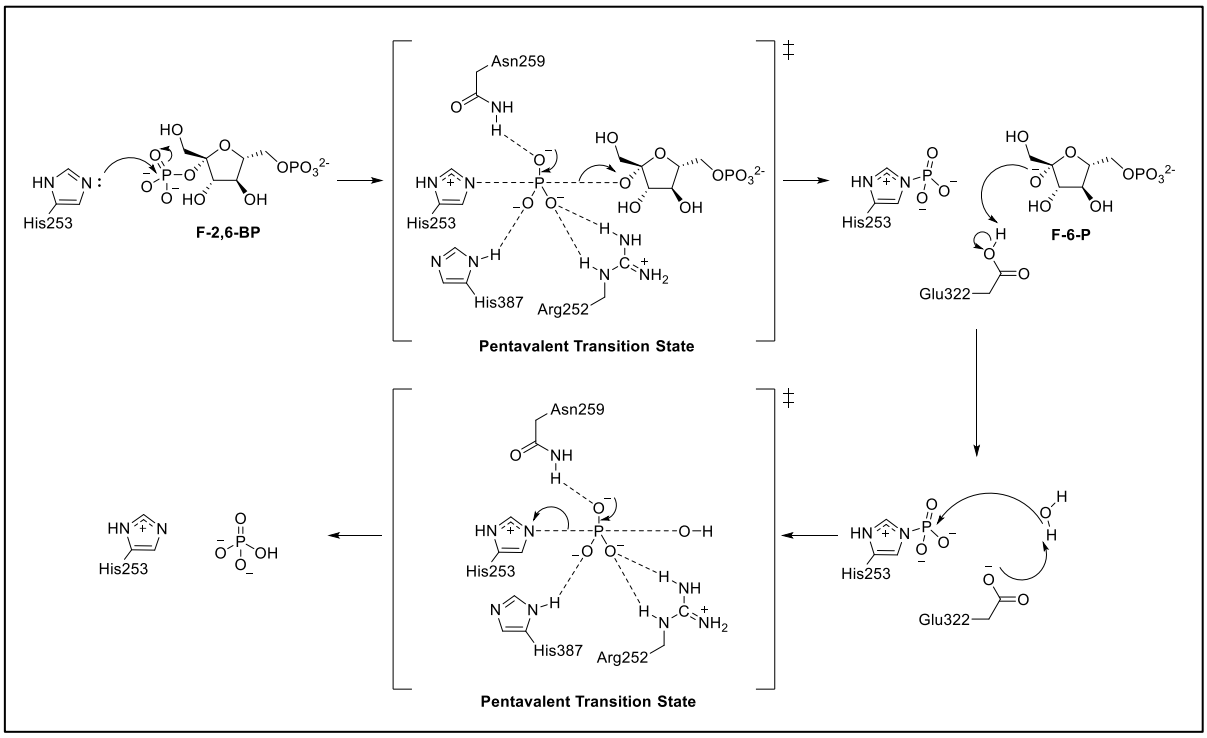

Scheme 1.2: PFK-2/FBPase-2 bisphosphatase reaction mechanism proposed by Cavalier and colleagues (Cavalier, Kim et al. 2012), which proceeds via two high-energy pentavalent transition states. His (histidine); Asn (asparagine); Arg (arginine); Glu (glutamic acid); F-6-P (fructose-6-phosphate); F-2,6-BP (fructose-2,6-bisphosphate).

Although both proposed mechanisms have been developed using PFKFB3 crystal structures, the high sequence homology in the core catalytic domains of the other PFK-2/FBPase-2 isoenzymes (> 85%) suggests that the mechanisms are likely to be conserved (Kim, Manes et al. 2006). A detailed understanding of the reaction mechanism and key residues involved in binding is likely to be important in facilitating the identification of potential small molecule inhibitors.

1.6.2: PFKFB1

In contrast to the other PFK-2/FBPase-2 isoenzymes, any potential role for PFKFB1 in carcinogenesis has yet to be fully elucidated, though *PFKFB1* mRNA expression has been found to be up-regulated in lung and gastric cancer (Minchenko, Ogura et al. 2005; Bobarykina, Minchenko et al. 2006). Three distinct promoters give rise to three mRNA variants, these being *F-PFK-2* (foetal), *L-PFK-2* (liver) and *M-PFK-2* (muscle), which differ at their 5'-end (Darville, Crepin et al. 1989; Darville, Antoine et al. 1992; Dupriez, Darville et al. 1993).

Two isoforms of PFKFB1 exist, these being the liver (L-PFK-2) isoform and the muscle (M-PFK-2) isoform. The L-PFK-2 isoform is derived from the *L-PFK-2* mRNA, it is the principle PFK-2/FBPase-2 enzyme expressed in the liver and is also expressed in white adipose tissue (Rider, Bertrand et al. 2004). The M-PFK-2 isoform is expressed in skeletal and white adipose tissue, where it is derived from the *M-PFK-2* mRNA. M-PFK-2 is also expressed in fibroblasts, foetal tissue, and of most relevance to cancer research, in proliferating tissues, where it derives from the *F-PFK-2* mRNA (Rider, Bertrand et al. 2004).

The two isoforms differ at their N-termini, where the L-PFK-2 isoform is distinct in possessing a Ser32 residue that can be phosphorylated by cAMP-dependent protein kinase, in response to glucagon (Murray, El-Maghrabi et al. 1984). This leads to inactivation of its kinase activity, mainly by increasing K_m for F-6-P, and activation of its bisphosphatase activity, thereby controlling glucose homeostasis, through promoting a switch from glycolysis to gluconeogenesis in liver cells (el-Maghrabi, Claus et al. 1982). The crystal structure of the liver isoform of PFKFB1 was reported in 2003, and exhibited structural features suitable for enhanced bisphosphatase activity, including an increase in the conformational stability of the

bisphosphatase domain, as compared with other PFK-2/FBPase-2 isoenzymes (Lee, Li et al. 2003).

1.6.3: PFKFB2

The *PFKFB2* gene encodes the cardiac isoform H-PFK-2 (PFKFB2), which is particularly important for regulating glycolysis in the heart, though its expression is not restricted to the heart (Hilliker, Darville et al. 1991; Chikri and Rousseau 1995; Heine-Suner, Diaz-Guillen et al. 1998). Four mRNA variants, denoted *H1-4*, are encoded by the *PFKFB2* gene. *H1*, *H2* and *H4* all encode the 58 kDa isoform of PFKFB2, whereas the *H3* variant encodes the shorter 54 kDa isoform, which arises due to alternative splicing and deletion of exon 15 (Rider, Vandamme et al. 1992; Vidal, Crepin et al. 1993).

Insulin, adrenalin and hypoxia are all known to stimulate PFKFB2 kinase activity, leading to a corresponding increase in F-2,6-BP concentration and elevated glycolytic flux (Rider and Hue 1984; Marsin, Bertrand et al. 2000). Activation is mediated through phosphorylation by a number of protein kinases, such as AMPK, Protein Kinase B (PKB) and Protein Kinase C (PKC) (Rider, van Damme et al. 1992; Deprez, Vertommen et al. 1997; Hue, Beauloye et al. 2002). Phosphorylation of two serine residues, Ser-466 and Ser-483, in the 58 kDa isoform increases PFKFB2 kinase activity (Bertrand, Alessi et al. 1999). These residues are absent in the 54 kDa isoform, leading some to postulate that the two isoforms of PFKFB2 may themselves have opposing effects on the regulation of glycolytic flux, though this has yet to be investigated (Ros and Schulze 2013).

The common elevation of F-2,6-BP in cancer cells may therefore be coupled with the regulation of PFKFB2 kinase activity, and one could suggest a potential role for this isoenzyme as a driver of carcinogenesis and cancer cell proliferation. Indeed, a recent report

linked androgen-stimulated glycolysis for *de novo* lipogenesis in the LNCaP prostate cancer cell line, at least in part, to increased activation of PFKFB2 kinase activity (Moon, Jin et al. 2011). Similar to *PFKFB1*, *PFKFB2* mRNA expression has also been found to be up-regulated in gastric and lung cancers (Minchenko, Ogura et al. 2005; Bobarykina, Minchenko et al. 2006), although studies of this isoenzyme in the context of carcinogenesis are limited.

1.6.4: PFKFB3

Originally identified in bovine brain (Ventura, Ambrosio et al. 1995) and human placenta (Sakai, Kato et al. 1996), at least six splice variants of PFKFB3 are now known to exist, which vary in the length of their C-termini. The two principle variants are inducible PFK-2 (iPFK-2) and ubiquitous (uPFK-2 or PFKFB3-ACG), also denoted UBI2K4 and UBI2K5, respectively. The remaining four variants were identified in human brain and are denoted UBI2K1-3 and UBI2K6 (Kessler and Eschrich 2001). *PFKFB3* mRNA is constitutively expressed in proliferating tissue (Hamilton, Callaghan et al. 1997; Goren, Manzano et al. 2000), and can be induced by stress stimuli (Novellasdemunt, Bultot et al. 2013), insulin (Riera, Manzano et al. 2002) and progestins (Hamilton, Callaghan et al. 1997; Novellasdemunt, Obach et al. 2012).

1.6.4.1: PFKFB3 and Cancer

PFKFB3 is over-expressed in a wide range of transformed cells (Hirata, Kato et al. 1998) and human cancers, including breast, colon (Minchenko, Ochiai et al. 2005), lung (Minchenko, Ogura et al. 2005), gastric (Bobarykina, Minchenko et al. 2006), glioblastoma (Kessler, Bleichert et al. 2008), ovarian and prostate (Atsumi, Chesney et al. 2002). Studies have also shown PFKFB3 is required for tumour cell growth *in vitro* and *in vivo* (Chesney, Mitchell et al. 1999) and that expression of PFKFB3 is selectively required to mediate the increase in

glycolytic flux that results from introduction of oncogenic *ras* to cells (Telang, Yalcin et al. 2006).

PFKFB3 has been observed to have the highest basal kinase:bisphosphatase (K:B) activity ratio of the four isoenzymes (740:1) (Sakakibara, Kato et al. 1997). The PFKFB3 crystal structure has revealed a structural rationale for this unusually high kinase activity (Kim, Manes et al. 2006). The N-terminus is found to bind to the FBPase-2 domain in the C-terminal region, leading to a local change in structure that enhances binding of the FBPase-2 catalytic site to the fructose-6-phosphate product, thereby slowing its release (the rate determining step), reducing turnover and lowering the FBPase-2 catalytic activity (Kim, Manes et al. 2006). A key catalytic Arg residue, present in the FBPase-2 domains of the other three isoenzymes, is replaced with a Ser residue, further reducing catalytic activity. Furthermore, a more rigid confirmation of the N-terminal kinase domain likely leads to higher affinity substrate (fructose-6-phosphate and ATP) binding, compared to other isoforms, promoting enhanced kinase activity (Kim, Manes et al. 2006).

Studies by Telang and colleagues have suggested that despite the co-expression of several isoenzymes, it is the relatively high kinase activity of PFKFB3 that determines the intracellular concentration of F-2,6-BP (Telang, Yalcin et al. 2006). This would suggest it is a critical activator of glycolysis, being largely responsible for malignant F-2,6-BP production (Atsumi, Chesney et al. 2002).

1.6.4.2: PFKFB3 and Hypoxia

PFKFB3 mRNA expression has been shown to be highly induced under hypoxic conditions in a range of cancer cell lines, including those derived from glioblastoma (Obach, Navarro-Sabate et al. 2004), colon (Atsumi, Chesney et al. 2002), gastric and pancreatic cancers

(Bobarykina, Minchenko et al. 2006). The hypoxic response was shown, at least in part, to be mediated by HIF-1α binding to a HRE in the 5'-promoter region of *PFKFB3* (Obach, Navarro-Sabate et al. 2004). A study of organs explanted from mice exposed to hypoxia showed that whilst all four PFK-2/FBPase-2 isoenzymes were induced, it was PFKFB3 mRNA that showed the highest induction (Minchenko, Opentanova et al. 2003).

1.6.4.3: PFKFB3 Regulation

PFKFB3 mRNA differs from the other isoforms by the presence of multiple copies of the AUUUA instability motif in its 3'-untranslated region, which confers instability and enhanced translational activity (Chen and Shyu 1995; Chesney, Mitchell et al. 1999). PFKFB3 has a phosphorylation site at Ser-461, which is phosphorylated by AMPK, leading to activation of its kinase activity (Marsin, Bouzin et al. 2002). The same residue is also a target for phosphorylation by Protein Kinase A (PKA) and PKC (Okamura and Sakakibara 1998). This is consistent with highly phosphorylated PFKFB3 observed in many human cancers (Bando, Atsumi et al. 2005). AMPK is known to activate PFKFB3 in this manner in response to prolonged exposure to low pH (Mendoza, Pocceschi et al. 2012), or hypoxia (Marsin, Bouzin et al. 2002).

PFKFB3 is unique among the PFK-2/FBPase-2 isoenzymes in that it contains a KEN box degradation motif, which allows recognition and proteasomal degradation by the E3 ubiquitin ligase anaphase-promoting complex/cyclosome APC/C-Cdh1 (Herrero-Mendez, Almeida et al. 2009; Almeida, Bolanos et al. 2010). This same complex is known to promote the degradation of cell cycle proteins, and therefore effectively co-ordinates proliferation with enhanced glycolysis, to supply the required biosynthetic intermediates (Almeida, Bolanos et al. 2010). It follows that PFKFB3 levels can be correlated with different stages of the cell cycle (Moncada, Higgs et al. 2012), and would explain why PFKFB3 expression is elevated

in normal proliferating tissue, e.g. thymus and testes, compared to non-proliferating normal tissue, e.g. heart and lung (Yalcin, Telang et al. 2009).

Deregulation of PFKFB3 degradation may be important in transformation and tumour progression. Indeed, mutations in APC subunits have been reported in colon (Wang, Moyret-Lalle et al. 2003) and breast cancer (Park, Choi et al. 2005). Furthermore, the tumour suppressor phosphatase and tensin homolog (PTEN), which promotes APC/C-Cdh1 activity, is also frequently mutated or deleted in cancer cells (Garcia-Cao, Song et al. 2012).

1.6.4.4: PFKFB3 Splice Variants

There has been a degree of confusion in the literature over the reported role of PFKFB3 splice variants, which has led to a number of findings being incorrectly ascribed to specific splice variants. For example, expression of inducible i-PFK-2, now referred to as UBI2K4, was originally found in tumours using a specific i-PFK-2 antibody (Chesney, Mitchell et al. 1999). However, cross-checking of the siRNA sequences and mRNA probes also used in the same widely-referenced study, reveals that these tools were not splice-variant specific. The study concluded i-PFK-2 was required for tumour cell growth (Chesney, Mitchell et al. 1999), but in fact, these conclusions should actually be applied to PFKFB3 protein in general. The importance of i-PFK-2 has thus received undue attention and it has now become clear that the splice variant UBI2K5, u-PFK-2, is the dominant variant expressed in transformed cells (Bando, Atsumi et al. 2005; Yalcin, Clem et al. 2009). A study by Calvo and colleagues (Calvo, Bartrons et al. 2006) also showed that specific siRNA-mediated reduction of UBI2K5 led to decreased F-2,6-BP, lactate and ATP production, and reduced viability of HeLa cells.

Zscharnack and colleagues (Zscharnack, Kessler et al. 2009) observed a change in PFKFB3 splice variant expression pattern with tumour progression, showing UBI2K3 and UBI2K4 (i-

PFK-2) to be restricted to low grade astrocytomas, whereas UBI2K5 (u-PFK-2) and UBI2K6 were found to predominate in rapidly proliferating, high-grade astrocytomas. Intriguingly, the group found that overexpression of UBI2K4 in the U87 glioblastoma cells elicited the expected increase in F-2,6-BP production, yet no increase in glycolytic rate, whilst also impeding their anchorage-independent growth (Zscharnack, Kessler et al. 2009). The authors extended their study to other cell lines and found an inverse correlation between *UBI2K4* expression and growth rate, suggesting it may function as a tumour-suppressor, the mechanism of which is currently unexplained.

Furthermore, the same group reported that common loss of heterozygosity (LOH) in high-grade gliomas targets the PFKFB3 gene locus, leading to reduced PFKFB3 expression, and in particular, reduced UBI2K4 expression levels in glioblastoma patients, which were found to correlate with poor prognosis (Fleischer, Kessler et al. 2011). This observation contrasts with previous studies linking elevated PFKFB3 expression to tumour progression. However, the authors suggest that the growth-advantage of LOH-mediated reduction of the tumour-suppressor function of UBI2K4 in gliomas may outweigh the reduction in other PFKFB3 splice variants that are known to promote tumour growth (Fleischer, Kessler et al. 2011). These findings await independent corroboration, but demonstrate the importance of furthering functional understanding of each of the splice variants.

It is becoming clear that PFKFB3 may have additional functional roles besides glycolysis. For example, Yalcin and colleagues (Yalcin, Clem et al. 2009) unexpectedly observed the splice variant UBI2K5 to be located in the nucleus of transformed cells, as opposed to the cytoplasm (the site of glycolysis). The production of F-2,6-BP at the nucleus was found to increase expression of cyclin-dependent kinase-1 (CDK-1), a key protein involved in cell cycle regulation, leading to increased proliferation. The different carboxyl-terminal domains of the

splice variants were shown to be responsible for differential sub-cellular trafficking (Yalcin, Clem et al. 2009) and nuclear localisation was later corroborated by Almeida and colleagues (Almeida, Bolanos et al. 2010; Rodriguez-Rodriguez, Fernandez et al. 2012).

1.6.4.5: PFKFB3 as a Therapeutic Target

These studies all suggest that PFKFB3 has an important role in transformation and tumour progression, both through regulation of glycolysis and cell proliferation, thus making it a very attractive therapeutic target. A series of non-selective PFK-2/FBPase-2 small molecule inhibitors were developed based on *N*-bromoacetylethanolamine phosphate, which was found to be an irreversible PFK-2/FBPase-2 inhibitor, and thought to act via alkylation at the kinase active site (Kitamura, Uyeda et al. 1989; Hirata, Watanabe et al. 2000). Other PFK-2/FBPase-2 inhibitors acted as non-specific alkylating agents, reacting with the sulfhydryl groups essential for enzymatic activity, e.g. the mercaptopurines (Mojena, Bosca et al. 1992).

However, the first step towards improved PFKFB3 selectivity came when Clem and colleagues published a computationally designed small-molecule inhibitor, 3PO (3-(3-pyridinyl)-1-(4-pyridinyl)-2-propen-1-one) (Figure 1.8) (Clem, Telang et al. 2008). This molecule was identified using a PFKFB3 homology model developed from the X-ray structure of rat testes PFKFB4. The authors found 3PO decreased intracellular F-2,6-BP and suppressed glycolytic flux in transformed cells. Furthermore, the compound suppressed growth of breast cancer, leukaemia and lung adenocarcinoma cells *in vivo*. The inhibitor was targeted to the F-6-P binding site and exhibited a combination of competitive and non-competitive activity (Clem, Telang et al. 2008). However, specificity of PFKFB3 inhibition was not validated during the study and high substrate binding domain homology between the kinase active sites of the PFK-2/FBPase-2 isoenzymes suggests that inhibition is likely to be non-specific.

A new series of 3PO derivatives were reported very recently (Clem, O'Neal et al. 2013), with one molecule, 1-(4-pyridinyl)-3-(2-quinolinyl)-2-propen-1-one (PFK-15) (Figure 1.8) showing 100-fold higher activity against PFKFB3, potent anti-tumour activity and improved isoenzyme selectivity, as compared to 3PO. An undisclosed derivative of PFK-15 will enter Phase I clinical trials sometime in 2013 (Clem, O'Neal et al. 2013).

The report of the PFKFB3 crystal structure (Kim, Manes et al. 2006) may facilitate the identification of more specific inhibitors, by exploiting distinct isoenzyme-specific topological features. Indeed, Seo and colleagues (Seo, Kim et al. 2011) used docking studies and similarity searches to identify two chromone derivatives, N4A and the more potent YN1, as competitive inhibitors of PFKFB3 (Figure 1.8). Chromones are molecules containing the core 1-benzopyran-4-one fragment, highlighted in red in Figure 1.8. The inhibitors reduced F-2,6-BP concentration, glycolytic flux and growth rate in transformed cells, and both showed strongest activity against PFKFB3, yet were still highly non-specific (Seo, Kim et al. 2011).

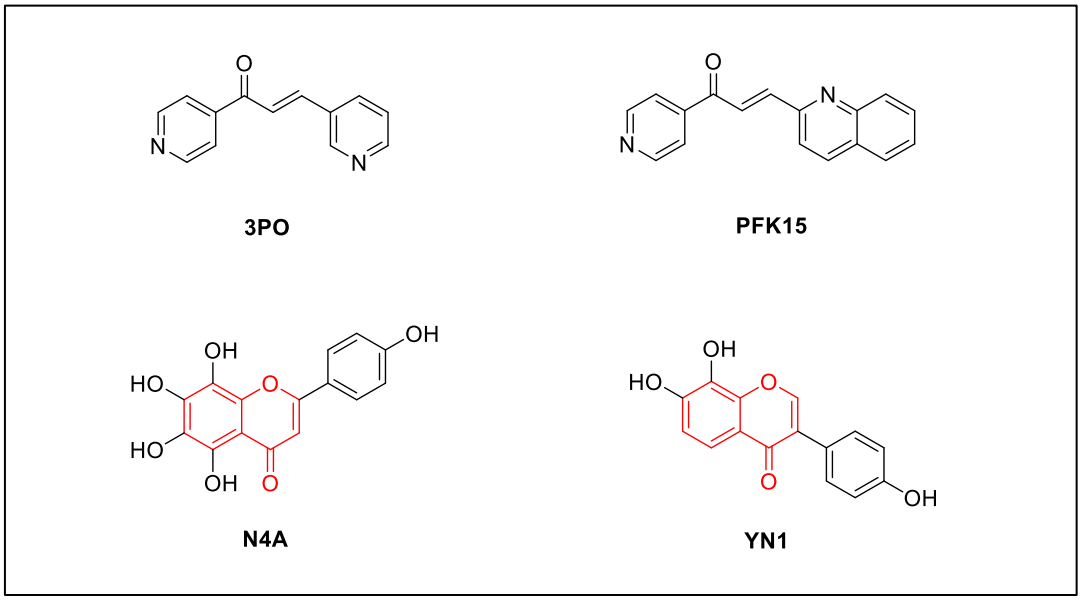

Figure 1.8: Current PFKFB3 inhibitors reported in the literature; 3PO (Clem, Telang et al. 2008), PFK15 (Clem, O'Neal et al. 2013), N4A and YN1 (Seo, Kim et al. 2011). The chromone motifs are indicated in red.

Chromone derivatives bind a wide variety of molecular targets and have been reported to have therapeutic effects in diseases such as asthma (Edwards and Howell 2000), cancer (Bhatnagar, Sahi et al. 2010) and HIV (Yu, Chen et al. 2004). However, our own group has found that molecules containing chromone-motifs are "frequent-hitters" in both computational and assay-based screens (unpublished data). Chromones are also highly electrophilic, making them susceptible to nucleophilic attack (Baell and Holloway 2010). Therefore a lack of specificity of N4A and YN1 may exist even beyond the PFK-2/FBPase-2 isoenzymes, due to potential promiscuous inhibition. This should be investigated through extensive kinome-screening.

1.6.5: PFKFB4

Human *PFKFB4* was first identified as a gene encoding a testis-specific PFK-2/FBPase-2 isoenzyme, T-PFK-2, which shares high amino acid sequence homology with the other human PFK-2/FBPase-2 isoenzymes (66-72%) (Manzano, Perez et al. 1999). The splice variant PFKFB4s was later identified (Minchenko, Ogura et al. 2005), and found to be co-expressed with the main isoform in DB-1 melanoma cells. PFKFB4s has a conserved PFK-2 catalytic domain, whilst the FBPase-2 is subject to modifications, which may confer different kinetic and/or regulatory properties, suggesting a potential role for different variants in tissue-specific regulation of glycolysis (Minchenko, Ogura et al. 2005; Ros and Schulze 2013).

1.6.5.1: PFKFB4 and Cancer

Elevated PFKFB4 expression has been reported in human breast, colon (Minchenko, Opentanova et al. 2005), lung (Minchenko, Ogura et al. 2005) and gastric cancers (Bobarykina, Minchenko et al. 2006). In fact, *PFKFB4* mRNA expression in the malignant tissue was generally found to exceed that of *PFKFB3* mRNA, and was found to be particularly high in the breast tumours (Minchenko, Ochiai et al. 2005; Bobarykina,

Minchenko et al. 2006). These findings, coupled with studies that have demonstrated basal expression of PFKFB4 in prostate, lung, hepatic and breast cell lines, as well as in brain cancer stem cells, all demonstrate expression in malignant cell lines, beyond those that are testis-specific (Minchenko, Opentanova et al. 2004; Minchenko, Ogura et al. 2005; Minchenko, Opentanova et al. 2005). PFKFB4 expression has also been reported as up-regulated in metastatic prostate cancer, compared with primary tumours (Ros, Santos et al. 2012).

However, it is only recently that elevated PFKFB4 expression has been linked with clinical outcome; one group showed positive correlation with reduced survival in primary glioblastoma patients (Goidts, Bageritz et al. 2011; Goidts, Bageritz et al. 2012). Furthermore, PFKFB4 expression correlates positively with bladder cancer tumour recurrence and progression, suggesting it could be used as a prognostic marker for disease management (Yun, Jo et al. 2011).

1.6.5.2: PFKFB4 and Hypoxia

Minchenko and colleagues (Minchenko, Opentanova et al. 2003) reported the first evidence for hypoxic induction of both splice variants of PFKFB4 *in vivo*, when they examined testis from mice exposed to 6 hours reduced oxygen concentration (7.5% oxygen). The same group observed induction of *PFKFB4* mRNA expression in a wide range of cell lines under hypoxic conditions, and after exposure to a series of hypoxia-mimics, including dimethyloxalylglycine (DMOG), a specific inhibitor of HIF hydroxylase enzymes (Minchenko, Opentanova et al. 2004; Minchenko, Opentanova et al. 2005). This suggested hypoxic regulation was mediated by HIF proteins, which the group confirmed through the use of a dominant-negative HIF-1α construct in transient transfection experiments with HeLa cells, which prevented induction of *PFKFB4* by DMOG (Minchenko, Opentanova et al. 2004). However, this final experiment

has not been extended to other cell lines and potential regulation of PFKFB4 expression by HIF-2α cannot currently be ruled out.

A HRE identified in the 5'-promoter region of PFKFB4 is now known to be responsible for mediating PFKFB4 gene transcription under hypoxic conditions (Minchenko, Opentanova et al. 2004). Intriguingly, Bobarykina and colleagues noted an inverse relationship between basal PFKFB4 protein expression and the degree of induction of *PFKFB4* mRNA under hypoxic conditions *in vitro* in a series of pancreatic and gastric cancer cell lines (Bobarykina, Minchenko et al. 2006). The group also found the degree of induction of PFKFB4 expression was far higher in malignant tumours derived from organs with low expression of the protein in non-malignant tissue, although the biological significance of this is yet to be understood.

1.6.5.3: PFKFB4 Regulation

Although no post-translational modifications of PFKFB4 have yet been reported, a recent study suggested that the heme oxygenase enzyme (HO-2) may have a role in regulating PFKFB4. Expression of the two enzymes was found to be co-ordinated, suggesting they both play a role in maintaining glucose homeostasis (Li, Takeda et al. 2012).

PFKFB4 lacks the key serine Ser-32 phosphorylation site, critical for down-regulation of PFKFB1 activity, so was hypothesised to have a high K:B activity, and therefore to play a significant role in promoting glycolytic flux (Okar, Manzano et al. 2001; Minchenko, Opentanova et al. 2004; Minchenko, Ochiai et al. 2005; Bartrons and Caro 2007). A number of studies have supported this (Sakata, Abe et al. 1991; Goidts, Bageritz et al. 2012; Gomez, Manzano et al. 2012), although PFKFB4 from human testis was found to have more balanced activity (K:B = 0.9, (Okar, Manzano et al. 2001)).

1.6.5.4: PFKFB4 as a Therapeutic Target

An elegant study by Ros and colleagues showed PFKFB4 was up-regulated under lipid-limited culture conditions, and that under such conditions, knockdown of PFKFB4 reduced prostate cancer cell growth *in vitro* (Ros, Santos et al. 2012). Furthermore, the group's *in vivo* study with PFKFB4 depletion showed remarkable tumour regression of PC3 xenografts. The group's findings were surprising in that they observed PFKFB4 kinase activity in the untransformed RWPE1 cell line, yet high PFKFB4 bisphosphatase activity in prostate cancer cells. Depletion of PFKFB4 in the prostate cancer cell lines resulted in a reduction in flux towards the PPP, reduced NADPH production and reduced ROS-scavenging by glutathione, promoting ROS-induced apoptosis. Their observation that the decrease in cell viability after *PFKFB4* silencing could be fully reversed by treatment with an anti-oxidant fully supported these findings (Ros, Santos et al. 2012). A reduction in PPP flux would also be consistent with greater PFKFB4 dependence in lipid-limited culture conditions, as NADPH is essential for lipid synthesis. It seems that PFKFB4 plays a key role in mediating the balance between glycolytic activity and antioxidant production, in order to maintain redox balance, an effect that may extend beyond prostate cancer cell lines (Ros and Schulze 2013).

This study could perhaps shed light on the observation (Atsumi, Chesney et al. 2002) made in SW620 colon adenocarcinoma cell lines, when they observed elevated PFKFB3 expression under hypoxic conditions, yet reduced F-2,6-BP concentration. These effects could potentially be explained by PFKFB4 induction under hypoxic conditions with elevated bisphosphatase activity, which would be interesting to investigate.

Importantly, Ros and colleagues showed that depletion of PFKFB4 selectively induced apoptosis only in the prostate cancer lines studied, and not the untransformed RWPE1 cell line (Ros, Santos et al. 2012). The authors also showed that PFKFB4-dependence extended to

other cancer cell lines, such as breast, colon and lung cancer cells, with effects more marked under lipid-limited culture conditions. Furthermore, other studies have now shown that PFKFB4 plays a key role in glioblastoma (Goidts, Bageritz et al. 2011) and hepatic cancer cell survival (Jeon, Jang et al. 2011). These results are encouraging and suggest PFKFB4 inhibition may allow selective targeting of tumour cells, although more extensive studies must be undertaken to assess the role of the individual splice variants, and whether the pro-survival role of PFKFB4 is generally tumour-specific (Dang 2012).

The relative kinase or bisphosphatase activity of PFKFB4 may be variable, but the studies outlined all suggest PFKFB4 is a potential target for the development of anti-cancer agents. To date, no specific small molecule inhibitors of PFKFB4 have been reported, either of its kinase or bisphosphatase activity, offering a potential window for the development of novel anti-cancer agents. However, it has been noted that the FBPase-2 domain lacks unique structural features, which may make the development of PFKFB4-specific competitive FBPase-2 inhibitors particularly challenging (Ros and Schulze 2013).

1.6.6: TIGAR

TIGAR (*TP53*-induced glycolysis and apoptosis regulator) is a p53-inducible gene, located on chromosome 12, p3-p13, which encodes a protein with bisphosphatase activity, similar to that of PFK-2/FBPase-2 (Bensaad, Tsuruta et al. 2006). Despite a lack of overall sequence homology with the FBPase-2 domain, the regions that are essential for the FBPase-2 catalytic activity are well conserved in TIGAR (Bensaad, Tsuruta et al. 2006), although the absence of 25 residues in the C-terminal region renders the active site comparatively open (Li and Jogl 2009). This explains why the bisphosphatase activity of TIGAR is less specific in nature, and so is able to exert a dual inhibitory effect on glycolysis, through reducing intracellular levels

of both the glycolytic intermediate F-1,6-BP and also the allosteric PFK-1 activator, F-2,6-BP (Li and Jogl 2009).

TIGAR thus diverts glycolytic intermediates towards the pentose phosphate pathway, promoting NADPH production, which acts as a co-factor in reduced glutathione (GSH) synthesis. The increase in GSH enables scavenging of reactive oxygen species (ROS), thereby protecting the cells from ROS-induced apoptosis and autophagy (Bensaad, Tsuruta et al. 2006; Bensaad, Cheung et al. 2009), an effect most apparent under conditions of cell stress, such as hypoxia (Wanka, Steinbach et al. 2012). This modulation of glycolytic flux towards the PPP neatly links increased glucose consumption to production of essential intermediates such as ribose-5-phosphate, important for nucleic acid production. This function may be vitally important for the promotion of cell growth, proliferation and the repair of DNA lesions (Green and Chipuk 2006; Bartrons and Caro 2007).

Intriguingly, a recent study has suggested an additional mechanism by which TIGAR is able to limit mitochondrial ROS in response to hypoxia, independent of its F-2,6-BPase function (Cheung, Ludwig et al. 2012). The group reported translocation of TIGAR to the outer mitochondrial membrane under hypoxic conditions. This facilitated interaction with, and stimulation of hexokinase-2 (HK2) activity, which is itself known to reduce mitochondrial ROS and promote cell survival (da-Silva, Gomez-Puyou et al. 2004). This would explain the observation that TIGAR overexpression more efficiently protected cells from apoptosis than overexpression of the FBPase-2 domain of PFK-2/FBPase-2 (Bensaad, Tsuruta et al. 2006).

The role that TIGAR plays in tumour progression is complex. One study links expression of TIGAR in highly glycolytic-dependent cells with reduced survival (Kimata, Matoba et al. 2010). In contrast, TIGAR has been shown to have a potential role in regulating cell-cycle

progression, through mediating G1-arrest and restricting entry into S-phase (Madan, Gogna et al. 2012), which the authors suggest may actually enhance drug-mediated tumour regression. In cells with functional p53, it seems induction of TIGAR has a protective role in response to mild cellular stress, or damage, forming part of the cell's tumour suppression system (Madan, Gogna et al. 2011). Prolonged cellular stress is correlated with a reduction in TIGAR levels, suggesting it may participate in the p53 induced switch from antioxidant targets to pro-apoptotic targets (Sablina, Budanov et al. 2005; Bensaad, Tsuruta et al. 2006). It is proposed that deregulation, leading to sustained TIGAR expression under prolonged stress, may inhibit the apoptotic response, thereby facilitating tumour progression (Bensaad, Cheung et al. 2009).

The observation that TIGAR is expressed in p53-null cells, suggests it can also be regulated in a p53-independent manner (Bensaad, Tsuruta et al. 2006). TIGAR function appears similar to that reported for PFKFB4, which was shown to have high bisphosphatase activity in prostate cancer cells (Ros, Santos et al. 2012). Whilst TIGAR's functional role is highly complex and inarguably cell and context dependent, ROS-dependent apoptosis, resulting from inhibition of TIGAR means the development of potential small molecule inhibitors for the prevention and possible treatment of cancer certainly warrants further investigation. No small molecule inhibitors have yet been developed, but the crystal structure of human TIGAR is now available (PDB: 3DCY), which should aid further investigations (Li and Jogl 2009).

1.6.7: PFK-2/FBPase-2 Isoenzymes and TIGAR – Modulators of Metabolic Flux

The high kinase activity of PFKFB3 and the exclusive bisphosphatase activity of TIGAR are well established (Figure 1.9) (Bensaad, Tsuruta et al. 2006). Whilst originally thought to have a more balanced K:B activity ratio, different reports in the literature suggest PFKFB4 may have elevated kinase activity (Gomez, Manzano et al. 2012) or elevated bisphosphatase activity (Ros, Santos et al. 2012) in different cell lines. PFKFB1 and PFKFB2 activities are

also subject to dynamic regulation. The interplay between the different isoenzymes and their relative K:B activities are intimately involved in regulating intracellular [F-2,6-BP], and therefore likely glycolytic flux. It will be essential to further understand this relationship in different tumour types, in order to explore the potential therapeutic applications of the development of effective small molecule inhibitors of PFK-2/FBPase-2.

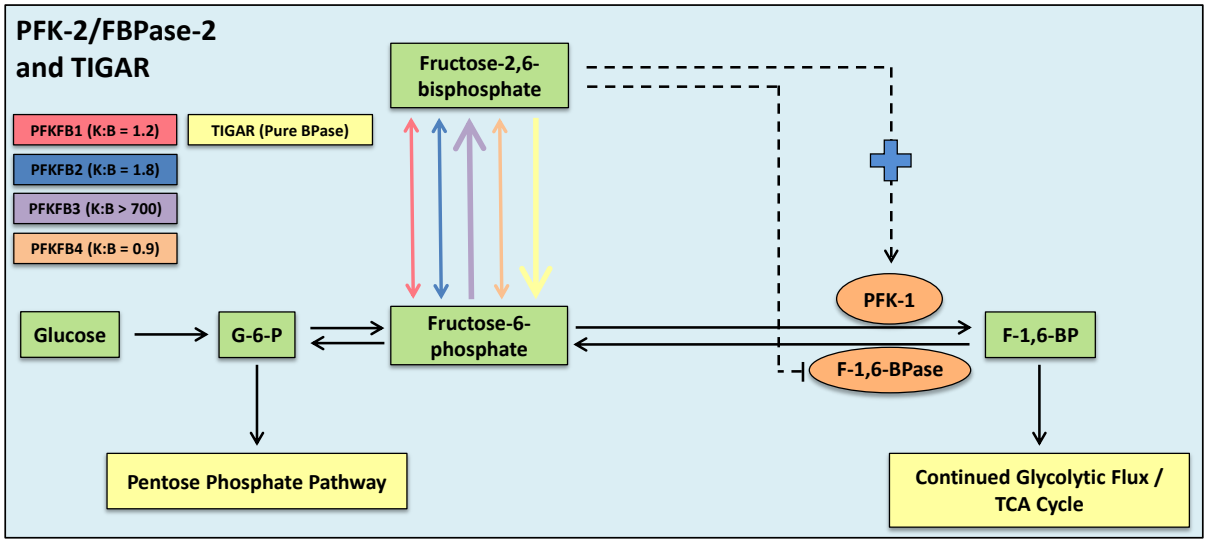

Figure 1.9: Basal kinase (K) and bisphosphatase (B) activities of each PFK-2/FBPase-2 isoenzyme and *TP53*-inducible glycolysis and apoptosis regulator (TIGAR), and their effect on PFK-1 activity. TCA (tricarboxylic acid); G-6-P (glucose-6-phosphate); BPase (bisphosphatase); F-1,6-BP (fructose-1,6-bisphosphate).

1.7: Project Aims

The literature clearly implicates PFK-1 and PFK-2/FBPase-2 as attractive targets for cancer therapy. In order to build on existing studies, this thesis has four broad aims:

- To examine the expression profiles of each of the PFK-1 and PFK-2/FBPase-2 isoenzymes in various cancer cell types and further probe their expression under hypoxic conditions, and regulation by hypoxia-inducible factors (HIFs).
- To validate PFK-2/FBPase-2 isoenzymes as anti-tumour targets and explore potential reciprocal relationships between isoenzymes.
- To investigate the requirement for isoenzyme-specific inhibition and further understanding of how individual PFK-2/FBPase-2 isoenzymes regulate metabolic flux.
- To undertake steps towards the development of an in-house assay to facilitate identification of potential PFK-2/FBPase-2 small molecule inhibitors.

Chapter 2: Materials and Methods

2.1: Cell Culture and *In Vitro* Techniques

2.1.1: Cell Lines and Media

MCF-7 breast and U87 glioblastoma cell lines were from Clare Hall laboratories, UK. BT20, BT549, MDA-MB-231, MDA-MB-468, SKBR3, T47D and MCF-10 breast cell lines, and DU145 and PC3 prostate cell lines were from CRUK Laboratories, Lincoln Inn Fields, UK. Roswell Park Memorial Institute-1640 (RPMI) media and foetal bovine serum (FBS) Gold were both from PAA Laboratories, and Dulbecco's Modified Eagle Medium (DMEM) was from Gibco (Invitrogen). All cell lines were cultured in DMEM media containing 10% FBS and 1% Penicillin-Streptomycin, with the exception of DU145 and PC3, which were cultured in RPMI, containing 10% FBS and 1% Penicillin-Streptomycin. All plasticware was purchased from Corning.

2.1.2: Culturing and Passaging Cells

Cells were grown in T175 cell culture flasks and passaged by first aspirating the media, washing with phosphate buffered saline solution (PBS) (10 mL) and incubating with 1x trypsin/ ethylenediaminetetraacetic acid (EDTA) solution (3 mL) for 3 minutes. Media (10 mL) was added and the cell suspension transferred to a 50 mL Falcon tube, before being centrifuged (Heraeus Biofuge primo, 1000 rpm, 4 minutes). The supernatant was aspirated and the cell pellet re-suspended in media (1 mL). The suspension was then typically split 1:10 and reseeded in T175 flasks with fresh media (30 mL).

2.1.3: Long-term Cell Storage and Recovery

Cell pellets were prepared as described above and re-suspended in FBS containing 10% DMSO at an approximate density of 2 million cells/mL. The cell suspension was aliquoted in individual cryo-vials (1 mL/vial). The vials were then transferred to a Mr Frosty (Nalgene) container, insulated with isopropanol, and placed in a -80 ºC freezer, which permitted freezing of the vials at a rate of 1 ºC per minute. Once frozen, cell vials were transferred to liquid nitrogen for long-term storage. To recover the cells, the vials were thawed rapidly using a water bath (37 ºC), before re-suspending in media (10 mL) and centrifuging (Heraeus Biofuge primo, 1000 rpm, 4 minutes). Cell pellets were re-suspended in media and transferred to a T75 cell culture flask with fresh media (20 mL) and incubated overnight. The media was replaced the following day and the cells incubated until reaching confluency. Cells were passaged twice before use in any experiments.

2.1.4: Cell Counting

A Coulter Particle counter Z2 (Beckman Coulter) was used to count cells. A 400 µL cell suspension was diluted in 19.6 mL isotonic buffered saline solution (isoton), and a cell count performed according to the manufacturer's instructions, between the particle size range 9-22 µm.

2.1.5: Hypoxic Exposure

Hypoxic incubations were performed using an INVIVO$_2$ 400 hypoxic work station (Pro-Lab Diagnostics), at 0.1% O_2 / 5% CO_2 / 37 ºC. Cells were allowed to adhere to plates for at least 4 hours after re-seeding, prior to hypoxic exposure. Media changes under hypoxic conditions were performed in the hypoxic chamber, with media that had been equilibrated under hypoxic conditions overnight.

2.2: Cell Transfection

2.2.1: Transient siRNA Suppression of Gene Expression

Cells were passaged and counted as described above, using media without Penicillin-Streptomycin, then re-suspended at a concentration of 104,167 cells/mL. Oligofectamine™ transfection reagent (Invitrogen, 18 µL/reaction) was diluted in Optimem™ (Invitrogen) (72 µL/reaction), and incubated for 5 minutes at room temperature (RT). Meanwhile, siRNA stock solutions (20 µM, 6 µL/reaction) were diluted in Optimem™ (1.10 mL/reaction), to which the diluted Oligofectamine™ (90 µL/reaction) was added. After incubation for 20 minutes at RT, the solution (1.2 mL) was added to the cell suspension (4.8 mL) in a 10 cm cell culture dish and incubated overnight at 37 ºC (final siRNA concentration 20 nM). The media was then aspirated and replaced with media (15 mL) containing Penicillin-Streptomycin (1%) and the plates treated in accordance with individual experiments. Volumes above are given for 10 cm culture dishes, and were scaled down by 50% for 6 cm dishes.

2.2.2: siRNA Sequences

An ON-TARGET*plus*™ non-targeting siRNA pool (D-Scramble), PFKFB3 siRNA pool (D-siPFKFB3) and PFKFB4 siRNA pool (D-siPFKFB4) were purchased from Dharmacon. The individual PFKFB3 and PFKFB4 sequences contained in these pools were then purchased from Invitrogen (siPFKFB3-1:siPFKFB3-4, siPFKFB4-1:siPFKFB4-4). A non-targeting scramble control, previously used in the literature (Reichert, Saur et al. 2007), was also purchased from Invitrogen. HIF-1α, HIF-2α and TIGAR siRNA sequences had previously been designed by other members of the Harris laboratory. Sequences were submitted to a Basic Local Alignment Search Tool (BLAST) search (National Centre for Biotechnology Information database), to confirm siRNA targeting of a single gene. Sequences are listed in Table 2.1.

siRNA	Supplier	Reverse (5'-3')
D-Scramble (Dharmacon pool)	Dharmacon (D-001810-10-20)	ON-TARGET*plus*™ Non-targeting Pool
D-siPFKFB3	Dharmacon (L-006763-00-0020)	ON-TARGET*plus*™ Pool of:- (1) CGACGACCCUACAGUUGUG (2) CAAGUACUAUUACCGCUAC (3) GGACCUAACCCGCUCAUGA (4) AAAGCUACCUGGCGAAAGA
D-siPFKFB4	Dharmacon (L-006764-00-0020)	ON-TARGET*plus*™ Pool of:- (1) GGAGAGCGACCAUCUUUAA (2) GAAAUGACCUACGAGGAAA (3) GAACAGAAUGGCUACAAGA (4) GGAAGGUCCUCAACGAGAU
Scramble	Invitrogen	AACAGTCGCGTTTGCGACTGG[dT][dT]
siPFKFB3.1	Invitrogen	CGACGACCCUACAGUUGUG[dT][dT]
siPFKFB3.2	Invitrogen	CAAGUACUAUUACCGCUAC[dT][dT]
siPFKFB3.3	Invitrogen	GGACCUAACCCGCUCAUGA[dT][dT]
siPFKFB3.4	Invitrogen	AAAGCUACCUGGCGAAAGA[dT][dT]
siPFKFB4.1	Invitrogen	GGAGAGCGACCAUCUUUAA[dT][dT]
siPFKFB4.2	Invitrogen	GAAAUGACCUACGAGGAAA[dT][dT]
siPFKFB4.3	Invitrogen	GAACAGAAUGGCUACAAGA[dT][dT]
siPFKFB4.4	Invitrogen	GGAAGGUCCUCAACGAGAU[dT][dT]
siHIF-1	Invitrogen	Pool of: CAAGCAACTGTCATATATA[dT][dT] TGCCACCACTGATGAATTA[dT][dT] TGACTCAGCTATTCACCAA[dT][dT]
siHIF-2	Invitrogen	Pool of: TAACGACCTGAAGATTGAA[dT][dT] CAAGCCACTGAGCGCAAAT[dT][dT] TGAATTCTACCATGCGCTA[dT][dT]
siTIGAR	Invitrogen	Pool of: GCAGCAGCTGCTGGTATAT[dT][dT] TTAGCAGCCAGTGTCTTAG[dT][dT]

Table 2.1: Small interfering RNA (siRNA) sequences and suppliers.

After validation, siRNA sequences used for further experiments were siPFKFB3 (siPFKFB3-1 and siPFKFB3-2), siPFKFB4 (siPFKFB4-1 and siPFKFB4-2) and siPFKFB3and4 (siPFKFB3-1, siPFKFB3-2, siPFKFB4-1 and siPFKFB4-2), all at a final concentration of 20 nM.

2.2.3: Transient PFKFB3 and PFKFB4 Over-expression

HEK 293T cells were plated in 10 cm dishes and incubated until reaching approximately 80% confluency. Prior to transfection, the media was removed and replaced with DMEM media, without Penicillin-Streptomycin (5.8 mL). To 3 sterile eppendorf tubes were added Optimem™ (176 µL) and one of either (1) PFKFB3 human cDNA clone (Origene, SC117283, 8 µL, 0.5 µg/µL), (2) PFKFB4 human cDNA clone (Origene, SC110972, 8 µL, 0.5 µg/µL), or (3) DEPC-treated water (8 µL, Mock). After equilibrating to room temperature, FuGENE® transfection reagent (16 µL) was added to each eppendorf tube and mixed immediately, taking care not to allow the transfection reagent to touch the sides of the tube. This was incubated at RT for 15 minutes, before adding the entire volume to the 10 cm dishes. Plates were incubated for 24 hours at 37 ºC, before lysing according to the standard protocol.

2.3: RNA Extraction, qRT-PCR and Analysis

2.3.1: RNA Extraction

Cells were aspirated and TRI Reagent® (Sigma Aldrich) added directly to the cells (10 cm dish: 1 mL) and transferred to a 1.5 mL eppendorf tube. Chloroform (200 µL) was added and the samples shaken vigorously for 15 seconds, before leaving at RT for 10 minutes. Samples were then centrifuged (Eppendorf Centrifuge 5424R, 14000 rpm, 4 ºC, 15 minutes) and the upper, aqueous phase, transferred to a fresh eppendorf tube, containing isopropanol (500 µL). The tubes were mixed immediately and incubated at RT for 15 minutes, then centrifuged (Eppendorf Centrifuge 5424R, 14000 rpm, 4 ºC, 15 minutes), before aspirating the supernatant from the pellet. A 75% ethanol solution (1 mL, containing nuclease-free diethylpyrocarbonate (DEPC)-treated water (Ambion)) was added to each tube and all samples were centrifuged (Eppendorf Centrifuge 5424R, 7500 rpm, 4 ºC, 5 minutes), before aspirating the supernatant and allowing the RNA pellets to air dry at RT for 10 minutes.

Pellets were re-suspended in 60 µL DEPC-treated water and heated at 60 ºC for 10 minutes, before vortexing. A NanoDrop ND 1000 Spectrophotometer (NanoDrop Technologies) was used to measure RNA concentration and quality. Volumes above are given for 10 cm plates, and were scaled down by 50% for 6 cm dishes.

2.3.2: cDNA Synthesis

RNA (1 µg per sample) was reverse transcribed using the High Capacity cDNA Synthesis Kit (Applied Biosystems), using the reaction components and cycling conditions detailed below (Tables 2.2 and 2.3, respectively) (thermal cycler PTC-2000, MJ Systems). cDNA samples (20 µL) were then diluted with DEPC treated water (200 µL), before use in quantitative real time polymerase chain reactions (qRT-PCR).

Component	Volume/reaction (µL)
RT buffer (10x)	2
dNTP mix (100 mM) (25x)	0.8
Random primers (10x)	2
Multiscribe (50U/µL)	1
DEPC treated water	4.2
RNA	1

Table 2.2: Volumes of components used for cDNA synthesis.

Cycling Conditions	
Temperature	**Time**
25 ºC	10 min
37 ºC	120 min
85 ºC	5 sec
4 ºC	Hold

Table 2.3: Cycling conditions used for cDNA synthesis.

2.3.3: Quantitative Real-Time PCR (qRT-PCR)

qRT-PCR reactions were performed in triplicate using the ABI 7900 sequence detector (Life Technologies). Master Mix was prepared containing SensiMix^{TM} SYBR No-Rox kit (Bioline) (5 µL/reaction), DEPC treated water (1 µL/reaction), forward primer (3 µM, 1 µL/reaction)

and reverse primer (3 µM, 1 µL/reaction). Reactions were performed in 384 well plates with each reaction well containing diluted cDNA (2 µL) and Master Mix (8 µL). Cycle conditions for the qRT-PCR reaction were (1) 50 ºC (2 min), (2) 95 ºC (10 min), (3) repeat of 95 ºC (15 sec) / 60 ºC (1 min) 50 times. A further dissociation step was included to confirm amplification of a single gene product. RNA content was normalised by amplification of β-actin as a reference gene. Relative expression levels of RNA were made using the modified comparative Ct method (Pfaffl 2001). Direct comparisons were made between the number of cycles required for the fluorescence signal to meet a threshold, chosen to be in the linear range of the cycle curves and above the non-specific background signal. Accordingly, the relative ratio of gene expression was calculated using Equation 2.1.

$$R = \frac{(E_{Target})^{\Delta CtTarget\ (Control - Sample)}}{(E_{Reference})^{\Delta CtReference\ (Control - Sample)}}$$

Equation 2.1: Calculation of relative mRNA expression levels using the comparative Ct method. E_{Target} (reaction efficiency of gene of interest); $E_{Reference}$ (reaction efficiency of reference gene: β-actin); ΔCt (difference in cycle number between control and sample of interest) (Pfaffl 2001). Assumption that $E_{Target}=E_{Reference}=2$ (100% amplification efficiency). Calculations based on mean value of 3 replicates.

2.3.4: qRT-PCR Primer Sequences

PFK-1 and PFK-2/FBPase-2 primer sequences were designed by Dr Anassuya Ramachandran, a member of the Harris laboratory, using the Exiqon universal ProbeLibary® system (Roche, Basal, Switzerland). β-actin, TIGAR, HIF-1α and HIF-2α primer sequences were previously designed in a similar manner by other members of the Harris laboratory. Primers were checked for specificity using a Basic Local Alignment Search Tool search (National Centre for Biotechnology Information database). Primer sequences are listed in Table 2.4.

Primer	Forward	Reverse
β-Actin	ATTGGCAATGAGCGGTTC	GGATGCCACAGGACTCCAT
PFKL	AAGAAGTAGGCTGGCACGACGT	GCGGATGTTCTCCACAATGGAC
PFKM	GCTTCTAGCTCATGTCAGACCC	CCAATCCTCACAGTGGAGCGAA
PFKP	AGGCAGTCATCGCCTTGCTAGA	ATCGCCTTCTGCACATCCTGAG
PFKFB1	GGCGAGAGTGAACTCAACATCAG	TGTGACTGGTCCACACCTTCAG
PFKFB2	TACCGACCTCTTGACCCAGACA	TAAATGGTGCGAGGCTGGACGT
PFKFB3	GGCAGGAGAATGTGCTGGTCAT	CATAAGCGACAGGCGTCAGTTTC
PFKFB4	GATCCTGAGGTCATAGCTGCCA	CTATCCAGGTCCTCATCTAGCG
TIGAR	TCCTCCAGGCGGGTGAACAGGGGC	CGGAGACTGGGTTTCGGCAAGCAGCGG
HIF-1α	CAGCTATTTGCGTGTGAGGA	TTCATCTGTGCTTTCATGTCATC
HIF-2α	CTGTGTCTGAGAAGAGTAACTTCC	TTGCCATAGGCTGAGGACTCCT

Table 2.4: Primer sequences.

2.4: Protein Extraction and Analysis

2.4.1: Protein Extraction

Cells were immediately placed on ice, the media aspirated, then washed with ice cold PBS (10 mL), which was aspirated, before adding 300 µL (10 cm plates) or 200 µL (6 cm plates) radioimmunoprecipitation assay (RIPA) lysis buffer (Sigma Aldrich), containing Complete® Mini Protease Inhibitor (Roche, 1 tablet/10 mL) and Phosphatase Inhibitor Cocktails 2 and 3 (Sigma Aldrich, 100 µL of each/10 mL). A cell scraper was used to remove the cells and the samples were then homogenised using a 25-gauge syringe, before vortexing (30 seconds).

2.4.2: Protein Quantification

Protein was quantified using Bio-Rad *DC*™ Protein Assay, according to the manufacturer's instructions. Briefly, protein samples were diluted 1:5 in PBS and 5 µL diluted sample added per well in a 96-well plate (5 replicates). Standard protein concentrations were also prepared (0.5 mg/mL – 2 mg/mL) and 5 µL added per well in duplicate. 25 µL Reagent A' (1 mL

Reagent A + 20 µL Reagent S) was added to each well, followed by 200 µL Reagent B. Plates were then incubated for 30 minutes before reading the absorbance at 690 nm; a standard curve was then plotted and the sample protein concentrations calculated accordingly.

2.4.3: Gel Electrophoresis

6x Laemmli sample buffer (72 mM Tris (pH 6.8), 20% glycerol, 10% β-mercaptoethanol, 4.5% SDS, 0.015% bromophenol blue) was added to protein sample diluted in PBS, such that the concentration of protein was 1 mg/mL. Samples were then heated at 70 ºC for 10 min. Protein samples were then loaded on 10 well (30 µL per lane) or 15 well (20 µL per lane) 4-12% gradient NuPAGE® Bis-Tris gels (Invitrogen) and 1x NuPAGE® MOPS SDS Running Buffer (500 mL) added to the gel chamber. Gels were run at 150 V for 90 minutes, before removing and transferring to a polyvinylidene fluoride (PVDF) membrane (Millipore) using 1 x NuPAGE® transfer buffer with 10 % methanol.

2.4.4: Membrane Blocking, Antibody Incubation and Detection

Membranes were blocked for 1 hour in Tris-buffered saline solution, with 0.1% Tween 20 (TBST), containing 5% milk powder (m-TBST), before incubation overnight at 4 ºC with the appropriate primary antibody diluted in m-TBST. Membranes were then washed in TBST solution (3 x 15 minutes) and incubated at RT for 1 hour with the appropriate horseradish peroxidase (HRP)-conjugated secondary antibody, diluted in m-TBST solution. Membranes were then washed in TBST solution (3 x 15 minutes) and antibody binding was detected using Amersham™ ECL™, ECL™ Plus or ECL™ Prime Western Blotting Detection Systems, and the ImageQuant LAS4000mini system (GE Healthcare). β-actin was used as a loading control.

2.4.4.1: Antibodies

Primary antibody suppliers and working concentrations were as shown in Table 2.5.

Antibody	Company / Catalogue Number	Host	Working Conc.	Detection System
Actin-HRP	Sigma Aldrich (A3854)	Mouse	1:10,000	ECL
HIF-1α	BD Transduction Laboratories (6109058)	Mouse	1:500	ECL Plus
HIF-2α	Novus Biologicals (NB100-122)	Rabbit	1:1000	ECL Plus
PFKFB3v5	Gift of Prof. Salvador Moncada(Colombo, Palacios-Callender et al. 2010)	Rabbit	1:1000	ECL Plus
PFKFB4	Epitomics (S1348)	Rabbit	1:1000	ECL Prime
TIGAR	Santa Cruz Biotechnology (sc-101535)	Mouse	1:100	ECL Plus

Table 2.5: Primary antibody suppliers, hosts, working concentrations and detection systems.

HRP-conjugated secondary antibodies (anti-rabbit, anti-mouse) were from Dako and used at a concentration of 1:1000. Western blot figures throughout the thesis showing PFKFB3 expression make use of an antibody specific to splice variant 5, UBI2K5 (PFKFB3v5), the predominant splice variant expressed in transformed cells.

2.5: *In vitro* Proliferation Assays

2.5.1: Sulforhodamine B (SRB) Assay

MCF-7 cells were transfected with siRNA in 6 cm dishes (300,000 cells per dish), according to the standard protocol, to provide a Mock (vehicle only), scramble control, PFKFB3-1:PFKFB3-4 knockdowns and PFKFB4-1:PFKFB4-4 knockdowns. After incubation overnight (37 ºC), cells were reseeded at 1000 cells/well (5 replicates per condition per plate), and allowed to adhere for 4 hours, before taking the first time point (t = 0 hours). The

remaining plates were incubated under normoxic conditions until the required time point (t = 1, 3 and 5 days), when the media was discarded and trichloroacetic acid (TCA) (10%, 200 µL) added to each well. Plates were then incubated at 4 ºC for 1 hour, the TCA solution removed from the wells and the plates washed 3 times with tap water, and allowed to air dry. SRB solution (0.4% SRB in 1% Acetic Acid, 100 µL) was added to each well and the plates incubated at RT for 30 minutes. The SRB solution was removed and the wells washed 3 times with acetic acid solution (1%, 100 µL), and allowed to air dry. The SRB stain was resolved by addition of Tris solution (10 mM, pH 9.5, 200 µL) to each well, and the plates were then incubated on a plate shaker at RT for 15 minutes. Absorbance was read at 540 nm.

2.5.2: CyQUANT® Cell Proliferation Assay

MCF-7, U87 and PC3 cells were transfected with siRNA in 6 cm dishes (300,000 cells per dish), according to the standard protocol, to provide a scramble control, PFKFB3 knockdown, PFKFB4 knockdown and a double PFKFB3/PFKFB4 knockdown. Cells were incubated overnight at 37 ºC and reseeded at a concentration of 1500 cells per well in 200 µL media (MCF-7/U87: DMEM; PC3: RPMI), 5 replicates per condition per plate. Cells were allowed to adhere at 37 ºC for 4 hours, before transferring hypoxic plates to the hypoxic incubator (0.1% O_2) (t = 0 hours). At t = 0 hours, a plate was assayed using the CyQUANT® NF Cell Proliferation Assay (Invitrogen), which was used according to the manufacturer's instructions. Briefly, the media was removed, and 100 µL CyQUANT® reagent (1:4:0.01 HBSS buffer/ DI water/ CyQUANT® NF dye reagent) added per well, before incubating in the dark at 37 ºC for 30 minutes. Fluorescence was then measured using a fluorescence microplate reader, with excitation at λ = 485 nm and emission detection at λ = 530 nm. Further plates were analysed at the appropriate time points and the values normalised to the t = 0 hours background control. Values were reported as relative fluorescence units.

2.5.3: 3D Spheroid Formation

MCF-7, U87 and PC3 cells were transfected with siRNA in 6 cm dishes (300,000 cells per dish), according to the standard protocol, to provide a scramble control, PFKFB3 knockdown, PFKFB4 knockdown and a double PFKFB3/PFKFB4 knockdown, and incubated overnight at 37 ºC. The cells were reseeded in non-adherent round bottom 96-well plates (Costar) at a concentration of 5000 cells/well in 200 µL media (MCF-7/U87: DMEM; PC3: RPMI), to generate 15 spheroids per condition used. Matrigel™ (BD BioSciences) was added to the MCF-7 and PC3 cells at a concentration of 25 µL/mL. The plates were then centrifuged (Beckmann Coulter Allegra 6R Centrifuge, 2000 rpm, 10 minutes), and incubated overnight at 37 ºC to allow the cells to adhere. Images were taken at t = day 1 (24 h after reseeding), day 2, day 4 and day 6, using an EVOS XL (AMG) inverted microscope, and saved as JPEGs. Media changes (100 µL) were made at t = day 4.

2.5.4: Quantifying Spheroid Volume

The images were processed as JPEGs and a threshold set using ImageJ® software so as to exclude any non-spheroid contributions. The number of pixels enclosed within the spheroid area was recorded and converted to mm^2, using a haemocytometer as a reference, and the spheroid radius calculated. Using the assumption that the spheroids were perfectly spherical, the spheroid volume was computed. Averages were calculated for each of the 15 spheroids per condition and the experiment repeated 3 times, final recorded results being the average and standard error of the mean (SEM) of at least 3 independent average readings per spheroid condition.

2.6: Metabolite Assays

2.6.1: ATP Assay

MCF-7, U87 and PC3 cells were transfected with siRNA in 6 cm dishes (300,000 cells per dish), according to the standard protocol, to provide a scramble control, PFKFB3 knockdown, PFKFB4 knockdown and a double PFKFB3/PFKFB4 knockdown. Cells were incubated overnight at 37 ºC and reseeded at a concentration of 5000 cells per well in 100 µL media (MCF-7/U87: DMEM; PC3: RPMI), 3 replicates per condition per plate. Cells were allowed to adhere at 37 ºC for 4 hours, before transferring hypoxic plates to the hypoxic incubator (0.1% O_2). Plates were incubated for a further 48 hours, before adding 100 µL Cell-Titer Glo® (Promega) to each well (prepared according to the manufacturer's instructions and equilibrated to RT before use). Plates were mixed on a plate shaker for 2 minutes to lyse the cells, before transferring 160 µL of each sample to a 96 well clear-bottomed white plate (Corning). Plates were incubated at RT for a further 10 minutes to allow the luminescence signal to stabilise, before measuring luminescence in a BMG LABTECH FLUOstar Omega multi-mode microplate reader and analysing the results using Soft Max Pro ™ software. Background luminescence was removed and the ATP values normalised to CyQUANT™ values for identical plates prepared at the same time.

2.6.2: Lactate Assay

MCF-7, U87 and PC3 cells were transfected with siRNA in 6 cm dishes (300,000 cells per dish), according to the standard protocol, and 96 well plates prepared in an identical manner to that described for the CyQUANT™ assay with 3 replicate plates (t = 0 h, t = 48 h (normoxia), t = 48 h (hypoxia)). A CyQUANT™ assay was performed on the t = 0 h plate at the appropriate time; media was collected from the t = 48 h (normoxia and hypoxia) time point plates and the relevant plates assayed using CyQUANT™. Sample media (10 µL) and

control media (10 µL) were added to a 96 well plate in triplicate. Serial dilutions of lactate standard (4.44 mM) were made across the plate in duplicate. Lactate reagent was prepared according to the manufacturer's instructions (INstruchemie, 2864) and 290 µL added to each well. The plate was mixed on a plate shaker, before incubating for 30 minutes at RT. Absorbance was measured at 340 nm and mean lactate concentrations calculated from the standard curve of serial dilutions. Lactate values were normalised to the geometric mean of cell number for each condition, calculated from the CyQUANT^{TM} values at t = 0 h and t = 48 h.

2.6.3: Glucose Assay

The same media samples were used as for the lactate assay, as described above. Sample media (5 µL) and control media (5 µL) were added to a 96 well plate in triplicate and diluted with distilled water (25 µL). Serial dilutions of glucose standard (5 g/L) (30 µL) were made across the plate in duplicate. Glucose reagent (150 µL) (INstruchemie, 2319) was added to each well and the plates mixed and incubated for 1 minute before reading the absorbance at 340 nm (OD1). Glucose starting reagent (30 µL) (INstruchemie, 2942) was added to each well and the plates mixed and incubated for 2 minutes, before reading the absorbance at 340 nm (OD2). The absorbance difference was calculated for each well (OD2-OD1) and the glucose concentration calculated using a standard curve plotted from the glucose standard dilutions. The mean glucose consumption was calculated from the concentration difference between the media control and test samples. Glucose consumption values were normalised to the geometric mean of cell number for each condition, calculated from the CyQUANT^{TM} values at t = 0 h and t = 48 h.

2.6.4: Glycolytic Efficiency

Glycolytic efficiency was estimated by dividing the amount of lactate produced by the amount of glucose consumed from the media, in the same experiment for each condition (mol lactate produced / mol glucose consumed).

2.6.5: Fructose-2,6-bisphosphate Assay and Analysis

MCF-7, U87 and PC3 cells were transfected with siRNA in 10 cm dishes (500,000 cells per dish), according to the standard protocol, to provide a scramble control, PFKFB3 knockdown, PFKFB4 knockdown and a double PFKFB3/PFKFB4 knockdown. Six identical plates for each condition were set up and incubated overnight at 37 ºC. The media was aspirated the following day and then replaced with 15 mL fresh media (MCF-7/U87: DMEM; PC3: RPMI), before transferring half of the plates to the hypoxic incubator (0.1% O_2). Plates were incubated, before removing and lysing 1 set of plates at 24 hours, 48 hours and 72 hours. Cells were washed twice with cold PBS (10 mL), before lysing with 0.4 mL extraction buffer (NaOH 100mM + Triton X-100 (0.1%)). Samples were stored at -20 ºC prior to determination. The F-2,6-BP assay was then performed by Dr Anna Manzano in Dr Ramon Bartrons' laboratory, at the University of Barcelona, using an adapted protocol by Van Schaftingen and colleagues (Van Schaftingen, Lederer et al. 1982; Van Schaftingen 1987) Values were normalised to protein content.

2.7: Reactive Oxygen Species Assay

MCF-7, U87 and PC3 cells were transfected with siRNA in 6 well dishes (100,000 cells per dish), according to the standard protocol (final transfection volume of 1 mL), to provide a scramble control, PFKFB3 knockdown, PFKFB4 knockdown and a double PFKFB3/PFKFB4 knockdown. Two replicates per condition were plated and cells were incubated overnight at

37 ºC, before aspirating the media and replacing with fresh media (3 mL, MCF-7/U87: DMEM; PC3: RPMI). One set of plates was transferred to the hypoxic incubator (0.1% O_2) and all plates incubated for a further 48 hours. A 10 mM ethanolic solution of 5(6)-carboxy-2',7'-dichlorodihydrofluorescein diacetate (carboxy-H_2DCFDA, Invitrogen) was freshly prepared and dissolved in PBS (pre-warmed to 37 ºC) at a final concentration of 10 µM. The media was aspirated from the cells and replaced with the diluted carboxy-H_2DCFDA solution (3 mL) and incubated at 37 ºC for 30 minutes. The solution was then aspirated from the cells and replaced with media (3 mL, pre-warmed to 37 ºC; MCF-7/U87: DMEM; PC3: RPMI) and incubated at 37 ºC for a further 30 minutes. The media was aspirated and the cells washed with PBS (3 mL), before adding 1x trypsin-EDTA (3 mL) and incubating at 37 ºC for 5 minutes. PBS (1 mL) was added to each well and the cell suspension transferred to a fluorescence activated cell sorting (FACS) tube, then centrifuged (Beckmann Coulter Allegra 6R Centrifuge, 1200 rpm, 5 minutes), before aspirating the supernatant and re-suspending in PBS (500 µL) and propidium iodide (aq) (5 µL, 1 mg/mL). All incubations were performed in the absence of light and for hypoxic samples, all steps prior to centrifugation were performed in the hypoxic incubator, using pre-equilibrated PBS and media. Approximately 50,000 cells per sample were analysed for ROS content using flow cytometry (CyAn^{TM} ADP Analyser, Beckman Coulter); unstained cells were used to account for background fluorescence and the final values were normalised to scramble (normoxia).

2.8: Lipid Droplet Assay

MCF-7, U87 and PC3 cells were transfected with siRNA in 10 cm dishes (500,000 cells per dish), according to the standard protocol, to provide a scramble control, PFKFB3 knockdown, PFKFB4 knockdown and a double PFKFB3/PFKFB4 knockdown. 2 identical plates for each condition were set up and incubated overnight at 37 ºC. The media was then aspirated and

replaced with 15 mL fresh media (MCF-7/U87: DMEM; PC3: RPMI), before transferring half of the plates to the hypoxic incubator (0.1% O_2). Plates were incubated for a further 48 hours, the media was aspirated and PBS-EDTA (5 mL) added to each plate and incubated at RT for 5 min. The cell suspension was collected in a 15 mL falcon tube and centrifuged (Beckmann Coulter Allegra 6R Centrifuge, 1500 rpm, 5 minutes), washed twice with PBS, fixed with paraformaldehyde (4%, 1 mL, 30 minutes, RT) and washed with PBS (3 x 10 mL). Centrifugation (Beckmann Coulter Allegra 6R Centrifuge, 1500 rpm, 5 minutes) was performed after each wash step in the protocol. LD540 (Spandl, White et al. 2009) stock was diluted 1:10,000 in PBS and each cell pellet was suspended in diluted LD540 solution (500 µL) and incubated at RT for 5 minutes in the absence of light. PBS (10 mL) was added, then centrifuged (Beckmann Coulter Allegra 6R Centrifuge, 1500 rpm, 5 minutes), and the pellet washed and re-suspended twice with PBS, before resolving the final pellet in PBS (500 µL). Approximately 50,000 cells per sample were analysed for lipid droplet content using flow cytometry (CyAn^{TM} ADP Analyser, Beckman Coulter). Unstained cells were used to account for background fluorescence and the final values were normalised to scramble (normoxia).

2.9: BODIPY-C16 Assay

MCF-7, U87 and PC3 cells were transfected with siRNA in 10 cm dishes (500,000 cells per dish), according to the standard protocol, to provide a scramble control, PFKFB3 knockdown, PFKFB4 knockdown and a double PFKFB3/PFKFB4 knockdown. 2 identical plates for each condition were set up and incubated overnight at 37 ºC. The media was then aspirated and replaced with 15 mL fresh media (MCF-7/U87: DMEM; PC3: RPMI), before transferring half of the plates to the hypoxic incubator (0.1% O_2). Plates were incubated for a further 48 hours, the media was aspirated and pre-warmed (37 ºC) BODIPY-C16 solution added (20 nM in 0.1% fatty acid free bovine serum albumin/PBS, 5 mL) to each plate. Plates were then

incubated in the dark for 15 minutes at 37 ºC, before removal of the BODIPY-C16 solution, washing with PBS (5 mL) and trypsinising the cells (1 mL, 5 min). Media was added (5 mL) and the cell suspensions transferred to 15 mL falcon tubes and centrifuged (Beckmann Coulter Allegra 6R Centrifuge, 1500 rpm, 5 minutes). Media changes and trypsinising cells from the hypoxic plates were performed in the hypoxic incubator with pre-equilibrated solutions. The cell pellets were washed and re-suspended with PBS (2 x 10 mL), before being fixed with paraformaldehyde (4%, 1 mL, 30 minutes, RT) and further washed with PBS (2 x 10 mL), being centrifuged after each wash (Beckmann Coulter Allegra 6R Centrifuge, 1500 rpm, 5 minutes). The pellets were re-suspended in PBS (500 µL), transferred to a FACS tube and approximately 50,000 cells assayed for BODIPY-C16 content using flow cytometry (CyAn^{TM} ADP Analyser, Beckman Coulter). Unstained cells were used to account for background fluorescence and the final values were normalised to scramble (normoxia).

2.10: Quantitative NMR Flux Analysis

2.10.1: Media Preparation

2-^{13}C glucose-DMEM	
Component	**Mass/Volume**
DMEM powder (Sigma, D5030)	8.3 g
Phenol red	15 mg
Sodium bicarbonate	3.7 g
Sodium pyruvate	110 mg
2-^{13}C glucose (Omicon Biochemicals)	4.5 g
Glutamine (200 mM)	20 mL
Milli-Q water	Make above up to 1 L total volume
Penicillin Streptomycin	11 mL
FBS	112 mL

Table 2.6: 2-^{13}C glucose-DMEM media components.

2-^{13}C glucose-RPMI	
Component	**Mass/Volume**
RPMI-1640 powder (Sigma, R1383)	8.4 g
Sodium bicarbonate	2.0 g
2-^{13}C glucose (Omicon Biochemicals)	2.0 g
Milli-Q water	Make above up to 1 L total volume
Penicillin Streptomycin	11 mL
FBS	112 mL

Table 2.7: 2-^{13}C glucose-RPMI media components.

2-^{13}C glucose-DMEM and 2-^{13}C glucose-RMPI media were prepared using the components listed in Table 2.6 and Table 2.7, before immediately passing through a sterile 0.22 µM filter.

2.10.2: Assay Procedure

MCF-7, U87 and PC3 cells were transfected with siRNA in 10 cm dishes (750,000 cells per dish), according to the standard protocol, to provide a scramble Control, PFKFB3 knockdown, PFKFB4 knockdown and a double PFKFB3/PFKFB4 knockdown. Four identical plates for each condition were set up and incubated overnight at 37 ºC. The media was then aspirated and replaced with 15 mL fresh media (MCF-7/U87: DMEM; PC3: RPMI), before transferring half of the plates to the hypoxic incubator (0.1% O_2). Plates were incubated for a further 24 hours, before aspirating the media (within the hypoxic chamber for the hypoxic samples), and replacing with 2-^{13}C glucose-containing media (8 mL, MCF-7/U87: DMEM; PC3: RPMI). The plates were incubated for a further 24 hours, after which time, the media was collected and transferred to a 30 mL Universal tube and sodium azide (2 mg) added in a fume hood. Samples were stored at -20 ºC before processing. Samples were purified to remove amino acids using a Dowex® 50W X8 resin (hydrogen form, strongly acidic, 200-400 mesh, Sigma Aldrich). Dry resin (500 mg) was loaded in a glass column and washed sequentially with water (3 x 20 mL), methanol (20 mL), water (20 mL), HCl (aq) (1 M, 20

mL), water (20 mL) and NH_4OH (aq) (1 M, 20 mL). This process was repeated, but prior to addition of NH_4OH (aq), the media samples were loaded on the column and allowed to filter under gravity into a 50 mL Falcon tube, before eluting with water (30 mL) under gravity filtration. The column was then washed with NH_4OH (aq) (1 M, 20 mL), and reactivated as detailed above. The combined column fractions were stored at -20 ºC, freeze-dried, and dissolved in D_2O (800 µL). The samples were vortexed (2 minutes) and the suspension passed through a 0.45 µM syringe filter to remove solids. 180 µL of this solution was transferred to an NMR tube (3 mm x 178 mm, sample vault tube, GPE Scientific Ltd.) and stored at 4 ºC, prior to running the spectra. NMR samples were run by Dr Tim Claridge (Chemistry Research Laboratory, University of Oxford) at 25 ºC on a Bruker AVIII 700 fitted with a 5 mm TCI cryoprobe. The proton observed carbon edited (POCE) spectra were obtained using parameters adapted from those published by Enthart and colleagues (Enthart, Freudenberger et al. 2008) and are a one dimensional variant of the CLIP-HSQC experiment. Advice on optimisation of the NMR technique was provided by Dr Nicola Sibson (Gray Institute for Radiation, Oncology and Biology, University of Oxford), Dr Sébastien Serres (Sibson Group) and Dr Tim Claridge. Analysis and processing of spectra was performed by the author using ACDLABS12.0 and TopSpin 3.1 (Bruker).

2.11: Quantitative Mass Spectrometry Assay

2.11.1: Cell Extraction

U87 cells were transfected with siRNA in 10 cm dishes (500,000 cells per dish), according to the standard protocol, to provide a scramble Control, PFKFB3 knockdown, PFKFB4 knockdown and a double PFKFB3/PFKFB4 knockdown. 8 identical plates for each condition were set up and incubated overnight at 37 ºC. The media was then aspirated and replaced with 15 mL fresh media (DMEM), before transferring half of the plates to the hypoxic incubator

(0.1% O_2). Plates were incubated for a further 48 hours, the media was aspirated and one set of plates counted. The remaining set (3 per condition) was treated with MeOH:H_2O (4:1, 666 µL), containing 0.5 mM fumaric acid-2,3-d_2 standard, and then scraped with a cell scraper. The extracts were then combined and transferred to a 2 mL eppendorf tube. After centrifuging (Spectrafuge 16M Microcentrifuge, 14000 rpm, 0 ºC, 5 minutes), the supernatant was transferred to a new tube and stored on dry ice, before freeze-drying and dissolving in distilled water (100 µL per sample) immediately prior to analysis. Analysis of the cell extracts using a triple quadrupole mass spectrometer (LC-MS) and optimisation of the corresponding protocol were performed by Khalid Al-Qahtani in Dr James McCullagh's research group in the Chemistry Research Laboratory, University of Oxford. In brief, a C18-pentafluorophenyl (PFP) column (2.1 x 250 mm ACE®) was used. The following eluents were used: solvent A (H_2O, 10mM tributylamine with 15 mM acetic acid (v/v)); solvent B (CH_3CN, 0.1% formic acid (v/v)). The gradient elution was as follows: 0–1 min (isocratic 5% B), 1–8 min (linear from 0% to 45% B), 8–9 min (isocratic 35% B), 9–17 min (linear from 35% to 0% B), 17-20 min (100% A for column equilibration). A constant flow rate at 0.2 mL/min was used. Sample injection was performed using partial-loop with needle overfill (loop size: 10 µL) mode; the sample injection volume used was 5 µL. A cone voltage of 60 V and a capillary voltage of 3.0 kV were used in negative ionisation mode. The de-solvation temperature was set to 190 °C and the source temperature to 120 °C.

2.11.2: Metabolite Standards

All metabolites standards used in the mass spectrometry assay were from Sigma Aldrich.

2.12: Kinase Assay Development

2.12.1: PFK-1 Kinase Glo® Plus assay

Fructose-6-phosphate Kinase (PFK-1) from *Bacillus stearothermophilus* (F0137) and all other assay components were purchased from Sigma Aldrich. The plate-reader used was BMG LABTECH FLUOstar Omega multi-mode microplate reader. The plates used were solid white, polystyrene, half area, 96 well plates (0.19 mL) from Corning. All reagents were equilibrated to RT before use and the assay was run at RT, to avoid temperature gradients across the plate. The assay was optimised using a protocol developed from the procedure reported in the "Handbook of Assay Development in Drug Discovery" (Minor 2010). A Z factor of 0.89 was calculated using the assay components and conditions detailed in Table 2.8 (final volume of 20 µL). All solutions were diluted with HEPES (0.5 M).

Component	Stock Conc.	Final Conc.	Final Volume
PFK-1	3.51 units/Ml	0.0063 units/mL	1.78 µL
ATP	125 µM	12.5 µM	2.00 µL
F-6-P	1.25 mM	125 µM	2.00 µL
HEPES (0.5 M)			11.82 µL
$MgCl_2$	100 mM	10 mM	2.00 µL
DMSO (+/- inhibitor)			0.40 µL
		Total	20 µL

Table 2.8: Final optimised component concentrations for the Kinase Glo® Plus assay.

The reaction was started by the addition of ATP (125 µM, 2.00 µL per well), then mixed on a plate shaker and incubated for 10 minutes at RT. Kinase Glo® Plus reagent (20 µL), prepared according to the manufacturer's instructions, was added to each well, then mixed on a plate shaker and incubated for 10 minutes at RT. The plate was then transferred to the plate reader and the end-point luminescence signal recorded using Soft Max Pro™ software. The assay was conducted in triplicate, with the mean value reported for each set being recorded.

Controls with no ATP and no PFK were also included in each experiment. Background luminescence (no ATP control) was removed from sample luminescence values, which were then reported as relative luminescence units (RLU). Percentage inhibition was calculated from the difference between the RLU value of the +PFK control and the RLU value of the test well, divided by the difference between the +PFK and –PFK controls. Inhibitors were added dissolved in DMSO.

2.12.2: PFKFB3 Kinase Glo® Plus assay

Human recombinant PFKFB3 was purchased from Abnova (H00005209-P01) and was tested for kinase activity in the Kinase Glo® assay using the same optimisation protocol developed from the procedure reported in the "Handbook of Assay Development in Drug Discovery" (Minor 2010).

2.12.3: PFKFB3 Thermal Shift Assay

PFKFB3 was buffered in 10 mM HEPES, 500 mM NaCl solution and assayed in a 96 well plate at a final concentration of 0.2 µM. SYPRO-Orange fluorescent probe was added at a dilution of 1:1000 (total volume 20 µL per well). Reactions were performed in triplicate, with an additional control triplicate with [PFKFB3] = 0 µM. Dimethylsulphoxide (DMSO) (0.4 µL per well) was added and the plate was then sealed with a Thermo-Seal (Fischer Scientific) and centrifuged (Beckmann Coulter Allegra 6R Centrifuge 1000 rpm, 1 minute). The thermal melting experiment was performed using a high temperature fluorescent microplate reader (FluoDia T70, Photon Tech. Int.) and excitation and emission filters were set to 465 and 590 nm, respectively. The temperature was then increased in 1 ºC increments per 90 seconds, from 20 ºC to 90 ºC, and the fluorescence signal recorded. Helen Storr (Russell laboratory) is gratefully acknowledged for advice given on running the assay. Dr Oleg Fedorov at the

Structural Genomics Consortium is also gratefully acknowledged for permitting use of the microplate reader.

2.13: Statistical Analysis

Data analysis and graph production was performed using GraphPad Prism® software (version 5.04). The unpaired, two-tailed Student's t-test or ANOVA, as appropriate, were used to test for statistical significance, with a confidence interval of >95%. The level of statistical significance is denoted throughout, using the following notation: * $p < 0.05$; ** $p < 0.01$; *** $p < 0.001$; **** $p < 0.0001$. Unless otherwise stated, data shown are the mean of three independent biological replicates, with error reported as standard error of the mean (SEM).

2.14: Chemistry

2.14.1: General Experimental

NMR spectra: Proton (^{1}H), carbon (^{13}C), fluorine (^{19}F) and phosphorous (^{31}P) NMR spectra were recorded on a Bruker AV 400 (400/100/376/162 MHz) and a Bruker AV 500 (500/125 MHz) spectrometer at 298 K in $CDCl_3$, d^3-MeOD, d^6-DMSO and D_2O solutions. Chemical shifts (δ_H, δ_C, δ_F, δ_P) are quoted in ppm (parts per million) downfield of tetramethylsilane, with residual protonated solvent as internal standard. Assignments were made on the basis of chemical shifts, coupling constants, COSY, DEPT, HMQC, HMBC data and comparison with spectra of related compounds. Resonances are described as s (singlet), d (doublet), t (triplet), q (quartet), app (apparent), m (multiplet), br (broad) and obs. (obscured). Coupling constants (*J*) are given in Hz, rounded to the nearest 0.1 Hz. H, H' and H'' refer to diastereotopic protons attached to the same carbon and imply no particular stereochemistry.

Mass spectra: Low resolution mass spectra were recorded on a Fisons Platform spectrometer (ESI). High resolution mass spectra were recorded by the mass spectrometry department of the Chemistry Research Laboratory using a Bruker Daltronics microTOF spectrometer (ESI). Mass-to-charge ratio (*m/z*) values are reported in Da with their percentage abundances and, where known, the relevant fragment ion in parenthesis. High resolution values are calculated to four decimal places from the molecular formula, all found values being within a tolerance of 5 ppm.

Infrared spectra: Infrared spectra were recorded on a Bruker Tensor 27 Fourier Transform spectrometer as either a thin film between NaCl plates (film) or as a KBr disc (KBr), as stated. Absorption maxima (ν_{max}) are described as s (strong), m (medium), w (weak) and br (broad) and selected characteristic peaks are quoted in wavenumbers (cm^{-1}).

Melting points: Melting points were determined using a Griffin heated metal block apparatus and are uncorrected.

Optical rotations: Optical rotations were recorded on a Perkin-Elmer 241 polarimeter with a water-jacketed 10 cm cell. Specific rotations are reported in 10^{-1} deg cm^2 g^{-1} and concentrations in g/100 mL.

Chromatography techniques: Thin layer chromatography (TLC) was performed on aluminium plates coated with VWR® 60 F_{254} silica. Plates were visualised by the quenching of UV fluorescence (λ_{max} = 254 nm) or staining with 1% $KMnO_{4(aq)}$, followed by heating. Flash chromatography was performed on Kieselgel 60 silica (Macherey-Nagel®) and DEAE-Sephadex® (Sigma-Aldrich) for polyol phosphates, with the solvent system used recorded in parenthesis.

Solvents and reagents: Solvents and commercially available reagents were dried and purified before use, or used as supplied (analytical or HPLC grade), as appropriate. CH_2Cl_2, THF and toluene were obtained dry and oxygen-free from Grubb solvent dispenser units. "Petrol" refers to the fraction of petroleum ether boiling in the range 30 ºC to 40 ºC. Water was purified by an Elix® UV-10 system.

Other reaction details: All reactions involving moisture or air-sensitive reagents were carried out under a nitrogen atmosphere, using glassware that had been oven-dried and cooled under nitrogen before use.

2.14.2: Synthesis

References in parenthesis indicate the original report of procedures utilised for each synthesis. Molecular structures illustrated indicate the final reaction product.

1.1.1.1: (E)- 3-(3-pyridinyl)-1-(4-pyridinyl)-2-propen-1-one (2)

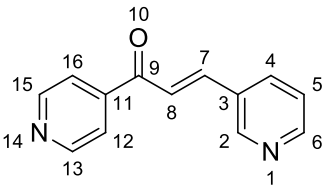

Triphenylphosphine (polymer bound, 200 mg, 1.6 mmol/g) was suspended in toluene (2 mL) and 4-bromoacetylpyridine hydrobromide (90 mg, 0.32 mmol) added, followed by dropwise addition of freshly distilled triethylamine (90 µL, 0.64 mmol). The reaction mixture was stirred overnight at RT, then filtered, and the resin washed with EtOAc (15 mL), EtOH (15 mL) and Et_2O (15 mL). The resin was suspended in chloroform (0.75 mL) and 3-pyridine carboxaldehyde (15 µL, 0.16 mmol) added, followed by stirring at RT for 48 h. The resin was then collected by filtration and washed with CH_2Cl_2 (30 mL). The filtrate and washings were combined and the solvent removed *in vacuo* to afford a white solid, which was redissolved in MeOH (10 mL), before addition of Amberlite® IRA-402 (1 g). The resulting suspension was stirred at RT for 1 h, then the resin was removed by filtration, and the solvent removed *in*

vacuo, to afford the title compound as a colourless oil (11 mg, 33%). δ_H ($CDCl_3$, 500 MHz) 8.87 (3H, m, ArCH-2, ArCH-13 and ArCH-15), 8.68 (1H, app. br. s., ArCH-6), 7.97 (1H, dt, *J* = 7.8 Hz, 1.6 Hz, ArCH-4), 7.84 (1H, d, *J* = 16.0 Hz, CH-8), 7.79 (2H, d, *J* = 7.8 Hz, ArCH-12 and ArCH-16), 7.51 (1H, d, *J* = 16.0 Hz, CH-7), 7.40 (1H, dd, *J* = 7.8 Hz, 4.9 Hz, ArCH-5); δ_C ($CDCl_3$, 125 MHz) 189.2 (C=O), 151.7 (ArCH-4), 150.9 (ArCH-13 and ArCH-15), 150.2 (ArCH-2), 143.8 (ArC-11), 142.9 (CH-8), 134.7 (ArCH-6), 130.1 (ArC-3), 123.9 (ArCH-5), 122.8 (CH-7), 121.5 (ArCH-12 and ArCH-16); *m/z* (ESI^+) 211 ($[M+H]^+$, 48%), 260 (100%); HRMS (ESI^+) Calc. for $C_{13}H_{11}N_2O$: 211.0866. Found: 211.0864.

1.1.1.2: ((1S,2S,3R,4S,6S)-4-Hydroxy-2,6-di(pyridin-3-yl)-4-(pyridin-4-yl)cyclohexane-1,3-diyl)bis(pyridin-4-ylmethanone) (5)

(Zhang, Dong et al. 2003; Vatsadze, Nuriev et al. 2004)

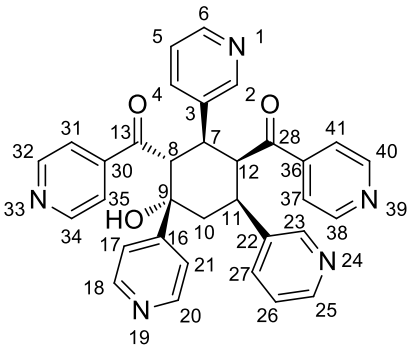

4-Acetyl pyridine (0.13 g, 1.05 mmol) and 3-pyridine carboxaldehyde (0.11 g, 1.00 mmol) were suspended in water (15 mL) and stirred at 70 °C in a pre-heated oil bath. A solution of sodium carbonate (26.5 mg, 0.25 mmol) in water (5 mL) was added to the reaction mixture and stirring continued at 70 °C for 1 h. After cooling to RT, the white precipitate that had formed was collected by filtration, then washed with water (20 mL) and Et_2O (30 mL) to afford the title compound as a white powder (0.19 g, 54%). The spectroscopic data were in agreement with the literature (Vatsadze, Nuriev et al. 2004). δ_H (d^6-DMSO, 500 MHz) 8.59 (1H, d, *J* = 1.9 Hz, ArCH-23), 8.52 (1H, d, *J* = 1.9 Hz, ArCH-2), 8.43-8.39 (4H, m, ArCH-32, ArCH-34, ArCH-38 and ArCH-40), 8.31 (2H, d, *J* = 5.8 Hz, ArCH-18 and ArCH-20), 8.20 (1H, dd, *J* = 4.7 Hz, 1.6 Hz, ArCH-6), 8.10 (1H, dd, *J* = 4.6 Hz, 1.6 Hz, ArCH-25), 7.63 (1H, d, *J* = 7.9 Hz, ArCH-4), 7.60 (1H, d, *J* = 8.1 Hz, ArCH-27), 7.55 (2H, d, *J* = 5.8 Hz, ArCH-17 and ArCH-21),

7.31-7.28 (2H, m, ArCH-31 and ArCH-35), 7.09 (1H, dd, *J* = 7.9 Hz, 4.7 Hz, ArCH-5), 7.06-7.03 (2H, m, ArCH-37 and ArCH-41), 6.99 (1H, dd, *J* = 8.1 Hz, 4.6 Hz, ArCH-26), 5.87 (1H, bs, OH), 5.16 (1H, d, *J* = 12.0 Hz, CH-8), 4.85 (1H, t, *J* = 4.8 Hz, CH-12), 4.49 (1H, dd, *J* = 12.0 Hz, 4.8 Hz, CH-7), 4.13-4.07 (1H, m, CH-11), 3.35 (1H, obs. m, CH-10), 1.89 (1H, dd, *J* = 13.4 Hz, 3.2 Hz, CH-10'); δ_C (d^6-DMSO, 125 MHz) 204.7 (C=O-28), 199.6 (C=O-13), 155.2 (ArC-16), 150.3 (ArCH-38 and ArCH-40), 150.0 (ArCH), 149.3 (ArCH), 149.3 (ArCH), 149.2 (ArCH-23), 147.9 (ArCH), 147.8 (ArCH), 144.5 (ArC-30), 143.7 (ArC-36), 136.6 (ArC), 136.5 (ArC), 134.7 (ArCH-27), 123.2 (ArCH-5 and ArCH-26), 120.8 (ArCH-17 and ArCH-21), 120.6 (ArCH-31 and ArCH-35), 120.0 (ArCH-37 and ArCH-41), 74.1 (COH-9), 51.1 (CH-8), 50.8 (CH-12), 41.2 (CH-7), 37.4 (CH-11), 37.2 (CH-10 and CH-10'); *m/z* (ESI^-) 540 ($[M-H]^-$, 34%), 576 (100%).

1.1.1.3: (E)-1-Phenyl-3-(pyridin-3-yl)prop-2-en-1-one (6)

(Westman 2001)

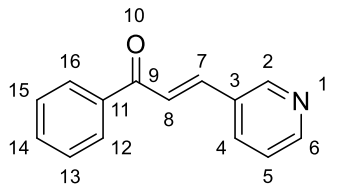

Acetophenone (0.93 mL, 8.00 mmol), 1,8-diazabicyclo[5.4.0]undec-7-ene (1.20 mL, 8.00 mmol) and 3-pyridine carboxaldehyde (1.50 mL, 16.0 mmol) were dissolved in THF (20 mL) and the mixture stirred at RT for 24 h. The solvent was evaporated *in vacuo* and Et_2O (20 mL) added. Evaporation of half of the solvent led initially to the formation of a precipitate and further precipitation was facilitated by addition of EtOH (1 mL). The flask was then stored at 4 °C for 24 h and the precipitate collected by filtration and washed with cold EtOH (10 mL) and Et_2O (20 mL), to afford the title compound as a yellow, crystalline solid (0.31 g, 75%). The spectroscopic data were consistent with the literature (Westman 2001). mp 95-97 °C; ν_{max} (KBr)/cm^{-1} 3085 (w), 3061 (m), 3038 (m), 1661 (s), 1604 (s), 1580 (s), 1565 (s), 1475 (s), 1447 (s), 1424 (m), 1338 (s), 1310 (s), 1221 (s), 1183 (m), 1122 (w), 1098 (w),

1043 (w), 1015 (s), 982 (s); δ_H (d^6-DMSO, 400 MHz) 9.02 (1H, d, *J* = 1.8 Hz, ArCH-2), 8.61 (1H, dd, *J* = 4.8 Hz, 1.3 Hz, ArCH-6), 8.33 (1H, d, *J* = 8.0 Hz, ArCH-4), 8.17 (2H, d, *J* = 7.3 Hz, ArCH-12 and ArCH-16), 8.06 (1H, d, *J* = 15.8 Hz, CH-8), 7.77 (1H, d, *J* = 15.8 Hz, CH-7), 7.68-7.62 (1H, m, ArCH-14), 7.59-7.52 (2H, m, ArCH-13 and ArCH-15), 7.46 (1H, dd, *J* = 8.0 Hz, 4.8 Hz, ArCH-5); δ_C (d^6-DMSO, 100 MHz) 188.9 (C=O), 151.0 (ArCH-6), 150.3 (ArCH-2), 140.5 (CH-7), 137.3 (ArC-11), 135.1 (ArCH-4), 133.3 (ArCH-14), 130.5 (ArC-3), 128.8 (ArCH-13 and ArCH-15), 128.6 (ArCH-12 and ArCH-16), 123.8 (CH-8 and ArCH-5); *m/z* (ESI^+) 210 ($[M+H]^+$, 10%), 232 ($[M+Na]^+$, 52%), 441 ($[2M+Na]^+$, 100%).

1.1.1.4: (E)-2,3-Dichloro-N-methoxy-N-methyl-3-(pyridin-3-yl)acrylamide (10)

(Kolly-Kovac and Renaud 2005)

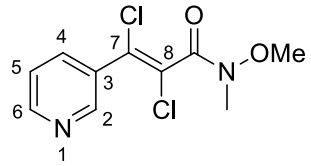

trans-3-(3-Pyridyl)-acrylic acid (1.00 g, 6.70 mmol) was suspended in thionyl chloride (6 mL) and heated at reflux for 4 h. The solvent was removed *in vacuo* and the resultant oil dissolved in anhydrous CH_2Cl_2 (70 mL) and *N*,*O*-dimethyl hydroxylamine hydrochloride (0.72 g, 7.39 mmol) added. The mixture was cooled to 0 °C and freshly distilled triethylamine (3.0 mL, 21.4 mmol) was added dropwise. After complete addition of triethylamine, the reaction mixture was stirred for 2 h at 0 °C and 1 h at RT. The solid triethylamine hydrochloride was filtered off and washed with CH_2Cl_2, then the filtrate and washings were combined and the solvent removed *in vacuo*. After partitioning the crude product between CH_2Cl_2/Et_2O (1:1, 50 mL) and brine (20 mL), the aqueous layer was extracted with CH_2Cl_2/Et_2O (1:1, 2 x 30 mL). The combined organic layers were washed with saturated aqueous $NaHCO_3$ solution (25 mL) and brine (25 mL), then dried over Na_2SO_4. The solvent was removed *in vacuo* and purification *via* column chromatography (SiO_2, EtOAc/petrol, 2:1) afforded the title compound as a yellow oil (0.63 g, 36%). Full analytical data were obtained. ν_{max} (film)/cm^{-1} 2940 (w), 1661 (s), 1584 (w),

1413 (m), 1385 (m), 1192 (w), 1128 (w), 1034 (w), 980 (w), 920 (w); δ_H ($CDCl_3$, 400 MHz) 8.67 (1H, s, ArCH-2), 8.59 (1H, d, *J* = 4.7 Hz, ArCH-6), 7.79 (1H, d, *J* = 7.7 Hz, ArCH-4), 7.31 (1H, dd, *J* = 7.7 Hz, 4.7 Hz, ArCH-5), 3.68 (3H, s, OCH_3), 3.08 (3H, s, NCH_3); δ_C ($CDCl_3$, 100 MHz) 163.7 (C=O), 150.5 (ArCH-6), 148.6 (ArCH-2), 135.9 (ArCH-4), 132.8 (CCl-8), 132.0 (ArC-3), 130.7 (CCl-7), 123.2 (ArCH-5), 62.0 (OCH_3), 32.4 (NCH_3); *m/z* (ESI^+) 261 ($[M+H]^+$, 11%), 283 ($[M+Na]^+$, 64%), 543 ($[2M+Na]^+$, 84%), 545 (100%); HRMS (ESI^+) Calc. for $C_{10}H_{10}Cl_2N_2NaO_2$: 283.0012. Found: 283.0002.

1.1.1.5: (Z)-2-Chloro-N-methoxy-N-methyl-3-(pyridin-4-yl)but-2-enamide (11)

(Kolly-Kovac and Renaud 2005)

trans-3-(4-Pyridyl)-acrylic acid (0.20 g, 1.34 mmol) was suspended in thionyl chloride (4 mL) and heated at reflux for 4 h. The solvent was removed *in vacuo* and the resultant oil dissolved in anhydrous CH_2Cl_2 (8 mL) before addition of *N,O*-dimethyl hydroxylamine hydrochloride (0.14 g, 1.48 mmol). The mixture was cooled to 0 °C and freshly distilled triethylamine (0.60 mL, 4.29 mmol) added dropwise; the reaction mixture was then stirred for 2 h at 0 °C and 1 h at RT. The solid triethylamine hydrochloride was filtered off and washed with CH_2Cl_2, then the filtrate and washings were combined and the solvent removed *in vacuo*. The crude product was partitioned between CH_2Cl_2/Et_2O (1:1, 20 mL) and brine (10 mL), and the aqueous layer extracted with CH_2Cl_2/Et_2O (1:1, 2 x 20 mL). The combined organic layers were washed with saturated aqueous $NaHCO_3$ solution (10 mL) and brine (10 mL), then dried over Na_2SO_4. Removal of the solvent *in vacuo*, followed by purification *via* column chromatography (SiO_2, EtOAc/petrol, 2:1), afforded the title compound as a yellow oil (0.10 g, 29%). ν_{max} (film)/cm^{-1} 2979 (w), 2940 (w), 1661 (s), 1548 (m), 1408 (m), 1386 (m), 1184 (w), 1038 (w), 983 (w), 930 (w); δ_H ($CDCl_3$, 400 MHz) 8.63 (2H, d, *J* = 4.7 Hz, ArCH-2 and ArCH-6), 7.37 (2H, d, *J*

= 4.7 Hz, ArCH-3 and ArCH-5), 3.65 (3H, s, OCH_3), 3.10 (3H, s, NCH_3); δ_C ($CDCl_3$, 100 MHz) 163.5 (C=O), 150.1 (ArCH-2 and ArCH-6), 143.1 (ArC-4), 131.0 (CCl-7), 124.3 (CCl-8), 122.2 (ArCH-3 and ArCH-5), 62.0 (OCH_3), 32.5 (NCH_3); *m/z* (ESI^+) 261 ($[M+H]^+$, 75%), 283 ($[M+Na]^+$, 100%); HRMS (ESI^+) Calc. for $C_{10}H_{11}Cl_2N_2O_2$: 261.0192. Found: 261.0194.

1.1.1.6: N-Methoxy-N-methylcinnamamide (12)

(Kolly-Kovac and Renaud 2005)

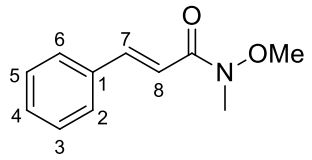

trans-Cinnamic acid (0.50 g, 3.38 mmol) was suspended in thionyl chloride (10 mL) and heated at reflux for 4 h. The solvent was removed *in vacuo* and the resultant oil dissolved in CH_2Cl_2 (20 mL) and *N,O*-dimethyl hydroxylamine hydrochloride (0.36 g, 3.71 mmol) added. The mixture was cooled to 0 °C and freshly distilled triethylamine (1.51 mL, 10.8 mmol) added dropwise. After complete addition of triethylamine, the reaction mixture was stirred for 2 h at 0 °C and 1 h at RT. The solid triethylamine hydrochloride was filtered off and washed with CH_2Cl_2, then the filtrate and washings were combined and the solvent removed *in vacuo*. The crude product was partitioned between CH_2Cl_2/Et_2O (1:1, 40 mL) and brine (20 mL), and the aqueous layer extracted with CH_2Cl_2/Et_2O (1:1, 2 x 30 mL). The combined organic layers were washed with saturated aqueous $NaHCO_3$ solution (10 mL) and brine (10 mL) and dried over Na_2SO_4. Following removal of the solvent *in vacuo*, purification *via* column chromatography (SiO_2, EtOAc/petrol, 2:1) afforded the title compound as a colourless, crystalline solid, in moderate yield (0.27 g, 42%). The spectroscopic data were in agreement with the literature (Niu, Zhang et al. 2009). δ_H ($CDCl_3$, 400 MHz) 7.74 (1H, d, *J* = 15.8 Hz, CH-7), 7.58 (2H, d, *J* = 6.6 Hz, CH-2 and CH-6), 7.45-7.33 (3H, m, CH-3, CH-4 and CH-5), 7.04 (1H, d, *J* = 15.8 Hz, CH-8), 3.77 (3H, s, OCH_3), 3.32 (3H, s, NCH_3); δ_C ($CDCl_3$, 100 MHz) 167.0 (C=O), 143.5 (CH-7), 135.2 (ArC-1), 129.8 (ArCH-4), 128.8 (ArCH-3 and ArCH-5), 128.1 (ArCH-2 and ArCH-6),

115.8 (CH-8), 61.9 (OCH_3), 32.5 (NCH_3); *m/z* (ESI^+) 192 ($[M+H]^+$, 22%), 214 ($[M+Na]^+$, 56%), 405 ($[2M+Na]^+$, 100%).

1.1.1.7: (E)-Perfluorophenyl 3-(pyridin-3-yl)acrylate (13)

(Brown, Bataille et al. 2002)

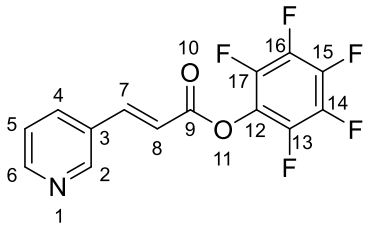

To a solution of *trans*-3-(3-pyridyl)-acrylic acid (300 mg, 2.01 mmol) and pentafluorophenol (389 mg, 2.11 mmol) in EtOAc (10 mL), a solution of *N*,*N*′-dicyclohexylcarbodiimide (440 mg, 2.13 mmol) in EtOAc (10 mL) was added dropwise, and the reaction stirred for 18 h at RT. The mixture was diluted with hexane (20 mL) and the solids removed by filtration. The filtrate was then washed with saturated aqueous $NaHCO_3$ solution (15 mL), dried over Na_2SO_4, and concentrated *in vacuo*. Purification *via* column chromatography (SiO_2, EtOAc/petrol, 2:1) afforded the title compound as a colourless powder (487 mg, 77%). mp 123-127 °C; ν_{max} (KBr)/cm^{-1} 2925 (w), 1749 (m), 1632 (m), 1521 (s), 1417 (m), 1320 (w), 1295 (m), 1224 (w), 1121 (s), 1028 (w), 997 (s); δ_H ($CDCl_3$, 400 MHz) 8.84 (1H, d, *J* = 1.3 Hz, ArCH-2), 8.69 (1H, d, *J* = 4.8 Hz, ArCH-6), 8.00-7.91 (2H, m, ArCH-4 and ArCH-7), 7.42 (1H, dd, *J* = 8.0 Hz, 4.8 Hz, ArCH-5), 6.75 (1H, d, *J* = 15.9 Hz, ArCH-8); δ_C ($CDCl_3$, 125 MHz) 162.0 (C=O), 152.0 (ArCH-6), 150.1 (ArCH-2), 145.6 (CH-7), 141.2 (dd, *J* = 251.8 Hz, 12.4 Hz, ArCF-13 and ArCF-17), 139.5 (dtt, *J* = 253.7 Hz, 13.4 Hz, 3.8 Hz, ArCF-15), 137.9 (dt, *J* = 253.7 Hz, 14.3 Hz, ArCF-14 and ArCF-16), 134.6 (ArCH-4), 129.3 (ArC-3), 125.0 (t, *J* = 14.8 Hz, ArC-12), 123.9 (ArCH-5), 116.5 (CH-8); δ_F ($CDCl_3$, 377 MHz) -152.4 (F-13 and F-17), -157.6 (F-15), -162.2 (F-14 and F-16); *m/z* (ESI^+) 316 ($[M+H]^+$, 56%), 471 (100%); HRMS (ESI^+) Calc. for $C_{14}H_7F_5NO_2$: 316.0391. Found: 316.0391.

1.1.1.8: (2R,3R,4R,5R)-2,5-Bis(acetoxymethyl)tetrahydrofuran-3,4-diyl diacetate (19)

(Cassel, Debaig et al. 2001)

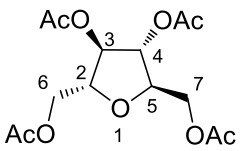

D-Glucosamine hydrochloride (4.00 g, 18.6 mmol) was stirred in water (44 mL) for 20 h at RT, in order to reach mutorotational equilibrium. The solution was cooled to 0 °C and sodium nitrite (4.73 g, 55.7 mmol) added in one portion. Whilst stirring and keeping the temperature below 2 °C, glacial acetic acid (3.2 mL, 55.7 mmol) was added dropwise, to form nitrous acid *in situ*. After an additional 2 h stirring at 0 °C, the temperature was allowed to rise to RT under a flow of nitrogen, in order to remove excess nitrous acid. The solution was then concentrated to dryness and the crude 2,5-anhydro-D-mannose reduced by slow addition of sodium borohydride (2.81 g, 74.2 mmol) in water (40 mL) at 0 °C. The reaction mixture was then allowed to stir for 1 h at RT. The excess sodium borohydride was destroyed by dropwise addition of glacial acetic acid until the evolution of gas had ceased. The solution was then allowed to stir for 1 h at RT to ensure complete decomposition of the sodium borohydride. The solvent was removed *in vacuo* and the residue redissolved and evaporated 3 times with MeOH (90 mL) *in vacuo* to remove methyl borate. For enhanced purification, the crude 2,5-anhydro-D-mannitol was acetylated by treating with pyridine/acetic anhydride (1:1, 50 mL) and the resulting mixture stirred overnight at RT. The solvents were removed *in vacuo*, using toluene to remove the acetic anhydride azeotropically. Water (40 mL) and EtOAc (40 mL) were then added to the residue and the aqueous layer extracted with EtOAc (2 x 40 mL). The organic layers were combined, dried over Na_2SO_4, and the solvents evaporated *in vacuo*, followed by purification *via* column chromatography (SiO_2, petrol/EtOAc, 2:1), to afford the title compound as a colourless oil (4.51 g, 73%). The spectroscopic data were in agreement with the literature (Cassel, Debaig et al. 2001). δ_H ($CDCl_3$, 400 MHz) 5.17 (2H, s, H-3 and H-4), 4.29-4.22 (6H, m, H-2, H-5, H-6, H-6', H-7 and H-7'), 2.12 (12H, s, 4 x CH_3); δ_C ($CDCl_3$, 100 MHz) 170.7 (C=O), 169.9

(C=O), 81.1 (CH-2 and CH-5), 78.1 (CH-3 and CH-4), 63.1 (2 x CH_2), 20.8 (2 x CH_3), 20.8 (2 x CH_3); *m/z* (ESI^+) 333 ($[M+H]^+$, 68%), 687 ($[2M+Na]^+$, 100%).

1.1.1.9: 2,5-Anhydro-D-mannitol (18)

(Cassel, Debaig et al. 2001)

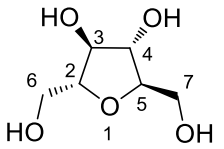

(2*R*,3*R*,4*R*,5*R*)-2,5-*Bis*(acetoxymethyl)tetrahydrofuran-3,4-diyl diacetate (**19**) (1.97 g, 5.93 mmol) was added to a solution of sodium methoxide (1.62 g, 30.0 mmol) in MeOH (30 mL) and stirred for 18 h at RT. Amberlite® IR-120 resin (H^+ form) was then added and the suspension stirred for 1 h at RT, whereupon the solution had become clear. The resin was removed by filtration and the solvent evaporated *in vacuo* to afford the title compound as a colourless oil (0.97 g, 99%). The spectroscopic data were in agreement with the literature (Cassel, Debaig et al. 2001). $[\alpha]_D^{25}$ +48.0 (*c* = 1.0, H_2O); lit ($[\alpha]_D^{20}$ +50.0 (*c* = 1.0, H_2O)); δ_H ($CDCl_3$, 400 MHz) 4.00-3.93 (2H, m, H-3 and H-4), 3.87-3.77 (2H, m, H-2 and H-5), 3.71 (2H, dd, *J* = 11.6 Hz, 3.3 Hz, H-6 and H-7), 3.62 (2H, dd, *J* = 11.6 Hz, 3.3 Hz, H-6' and H-7'); δ_C ($CDCl_3$, 100 MHz) 85.2 (CH-2 and CH-5), 78.9 (CH-3 and CH-4), 63.4 (2 x CH_2); *m/z* (ESI^+) 187 ($[M+Na]^+$, 100%), 329 ($[2M+H]^+$, 11%), 351 ($[2M+Na]^+$, 20%).

1.1.1.10: (2S,3S,4S,5S)-1,6-Dibromohexane-2,3,4,5-tetrayl tetraacetate (22)

(CrombezRobert, Benazza et al. 1997; Schmidt and Nave 2007)

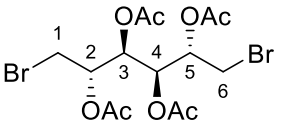

To a suspension of D-mannitol (8.00 g, 43.9 mmol) in anhydrous 1,4-dioxane (72 mL), was slowly added acetyl bromide (7.80 mL, 105.2 mmol) and the reaction mixture left to stir for 72 h at RT, under a nitrogen atmosphere. The solvent was then removed *in vacuo* and the pale yellow residue dissolved in anhydrous pyridine (30 mL), before slow addition of acetic anhydride (30 mL). The reaction was then

left to stir at RT for 18 h. Toluene was added and the off-white precipitate removed by filtration. The solvents were then removed *in vacuo* and the viscous residue kept at 4 °C for 18 h, after which the title compound had precipitated as a white, crystalline solid. The crystals were collected by filtration and washed with petrol to afford the title compound (10.0 g, 48%). The spectroscopic data were in agreement with the literature (CrombezRobert, Benazza et al. 1997; Schmidt and Nave 2007). δ_H (d^6-DMSO, 400 MHz) 5.27 (2H, d, *J* = 7.3 Hz, H-3 and H-4), 5.04 (2H, m, H-2 and H-5), 3.74 (2H, dd, *J* = 11.4 Hz, 3.3 Hz, H-1' and H-6'), 3.56 (2H, dd, *J* = 11.4 Hz, 6.6 Hz, H-1 and H-6), 2.07 (6H, s, CH_3), 2.03 (6H, s, CH_3); δ_C (d^6-DMSO, 100 MHz) 169.5 (C=O), 169.3 (C=O), 68.9 (CH-2 and CH-5), 68.4 (CH-3 and CH-4), 31.7 (2 x CH_2), 20.6 (2 x CH_3), 20.5 (2 x CH_3); *m/z* (ESI^+) 499 ($[M+Na]^+$, 100%).

1.1.1.11: (3R,4R)-Hexa-1,5-diene-3,4-diyl diacetate (23)

(CrombezRobert, Benazza et al. 1997; Schmidt and Nave 2007)

(2*S*,3*S*,4*S*,5*S*)-1,6-Dibromohexane-2,3,4,5-tetrayl tetraacetate (**22**) (5.00 g, 10.5 mmol) was dissolved in glacial acetic acid (60 mL). Sodium acetate

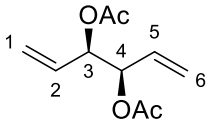

(1.89 g, 23.1 mmol) and zinc dust (2.75 g, 42.0 mmol) were added and the reaction mixture heated to 100 °C until the evolution of gas had ceased, and the solution had become clear (approx. 3 h). After cooling, the zinc was removed by filtration and the filtrate evaporated *in vacuo* to afford a viscous, colourless residue, which was dissolved in water (50 mL) and extracted with Et_2O (3 x 50 mL). The combined organic layers were then washed carefully (vigorous gaseous evolution) with saturated aqueous $NaHCO_3$ solution, dried over $MgSO_4$, filtered, and the solvent removed *in vacuo*. The crude product was purified by flash chromatography (SiO_2, petrol/EtOAc, 10:1) to afford the title compound as a colourless oil (1.69 g, 81%) The spectroscopic data were in agreement with the literature (CrombezRobert, Benazza et al. 1997; Schmidt and Nave 2007). δ_H ($CDCl_3$, 400 MHz) 5.83-5.70 (2H, m, H-2

and H-5), 5.41 (2H, d, J = 5.0 Hz, H-3 and H-4), 5.34 (2H, d, J = 17.2 Hz, H-1_{trans} and H-6_{trans}), 5.29 (2H, d, J = 10.6 Hz, H-1_{cis} and H-6_{cis}), 2.10 (6H, s, CH_3); δ_C ($CDCl_3$, 100 MHz) 169.8 (C=O), 132.0 (CH-2 and CH-5), 119.2 (2 x CH_2), 74.3 (CH-3 and CH-4), 20.9 (2 x CH_3); *m/z* (ESI^+) 221 ($[M+Na]^+$, 100%).

1.1.1.12: (3R,4R)-Hexa-1,5-diene-3,4-diol (24)

(CrombezRobert, Benazza et al. 1997; Schmidt and Nave 2007)

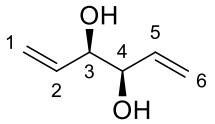

(3*R*,4*R*)-Hexa-1,5-diene-3,4-diyl diacetate (**23**) (1.35 g, 6.81 mmol) was dissolved in a solution of sodium methoxide (1.62 g, 30.0 mmol) in MeOH (30 mL), and stirred for 18 h at RT. Amberlite® IR-120 resin (H^+ form) was then added and the reaction mixture stirred for 1 h at RT. The resin was removed by filtration and the solvent evaporated *in vacuo* to afford the title compound as a colourless oil (0.76 g, 99%). The spectroscopic data were in agreement with the literature (CrombezRobert, Benazza et al. 1997; Schmidt and Nave 2007). δ_H (d^3-MeOD, 400 MHz) 5.94-5.82 (2H, m, H-2 and H-5), 5.29 (2H, d, J = 17.4 Hz, H-1_{trans} and H-6_{trans}), 5.16 (2H, d, J = 10.6 Hz, H-1_{cis} and H-6_{cis}), 3.98-3.92 (2H, m, H-3 and H-4); δ_C (d^3-MeOD, 100 MHz) 138.8 (CH-2 and CH-4), 116.9 (2 x CH_2), 77.1 (CH-3 and CH-4); *m/z* (ESI^-) 113 ($[M-H]^-$, 55%), 255 (100%).

1.1.1.13: (((3R,4R)-Hexa-1,5-diene-3,4-diylbis(oxy))bis(methylene))dibenzene (25)

(Kufner and Schmidt 1985; Kim, Oh et al. 2007)

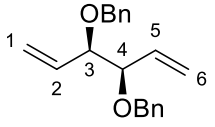

To a solution of (3*R*,4*R*)-hexa-1,5-diene-3,4-diol (**24**) (0.84 g, 7.32 mmol) in THF/DMF (1:1, 40 mL) were added sodium hydride (60% dispersed in oil, 0.70 g, 17.6 mmol) and benzyl bromide (2.26 mL, 19.0 mmol), at 0 °C. The reaction mixture was stirred for 18 h at RT, then quenched with water (20 mL) and the aqueous layer extracted with EtOAc (3 x 30 mL). The organic layers were combined, washed with water (15

mL), brine (15 mL) and then dried over $MgSO_4$, before removal of the solvent *in vacuo*. The crude product was purified by flash chromatography (SiO_2, petrol/EtOAc, 40:1), to afford the title compound as a colourless oil (1.55 g, 72%). The spectroscopic data were in agreement with the literature (Kufner and Schmidt 1985; Kim, Oh et al. 2007). δ_H ($CDCl_3$, 400 MHz) 7.39-7.23 (10H, m, ArH), 5.89-5.77 (2H, m, H-2 and H-5), 5.32-5.25 (4H, m, H-1, H-1', H-6 and H-6'), 4.67 (2H, d, *J* = 12.1 Hz, CH**H'** (benzyl)), 4.47 (2H, d, *J* = 12.1 Hz, C**H**H'(benzyl)), 3.93-3.88 (2H, m, H-3 and H-4); δ_C ($CDCl_3$, 100 MHz) 138.6 (ArC), 135.1 (CH-2 and CH-5), 128.2 (ArCH), 127.6 (ArCH), 127.4 (*p*-ArCH), 118.5 (2 x CH_2), 82.4 (CH-3 and CH-4), 70.7 (2 x CH_2(benzyl)); *m/z* (ESI^+) 295 ($[M+H]^+$, 4%), 317 ($[M+Na]^+$, 100%).

1.1.1.14: ((2R,3R,4R,5S)-3,4-Bis(benzyloxy)tetrahydrofuran-2,5-diyl)dimethanol (26)

(Donohoe and Butterworth 2003)

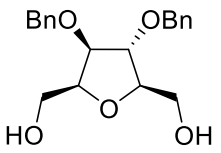

To a stirred solution of (((3*R*,4*R*)-hexa-1,5-diene-3,4-diyl*bis*(oxy))*bis*(methylene))-dibenzene (**25**) (0.87 g, 2.96 mmol) in CH_2Cl_2 (150 mL) were added trimethylamine *N*-oxide dihydrate (1.78 g, 23.7 mmol) and (+)-camphor-10-sulphonic acid (8.25 g, 35.5 mmol), followed by osmium tetroxide (38 mg, 0.15 mmol). The mixture was stirred for 48 h and then quenched with sodium sulfite (0.13 g, 1.0 mmol) and saturated aqueous Na_2CO_3 solution (100 mL), followed by the addition of EtOAc (250 mL). The biphasic solution was extracted into EtOAc (3 x 100 mL) and the combined organic layers dried over Na_2SO_4, followed by removal of the solvents *in vacuo*. The crude product was purified by flash chromatography (SiO_2, Et_2O), to afford the title compound as a colourless oil (0.77 g, 76%). The spectroscopic data were in agreement with the literature (Donohoe and Butterworth 2003). δ_H ($CDCl_3$, 400 MHz) 7.40-7.27 (10H, m, ArCH), 4.64 (1H, d, *J* = 11.7 Hz, C**H**H'Ph), 4.58 (2H, s, CH_2Ph), 4.45 (1H, d, *J* = 11.7 Hz, CH**H'**Ph), 4.17-4.11 (3H, m, C**H**OBnC**H**OBnC**H**), 4.04 (1H, td, *J* = 4.0 Hz, 3.0 Hz,

C**H**CH_2OH), 3.92 (1H, dd, *J* = 12.4 Hz, 4.0 Hz, C**H**H'OH), 3.88-3.81 (2H, m, CH**H'**OH and CH**H''**OH), 3.68 (1H, dd, *J* = 11.9 Hz, 3.3 Hz, C**H**H''OH), 2.67 (1H, bs, OH), 2.52 (1H, bs, OH); δ_C ($CDCl_3$, 100 MHz) 137.5 (ArC), 137.1 (ArC), 128.6 (ArCH), 128.6 (ArCH), 128.2 (*p*-ArCH), 128.0 (*p*-ArCH), 127.8 (ArCH), 127.6 (ArCH), 83.9 (CH), 83.8 (CH), 82.9 (CH), 80.4 (CH), 72.1 (CH_2(benzyl)), 71.9 (CH_2(benzyl)), 62.9 (CH_2OH), 61.7 (CH_2OH); *m/z* (ESI^+) 345 ($[M+H]^+$, 1%), 367 ($[M+Na]^+$, 55%), 689 ($[2M+H]^+$, 2%), 711 ($[2M+Na]^+$, 100%).

1.1.1.15: 2,5-Anhydro-D-glucitol (27)

(Donohoe and Butterworth 2003)

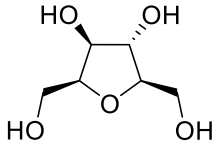

To a solution of ((2*R*,3*R*,4*R*,5*S*)-3,4-*bis*(benzyloxy)tetrahydrofuran-2,5-diyl)dimethanol (**26**) (59 mg, 0.17 mmol) in THF/EtOH (1:1, 10 mL), was added Pd/C (72 mg, 10 mol%) and the flask thoroughly evacuated and filled with nitrogen (x 3). The flask was then flushed with hydrogen (x 3), and hydrogen was allowed to bubble through the reaction mixture for 2 h using a hydrogen-filled balloon, whilst stirring vigorously. The suspension was left to stir under a sealed hydrogen atmosphere for 48 h at RT, and then carefully filtered through a plug of Celite®. After washing the filter plug with EtOH (2 x 20 mL) and removal of the solvent *in vacuo*, the resultant oil was dissolved in water (10 mL), washed with CH_2Cl_2 (3 x 20 mL) and the aqueous phase evaporated *in vacuo*, to afford the title compound as a colourless oil (26 mg, 94%). The spectroscopic data were in agreement with the literature (Donohoe and Butterworth 2003). $[\alpha]_D^{25}$ +21.6 (*c* = 1.0, MeOH); lit ($[\alpha]_D^{20}$ +18.8 (*c* = 1.0, CH_2Cl_2)); δ_H (D_2O, 400 MHz) 4.12 (1H, dd, *J* = 4.1 Hz, 2.4 Hz, C**H**OH), 4.09-4.03 (1H, m, C**H**CH_2OH), 3.96 (1H, dd, *J* = 4.1 Hz, 2.5 Hz, C**H**OH), 3.80-3.61 (5H, m, 2 x C**H₂**OH, C**H**CH_2OH); δ_C (D_2O, 100 MHz) 84.9 (**C**HCH_2OH), 81.3 (**C**HCH_2OH), 78.3 (CHOH), 77.2 (CHOH), 62.1 (CH_2OH), 60.5 (CH_2OH); *m/z* (ESI^+) 187 ($[M+Na]^+$, 100%).

Chapter 3: Hypoxic Regulation of PFK Isoenzymes

3.1: Introduction and Aims

Numerous studies have shown that PFK-1 and PFK-2/FBPase-2 isoenzymes are over-expressed in cancer and also induced under hypoxic conditions (Sanchez-Martinez and Aragon 1997; Minchenko, Opentanova et al. 2003; Minchenko, Ochiai et al. 2005). The kinase/bisphosphatase activity of PFK-2/FBPase-2 and bisphosphatase activity of TIGAR cooperate to control the intracellular concentration of F-2,6-BP, which is able to promote glycolysis through allosteric activation of PFK-1 (Bensaad, Tsuruta et al. 2006; Bartrons and Caro 2007). The PFK-1, PFK-2/FBPase-2 and TIGAR isoenzymes are thought to be intimately involved in maintaining the glycolytic phenotype and therefore present themselves as potential anti-tumour targets (Herrero-Mendez, Almeida et al. 2009).

At the outset it was therefore important to gain a deeper understanding of the relationship between PFK-1, PFK-2/FBPase-2 and TIGAR isoenzyme expression, and explore how that relationship changes under hypoxic conditions, as well as the nature of hypoxic regulation. It was also necessary to narrow the focus by identifying the most important isoenzymes for further study. It was then desirable to select suitable cell lines with differing expression profiles of those isoenzymes, to progress to *in vitro* small interfering RNA (siRNA) studies, in order to further probe any relationship between them.

3.2: Results

3.2.1: Basal expression and hypoxic induction of the *PFK-1* and *PFK-2/FBPase-2* isoenzymes differed markedly in U87, MCF-7 and PC3 cells.

In order to gain a greater understanding of basal expression and hypoxic induction of the PFK isoenzymes and TIGAR, it was decided to examine the mRNA expression of each isoenzyme in a panel of three cancer cell lines. U87 (glioblastoma), MCF-7 (breast adenocarcinoma) and PC3 (prostate) were chosen as an initial starting point, as they each originate from tissues known to up-regulate PFK isoenzymes during carcinogenesis (Staal, Kalff et al. 1987; Minchenko, Ochiai et al. 2005; Kessler, Bleichert et al. 2008; Ros, Santos et al. 2012).

The cells were plated and left to adhere overnight, then exposed to hypoxia (0.1% O_2) for either 0, 4, 8, 24, 48 or 72 hours, before extraction of the RNA. *PFK-1 (PFKL*, *PFKM* and *PFKP)*, *PFK-2/FBPase-2 (PFKFB1*, *PFKFB2*, *PFKFB3* and *PFKFB4)* and *TIGAR* mRNA expression were then quantified by quantitative real-time polymerase chain reaction (qRT-PCR), using sequence-specific primers. The relative isoenzyme expression was calculated, as shown in Figures 3.1 (U87), 3.2 (MCF-7) and 3.3 (PC3). For ease of reference, the hypoxic induction of each individual isoenzyme, normalised to t = 0 h, is shown in Figures 3.4 (U87), 3.5 (MCF-7) and 3.6 (PC3).

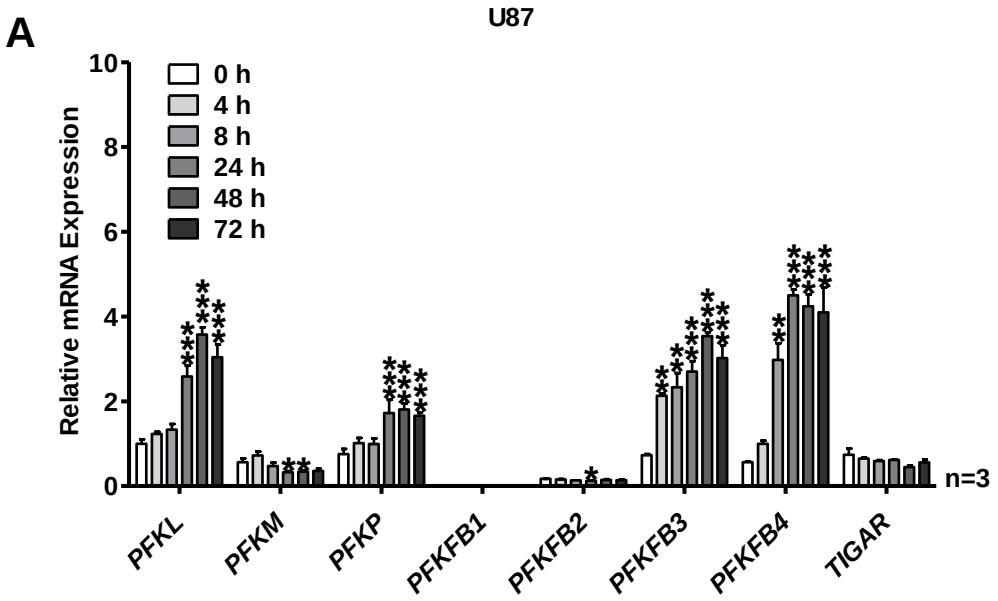

B

	Relative mRNA Expression	
	Normoxia	**Hypoxia (48 h)**
PFKL	1.0 (+/- 0.1)	3.6 (+/- 0.2)
PFKM	0.6 (+/- 0.1)	0.3 (+/- 0.1)
PFKP	0.8 (+/- 0.1)	1.8 (+/- 0.1)

C

	Relative mRNA Expression	
	Normoxia	**Hypoxia (48 h)**
PFKFB1	3.0 (+/- 0.7)x10^{-3}	4.0 (+/-0.7)x10^{-3}
PFKFB2	1.0 (+/- 0.1)	0.8 (+/- 0.1)
PFKFB3	4.3 (+/- 0.2)	20.8 (+/- 0.5)
PFKFB4	3.3 (+/- 0.1)	24.9 (+/- 1.6)
TIGAR	4.3 (+/- 0.9)	2.6 (+/- 0.2)

Figure 3.1: Hypoxic time course of relative *PFK-1*, *PFK-2/FBPase-2* and *TIGAR* mRNA expression in U87 cells. Relative expression was markedly different under normoxic conditions and over a 72 h hypoxic time course. **(A)** Normalised to *PFKL* (normoxia); **(B)** Relative mRNA expression of the *PFK-1* isoenzymes under normoxic and hypoxic conditions, normalised to *PFKL* (normoxia) shows *PFKL* and *PFKP* were predominant; **(C)** Relative mRNA expression of the *PFK-2/FBPase-2* isoenzymes and *TIGAR* under normoxic and hypoxic conditions, normalised to *PFKFB2* (normoxia) shows *PFKFB3* and *PFKFB4* were the predominant *PFK-2/FBPase-2* isoenzymes. n=3; One-way ANOVA analysis performed with Dunnett's post-test, comparing isoenzyme mRNA expression at each time point to the corresponding expression level at t = 0 h; *($p<0.05$), **($p<0.01$), ***($p<0.001$), ****($p<0.0001$).

A

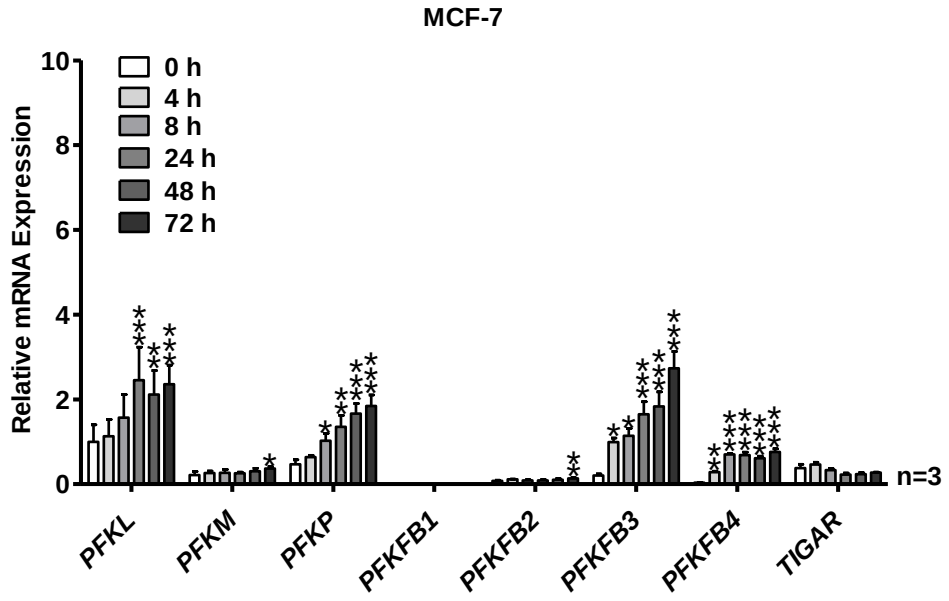

B

	Relative mRNA Expression	
	Normoxia	**Hypoxia (48 h)**
PFKL	1.0 (+/- 0.4)	2.1 (+/- 0.6)
PFKM	0.2 (+/- 0.1)	0.3 (+/- 0.1)
PFKP	0.5 (+/- 0.1)	1.7 (+/- 0.2)

C

	Relative mRNA Expression	
	Normoxia	**Hypoxia (48 h)**
PFKFB1	7.2 (+/- 2.5)x10^{-3}	16.1 (+/- 4.2)x10^{-3}
PFKFB2	1.0 (+/- 0.2)	1.4 (+/- 0.3)
PFKFB3	2.6 (+/- 0.5)	23.8 (+/- 4.4)
PFKFB4	0.5 (+/- 0.1)	7.9 (+/- 0.6)
TIGAR	4.9 (+/- 1.2)	3.1 (+/- 0.5)

Figure 3.2: Hypoxic time course of relative *PFK-1*, *PFK-2/FBPase-2* and *TIGAR* mRNA expression in MCF-7 cells. Relative expression was markedly different under normoxic conditions and over a 72 h time course. **(A)** Normalised to *PFKL* (normoxia); **(B)** Relative mRNA expression of the *PFK-1* isoenzymes under normoxic and hypoxic conditions, normalised to *PFKL* (normoxia) shows *PFKL* and *PFKP* were predominant; **(C)** Relative mRNA expression of the *PFK-2/FBPase-2* isoenzymes and *TIGAR* under normoxic and hypoxic conditions, normalised to *PFKFB2* (normoxia) shows *PFKFB2* and *PFKFB3* were the predominant *PFK-2/FBPase-2* isoenzymes in normoxia, whereas *PFKFB3* and *PFKFB4* predominated in hypoxia. n=3; One-way ANOVA analysis performed with Dunnett's post-test, comparing isoenzyme mRNA expression at each time point to the corresponding expression level at t = 0 h; *($p<0.05$), **($p<0.01$), ***($p<0.001$), ****($p<0.0001$).

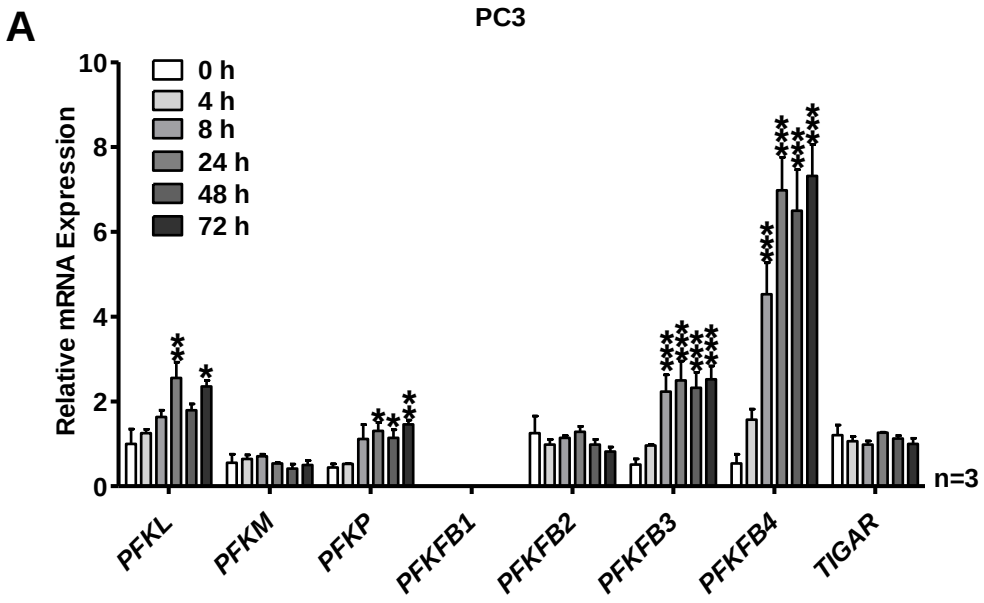

B

	Relative mRNA Expression	
	Normoxia	**Hypoxia (48 h)**
PFKL	1.0 (+/- 0.4)	1.8 (+/- 0.2)
PFKM	0.6 (+/- 0.2)	0.4 (+/- 0.1)
PFKP	0.4 (+/- 0.1)	1.1 (+/- 0.2)

C

	Relative mRNA Expression	
	Normoxia	**Hypoxia (48 h)**
PFKFB1	1.4 (+/-0.5)x10^{-3}	1.7 (+/- 0.1)x10^{-3}
PFKFB2	1.0 (+/- 0.3)	0.8 (+/-0.1)
PFKFB3	0.4 (+/- 0.1)	1.9 (+/- 0.3)
PFKFB4	0.4 (+/- 0.2)	5.2 (+/- 0.8)
TIGAR	1.0 (+/- 0.2)	0.9 (+/- 0.1)

Figure 3.3: Hypoxic time course of relative *PFK-1*, *PFK-2/FBPase-2* and *TIGAR* mRNA expression in PC3 cells. Relative expression was markedly different under normoxic conditions and over a 72 h hypoxic time course. **(A)** Normalised to *PFKL* (normoxia); **(B)** Relative mRNA expression of the *PFK-1* isoenzymes under normoxic and hypoxic conditions, normalised to *PFKL* (normoxia) shows *PFKL* and *PFKP* were predominant in hypoxia; **(C)** Relative mRNA expression of the *PFK-2/FBPase-2* isoenzymes and *TIGAR* under normoxic and hypoxic conditions, normalised to *PFKFB2* (normoxia) shows *PFKFB2* was the predominant *PFK-2/FBPase-2* isoenzyme in normoxia, whereas *PFKFB3* and *PFKFB4* predominated in hypoxia. n=3; One-way ANOVA analysis performed with Dunnett's post-test, comparing isoenzyme mRNA expression at each time point to the corresponding expression level at t = 0 h; *($p<0.05$), **($p<0.01$), ***($p<0.001$), ****($p<0.0001$).

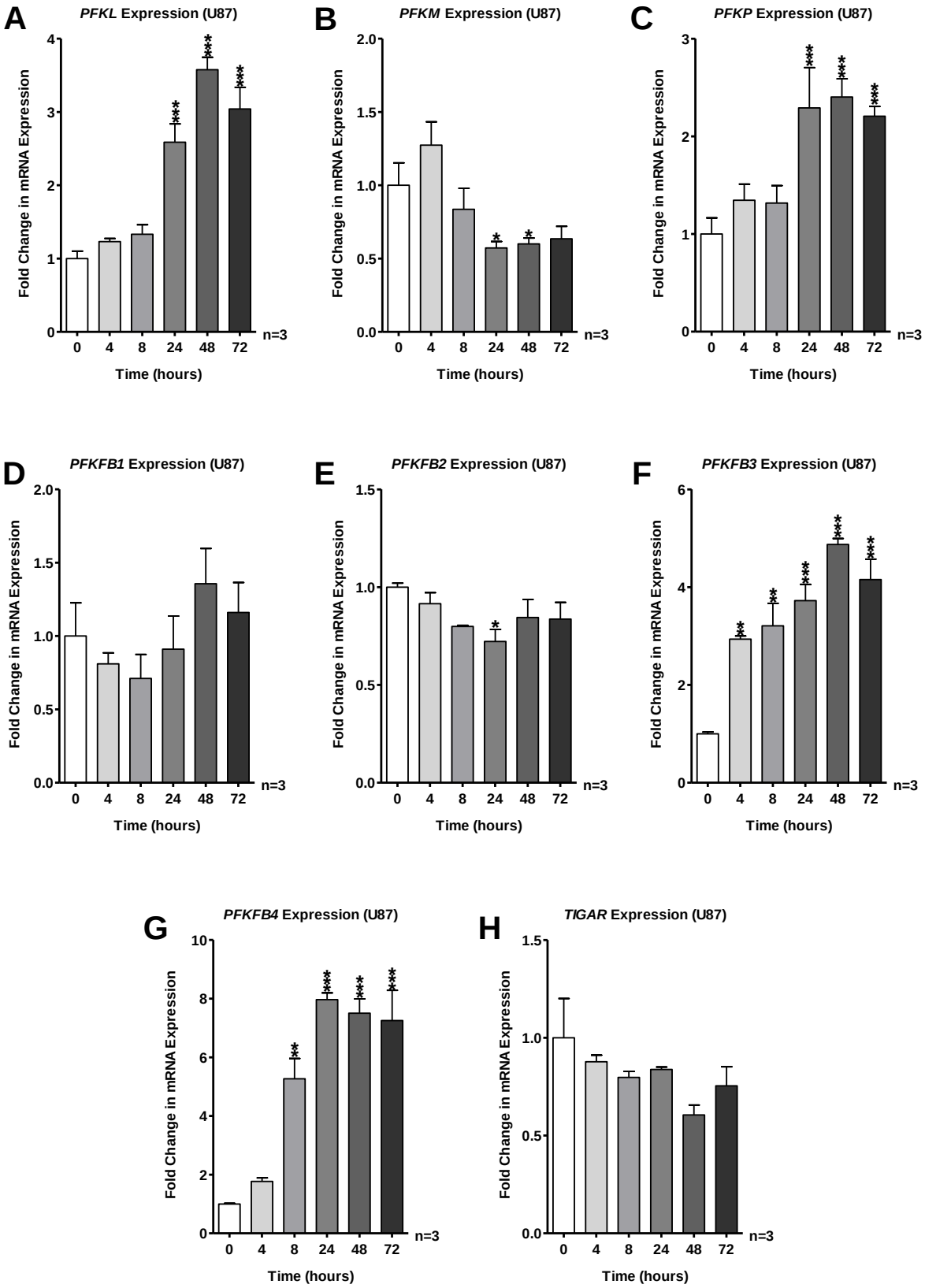

Figure 3.4: Hypoxic time course (0-72 h) of **(A)-(C)** *PFK-1*, **(D)-(G)** *PFK-2/FBPase-2* and **(H)** *TIGAR* isoenzyme mRNA expression in U87 cells, normalised to t = 0 h. **(A)** *PFKL* and **(C)** *PFKP* were both induced in hypoxia, but the highest induction was observed for **(F)** *PFKFB3* and **(G)** *PFKFB4*. **(B)** *PFKM* expression decreased in hypoxia. n=3; One-way ANOVA analysis performed with Dunnett's post-test, comparing isoenzyme mRNA expression at each time point to the corresponding expression level at t = 0 h; *($p<0.05$), **($p<0.01$), ***($p<0.001$), ****($p<0.0001$).

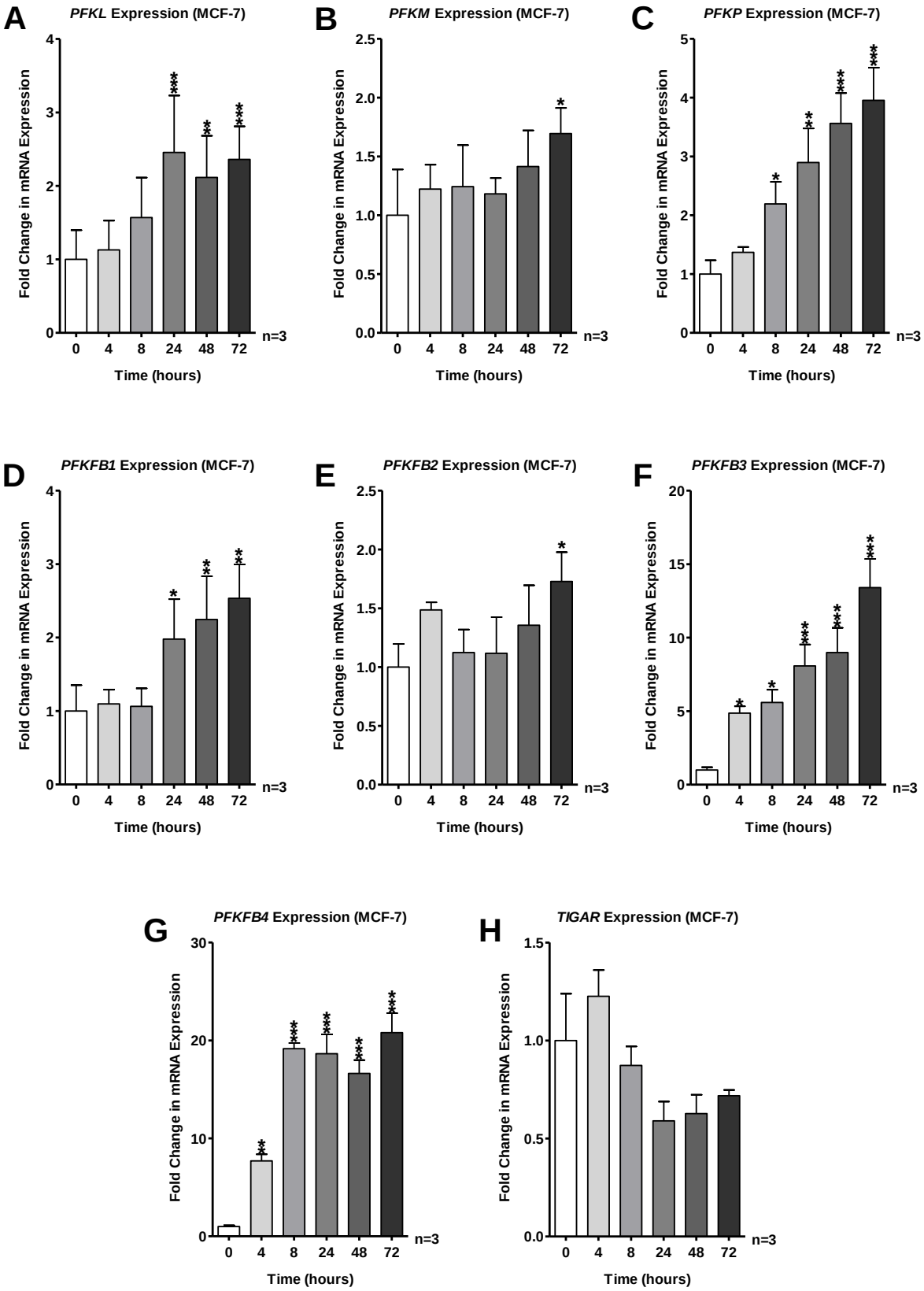

Figure 3.5: Hypoxic time course (0-72 h) of **(A)-(C)** *PFK-1*, **(D)-(G)** *PFK-2/FBPase-2* and **(H)** *TIGAR* isoenzyme mRNA expression in MCF-7 cells, normalised to t = 0 h. **(A)** *PFKL*, **(B)** *PFKM*, **(C)** *PFKP* and **(D)** *PFKFB1* were all induced in hypoxia, but the highest induction was observed for **(F)** *PFKFB3* and **(G)** *PFKFB4*. n=3; One-way ANOVA analysis performed with Dunnett's post-test, comparing isoenzyme mRNA expression at each time point to the corresponding expression level at t = 0 h; *($p<0.05$), **($p<0.01$), ***($p<0.001$), ****($p<0.0001$).

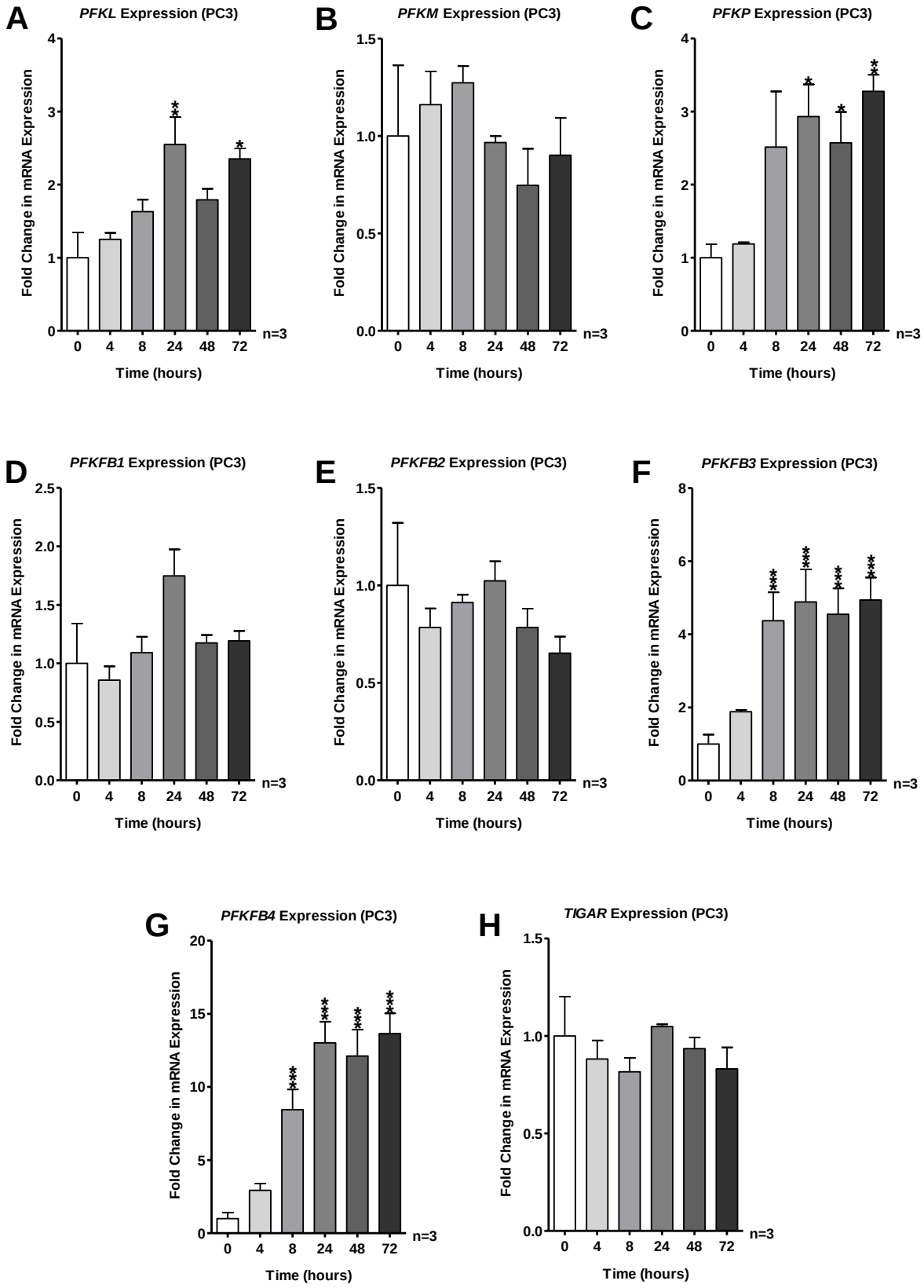

Figure 3.6: Hypoxic time course (0-72 h) of **(A)-(C)** *PFK-1*, **(D)-(G)** *PFK-2/FBPase-2* and **(H)** *TIGAR* isoenzyme mRNA expression in PC3 cells, normalised to t = 0 h. **(A)** *PFKL* and **(C)** *PFKP* were both induced in hypoxia, but the highest induction was observed for **(F)** *PFKFB3* and **(G)** *PFKFB4*. n=3; One-way ANOVA analysis performed with Dunnett's post-test, comparing isoenzyme mRNA expression at each time point to the corresponding expression level at t = 0 h; *($p<0.05$), **($p<0.01$), ***($p<0.001$), ****($p<0.0001$).

The most striking observation was the marked difference in basal expression and hypoxic induction of each of the isoenzymes. Under both normoxic and hypoxic conditions, *PFKL* was the predominant PFK-1 isoenzyme expressed in all three cell lines (Figures 3.1B, 3.2B and 3.3B). Both *PFKL* and *PFKP* were consistently induced under hypoxic conditions (Figures 3.1A-3.3A and 3.1B-3.3B). The pattern for *PFKM* expression was more variable, showing a significant decrease in U87 cells at 24 hours (43(+/-16)% decrease ($p<0.05$)) (Figure 3.4B), but a significant increase in MCF-7 cells at 72 hours (69(+/-45)% increase ($p<0.05$)) (Figure 3.5B). However, the net effect in all cases was a reduction in the relative contribution of *PFKM* under hypoxic conditions, compared to *PFKL* and *PFKP* (Figures 3.1B, 3.2B and 3.3B). During the course of this work, a study was published by Marunych and colleagues (Marunych, Minchenko et al. 2011), which confirmed the general pattern of findings presented in Figures 3.1 and 3.4, for the effect of hypoxia on *PFK-1* isoenzyme expression in U87 cells. However, their study did not make any comparison between the different isoenzymes. The observed 2.6-fold increase in *PFKL* expression (24 hours exposure to 0.1% oxygen) (Figure 3.4A) differed considerably from Marunych and colleagues' reported 19-fold increase (16 hours exposure to 3% oxygen), the reasons for which remain unclear.

The relative *PFKFB1* expression was over an order of magnitude lower than the other PFK-2/FBPase-2 isoenzymes under basal conditions in all cell lines (Figures 3.1C, 3.2C and 3.3C) and was only found to be significantly increased in the MCF-7 cell line (2.5-fold ($p<0.01$) after 72 hours) (Figure 3.5D). Accordingly, it is unlikely to exert much influence on [F-2,6-BP] and therefore glycolytic flux in these cell lines.

Relative basal *PFKFB2* expression exceeded both *PFKFB1* and *PFKFB4* expression in the MCF-7 cell line and was actually the predominant *PFK-2/FBPase-2* isoenzyme in PC3 cells under basal conditions (Figures 3.2C and 3.3C, respectively). Hypoxia-inducibility was only

observed for *PFKFB2* in the MCF-7 cell line, which exhibited a comparatively small increase after 72 hours (1.7-fold ($p<0.05$)) (Figure 3.5E). The relative contribution of *PFKFB2* to the total *PFK-2/FBPase-2* expression was therefore much reduced after hypoxic exposure in all three cell lines (Figures 3.1C, 3.2C and 3.3C).

In all cases *PFKFB3* and *PFKFB4* were strongly induced in hypoxia, more so than any other isoenzyme, and were the predominant isoenzymes expressed under hypoxic conditions. Respective fold-changes in expression after 72 hours were: *PFKFB3* (U87: 4.2 ($p<0.001$); MCF-7: 13.4 ($p<0.001$); PC3: 4.9 ($p<0.001$)) and *PFKFB4* (U87: 7.3 ($p<0.001$); MCF-7: 20.8 ($p<0.001$); PC3: 13.7 ($p<0.001$)) (Figures 3.4F-3.6F and 3.4G-3.6G, respectively). The rate of hypoxic induction differed between cell lines. It was interesting that PC3 cells, which had the lowest relative basal *PFKFB3* expression of the three cell lines, showed the highest rate of *PFKFB3* induction, reaching maximal extent after just 8 hours (Figure 3.6F), compared to U87 cells (48 hours, Figure 3.4F) and MCF-7 cells (72 hours, Figure 3.5F). Conversely, MCF-7 cells, which had the lowest relative basal *PFKFB4* expression of the three cell lines, showed the highest relative rate of *PFKFB4* induction, reaching maximal expression after just 8 hours (Figure 3.5G), compared to U87 (24 hours, Figure 3.4G) and PC3 (24 hours, Figure 3.6G). This suggested the adaptive response to hypoxia might require high levels of both PFKFB3 and PFKFB4 proteins. Those cell lines with lower basal abundance of either of the corresponding mRNAs might be required to induce their expression more rapidly in response to reduced oxygen concentration.

No significant change in *TIGAR* expression was observed in any of the cell lines after hypoxic exposure (Figures 3.4H, 3.5H and 3.6H). Hence, under hypoxic conditions, the relative expression compared to *PFKFB3* and *PFKFB4* was much reduced (for example, the change in *PFKFB3:PFKFB4:TIGAR* mRNA expression ratio from (1 : 1 : 2.3) to (1 : 2.8 : 0.5) in

PC3 cells after 48 hours hypoxia). This suggested that TIGAR has comparatively less effect on intracellular [F-2,6-BP] under hypoxic conditions.

The consistently high relative basal *PFKFB3* and *PFKFB4* expression and hypoxia-inducibility supported the view that these isoenzymes are intimately involved in the hypoxic response and maintenance of the glycolytic phenotype. Changes in mRNA expression levels are often a good indicator of effects at the protein level, but it was necessary to confirm this was the case for both PFKFB3 and PFKFB4. TIGAR protein expression was also investigated because of high basal mRNA expression and its known importance as a bisphosphatase (Bensaad, Tsuruta et al. 2006).

3.2.2: Validation of PFKFB3 and PFKFB4 antibodies.

In order to further investigate function and regulation of PFKFB3 and PFKFB4, it was necessary to obtain and validate specific antibodies. The highly-transfectable HEK 293T cell line was chosen, and the cells reverse transfected with either PFKFB3 or PFKFB4 expression plasmids, or transfection reagent only (Mock). The cells were then incubated for 48 hours, before lysing. The corresponding cell lysates were probed by Western Blot for PFKFB3 and PFKFB4 expression using a series of commercially available antibodies (listed in Tables A1.1 and A1.2, Appendix). In our hands, the commercial PFKFB3 antibodies tested showed a lack of specificity and were unsuitable for use. However, a specific antibody targeting PFKFB3 splice variant 5 (UBI2K5) was kindly provided as a gift from Professor Salvador Moncada (University College, London), and showed high specificity (Figure 3.7A, predicted molecular weight = 67 kDa). UBI2K5 has been reported as the dominant PFKFB3 splice variant expressed in transformed cells (Bando, Atsumi et al. 2005; Yalcin, Clem et al. 2009).

The PFKFB4 antibody from Epitomics (S1348) was identified as likely the most selective (Figure 3.7B, predicted molecular weight = 54 kDa), but low basal expression in the control samples hindered confirmation of the protein band identity. A further experiment in PC3 cells, which express particularly high PFKFB4 levels under hypoxic conditions, was performed using scramble control and PFKFB4-specific siRNA sequences. Western Blot comparison with the HEK 293T lysate using lower sensitivity ECL™ reagent (Figure 3.7C) and higher sensitivity ECL™ Prime reagent (Figure 3.7D) confirmed the band at 54 kDa was PFKFB4.

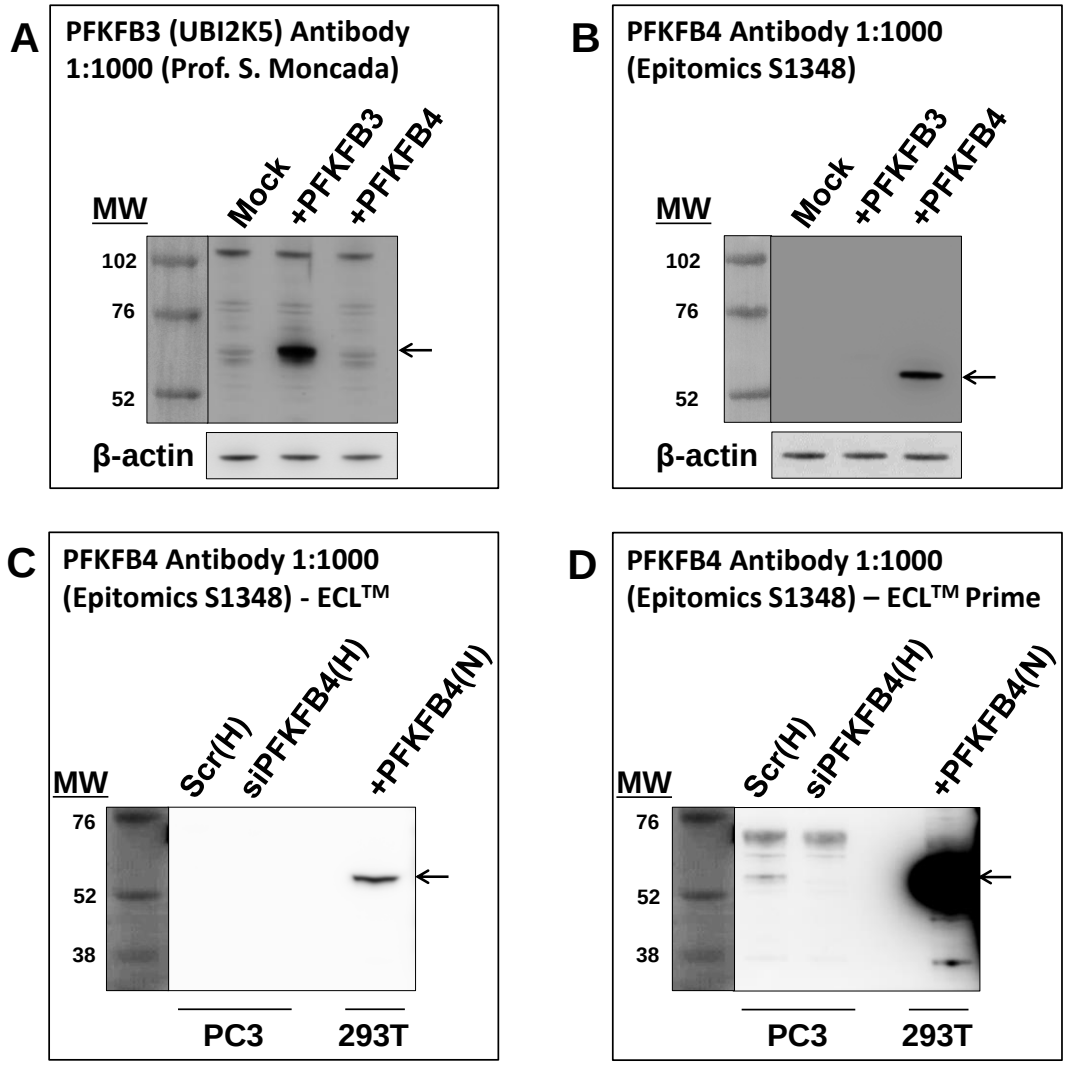

Figure 3.7: PFKFB3 and PFKFB4 antibody validation. Over-expression of PFKFB3 (+PFKFB3) and PFKFB4 (+PFKFB4) compared to control (Mock) in HEK 293T cells allowed selection of specific **(A)** PFKFB3 (UBI2K5) and **(B)** PFKFB4 antibodies. PFKFB4 band identity was confirmed using lysates from scramble control (Scr) siRNA and PFKFB4 siRNA-transfected PC3 cells exposed to 48 h hypoxia. These were compared with the PFKFB4 over-expression lysate (HEK 293T cells) at low-sensitivity ECL™ exposure **(C)** and high sensitivity ECL™ Prime exposure **(D)**. N: Normoxia, H: Hypoxia, MW: Molecular weight (kDa), 293T: HEK 293T cells.

A commercially available TIGAR antibody (T8828, Sigma Aldrich) was originally produced and had previously been validated by Dr Karim Bensaad, a member of the Harris laboratory (Bensaad, Tsuruta et al. 2006). This antibody was selected for further use.

3.2.3: PFKFB3 and PFKFB4 proteins were induced under hypoxic conditions in U87, MCF-7 and PC3 cells.

Having validated the PFKFB3 and PFKFB4 antibodies, U87, MCF-7 and PC3 cell lysates were prepared at corresponding time points to the RNA-level study, and probed using Western blot. Additional antibodies specific for HIF-1α and TIGAR were also used to probe protein expression (Figures 3.8A, 3.8B and 3.8C, respectively).

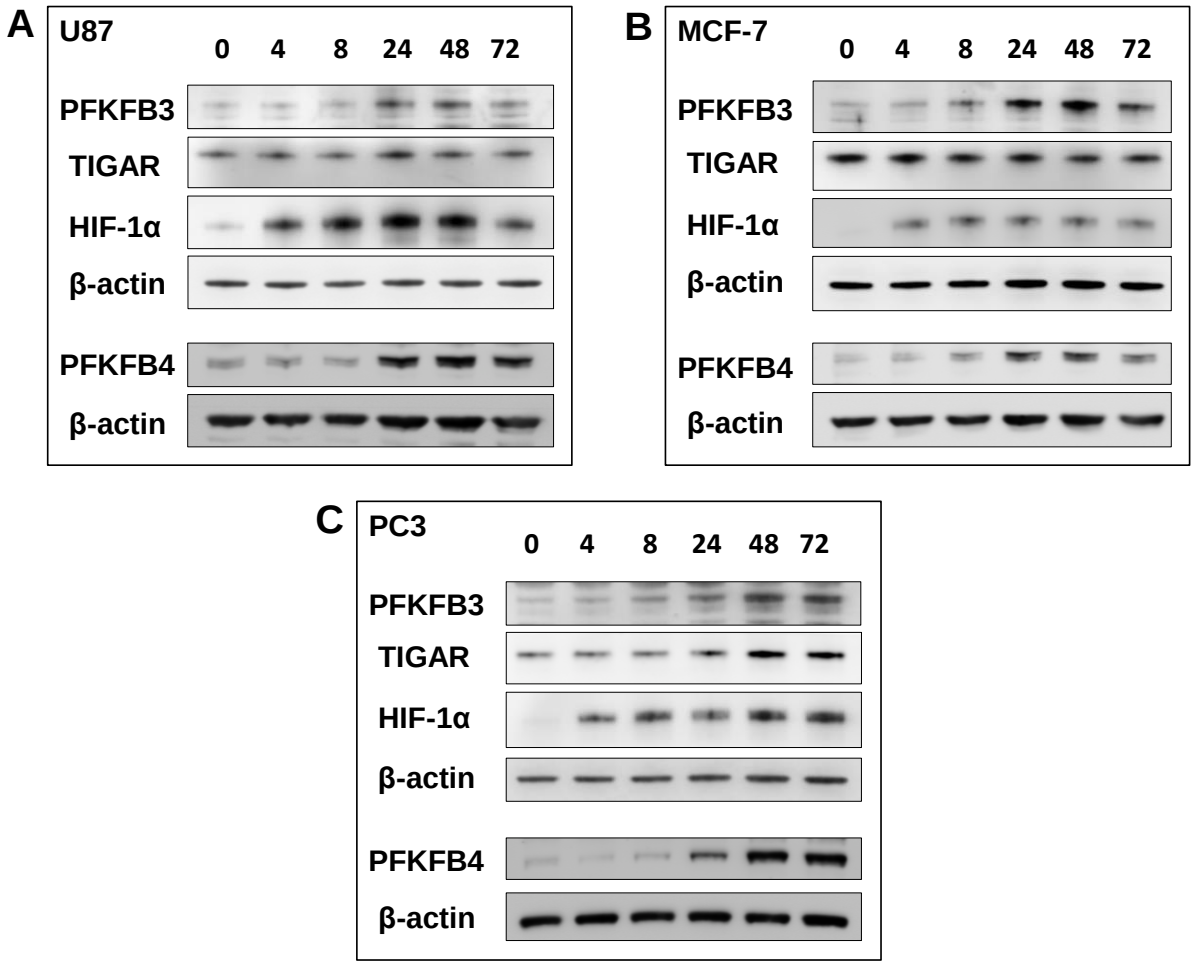

Figure 3.8: Western blot showing expression of PFKFB3, PFKFB4 and TIGAR in hypoxia. PFKFB3 and PFKFB4 expression were induced during a 72 h hypoxic time course, whereas TIGAR expression showed no consistent change in **(A)** U87, **(B)** MCF-7 and **(C)** PC3 cells. β-actin was used as a loading control. Representative images of n≥2 replicates.

The Western blot data corroborated the RNA-level findings, with strong induction of both PFKFB3 and PFKFB4 in all three cell lines, with no consistent change over time in TIGAR expression between replicates (Figure 3.8). The differences seen in the rate of *PFKFB3* and *PFKFB4* induction in the qRT-PCR data were not borne out at the protein level, with both isoenzymes reaching maximal protein expression at the 24 / 48 hour time points in all three cell lines (Figure 3.8).

3.2.4: *PFKL, PFKP, PFKFB3* and *PFKFB4* mRNAs were induced and *PFKFB1* mRNA expression repressed under hypoxic conditions in a HIF-1α-dependent and HIF-2α-independent manner in U87, MCF-7 and PC3 cells.

To further understand regulation of PFK-1 and PFK-2/FBPase-2 isoenzyme expression under hypoxic conditions, it was important to investigate control at the transcriptional level. HIF-1α and HIF-2α are the two principal transcription factor subunits responsible for mediating the physiologic response to hypoxia (Hu, Wang et al. 2003). A number of previous studies have shown that both the *PFKFB3* and *PFKFB4* genes possess hypoxia response elements (HREs) in their promoter regions and are HIF-regulated (Minchenko, Leshchinsky et al. 2002; Minchenko, Opentanova et al. 2004; Obach, Navarro-Sabate et al. 2004). However, most of these studies used dimethyloxalylglycine (DMOG, an oxoglutarate analogue), desferrioxamine (DFO, an iron-chelator) and cobalt chloride (an iron-substitute), to inhibit PHD-mediated hydroxylation of HIF-α. This leads to HIF-α accumulation, thereby mimicking hypoxia. The authors of these studies observed increased *PFKFB3* and *PFKFB4* expression in response to these hypoxia-mimics and concluded their expression was HIF-1α-dependent (Minchenko, Leshchinsky et al. 2002; Minchenko, Opentanova et al. 2005). However, these PHD-inhibitors do not exert their effect specifically on HIF-1α, and the observations presented in these reports do not preclude regulation by HIF-2α. Furthermore, their inhibitory effect will likely extend to other 2-oxogluterate-dependent enzymes, in addition to the PHDs.

It was believed that only one study had previously shown conclusive HIF-1α regulation of *PFKFB4*, using a dominant-negative HIF-1α construct in HeLa cells (Minchenko, Opentanova et al. 2004). It was therefore of interest to investigate the nature of hypoxic PFK-1 and PFK-2/FBPase-2 regulation across the three different cell lines, using small interfering RNAs (siRNAs).

RNA interference is the intracellular process of specifically silencing gene expression at the post-transcriptional level, mediated by double-stranded RNAs that direct degradation of homologous mRNA targets. The development of synthetic siRNAs (19-22 base pairs) enables researchers to selectively silence target genes of interest (Elbashir, Harborth et al. 2001; Elbashir, Lendeckel et al. 2001). U87, MCF-7 and PC3 cells were reverse transfected with control scramble, or specific siRNA sequences targeting HIF-1α or HIF-2α. The following day, cells were transferred to hypoxia for 48 hours and a set of control scramble-transfected plates were kept in normoxic conditions. RNAs were extracted from the cells and qRT-PCR performed using sequence-specific primers, to quantify relative *PFK-1* and *PFK-2/FBPase-2* isoenzyme mRNA expression (U87: Figure 3.9; MCF-7: Figure 3.10; PC3: Figure 3.11).

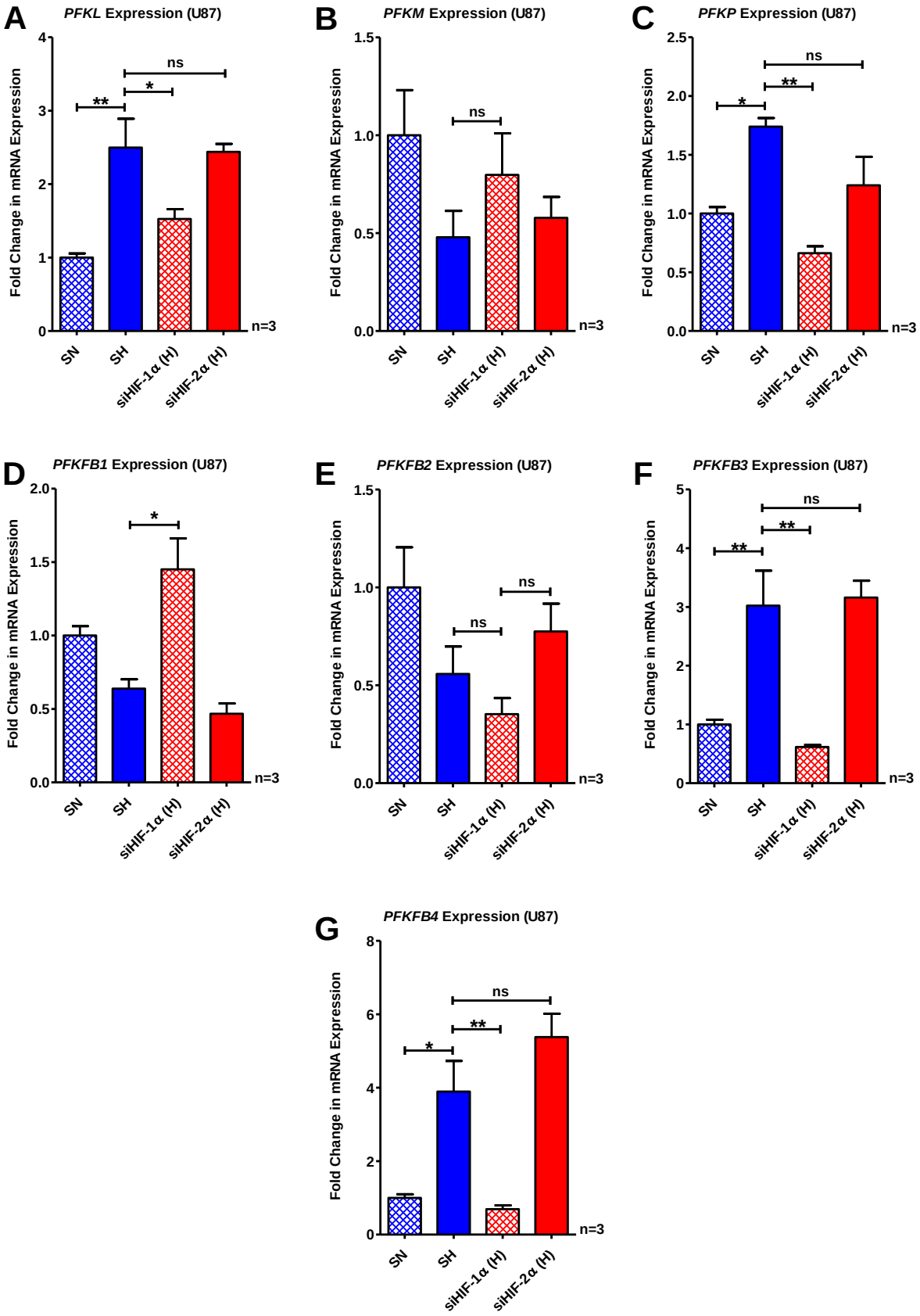

Figure 3.9: qRT-PCR analysis of the effect of HIF-1α and HIF-2α siRNA knockdown on *PFK-1* and *PFK-2/FBPase-2* isoenzyme mRNA expression in U87 cells **(A)** *PFKL*, **(C)** *PFKP*, **(F)** *PFKFB3* and **(G)** *PFKFB4* were all regulated in a HIF-1α-dependent and HIF-2α-independent manner. 48 hours normoxic/hypoxic exposure. n=3; One-way ANOVA analysis performed with Bonferroni post-test, comparing isoenzyme mRNA expression of SH to each of the other three conditions; *(p<0.05), **(p<0.01), ***(p<0.001), ****(p<0.0001), ns (not significant); S: Scramble siRNA, N: Normoxia, H: Hypoxia.

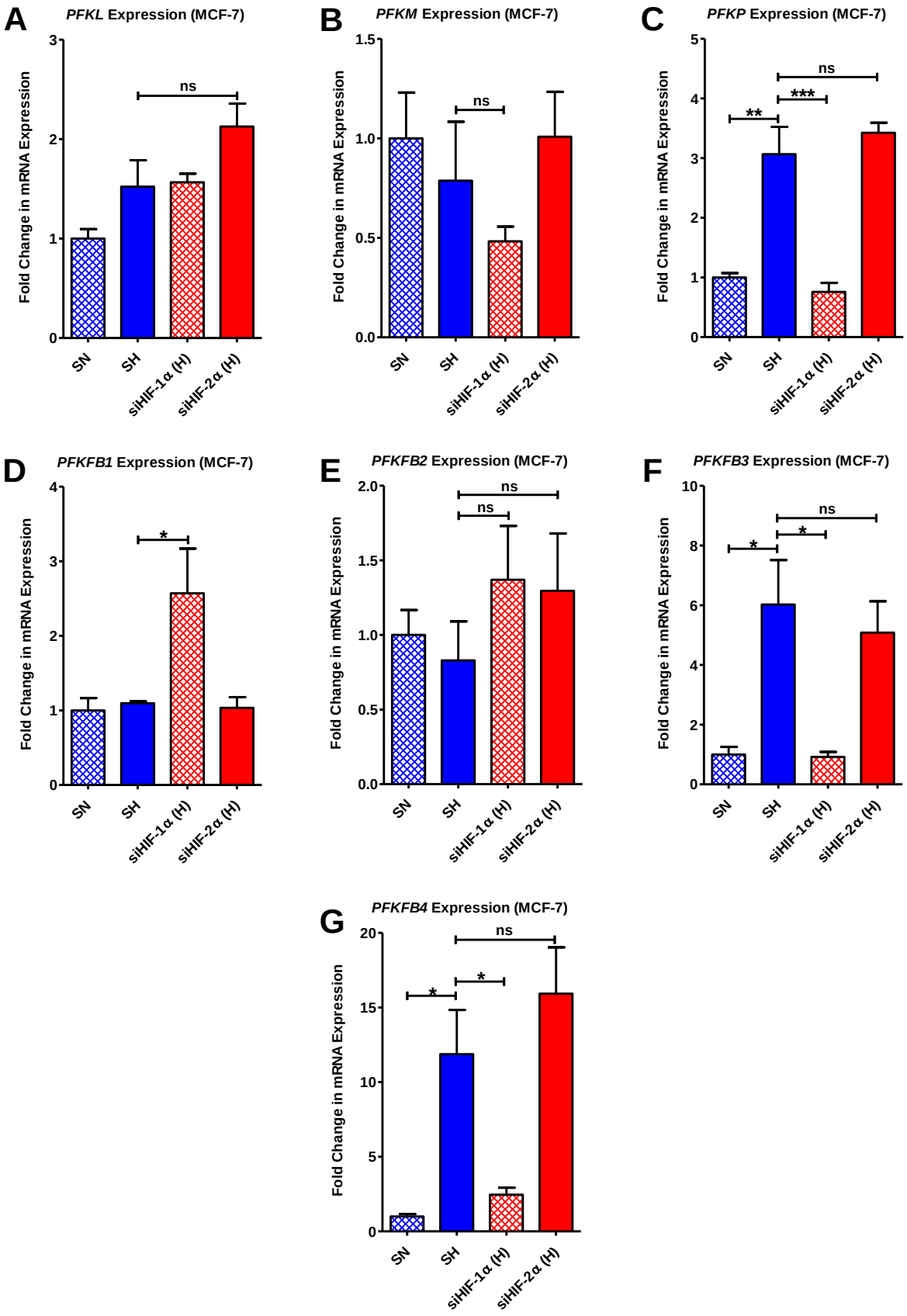

Figure 3.10: qRT-PCR analysis of the effect of HIF-1α and HIF-2α siRNA knockdown on *PFK-1* and *PFK-2/FBPase-2* isoenzyme mRNA expression in MCF-7 cells **(C)** *PFKP*, **(F)** *PFKFB3* and **(G)** *PFKFB4* were all regulated in a HIF-1α-dependent and HIF-2α-independent manner. 48 hours normoxic/hypoxic exposure. n=3; One-way ANOVA analysis performed with Bonferroni post-test, comparing isoenzyme mRNA expression of SH to each of the other three conditions; *($p<0.05$), **($p<0.01$), ***($p<0.001$), ****($p<0.0001$), ns (not significant); S: Scramble siRNA, N: Normoxia, H: Hypoxia.

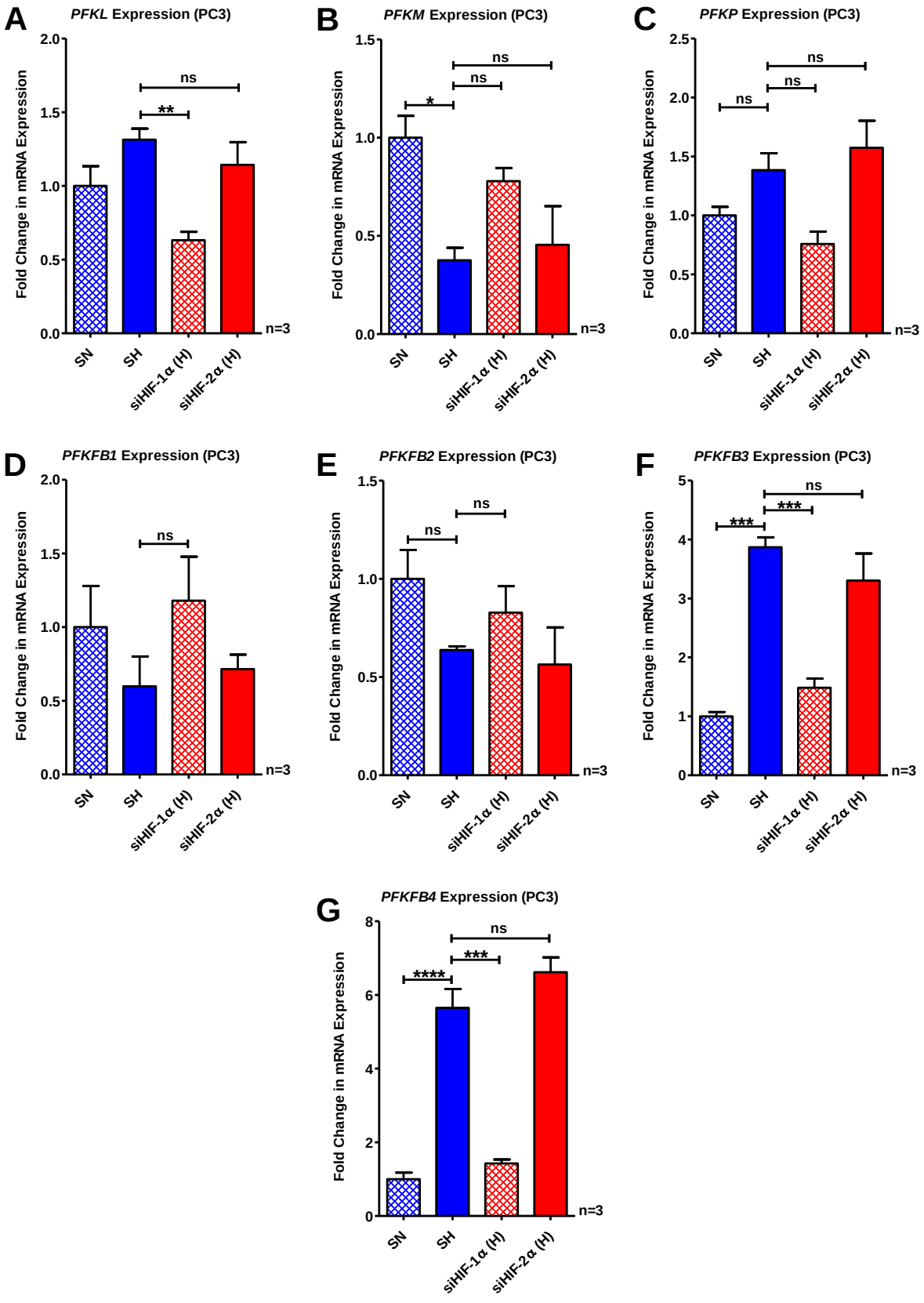

Figure 3.11: qRT-PCR analysis of the effect of HIF-1α and HIF-2α siRNA knockdown on *PFK-1* and *PFK-2/FBPase-2* isoenzyme mRNA expression in PC3 cells. **(A)** *PFKL*, **(F)** *PFKFB3* and **(G)** *PFKFB4* were all regulated in a HIF-1α-dependent and HIF-2α-independent manner. 48 hours normoxic/hypoxic exposure. n=3; One-way ANOVA analysis performed with Bonferroni post-test, comparing isoenzyme mRNA expression of SH to each of the other three conditions; *(p<0.05), **(p<0.01), ***(p<0.001), ****(p<0.0001), ns (not significant); S: Scramble siRNA, N: Normoxia, H: Hypoxia.

There was no significant change in *PFKM* or *PFKFB2* expression in any of the cell lines in response to knockdown of either HIF-1α or HIF-2α (Figures 3.9B-3.11B and 3.9E-3.11E, respectively). Minchenko and colleagues had previously shown hypoxia-mimics, including DMOG and desferrioxamine (DFO), to induce *PFKFB2* expression in MCF-7 cells, which they suggested meant involvement of HIF-α proteins in *PFKFB2* regulation (Minchenko, Opentanova et al. 2003). The findings presented in Figure 3.10E suggest this is not the case.

There was a trend for increased *PFKFB1* expression in response to HIF-1α knockdown in all three cell lines and this was significant for the U87 cell line (127(+/-34)% increase; $p<0.05$) (Figure 3.9D) and the MCF-7 cell line (134(+/-54)% increase; $p<0.05$) (Figure 3.10D). As previously noted, *PFKFB1* expression was markedly lower in all three cell lines compared to the other PFK-2/FBPase-2 isoenzymes (Figures 3.1, 3.2 and 3.3). Whilst this was not investigated further, repression of *PFKFB1* expression by HIF-1α, i.e. regulation in a manner opposite to the other PFK-2/FBPase-2 isoenzymes, further suggests PFKFB1 expression is less relevant in determining overall [F-2,6-BP] under hypoxic conditions. *PFKFB1* mRNA expression was found to be independent of HIF-2α expression in all three cell lines (Figures 3.9D, 3.10D and 3.11D).

PFKL expression was insensitive to HIF-1α knockdown in the MCF-7 cell line (Figure 3.10A), but was significantly decreased in the U87 and PC3 cell lines upon treatment with siHIF-1α (39(+/-17)% ($p<0.05$) and 52(+/-7)% ($p<0.01$), respectively) (Figures 3.9A and 3.11A, respectively). There was a consistent trend for reduced *PFKP* expression after HIF-1α knockdown in all three cell lines, which was significant in the U87 and MCF-7 cell lines (decreases of 62(+/-5)% ($p<0.01$) and 75(+/-16)% ($p<0.01$), respectively) (Figures 3.9C and 3.10C, respectively). Both *PFKL* and *PFKP* expression were unaffected by HIF-2α knockdown in all three cell lines (Figures 3.9A-3.11A and 3.9C-3.11C, respectively). These

findings confirmed that *PFK-1* regulation occurs in a cell-specific manner and that *PFKL* and *PFKP* can be regulated by HIF-1α, but are independent of HIF-2α expression.

The most uniform findings were for *PFKFB3* and *PFKFB4* expression, which were shown to be HIF-1α-dependent and HIF-2α-independent in all three cell lines. The reduction in *PFKFB4* expression with HIF-1α knockdown was consistent in the three cell lines (U87: 82(+/-22)% ($p<0.01$); MCF-7: 79(+/-25)% ($p<0.05$); PC3: 75(+/-9)% ($p<0.001$)) (Figures 3.9G, 3.10G and 3.11G, respectively). However, *PFKFB3* expression in the PC3 cell line was apparently less sensitive to HIF-1α knockdown (decrease of 62(+/-6)% from the control, ($p<0.001$)) (Figure 3.11F), compared to the U87 and MCF-7 cell lines (decreases of 80(+/-20)% ($p<0.01$) and 85(+/-25)% ($p<0.05$), respectively, from the scramble hypoxic controls) (Figures 3.9F and 3.9G, respectively). This decreased sensitivity was unrelated to fold change of expression compared to basal *PFKFB3* levels. However, it was noted that the degree of siRNA-mediated *HIF-1α* suppression was proportionally lower for the PC3 cell line (expression decreased by 60(+/-7)% ($p<0.01$) from scramble hypoxic control), compared to the U87 and MCF-7 cell lines (decreases of 76(+/-3%) ($p<0.01$) and 73(+/-11%) ($p<0.05$) respectively, from the scramble hypoxic controls) (Figure A2.1, Appendix). This could potentially account for that observation.

3.2.5: PFKFB3 and PFKFB4 proteins were induced in hypoxia in a HIF-1α-dependent and HIF-2α-independent manner in U87, MCF-7 and PC3 cells.

The clear relationship between *HIF-1α* and *PFKFB3*/*PFKFB4* expression at the RNA level was then examined at the protein level, using U87, MCF-7 and PC3 cell lysates taken at the same time as RNA extracts from the reverse transfection experiment. The lysates were probed with specific PFKFB3, PFKFB4, HIF-1α and HIF-2α antibodies, with β-actin used as a loading control (U87: Figure 3.12A; MCF-7: Figure 3.12B; PC3: Figure 3.12C).

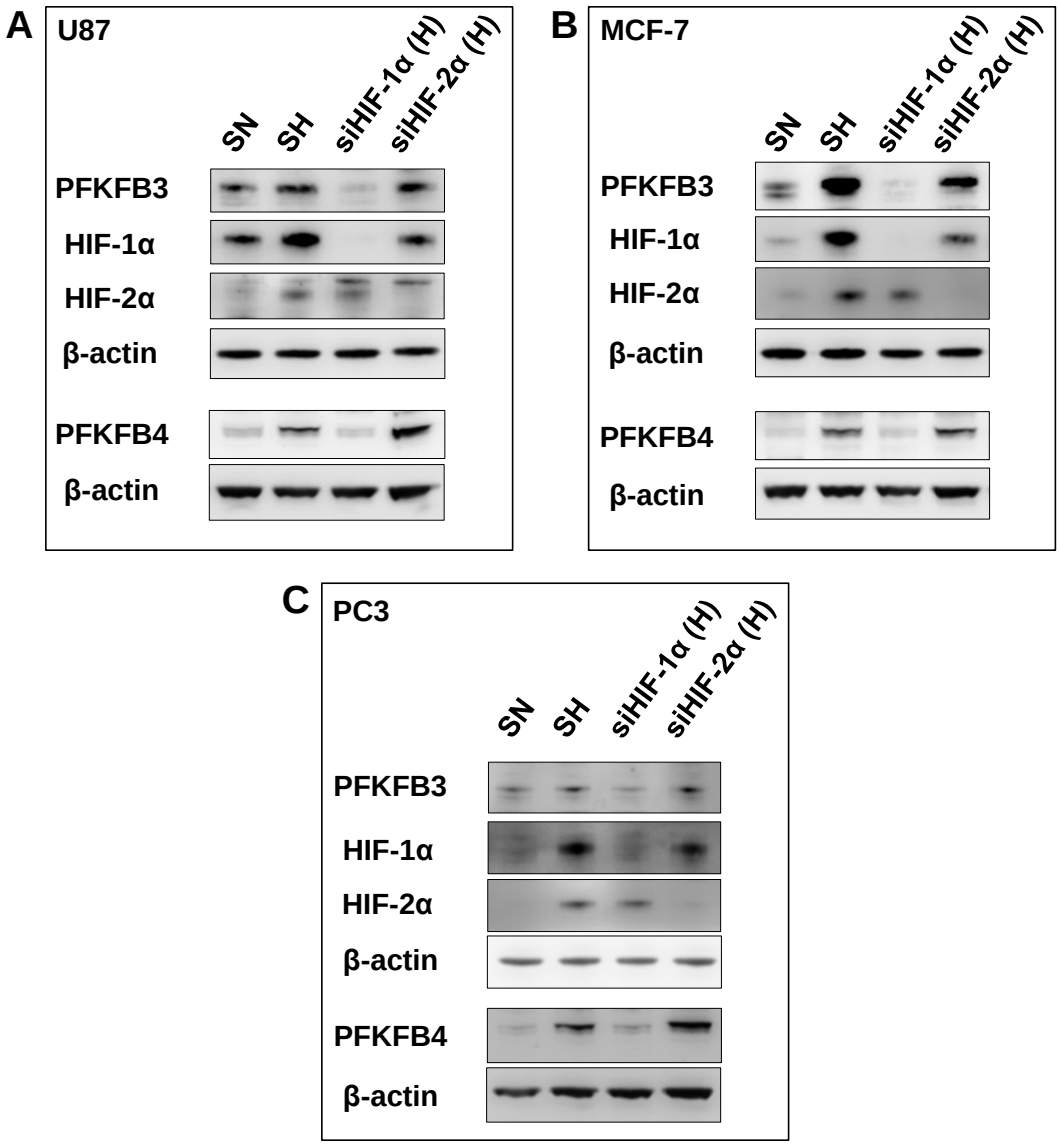

Figure 3.12: Western blot showing HIF-1α-dependence and HIF-2α-independence of PFKFB3 and PFKFB4 expression. siRNA knockdown of HIF-1α suppressed hypoxic PFKFB3 and PFKFB4 induction in **(A)** U87, **(B)** MCF-7 and **(C)** PC3 cells after 48 hours hypoxic exposure, whereas their expression was unaffected by siHIF-2α. S: Scramble siRNA, N: Normoxia, H: Hypoxia. Representative images of n≥2 replicates.

The Western blots confirmed efficient knockdown of HIF-1α and HIF-2α and demonstrated clear HIF-1α dependence, and HIF-2α independence of both PFKFB3 and PFKFB4 expression in all three cell lines (Figure 3.12), supporting findings at the RNA level. siRNA knockdown of HIF-1α and HIF-2α had no effect on TIGAR protein expression in the three cell lines (Figure A3.1, Appendix). This was anticipated, having previously observed TIGAR expression to be unchanged under hypoxic conditions (Figures 3.4-3.6).

3.2.6: High *PFKFB4* mRNA expression was correlated with poor prognosis in breast cancer patients.

As PFKFB3 and PFKFB4 had emerged as the most important isoenzymes from the current study, it was interesting to examine literature reports for any relationship between PFKFB3 or PFKFB4 expression and prognosis. In fact, very few such studies exist, although a recent report showed increased *PFKFB4* expression was significantly correlated with reduced overall survival of glioblastoma patients (Goidts, Bageritz et al. 2011). Furthermore, as part of the current study, an in-house clinical data set of 216 breast cancer patients was analysed by Dr Laura Winchester and Dr Francesca Buffa (Harris Lab) to examine any relationship between *PFKFB4* expression and prognosis. The samples were ranked according to *PFKFB4* expression and split into approximately equal groups according to level of expression; high, medium and low (Figure 3.13).

The data showed a significant correlation ($p<0.01$) between *PFKFB4* mRNA expression and relapse- free survival over a 10 year period, suggesting *PFKFB4* may be an important prognostic marker. These findings support an important role for PFKFB4 in carcinogenesis. No significant correlation between *PFKFB3* mRNA expression and relapse free survival was observed in the same data set.

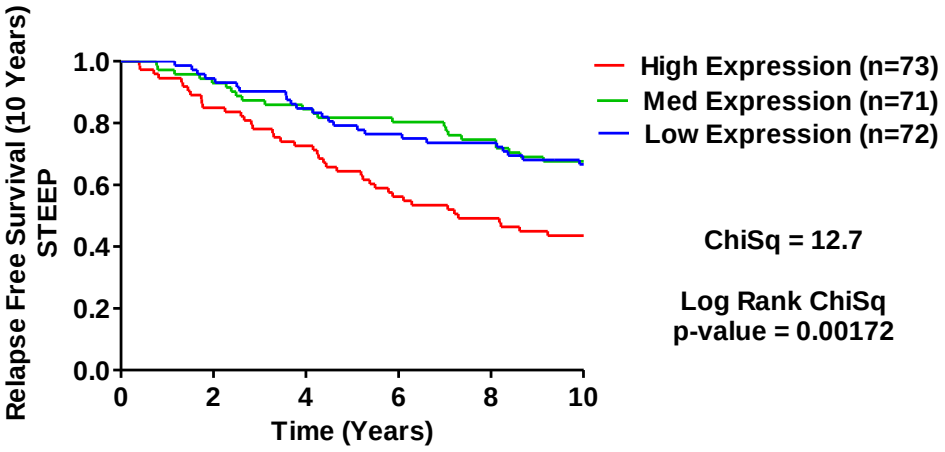

Figure 3.13: Analysis of relapse free survival and *PFKFB4* mRNA expression in breast cancer patients. High *PFKFB4* mRNA expression was correlated with reduced relapse free survival of breast cancer patients. Analysis performed by Dr Laura Winchester and Dr Francesca Buffa, using an in-house breast cancer data set.

3.2.7: Relative *PFKFB3, PFKFB4* and *TIGAR* mRNA expression varied markedly in a panel of cell lines under normoxic and hypoxic conditions.

In order to further explore the relationship between *PFKFB3*, *PFKFB4* and *TIGAR* expression, the study was extended to include an additional 6 breast cancer cell lines (T47D, MDA-MB-231, BT549, SKBR3, MDA-MB-468 and BT20), 1 prostate cancer cell line (DU145) and the untransformed MCF-10 breast cell line as a control (Figure 3.14). Relative expression of the three enzymes in all cell lines was normalised to DU145 normoxic *PFKFB3* expression, which had the highest basal *PFKFB3* expression, as shown in Figures 3.14A normoxia) and 3.14B (48 hours hypoxia). For ease of reference, hypoxic time courses for individual cell lines, normalised to t = 0 h *PFKFB3* expression, are shown in Figures A4.1A-A4.1K of the Appendix. Graphs displaying relative isoenzyme mRNA expression at the 24 hours and 72 hours hypoxia time points are also shown in Figure A5.1, Appendix. It was immediately apparent that constitutive enzyme expression again varied markedly between cell lines, including those of the same tissue type (Figure 3.14). *PFKFB3* expression exceeded *PFKFB4* expression in most of the cell lines under normoxic conditions, with the exception of PC3 (Figure 3.14A). *TIGAR* expression also exceeded *PFKFB4* expression in all cell lines

under basal conditions, but no general relationship with *PFKFB3* expression was observed (Figure 3.14A). Interestingly, the untransformed MCF-10 cell line was not distinguished from other cell lines by its expression pattern (Figure 3.14).

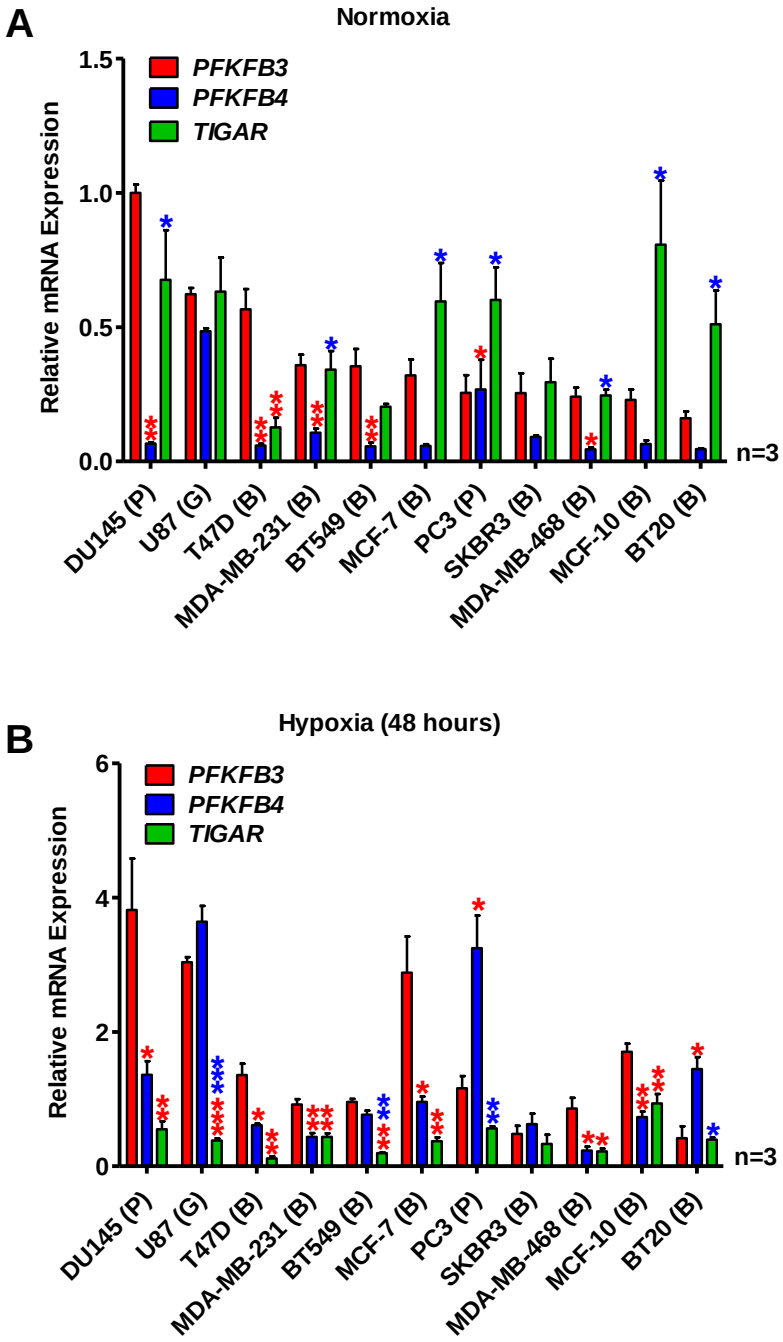

Figure 3.14: Relative *PFKFB3*, *PFKFB4* and *TIGAR* mRNA expression in a panel of cell lines under **(A)** normoxic and **(B)** hypoxic (48 hours) conditions. Relative mRNA expression varied markedly and was normalised to normoxic DU145 *PFKFB3* expression and cell lines ordered by decreasing normoxic *PFKFB3* expression. n=3; *(p<0.05), **(p<0.01), ***(p<0.001), ****(p<0.0001); One-way ANOVA analysis with Bonferroni correction performed within each cell line, with * denoting a significant difference from *PFKFB3* expression, and * denoting a significant difference from *PFKFB4* expression. B (breast cell line), G (glioblastoma cancer cell line), P (prostate cancer cell line).

The relative expression of *PFKFB3* and *PFKFB4* mRNA were not correlated under normoxic conditions (linear regression analysis: R^2 = 0.04, p = 0.28; not significant) (Figure 3.15A), and there was only weak positive correlation under hypoxic conditions (linear regression analysis: R^2 = 0.12, p = 0.048; significant) (Figure 3.15B). This suggested that *PFKFB3* and *PFKFB4* expression are regulated independently of one another, in a cell-specific manner.

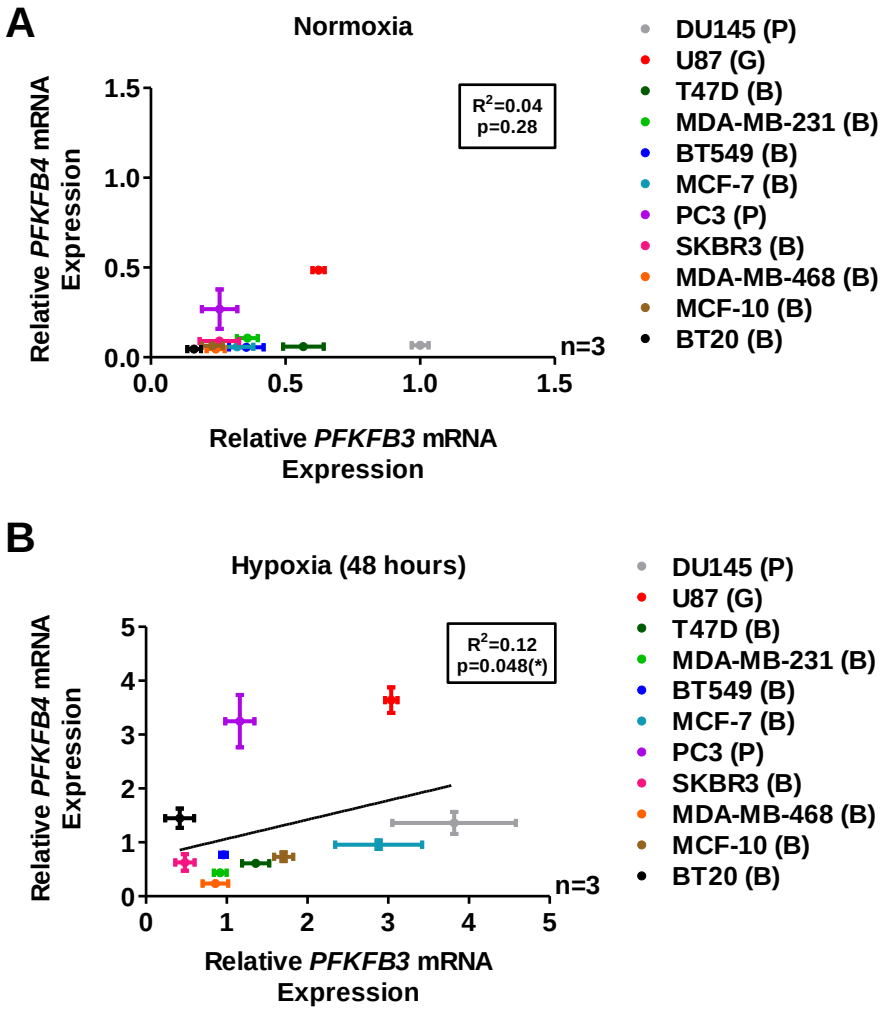

Figure 3.15: Comparison of relative *PFKFB3* and *PFKFB4* mRNA expression in a panel of cell lines under **(A)** normoxic and **(B)** hypoxic conditions. There was no correlation between relative *PFKFB3* and *PFKFB4* mRNA expression under **(A)** normoxic conditions and only weak positive correlation after **(B)** 48 hours hypoxia. mRNA expression values were normalised to normoxic DU145 *PFKFB3* expression. n=3. Linear regression analysis performed; *(p<0.05), **(p<0.01), ***(p<0.001), ****(p<0.0001). B (breast cell line), G (glioblastoma cancer cell line), P (prostate cancer cell line).

In all cell lines examined there was a significant increase in *PFKFB3* and *PFKFB4* expression under hypoxic conditions. The hypoxic fold change (48 hours) of *PFKFB3* was lowest in

SKBR3 breast cancer cells (1.9-fold) and highest in MCF-7 breast cancer cells (9.0-fold). The hypoxic fold change (48 hours) of *PFKFB4* was more variable, being lowest in MDA-MB-231 breast cancer cells (4.1-fold) and highest in BT20 breast cancer cells (31.6-fold) (Table 3.1 and Figure A4.1, Appendix). A previous study reported 3.0-fold and 3.5-fold *PFKFB4* mRNA induction under hypoxic conditions for T47D and MCF-7 breast cancer cells, respectively, after 6 hours exposure to 1% oxygen (Minchenko, Opentanova et al. 2005). The results presented in Table 3.1 demonstrate respective fold-induction values of 10.4-fold and 16.6-fold for the same cell lines after 48 hours exposure to 0.1% oxygen, demonstrating higher maximal *PFKFB4* fold-induction than previously reported.

It was interesting to note that there was no correlation between hypoxic fold change of *PFKFB3* and *PFKFB4* mRNA expression after 48 hours hypoxia (linear regression analysis: $R^2 = 0.005$, $p = 0.84$; not significant) (Figure 3.16 and Table 3.1). This further indicated the two isoenzymes are regulated independently of one another, in a cell-specific manner. In all cases the hypoxic fold change of *PFKFB4* expression exceeded that of *PFKFB3* expression (Table 3.1). This tentatively suggested PFKFB4 may be more important in adapting to hypoxia and regulating the glycolytic phenotype under such conditions.

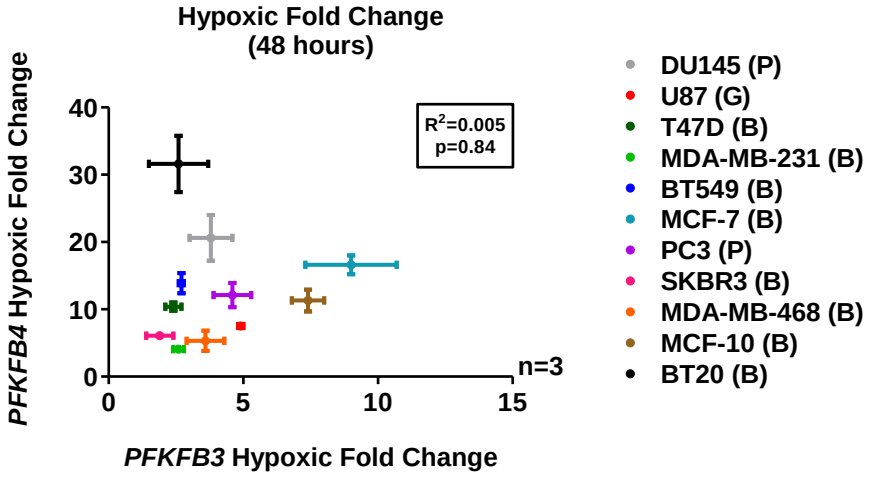

Figure 3.16: Comparison of fold change of *PFKFB3* and *PFKFB4* mRNA expression after exposure to hypoxia (48 hours) in a panel of cell lines. No correlation was observed. n=3. Linear regression analysis performed. B (breast cell line), G (glioblastoma cancer cell line), P (prostate cancer cell line).

Consistent with previous findings, no significant change in *TIGAR* mRNA expression was observed under hypoxic conditions in any of the cell lines examined (Figure 3.14 and Figure A4.1, Appendix). This indicated that under hypoxic conditions, PFKFB3 and PFKFB4 would have greater importance in regulating [F-2,6-BP] and therefore glycolytic flux, with TIGAR comparatively more important under basal conditions.

	Fold Change in mRNA Expression (48 h Hypoxia)				**Relative Normoxic mRNA Expression**
Cell Line	***PFKFB3***	***PFKFB4***	**ER Status**	**p53 Status**	***TIGAR***
SKBR3 (B)	1.9 (+/- 0.5)	6.1 (+/- 0.3)	Negative	Mutant	0.29 (+/- 0.09)
T47D (B)	2.4 (+/- 0.3)	10.4 (+/- 0.6)	Positive	Mutant	0.13 (+/- 0.04)
MDA-MB-231 (B)	2.6 (+/- 0.2)	4.1 (+/- 0.4)	Negative	Mutant	0.34 (+/- 0.07)
BT20 (B)	2.6 (+/- 1.1)	31.6 (+/- 4.2)	Negative	Mutant	0.51 (+/- 0.13)
BT549 (B)	2.7 (+/- 0.1)	13.9 (+/- 1.5)	Negative	Mutant	0.20 (+/- 0.01)
MDA-MB-468 (B)	3.6 (+/- 0.7)	5.3 (+/- 1.5)	Negative	Mutant	0.25 (+/- 0.02)
DU145 (P)	3.8 (+/- 0.8)	20.6 (+/- 3.4)	N/A	Mutant	0.68 (+/- 0.19)
PC3 (P)	4.6 (+/- 0.7)	12.1 (+/- 1.8)	N/A	Null	0.60 (+/- 0.12)
U87 (G)	4.9 (+/- 0.1)	7.5 (+/- 0.5)	N/A	WT	0.63 (+/- 0.13)
MCF-10 (B)	7.4 (+/- 0.6)	11.3 (+/- 1.6)	Negative	WT	0.81 (+/- 0.24)
MCF-7 (B)	9.0 (+/- 1.7)	16.6 (+/- 1.4)	Positive	WT	0.60 (+/- 0.14)

Table 3.1: Comparison of hypoxic fold change of *PFKFB3* and *PFKFB4* mRNA expression, ER status, p53 status and relative basal *TIGAR* mRNA expression in a panel of cell lines. The fold change of *PFKFB3* and *PFKFB4* mRNA expression after 48 hours hypoxic exposure were not correlated with one another. No correlation was observed in the breast cell lines between hypoxic fold change of *PFKFB3* or *PFKFB4* mRNA expression and estrogen receptor (ER) status. Fold change of *PFKFB3* appeared to be linked to p53 status, being highest in those cell lines with wild-type p53. Constitutive *TIGAR* expression was highest in those breast cell lines with wild-type *p53*. n=3. B (breast cell line), G (glioblastoma cancer cell line), P (prostate cancer cell line), ER (estrogen-receptor), WT (wild type).

It might be predicted that those cell lines with lowest basal *PFKFB3* or *PFKFB4* expression would exhibit the highest fold induction of these isoenzymes under hypoxic conditions, in order to promote the pro-survival glycolytic phenotype to the maximum extent. However, a general analysis of all cell lines examined showed no correlation between basal expression and hypoxic fold change for either isoenzyme (data not shown). Nevertheless, examination of the breast cell lines alone showed no correlation for *PFKFB3* expression, but there was a significant inverse relationship between basal *PFKFB4* expression and hypoxic fold induction of *PFKFB4* (linear regression analysis: $R^2 = 0.29$, $p = 0.007$; significant) (Figures 3.17A and

3.17B). This supported the findings of a previous study by Bobarykina and colleagues (Bobarykina, Minchenko et al. 2006), which examined pancreatic and gastric cancer cell lines. The authors of that study observed a similar inverse relationship between basal *PFKFB4* expression and hypoxic fold change. It may well be the case that this is a general phenomenon within cell lines from the same tissue origin. The more predictable nature of *PFKFB4* mRNA expression across cell lines under hypoxia would again be consistent with a more important role for PFKFB4 in mediating the physiologic response to hypoxia.

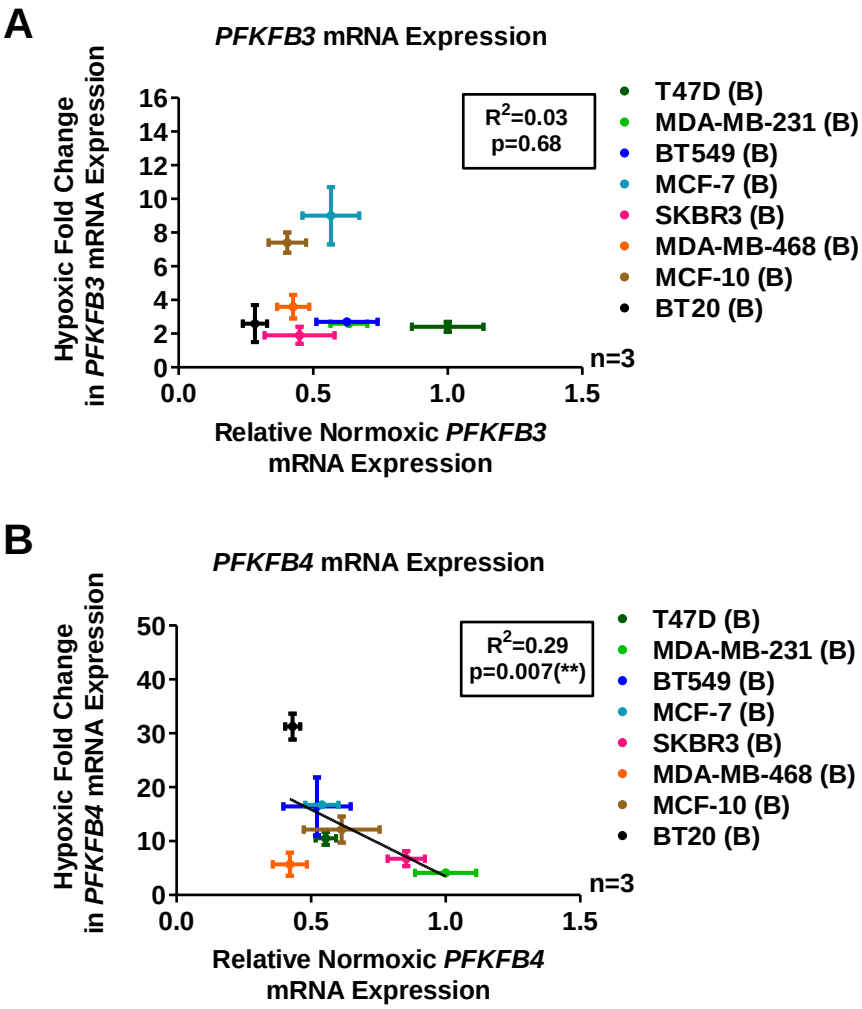

Figure 3.17: Comparison of relative basal mRNA expression and hypoxic fold change of **(A)** *PFKFB3* and **(B)** *PFKFB4* in a panel of breast cell lines. **(A)** There was no correlation between basal expression and hypoxic fold-induction of *PFKFB3* mRNA expression after 48 hours in a panel of breast cell lines. **(B)** There was significant inverse correlation between basal expression and hypoxic-fold induction of *PFKFB4* mRNA expression after 48 hours in a panel of breast cell lines. Normoxic *PFKFB3* mRNA expression normalised to T47D **(A)** and normoxic *PFKFB4* mRNA expression normalised to MDA-MB-231 **(B)**. n=3. Linear regression analysis performed; *(p<0.05), **(p<0.01), ***(p<0.001), ****(p<0.0001). B (breast cell line).

In their published study, Minchenko and colleagues (Minchenko, Opentanova et al. 2005) reported elevated hypoxic induction of *PFKFB3* for breast cell lines that were estrogen-receptor (ER) positive, compared to those that were estrogen-receptor negative. The present study examined a more extensive panel of breast cell lines and found no such relationship between ER status and hypoxic fold-induction of *PFKFB3* or *PFKFB4* mRNA expression (Table 3.1). Minchenko and colleagues used a nuclease protection assay to measure RNA expression in their study, whereas the experiments described in this Chapter made use of qRT-PCR, which is a more sensitive method for detecting and quantifying gene expression. It is possible differences in assay sensitivity would account for the disparate observations. Intriguingly, the degree of *PFKFB3* induction in the cell lines appeared to be stratified according to *p53* status, with those cell lines exhibiting the highest *PFKFB3* induction possessing wild-type *p53* (U87, MCF-10, MCF-7) (Table 3.1). A more extensive cell line screen would need to be performed to assess whether this is a general phenomenon. It would potentially mean the tumour suppressor protein p53 might have a role in regulating the balance of PFK-2/FBPase-2 isoenzyme expression, leading to dysregulation of [F-2,6-BP] upon *p53* mutation.

Furthermore, within the breast cell lines there appeared to be a relationship between *p53* status and constitutive *TIGAR* expression, with those cell lines expressing wild-type *p53* (MCF-10 and MCF-7) having the highest basal *TIGAR* levels (Table 3.1). This was consistent with studies showing *TIGAR* to be a *p53*-inducible gene (Bensaad, Tsuruta et al. 2006). High relative *TIGAR* expression levels in the *p53*-mutant prostate cancer cell lines DU145 and PC3 indicated that *p53*-independent regulation of *TIGAR* expression might be more important in these cell lines.

3.2.8: U87, MCF-7 and PC3 cell lines were selected for further study, due to their differing relative *PFKFB3:PFKFB4* mRNA expression ratios

PFKFB3 and PFKFB4 had emerged from this study as the most strongly induced PFK isoenzymes under hypoxic conditions, as well as showing consistently high constitutive expression across different cell lines. With a view to further studying the relationship between these two isoenzymes, it was necessary to select suitable cell lines with differing isoenzyme expression profiles under normoxic and hypoxic conditions. In considering the full panel of cell lines examined, the three cell lines originally chosen (U87, MCF-7 and PC3) were selected. MCF-7 was selected for its high *PFKFB3:PFKFB4* expression ratio, U87 for its similar expression ratio, and PC3 for its low expression ratio, with these differences particularly apparent under hypoxic conditions (Table 3.2). A Western blot comparing relative PFKFB3 and PFKFB4 protein expression levels between the cell lines over a 72 hour hypoxic time course corroborated the RNA-level findings (Figure 3.18). PFKFB3 expression was highest in the MCF-7 cells at the end of the time course, whereas PFKFB4 expression was highest in the PC3 cells; TIGAR showed no consistent difference between replicates (Figure 3.18).

	Relative *PFKFB3:PFKFB4* mRNA Expression	
Cell Line	**Normoxia**	**Hypoxia (48 h)**
MCF-7	5.3 (+/- 0.8)	2.9 (+/- 0.4)
U87	1.3 (+/- 0.04)	0.8 (+/- 0.1)
PC3	1.0 (+/- 0.3)	0.4 (+/- 0.04)

Table 3.2: Relative *PFKFB3:PFKFB4* mRNA expression ratios in MCF-7, U87 and PC3 cell lines under normoxic and hypoxic conditions. The expression ratios were markedly different, being highest in MCF-7 and lowest in PC3 cells. This made these three cell lines suitable for further study to investigate the relationship between PFKFB3 and PFKFB4.

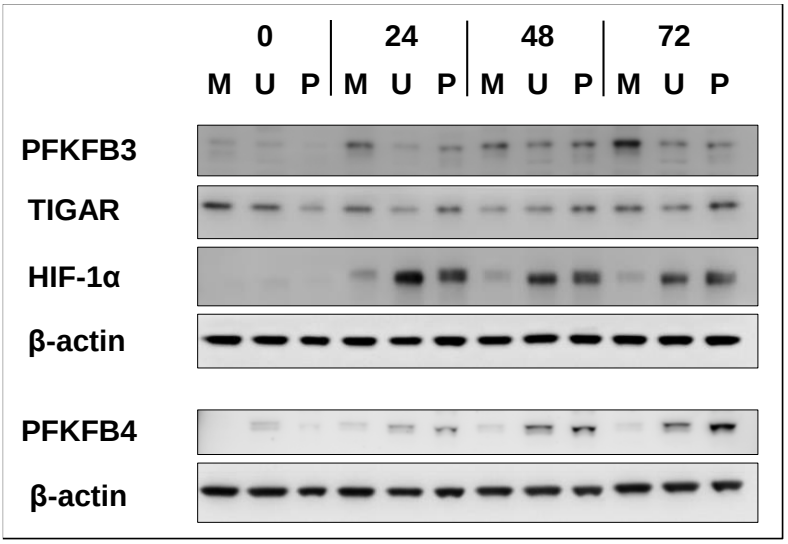

Figure 3.18: Western blot of HIF-1α, PFKFB3, PFKFB4 and TIGAR expression in MCF-7 (M), U87 (U) and PC3 (P) cells during a 0-72 h hypoxia time course. PFKFB3 expression was highest in MCF-7 cells, whereas PFKFB4 expression was highest in PC3 cells, after 72 hours hypoxia. TIGAR expression showed no consistent pattern between replicates. β-actin was used as a loading control. n≥2 independent replicates.

3.3: Discussion

The marked variation in relative levels of the individual *PFK-1*, *PFK-2/FBPase-2* and *TIGAR* isoenzymes under basal conditions between the cell lines examined was very clear, with this pattern changing significantly under hypoxic conditions (Figures 3.14A and 3.14B). A complex relationship of regulation and expression pattern of individual isoenzymes had emerged.

The relative contribution of the PFKL and PFKP subunits to total PFK-1 expression is known to increase in transformed cells (Sanchez-Martinez and Aragon 1997), these subunits being less sensitive to inhibition by ATP and citrate. The observation presented in this Chapter, that the relative expression of both *PFKL* and *PFKP* further increase in hypoxia (Figures 3.4A-3.6A and 3.4C-3.6C) is consistent with their role in promoting a more glycolytic phenotype through higher PFK-1 activity, which is favoured under such conditions. The results demonstrate that regulation of both subunits is HIF-1α-dependent, and HIF-2α-independent (Figures 3.9A-3.11A and 3.9C-3.11C).

The expression of *PFKFB1* was over an order of magnitude lower than the other *PFK-2/FBPase-2* isoenzymes in all cell lines examined (Figures 3.1C, 3.2C and 3.3C), suggesting that its role in regulating intracellular [F-2,6-BP] would be less important than the other isoenzymes. HIF-1α-mediated repression of *PFKFB1* expression (Figures 3.9D, 3.10D and 3.11D) would further diminish the influence of PFKFB1 expression on intracellular [F-2,6-BP] in hypoxia. Although basal *PFKFB2* expression was comparatively high in MCF-7 and PC3 cells, its relative expression ratio was diminished under hypoxic conditions. This indicates that PFKFB2 would be a less suitable target for a more general therapy for solid tumours and across different tumour types, compared to PFKFB3 and PFKFB4. The latter two isoenzymes were more consistently expressed in different cell lines, under both normoxic and hypoxic conditions.

In fact, the findings of this study confirmed that PFKFB3 and PFKFB4 were the most strongly induced isoenzymes under hypoxic conditions in all cell lines examined, at both the RNA and protein level (Figures 3.4F-3.6F, 3.4G-3.6G, 3.8 and 3.14). This induction was regulated in a HIF-1α-dependent and HIF-2α-independent manner (Figures 3.9F-3.11F, 3.9G-3.11G and 3.12). Comparison of the relative expression of HIF-1α protein in the different cell lines under hypoxic conditions, showed U87 and PC3 cells to have much higher levels of HIF-1α than MCF-7 cells (Figure 3.18). It was somewhat surprising then that *PFKFB3* and *PFKFB4*, as HIF-1α-target genes, were the most strongly induced in the MCF-7 cells under hypoxic conditions (Figures 3.5F and 3.5G). This demonstrated the complexity of regulation, which extends beyond HIF-1α expression alone. In all cases, *PFKFB4* hypoxic fold-induction exceeded that of *PFKFB3*, potentially suggesting PFKFB4 is relatively more important under hypoxic conditions. This will be further investigated.

TIGAR is known to have high F-2,6-BPase activity and was found to be consistently expressed at comparatively high basal levels in all cell lines studied (Figure 3.14A). Although the relative catalytic activities were not investigated, the lack of hypoxic induction led to a reduced relative expression level under hypoxic conditions (Figure 3.14B), suggesting the effect of TIGAR on total [F-2,6-BP] would be most pronounced in normoxia.

Targeting PFK-1 enzymes in cancer cells enriched with PFK-L or PFK-P subunits may provide a therapeutic opportunity, due to their elevation under hypoxic conditions, and promotion of increased glycolytic activity. However, targeting of specific monomer subunits would likely be more difficult than targeting individual enzymes. Furthermore, changes in protein expression in the hypoxic tumour micro-environment provide an opportunity for specific targeting. *PFK-L* and *PFK-P* were induced to a lesser extent under hypoxic conditions than *PFKFB3* and *PFKFB4*, suggesting the latter would be far more promising targets for selective, hypoxia-targeted therapy (Figures 3.4-3.6). The decision to focus attention on *PFKFB3* and *PFKFB4* was also supported by the literature study from Goidts and colleagues (Goidts, Bageritz et al. 2011) and an in-house analysis (Figure 3.13), which both correlated increased *PFKFB4* mRNA expression with poor prognosis. Furthermore, PFKFB3 has been reported to have the highest basal K:B activity ratio of the four isoenzymes at 740:1 (Sakakibara, Kato et al. 1997), and is therefore thought to be a key determinant of the overall intracellular concentration of F-2,6-BP. This, when coupled with data presented in this Chapter, indicated that both PFKFB3 and PFKFB4 warranted further investigation as therapeutic targets.

It was particularly striking that the relative *PFKFB3* and *PFKFB4* expression levels were so markedly different, even between cell lines of the same tissue origin e.g. breast cell lines (Figure 3.15). The hypoxia-responsiveness of *PFKFB3* did not correlate with basal expression

(Figure 3.17A), but *PFKFB4* induction was inversely correlated with basal expression in the breast cell lines (Figure 3.17B). This indicated that sufficient PFKFB4 expression may be essential for mediating the cell's physiologic response to hypoxia. Cancer cells may therefore be comparatively more sensitive to PFKFB4 depletion under hypoxic conditions and this will be further investigated.

It follows then that further study should validate both PFKFB3 and PFKFB4 as anti-tumour targets and investigate the relationship between them, in order to determine their combined effect on cancer cell growth, i.e. whether these bifunctional isoenzymes act synergistically, additively, or antagonise one another *in vitro*. If the isoenzymes were to antagonise one another, it would reduce the effectiveness of any non-specific PFK-2/FBPase-2 therapy targeting total enzyme activity. If this were the case, the findings in this Chapter would have major implications in a clinical setting. They suggest that not only will relative PFKFB3 and PFKFB4 expression vary between tumours originating from different tissues, but also between cancers from the same host tissue. Furthermore, the heterogeneic nature of individual tumours, and the intermittent hypoxic exposure, may result in markedly different PFKFB3:PFKFB4 expression ratios even between cells in the same tumour. These differing expression ratios may be difficult to predict.

This would be particularly important if cancer cells are sensitive to either individual PFKFB3 or PFKFB4 inhibition alone. It would then be vital to gain a full understanding of the tumour PFK-2/FBPase-2 expression pattern in individual patients. This would allow stratification of those patients most likely to respond to a PFKFB3-specific or a PFKFB4-specific therapy.

The lack of correlation between ER-status and basal expression / fold-change of isoenzyme expression in the breast cancer cell lines (Table 3.1) precludes ease of patient stratification

with differing PFKFB3:PFKFB4 expression ratios using this marker. PFKFB3 and PFKFB4 have both previously been reported to be up-regulated in tumour tissue (Minchenko, Ochiai et al. 2005; Minchenko, Ogura et al. 2005). However, the findings presented in this Chapter showed that the *PFKFB3:PFKFB4:TIGAR* expression pattern in the untransformed cell line MCF-10 did not distinguish this cell line from the other cancer cell lines (Figure 3.14). This suggested that the most effective PFKFB3/PFKFB4-targeted therapies might be those more specifically targeted to cancer cells, e.g. hypoxia-targeted therapies. It will therefore be important to determine the sensitivity of cancer cell lines to depletion of these isoenzymes, particularly under hypoxic conditions.

The selection of MCF-7, U87 and PC3 for further study due to their differing PFKFB3/PFKFB4 expression ratios was made in order to permit the interplay of these isoenzymes to be fully explored and the issue of isoenzyme-specificity as an anti-cancer treatment to be addressed. This will enable the therapeutic potential of PFK-2/FBPase-2 inhibition to be more fully explored in the next Chapter.

Chapter 4: Examining the Effect of PFKFB3 and PFKFB4 on Cancer Cell Growth

4.1: Introduction and Aims

Having established that PFKFB3 and PFKFB4 were the most strongly induced PFK-2/FBPase-2 isoenzymes in a panel of cancer cell lines, it was necessary to validate them individually, and collectively, as potential anti-tumour targets. As previously discussed, a number of literature reports have linked suppression of both PFKFB3 and PFKFB4 expression with reduced cancer cell proliferation (Clem, Telang et al. 2008; Goidts, Bageritz et al. 2011; Jeon, Jang et al. 2011; Ros, Santos et al. 2012).

However, there have been no reports relating these findings to the relative basal expression levels of the isoenzymes in the relevant cell lines, or any studies examining their effect on cancer cell growth under hypoxic conditions. The marked increase in PFKFB3 and PFKFB4 expression under hypoxic conditions suggests they are intimately involved in regulating [F-2,6-BP] and therefore the glycolytic pro-survival phenotype in hypoxia. This may potentially enhance the sensitivity of hypoxic cells to PFKFB3/PFKFB4 depletion.

The hypoxic tumour microenvironment is a feature almost exclusive to solid tumours and so inhibiting these isoenzymes may offer the means to selectively target the hypoxic sub-fraction of a tumour, providing that such inhibitors can be delivered effectively. An understanding of how cells in the hypoxic fraction of tumours might respond to PFKFB3 or PFKFB4 inhibition is therefore required.

PFKFB3 has an unusually high basal kinase:bisphosphatase (K:B) activity ratio and is thus considered to be the key determinant of intracellular [F-2,6-BP], and correspondingly glycolytic flux (Sakakibara, Kato et al. 1997; Atsumi, Chesney et al. 2002). The predominant

function of PFKFB4 is less clear. Although originally thought to possess a near-equal K:B ratio (Okar, Manzano et al. 2001), recent reports have questioned this notion. A study by Goidts and colleagues observed decreased lactate and ATP production in glioma stem-like cells in response to PFKFB4 shRNA knockdown, implying PFKFB4 might have predominant kinase activity in these cells (Goidts, Bageritz et al. 2011). However, a further study by Ros and colleagues reported PFKFB4 in prostate cancer cell lines to have high bisphosphatase activity under lipid-limited growth conditions (Ros, Santos et al. 2012).

The relative K:B activity of PFKFB4 in cancer cells may be crucial, for if it were to have high bisphosphatase activity and thus antagonise PFKFB3 kinase activity, it would potentially decrease the efficacy of non-specific PFK-2/FBPase-2 inhibitors targeting total isoenzyme enzymatic activity. This would signal a requirement for isoenzyme-specific inhibition, unless the kinase or bisphosphatase activity of these isoenzymes could be inhibited separately. To date, the only study examining this possibility is a recent report by Ros and colleagues, which showed double PFKFB3/PFKFB4 knockdown to reduce apoptosis mediated by PFKFB4 silencing in prostate cancer cells under normoxic, lipid-limited growth conditions (Ros, Santos et al. 2012).

The development of isoenzyme-specific PFKFB3 or PFKFB4 inhibitors would likely be extremely challenging given that the isoenzymes share >85% sequence homology in their core catalytic domains (Kim, Manes et al. 2006). Indeed, the PFKFB3 inhibitors identified in a recent docking study that made use of the PFKFB3 crystal structure still showed a lack of specificity (Seo, Kim et al. 2011).

It was clear that the reciprocal relationship between PFKFB3 and PFKFB4 required further investigation, particularly in the context of hypoxia and cell lines with differing

PFKFB3:PFKFB4 expression ratios. Furthermore, a consistently high relative basal level of *TIGAR* mRNA expression was previously observed in a panel of cell lines (Figure 3.14, Chapter 3). TIGAR has high bisphosphatase activity (Bensaad, Tsuruta et al. 2006), so this warranted further investigation of its expression, to probe any compensatory relationship with PFKFB3 and/or PFKFB4 expression.

The work in this Chapter aimed to address all of these issues through initially validating the isoenzymes as potential anti-tumour targets, exploring potential antagonism between them in growth assays and then relating these observations to changes in [F-2,6-BP] and metabolic outputs, including lactate and ATP production. In doing so, it was intended that an answer to the question of isoenzyme-specific or non-specific PFK-2/FBPase-2 inhibition as an anti-cancer strategy should emerge.

4.2: Results

4.2.1: siRNA Validation

To further investigate function and also validate PFKFB3 and PFKFB4 as potential anti-tumour targets, it was necessary to obtain and validate siRNAs to selectively suppress the expression of the corresponding genes. Both small molecule inhibitors and siRNAs eliminate enzymatic function, but it is important to consider that the inactivated enzyme is still present after small molecule inhibition.

4.2.1.1: Single and double siRNA knockdown reduced constitutive expression of PFKFB3 and PFKFB4 at the mRNA and protein level.

Commercially available siRNA pools (combination of 4 individual sequences) for both PFKFB3 and PFKFB4 were purchased (Dharmacon) and their activity and PFK-2/FBPase-2 specificity confirmed in a reverse transfection experiment with MCF-7 cells (Figure A6.1,

Appendix). The use of multiple siRNA sequences in a pool risks potential off-target effects, so the individual sequences used in the Dharmacon pools were purchased from Invitrogen^{TM}, and each tested in an *in vitro* sulforhodamine B (SRB) 2D growth assay (Figure 4.1). The SRB assay measures cellular protein content, and is thus a good indicator of relative cell number. Any chemical modifications of the scramble control siRNA sequence and the test sequences should be kept consistent, and the phenotype and viability of control siRNA-treated cells should be closely matched to samples treated with transfection reagent only (Mock). The selected scramble control (Invitrogen^{TM}) fulfilled these criteria (Figure 4.1). If two independent siRNA sequences elicit the same phenotypic effect, the effect is most likely due to gene-specific silencing.

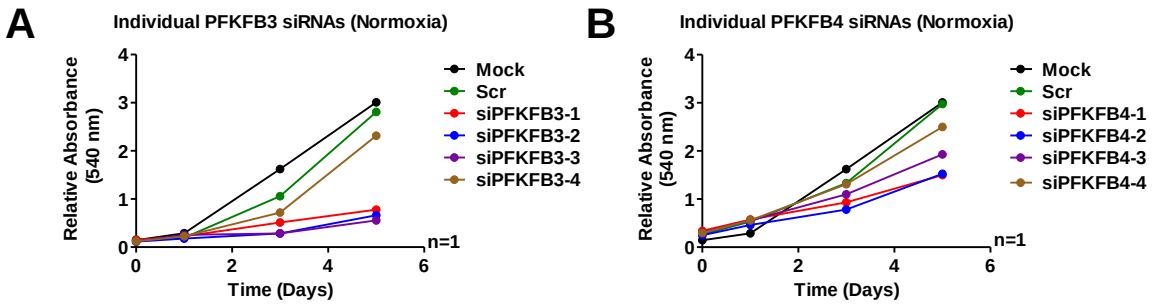

Figure 4.1: Validation of individual **(A)** PFKFB3 and **(B)** PFKFB4 siRNA sequences in MCF-7 cells using an SRB proliferation assay. This resulted in selection of siPFKFB3-1/siPFKFB3-2 and siPFKFB4-1/siPFKFB4-2 for further study. Relative absorbance at 540 nm indicates relative protein content, an indicator of relative cell number. n=1. Scr (scramble).

Accordingly, sequences siPFKFB3-1 and siPFKFB3-2 were selected and pooled for further use (future notation: siPFKFB3), as were sequences siPFKFB4-1 and siPFKFB4-2 (future notation: siPFKFB4). These pools were used at a final concentration of 20 nM. All four sequences were pooled to enable double PFKFB3/PFKFB4 knockdown (future notation: siPFKFB3and4), with use at a final concentration of 20 nM.

The pooled siRNAs were validated in reverse transfection experiments with MCF-7, U87 and PC3 cells, first at the RNA level (Figure 4.2) and then at the protein level (Figure 4.3), under

both normoxic and hypoxic conditions. Isoenzyme-specific silencing was confirmed and double PFKFB3/PFKFB4 knockdown was equally effective at reducing mRNA and protein expression as the single knockdowns (Figures 4.2 and 4.3).

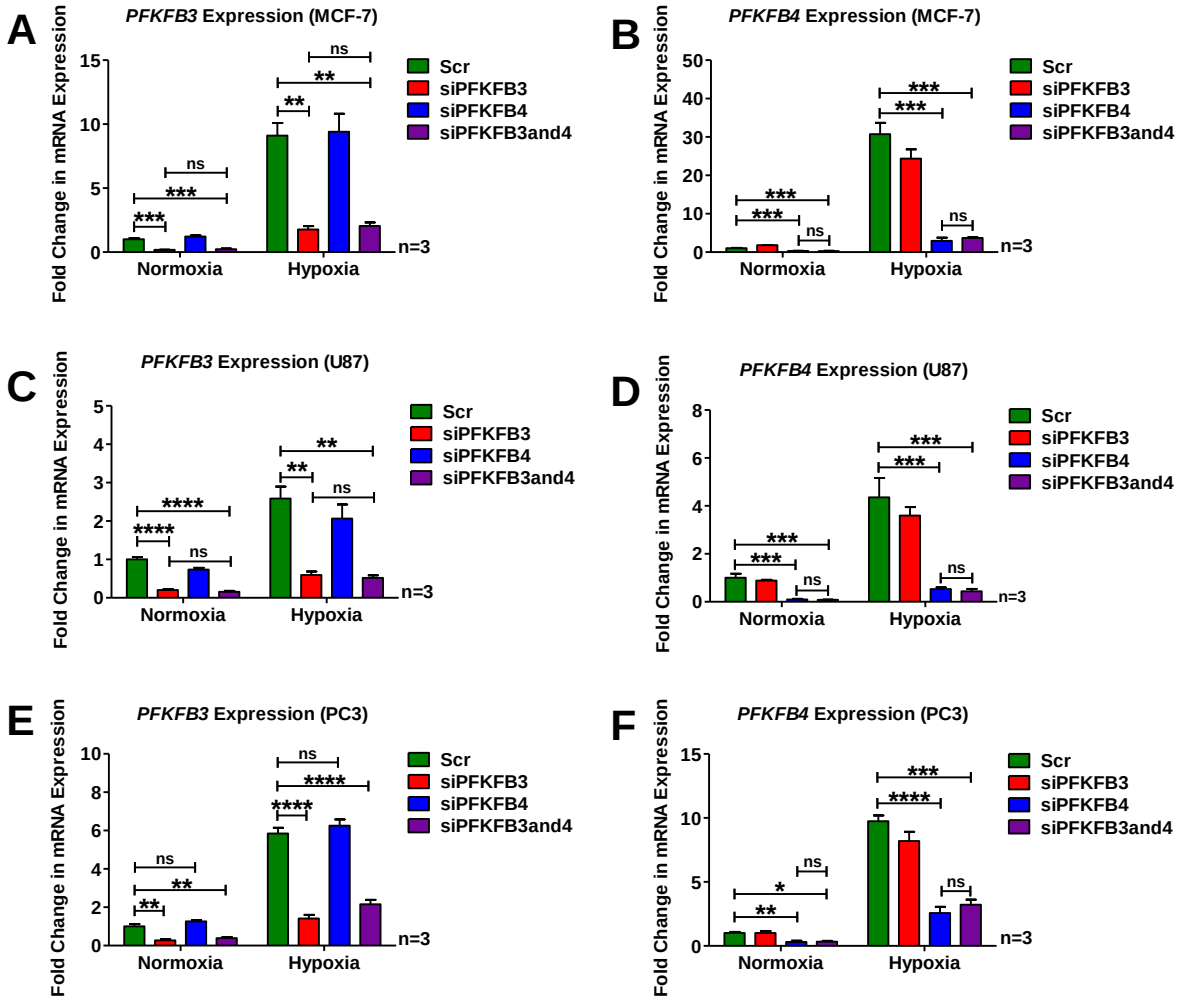

Figure 4.2: qRT-PCR validation of single and double PFKFB3/PFKFB4 siRNA knockdown at the mRNA level in MCF-7, U87 and PC3 cells under normoxic and hypoxic conditions. Single and double siRNA knockdown selectively suppressed *PFKFB3* mRNA expression in **(A)** MCF-7, **(C)** U87 and **(E)** PC3 cells, and *PFKFB4* mRNA expression in **(B)** MCF-7, **(D)** U87 and **(F)** PC3 cells under both normoxic and hypoxic conditions. siPFKFB3 was a pool of siPFKFB3-1 and siPFKFB3-2 sequences; siPFKFB4 was a pool of siPFKFB4-1 and siPFKFB4-2 sequences; siPFKFB3and4 was a pool of all 4 sequences; Scr (scramble) was a non-targeting control sequence. All siRNAs were purchased from Invitrogen™. Reverse transfections were performed at a final total siRNA concentration of 20 nM (48 h normoxia/hypoxia). n=3; One-way ANOVA analysis performed with Bonferroni correction, comparing all normoxic data sets with one another, and all hypoxic data sets with one another, for an individual isoenzyme and cell line; *($p<0.05$), **($p<0.01$), ***($p<0.001$), ****($p<0.0001$), ns (not significant).

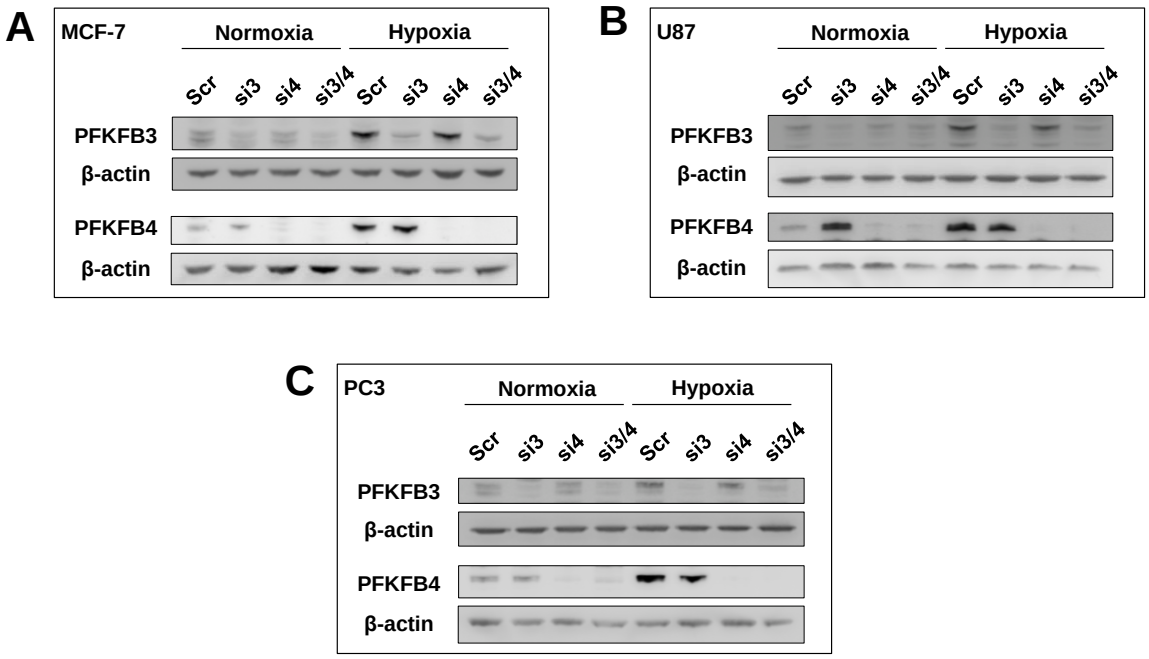

Figure 4.3: Western blot validation of single and double PFKFB3/PFKFB4 siRNA knockdown at the protein level in **(A)** MCF-7, **(B)** U87 and **(C)** PC3 cells under normoxic and hypoxic conditions. Specificity of single and double siPFKFB3 (pooled siPFKFB3-1 and siPFKFB3-2) and siPFKFB4 (pooled siPFKFB4-1 and siPFKFB4-2) knockdown were validated in **(A)** MCF-7, **(B)** U87 and **(C)** PC3 cells after 48 h normoxia/hypoxia. β-actin was used as a loading control. Representative images of n=2 replicates. Scr (scramble), si3 (siPFKFB3), si4 (siPFKFB4), si3/4 (siPFKFB3 and siPFKFB4).

It was important to identify any compensatory changes in PFKFB3 or PFKFB4 isoenzyme expression in response to knockdown of the other isoenzyme, which could impact on the effectiveness of an isoenzyme-specific inhibitor. No such changes were observed at the RNA level (Figure 4.2), but an increase in PFKFB4 protein expression was observed in U87 cells under normoxic conditions, in response to PFKFB3 knockdown (Figure 4.3B). The biological effect of this was unclear at this stage, but highlighted the importance of monitoring changes in protein expression, rather than at the mRNA level alone.

4.2.1.2: Single and double siRNA knockdown of PFKFB3 and PFKFB4 had no effect on TIGAR protein expression.

Results had previously shown high basal *TIGAR* expression in all three cell lines, as compared to expression of the PFK-2/FBPase-2 isoenzymes (Figures 3.1, 3.2 and 3.3, Chapter 3). TIGAR is known to have high F-1,6-BPase and F-2,6-BPase activity, which leads to a

decrease in the intracellular concentration of the glycolytic intermediate F-1,6-BP and the allosteric PFK-1-activator F-2,6-BP, thereby reducing glycolytic flux (Li and Jogl 2009). It was hypothesised that selective suppression of PFKFB3 or PFKFB4 expression might cause the cell to elicit a change in TIGAR expression in order to compensate for resulting changes in [F-2,6-BP]. If such a compensatory mechanism were to operate, it would reduce the efficacy of a PFK-2/FBPase-2-specific therapy and point towards a requirement for combination therapies that would allow concomitant inhibition of a PFK-2/FBPase-2 isoenzyme and modulation of TIGAR expression.

TIGAR mRNA expression was analysed in response to siPFKFB3, siPFKFB4 and siPFKFB3and4 knockdown in MCF-7, U87 and PC3 cells (Figure 4.4). A significant increase in expression in response to PFKFB4 knockdown in normoxic MCF-7 cells was observed (increase of 156(+/-51)% compared to normoxic control, $p<0.05$) (Figure 4.4A), whilst there was a significant decrease in expression in response to PFKFB3 knockdown in hypoxic PC3 cells (29(+/-9)% decrease compared to hypoxic control, $p<0.05$) (Figure 4.4C).

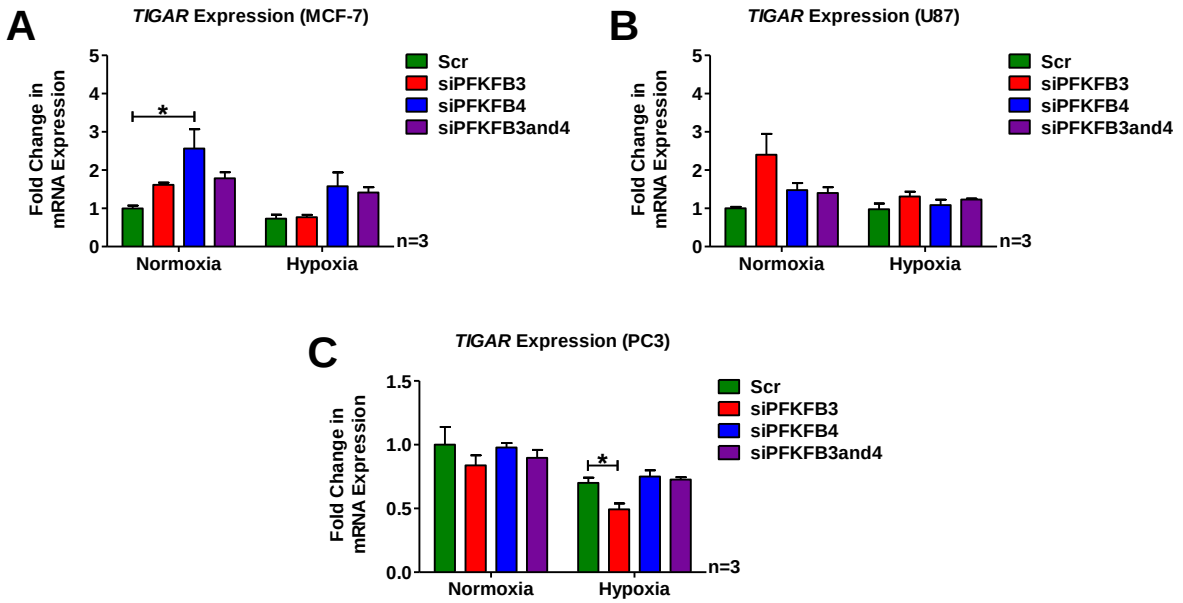

Figure 4.4: *TIGAR* mRNA expression in response to single and double PFKFB3/PFKFB4 knockdown in **(A)** MCF-7, **(B)** U87 and **(C)** PC3 cells. Expression significantly increased in response to siPFKFB4 in MCF-7 cells (normoxia) **(A)** and significantly decreased in response to siPFKFB3 in PC3 cells (hypoxia) **(B)**. n=3; One-way ANOVA analysis performed with Bonferroni correction, comparing all normoxic data sets with one another, and all hypoxic data sets with one another, for each individual cell line *($p<0.05$), **($p<0.01$), ***($p<0.001$), ****($p<0.0001$).

However, Western blot analysis of TIGAR protein expression in all three cell lines (Figures 4.5A, 4.5B and 4.5C) was inconsistent with the observed RNA-level changes. Indeed, there appeared to be no consistent change in TIGAR protein expression between replicates in response to siRNA knockdown of PFKFB3 and/or PFKFB4, which suggested that the proposed compensatory mechanism was not active in these cell lines. Accordingly, it was decided to focus further study on the PFKFB3 and PFKFB4 isoenzymes alone. This demonstrated the importance of validating RNA-level changes at the protein level.

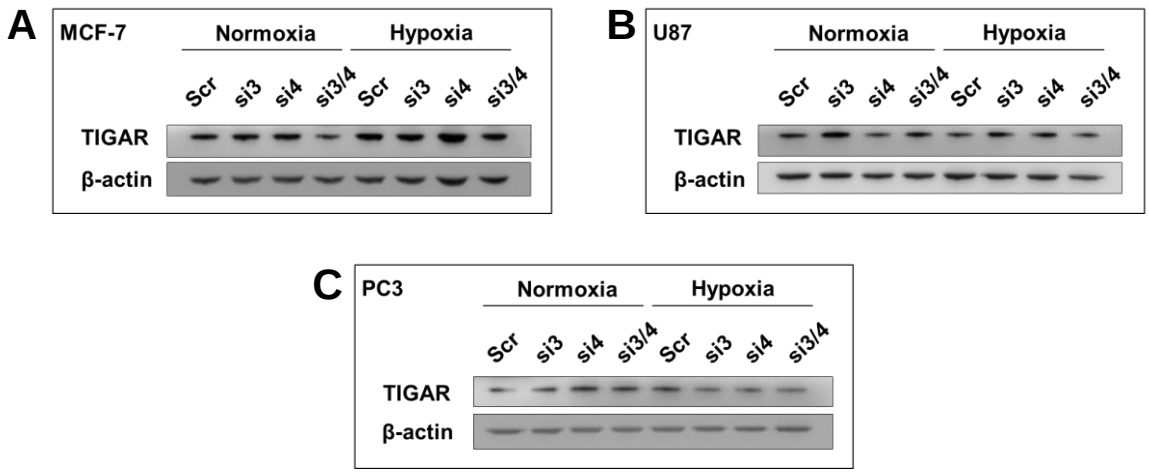

Figure 4.5: Western blots of TIGAR protein expression in response to single and double PFKFB3/PFKFB4 knockdown in **(A)** MCF-7, **(B)** U87 and **(C)** PC3 cells. No consistent changes in TIGAR protein expression were observed in response to single or double PFKFB3 or PFKFB4 knockdown after 48 h incubation in normoxia/hypoxia. β-actin was used as a loading control. Representative images of n=2 replicates. Scr (scramble), si3 (siPFKFB3), si4 (siPFKFB4), si3/4 (siPFKFB3 and siPFKFB4).

4.2.2: 2D Proliferation Studies

4.2.2.1: siRNA knockdown of PFKFB3 and PFKFB4 reduced 2D MCF-7 cell growth in vitro; double PFKFB3/PFKFB4 knockdown was less effective than PFKFB3 knockdown alone.

To validate PFKFB3 and PFKFB4 as potential anti-tumour targets, it was first necessary to conduct a 2D proliferation assay to examine their effect on cell growth. Initially, MCF-7 cells were reverse transfected with the validated siRNA sequences targeting PFKFB3 and PFKFB4, as well as a non-targeting scramble control. Furthermore, to begin addressing the question of whether isoenzyme-specific PFK-2/FBPase-2 inhibition would be necessary, a double siRNA knockdown of PFKFB3 and PFKFB4 was also performed. After transfection, cells were incubated overnight at 37 ºC, before reseeding in 96 well plate format and transferring half the plates to hypoxic conditions 4 hours later (t = 0 hours). The CyQUANT® cell proliferation assay was used to measure cell growth at t = 0 hours, 2 days, 4 days and 6 days. Separate graphs were plotted for normoxic (Figure 4.6A) and hypoxic (Figure 4.6B) conditions. The CyQUANT® assay is a fluorescence based assay that measures cellular DNA content. The tight regulation of cellular DNA content means it is closely proportional to cell number.

At the end of the six day time course, both PFKFB3 and PFKFB4 knockdown in normoxia showed a significant reduction in proliferation compared to the scramble control, these decreases being 66(+/-4)% ($p<0.0001$) and 31(+/-6)% ($p<0.0001$), respectively (Figure 4.6A). The most striking finding was that double PFKFB3/PFKFB4 knockdown significantly reduced growth (reduction of 44(+/-6)% ($p<0.0001$) compared to the control). However, rather than compounding the effect seen with the individual knockdowns, it was actually significantly less effective than PFKFB3 knockdown alone (22% less effective, $p<0.0001$) (Figure 4.6A).

Exposure to hypoxia for 6 days led to a 42(+/-8)% decrease in proliferation of the MCF-7 scramble control siRNA-treated cells, compared to normoxia (Figure 4.6B). The effect of both PFKFB3 and PFKFB4 knockdown was again to reduce proliferation, this time by 78(+/-13)% ($p<0.0001$) and 50(+/-14)% ($p<0.0001$), respectively, compared to the hypoxic scramble control (Figure 4.6B). This effect was markedly higher compared to the effect in normoxia. Double PFKFB3/PFKFB4 knockdown significantly reduced cell growth under hypoxic conditions (67(+/-13)% decrease, ($p<0.0001$)), but no significant difference from the effect of PFKFB3 knockdown alone was observed (Figure 4.6B).

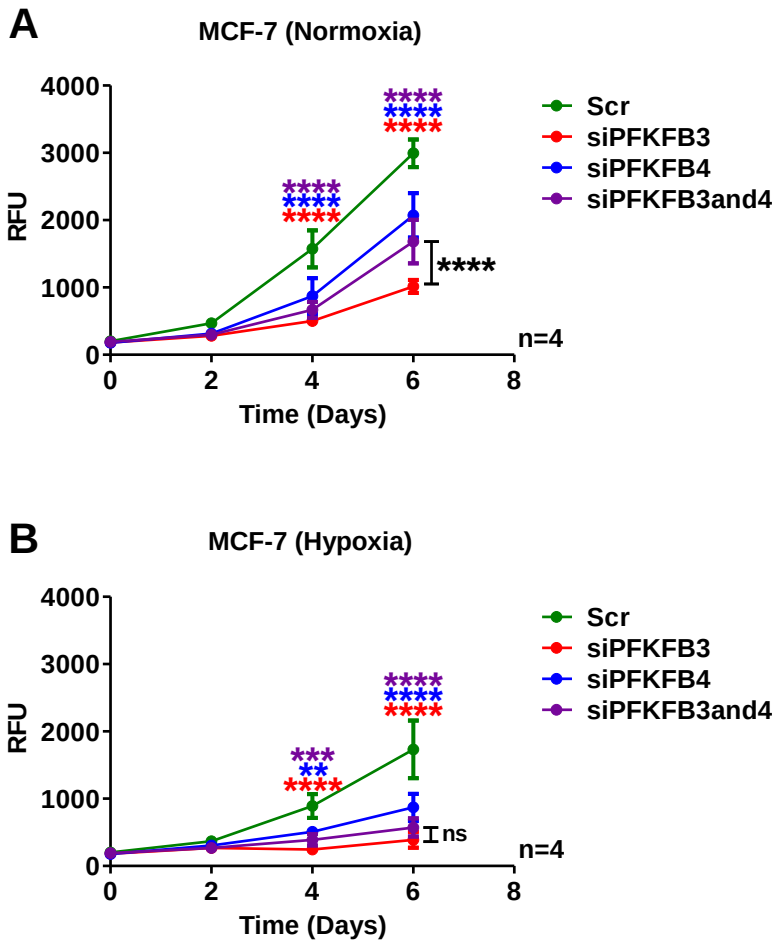

Figure 4.6: CyQUANT® cell proliferation time-course with single and double PFKFB3/PFKFB4 knockdown in MCF-7 cells under **(A)** normoxic and **(B)** hypoxic conditions. siRNA knockdown of PFKFB3, PFKFB4 and double PFKFB3/PFKFB4 knockdown decreased 2D growth under **(A)** normoxic and **(B)** hypoxic conditions during a 6 day time course. Double siPFKFB3and4 knockdown was significantly less effective at reducing proliferation compared with single siPFKFB3 knockdown under **(A)** normoxic conditions. n=4; Two-way repeated measures ANOVA, with Bonferroni post-test; *($p<0.05$), **($p<0.01$), ***($p<0.001$), ****($p<0.0001$), ns (not significant); significant differences from Scr control denoted *siPFKFB3, *siPFKFB4 and *siPFKFB3and4; significant differences between siPFKFB3 and siPFKFB3and4 denoted *. RFU (relative fluorescence units).

4.2.2.2: siRNA knockdown of PFKFB3 and PFKFB4 reduced 2D U87 cell growth in vitro; double PFKFB3/PFKFB4 knockdown was less effective than PFKFB3 knockdown alone.

The same experiment was extended to the U87 cell line with a view to investigating any differences in susceptibility to PFKFB3 or PFKFB4 knockdown in terms of differing relative *PFKFB3:PFKFB4* expression ratios (Figure 4.7). U87 cells had previously been shown to have a lower *PFKFB3:PFKFB4* expression ratio than MCF-7 cells (Table 3.2, Chapter 3).

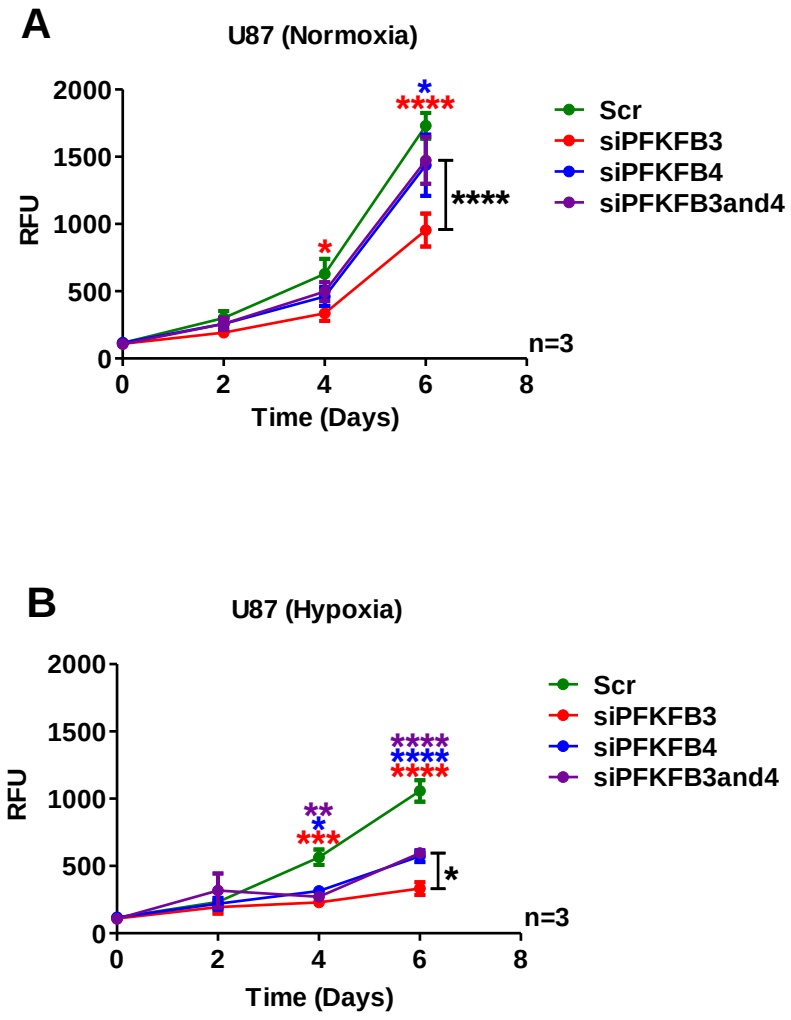

Figure 4.7: CyQUANT® cell proliferation time-course with single and double PFKFB3/PFKFB4 knockdown in U87 cells under **(A)** normoxic and **(B)** hypoxic conditions. siRNA knockdown of PFKFB3 and PFKFB4 decreased 2D growth under **(A)** normoxic and **(B)** hypoxic conditions during a 6 day time course. Double siPFKFB3and4 knockdown significantly reduced growth only under **(B)** hypoxic conditions and was less effective at reducing cell growth compared to single siPFKFB3 knockdown under both **(A)** normoxic and **(B)** hypoxic conditions. n=3; Two-way repeated measures ANOVA, with Bonferroni post-test; *(p<0.05), **(p<0.01), ***(p<0.001), ****(p<0.0001); significant differences from Scr control denoted *siPFKFB3, *siPFKFB4 and *siPFKFB3and4; significant differences between siPFKFB3 and siPFKFB3and4 denoted *. RFU (relative fluorescence units).

PFKFB3 knockdown under normoxic conditions was again more effective at reducing cell proliferation than PFKFB4 knockdown (decreases of 45(+/-5)% ($p<0.0001$) and 17(+/-8)% ($p<0.05$), respectively) (Figure 4.7A). However, their respective effects on U87 cells were noticeably less pronounced than that seen for the MCF-7 cells. It was remarkable that double PFKFB3/PFKFB4 knockdown completely abrogated the significant decrease in proliferation seen with PFKFB3 knockdown alone, with the double knockdown growth curve following a profile more similar to the single PFKFB4 knockdown (Figure 4.7A). These results led to the conclusion that PFKFB3 is more important for 2D U87 cell growth than PFKFB4 under normoxic conditions.

The findings under hypoxic conditions, which reduced growth of scramble siRNA-treated cells by 39(+/-6)%, were slightly different (Figure 4.7B). PFKFB3 knockdown was again the most effective at reducing proliferation, leading to a decrease of 69(+/-9)% ($p<0.0001$), compared to the hypoxic control. This was more marked than its effect under normoxic conditions (decrease of 45(+/-5)% compared to normoxic control, ($p<0.0001$)). However, it was particularly striking that under hypoxic conditions, both PFKFB4 and double PFKFB3/4 knockdown led to a considerable reduction in cell growth, with decreases of 46(+/-9)% ($p<0.0001$) and 44(+/-8)% ($p<0.0001$), respectively (Figure 4.7B). Yet again, the double knockdown was significantly less effective than PFKFB3 alone ($p<0.05$), with its growth curve following a similar profile to that of siPFKFB4. The increased sensitivity of U87 cells to depletion of both isoenzymes, but particularly PFKFB4, under hypoxic conditions was very clear (Figure 4.7B).

4.2.2.3: siRNA knockdown of PFKFB3 and PFKFB4 reduced PC3 normoxic cell growth in vitro; double PFKFB3 /PFKFB4 knockdown was less effective than PFKFB3 knockdown alone.

The final cell line to be investigated under the same experimental conditions was PC3 (Figure 4.8), which had previously been found to have the highest *PFKFB4:PFKFB3* ratio out of the three cell lines (Table 3.2, Chapter 3), under both normoxic and hypoxic conditions.

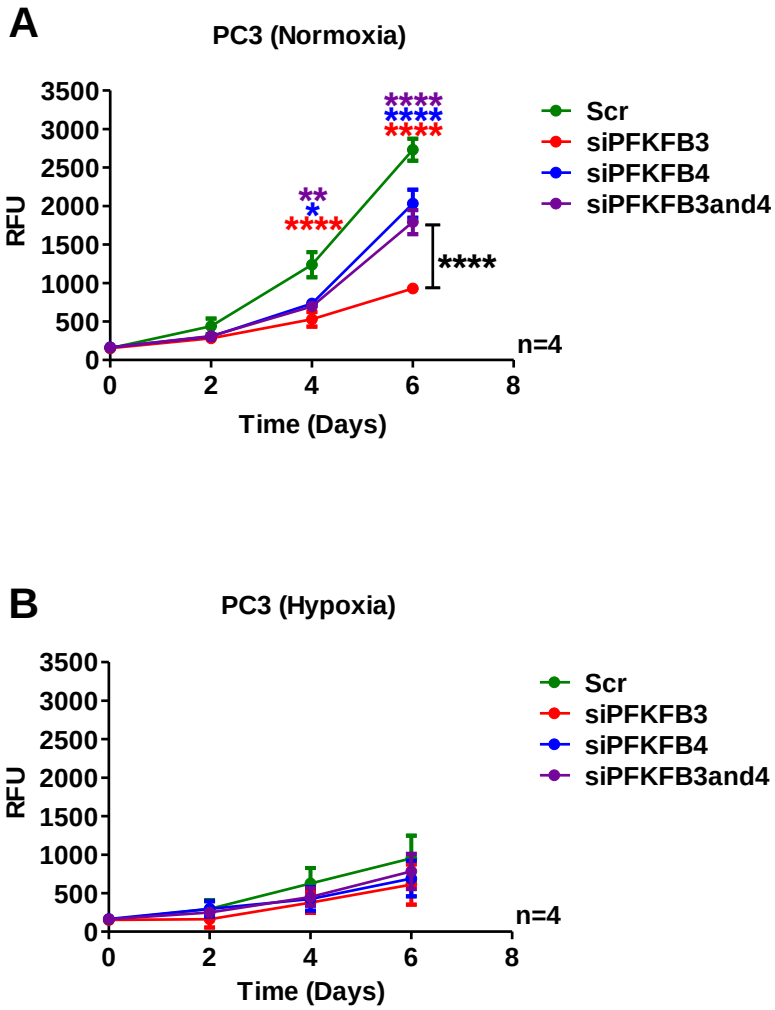

Figure 4.8: CyQUANT® cell proliferation time-course with single and double PFKFB3/PFKFB4 knockdown in PC3 cells under **(A)** normoxic and **(B)** hypoxic conditions. siRNA knockdown of PFKFB3, PFKFB4 and double PFKFB3/PFKFB4 knockdown decreased 2D growth under **(A)** normoxic conditions, whereas there was no significant difference under **(B)** hypoxic conditions during a 6 day time course. Double siPFKFB3and4 knockdown was significantly less effective at reducing cell growth compared to single siPFKFB3 knockdown under **(A)** normoxic conditions. n=4; Two-way repeated measures ANOVA with Bonferroni post-test; *(p<0.05), **(p<0.01), ***(p<0.001), ****(p<0.0001); significant differences from Scr control denoted *siPFKFB3, *siPFKFB4 and *siPFKFB3and4; significant differences between siPFKFB3 and siPFKFB3and4 denoted *. RFU (relative fluorescence units).

Under normoxic conditions, siRNA knockdown of PFKFB3 was again the most effective at reducing cell growth (decrease of 66(+/-6)% ($p<0.0001$)), with single PFKFB4 knockdown and double PFKFB3/PFKFB4 knockdown having comparable effects to one another, with decreases of 26(+/-8)% and 34(+/-8)%, respectively (Figure 4.8A). Double knockdown of PFKFB3/PFKFB4 was significantly less effective at reducing PC3 cell proliferation than single PFKFB3 knockdown alone (32% less effective, $p<0.0001$).

The proliferation of scramble control siRNA-treated PC3 cells was reduced by 65(+/-8)% under hypoxic conditions (Figure 4.8B), which was considerably higher than the corresponding effects in MCF-7 and U87 cells (decreases of 42(+/-8)% and 39(+/-6)%, respectively (Figures 4.6 and 4.7)). The pattern suggested there might have been a significant difference with the siRNA-treated groups in PC3 cells under hypoxic conditions, if the time course was allowed to proceed. However, siRNAs function via transient knockdown, the efficacy of which was reduced beyond 6 days, so further extension of the experiment was not an option. It was therefore not possible to draw any firm conclusions about the respective effect of the PFKFB3 and PFKFB4 isoenzymes in PC3 cells under hypoxic conditions. Future work could potentially examine the effect of siRNA knockdown of these isoenzymes on PC3 cells at a slightly higher oxygen concentration (1%).

The findings from these 2D growth curve studies are summarised in Table 4.1.

% Reduction in Cell Proliferation			MCF-7	U87	PC3
A	**Normoxia**	**si3**	66 (+/-4)%	45 (+/-5)%	66 (+/-6)%
		si4	31 (+/-6)%	17 (+/-8)%	26 (+/-8)%
		si3and4	44 (+/-6)%	15 (+/-7)%	34 (+/-8)%
B	**Hypoxia**	**si3**	78 (+/-13)%	69 (+/-9)%	n/a
		si4	50 (+/-14)%	46 (+/-9)%	n/a
		si3and4	67 (+/-13)%	44 (+/-8)%	n/a

Table 4.1: Percentage reduction in cell proliferation in response to single and double PFKFB3 and PFKFB4 knockdown, as compared to the scramble control after a 6 day time course under **(A)** normoxic and **(B)** hypoxic conditions. MCF-7, U87 and PC3 cell lines, as measured by CyQUANT® proliferation assay. n=3. si3 (siPFKFB3), si4 (siPFKFB4) and si3/4 (siPFKFB3and4), n/a (not applicable).

The sensitivity of MCF-7 and U87 cells to PFKFB3 and PFKFB4 knockdown was increased under hypoxic conditions, which would be consistent with these isoenzymes playing an important role in promotion of the glycolytic phenotype as an adaptation to hypoxia. siRNA knockdown of PFKFB3 consistently suppressed cell proliferation to a greater extent than siRNA knockdown of PFKFB4. PFKFB3 is known to have the highest basal K:B activity ratio (740:1) of the PFK-2/FBPase-2 isoenzymes, so is thought to have a strong influence on intracellular [F-2,6-BP] and therefore the glycolytic rate (Sakakibara, Kato et al. 1997). This would again be consistent with the findings presented in this Chapter.

U87 was comparatively less sensitive to both PFKFB3 and PFKFB4 inhibition than the other two cell lines under normoxic conditions. Previous work had found U87 to have the highest basal *PFKFB3* and *PFKFB4* mRNA expression of the three cell lines, which could potentially make it less sensitive to their suppression (Figure 3.14A, Chapter 3). However, the sensitivity to PFKFB3 and PFKFB4 inhibition under hypoxic conditions was comparable between the MCF-7 and U87 cell lines. Previous results had found that hypoxic fold-induction of the two isoenzymes was considerably lower in U87 cells (Figure 3.4, Chapter 3), which may account for the comparatively larger increase in sensitivity under hypoxic conditions.

A consistent, and somewhat surprising finding, was that double PFKFB3/PFKFB4 knockdown was less effective at reducing cell proliferation than single PFKFB3 knockdown alone, in all three cell lines under normoxic conditions (Figures 4.6, 4.7 and 4.8). The same effect was only observed to be significant under hypoxic conditions in the U87 cell line (Figure 4.7B), suggesting it may be of less relevance under these conditions. This observation was despite comparable levels of PFKFB3 mRNA and protein suppression after single or double knockdown (Figures 4.2 and 4.3), strongly implicating reduction of PFKFB4 expression as being responsible for this effect. It was noteworthy that the growth curves for

double PFKFB3/PFKFB4 knockdown in both U87 and PC3 cell lines (Figures 4.7A and 4.8A) more closely mirrored those of single PFKFB4 knockdown than in the MCF-7 cell line (Figure 4.6A) under normoxic conditions. At this point, it would be reasonable to speculate that the magnitude of the rescue effect could be directly related to the differing relative *PFKFB3:PFKFB4* expression ratios of the three cell lines, with *PFKFB3:PFKFB4* being far higher in the MCF-7 cell line than U87 and PC3 (Table 3.2, Chapter 3). Indeed, previous results had found U87 and PC3 cells to have higher absolute expression of PFKFB4 protein (Figure 3.18, Chapter 3). It follows that if the two isoenzymes antagonise one another (PFKFB3 with high kinase activity, PFKFB4 with high bisphosphatase activity), then lower relative PFKFB3:PFKFB4 expression would increase the degree to which PFKFB4 modulates intracellular [F-2,6-BP]. Accordingly, this would therefore increase the degree to which suppression of PFKFB4 expression could "rescue" the reduction in cell growth mediated by PFKFB3 knockdown.

4.2.3: 3D Proliferation Studies

Having established the differing sensitivities of the three cell lines to siRNA knockdown of PFKFB3 and PFKFB4, and with a view to further understanding the interplay of the two isoenzymes, it was decided to examine their effect in 3D spheroid models. The nature of these models mimics the avascular areas of a tumour, which experience nutrient/oxygen diffusion gradients and reduced proliferation rate, as well as providing a more realistic model of intratumoural cell-cell interactions (Ivascu and Kubbies 2007). Cells were reverse transfected as with the 2D experiment, and reseeded into 96-well low-adherence round bottom plates, before centrifuging and incubating at 37 ºC. 3D spheroid formation followed, with average tumour volume estimated from images of 15 replicates per condition, taken on days 2, 4 and 6 after reseeding.

4.2.3.1: Single PFKFB4 siRNA knockdown reduced 3D MCF-7 cell growth in vitro; PFKFB3 knockdown alone prevented spheroid formation.

MCF-7 cells did not grow well as spheroids, even in the presence of Matrigel® (reconstituted basement membrane), which promotes aggregation. The growth curve (Figure 4.9A) and representative spheroid images (Figure 4.9B) show that transformation of scramble siRNA-treated cells from an aggregate of cells to a fully-formed spheroid took 4 days. In contrast, treatment with PFKFB4 siRNA and the PFKFB3/PFKFB4 siRNA pools promoted spheroid formation by day 2. Intriguingly, knockdown of PFKFB3 prevented spheroid formation during the course of the experiment, with the cells still remaining an aggregate at day 6 (Figure 4.9B), hence their exclusion from Figure 4.9A. An explanation for this was not easily forthcoming, though it demonstrated very distinct and opposing effects of each isoenzyme on spheroid formation. Further work outside the scope of this thesis would seek to examine this in detail, but the effect would only be likely to enhance any metabolic effects resulting from inhibition of PFKFB3. Recent evidence suggests PFKFB3 has a role in promoting migration in endothelial cells (unpublished data presented at a meeting by Prof. Peter Carmeliet). This, together with a potential role in adhesion, might offer an explanation for these findings in the MCF-7 cell line.

There was a significant reduction in spheroid volume with PFKFB4 knockdown compared to scramble control at day 6 (decrease of 40(+/-14)%, $p<0.05$) (Figure 4.9). However, it is difficult to draw conclusions from this data because the reduced rate of spheroid formation for the scramble control would have meant those cells had higher oxygen and nutrient exposure, due to more cell surface area exposed to media. This could have promoted a higher rate of proliferation compared to the PFKFB4 or PFKFB3/PFKFB4 knockdown spheroids, beyond the effect on growth mediated by differences in isoenzyme expression alone.

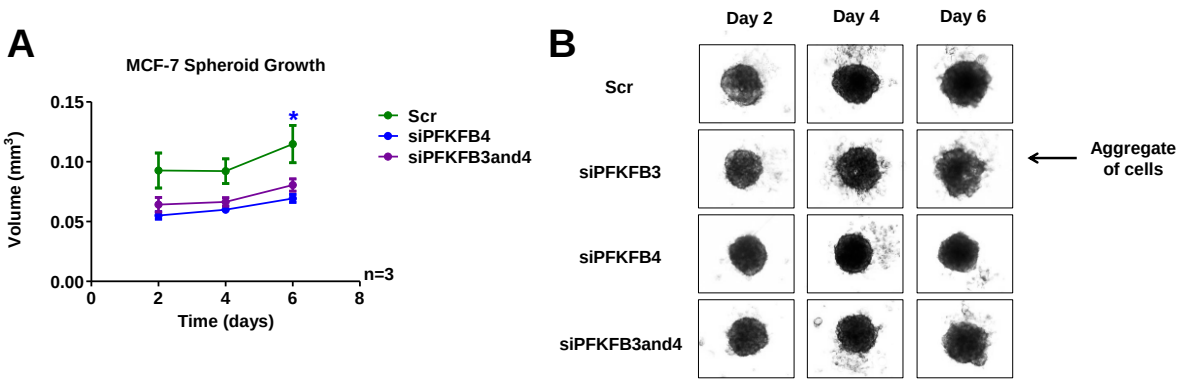

Figure 4.9: Spheroid 3D proliferation time-course with single and double PFKFB3/PFKFB4 knockdown in MCF-7 cells. siRNA knockdown of PFKFB4 significantly decreased 3D growth in MCF-7 cells **(A)** during a 6 day time course. PFKFB3 knockdown prevented spheroid formation so these results are excluded from **(A)**. Representative images of spheroids at each time point are displayed in **(B)**. n=3; Two-way repeated measures ANOVA with Bonferroni post-test; *(p<0.05), **(p<0.01), ***(p<0.001), ****(p<0.0001); significant differences from Scr control denoted *siPFKFB3, *siPFKFB4 and *siPFKFB3and4.

4.2.3.2: Single PFKFB3 siRNA knockdown reduced 3D U87 cell growth in vitro, whereas PFKFB4 knockdown and double PFKFB3/PFKFB4 knockdown had no effect.

The U87 cell line grew well as spheroids in the absence of Matrigel®, with all 4 siRNA-treatment conditions (Figure 4.10). There was a significant reduction in spheroid volume with PFKFB3 knockdown compared to the control (decrease of 28(+/-5)%, p<0.001). There was no significant effect on U87 spheroid volume with either PFKFB4 or PFKFB3/PFKFB4 knockdown. This significant (p<0.01) "rescue" by double knockdown of the reduction in spheroid volume effected by single PFKFB3 knockdown alone, was akin to that seen in 2D.

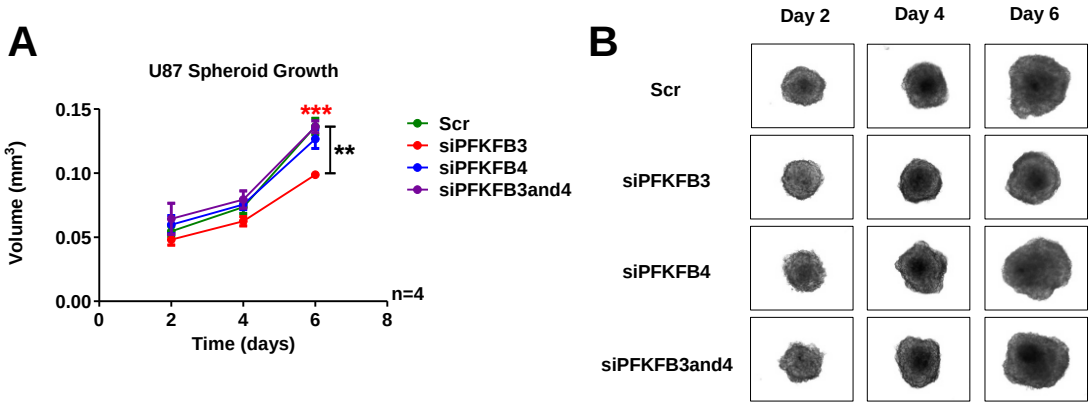

Figure 4.10: Spheroid 3D proliferation time-course with single and double PFKFB3/PFKFB4 knockdown in U87 cells. siRNA knockdown of PFKFB3 decreased 3D growth in U87 cells, whereas knockdown of PFKFB4 and double PFKFB3/PFKFB4 knockdown had no significant effect on growth **(A)** during a 6 day time course. Representative images of spheroids at each time point are displayed in **(B)**. n=4; Two-way repeated measures ANOVA with Bonferroni post-test; *(p<0.05), **(p<0.01), ***(p<0.001), ****(p<0.0001); significant differences from Scr control denoted *siPFKFB3, *siPFKFB4 and *siPFKFB3and4; significant difference between siPFKFB3 and siPFKFB3and4 denoted *.

4.2.3.3: PFKFB3, PFKFB4 and double PFKFB3/PFKFB4 siRNA knockdown all reduced 3D PC3 cell growth in vitro.

In the presence of Matrigel®, PC3 spheroids grew well with all four siRNA-treatment conditions (Figure 4.11). After 6 days, there was a significant reduction in volume with PFKFB3 knockdown (58(+/-5)%, p<0.0001), PFKFB4 knockdown (27(+/-9)%, p<0.01) and double PFKFB3/PFKFB4 knockdown (43(+/-5)%, p<0.0001), compared with the scramble control. These results were consistent with previous observations from the 2D studies in PC3 cells (Table 4.1). There appeared to be a trend for reduced effect on spheroid volume of the double PFKFB3/PFKFB4 knockdown, compared to single PFKFB3 knockdown alone, which would likely be significant with an increased number of experimental replicates (Figure 4.11A). This would be consistent with the "rescue" effect clearly observed in the 2D assay.

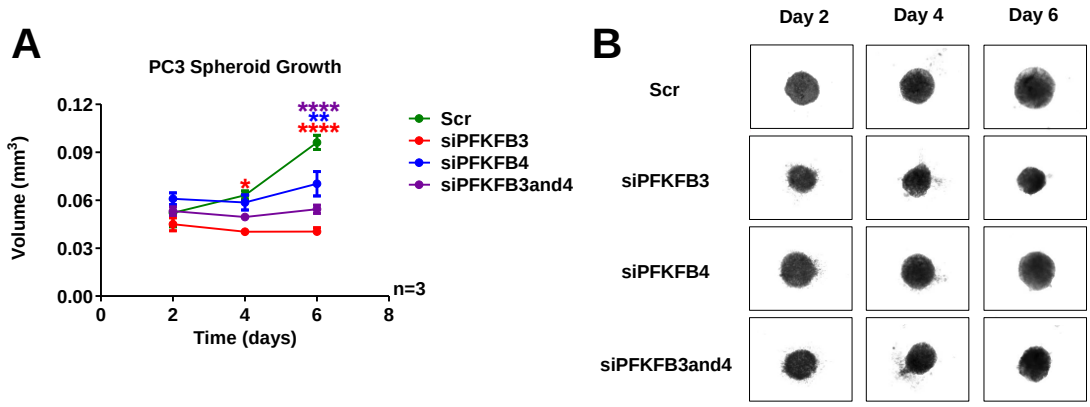

Figure 4.11: Spheroid 3D proliferation time-course with single and double PFKFB3/PFKFB4 knockdown in PC3 cells. siRNA knockdown of PFKFB3, PFKFB4 and double PFKFB3/4 knockdown decreased 3D growth in PC3 cells **(A)** during a 6 day time course. Representative images of spheroids at each time point are displayed in **(B)**. n=3; Two-way repeated measures ANOVA with Bonferroni post-test; *(p<0.05), **(p<0.01), ***(p<0.001), ****(p<0.0001); significant differences from Scr control denoted *siPFKFB3, *siPFKFB4 and *siPFKFB3and4; significant differences between siPFKFB3 and siPFKFB3and4 denoted *.

4.2.4: Fructose-2,6-bisphosphate Assay

The growth curve data had provided evidence that PFKFB3 and PFKFB4 may be acting to antagonise one another. It was therefore important to investigate whether this effect was due to opposing effects of the isoenzymes on intracellular [F-2,6-BP], through differing K:B activity ratios. It was originally intended to set up an in-house assay to measure [F-2,6-BP], but it was not possible to obtain F-2,6-BP, which was required as a standard. Commercial suppliers had stopped producing the compound and potential collaborators had insufficient stock remaining. It was therefore necessary to outsource the assay and so a collaboration was initiated with Dr Ramon Bartrons' group at the University of Barcelona. Reverse transfections and sample preparation were performed by the author of the thesis, the assays were performed by Dr Anna Manzano (Bartrons group) and raw data was analysed and interpreted by the author. The assay method used was adapted from that previously reported by Van Schaftingen and colleagues (Van Schaftingen, Lederer et al. 1982; Van Schaftingen 1987).

4.2.4.1: Changes in [F-2,6-BP] under normoxic and hypoxic conditions and differences between cell lines were correlated with different PFKFB3/PFKFB4 expression ratios.

An initial comparison of intracellular [F-2,6-BP] in scramble control-transfected MCF-7, U87 and PC3 cells was conducted under both normoxic (0 hours) and hypoxic conditions (72 hours) (Figure 4.12). Under basal conditions, [F-2,6-BP] was highest in MCF-7 cells (58(+/-7) pmol/mg protein), slightly lower in U87 cells (45(+/-3) pmol/mg protein) and markedly lower in PC3 cells (14(+/-2) pmol/mg protein). These results could be rationalised by comparing the relative *PFKFB3:PFKFB4* expression profiles that had previously been calculated (Table 3.2, Chapter 3). PFKFB3 is widely thought to be the most important isoenzyme for controlling intracellular [F-2,6-BP], through its unusually high kinase activity (Telang, Yalcin et al. 2006). One might therefore expect the [F-2,6-BP] in the three cell lines

to correlate with basal expression of *PFKFB3*. In fact, U87 had previously been found to have the highest absolute *PFKFB3* expression, whereas MCF-7 and PC3 expression levels were comparable (Figure 3.14A, Chapter 3). At first sight then, it seemed counter-intuitive that MCF-7 should have a higher basal [F-2,6-BP] than the U87 cell line. However, MCF-7 differed from the other two cell lines in that it had a much higher *PFKFB3:PFKFB4* expression ratio (Table 3.2, Chapter 3). If the two isoenzymes were acting to antagonise one another through opposing effects on [F-2,6-BP], this would explain the higher [F-2,6-BP] observed for the MCF-7 cells (Figure 4.12).

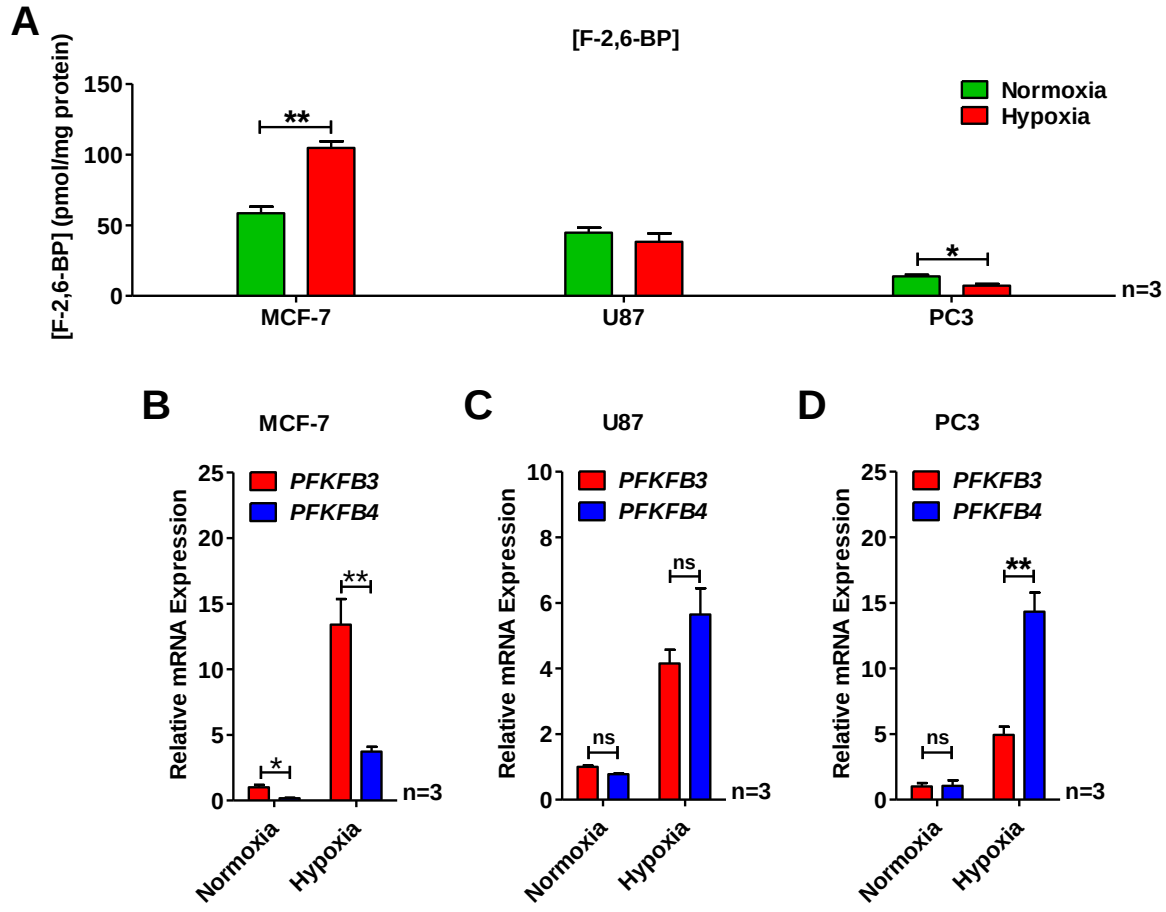

Figure 4.12: (A) Assay of fructose-2,6-bisphosphate in MCF-7, U87 and PC3 cells under normoxic and hypoxic conditions and **(B)** relative *PFKFB3*:*PFKFB4* mRNA expression in MCF-7, U87 and PC3 cells under normoxic and hypoxic conditions. **(A)** [F-2,6-BP] increased in MCF-7 cells, was unchanged in U87 cells and decreased in PC3 cells after 72 hours hypoxic exposure. This correlated with changes in the *PFKFB3:PFKFB4* mRNA expression ratios after 72 hours hypoxic exposure: *PFKFB3*>*PFKFB4* in MCF-7 cells **(B)**, *PFKFB3*≈*PFKFB4* in U87 cells **(C)** and *PFKFB3*<*PFKFB4* in PC3 cells **(D)**. [F-2,6-BP] assay samples were prepared by the author and the assay was performed by Dr Anna Manzano in Dr Ramon Bartrons' group at the University of Barcelona, Spain. Analysis and interpretation of the raw data was performed by the author. Relative expression values in **(B)**-**(D)** were normalised to normoxic *PFKFB3* expression. n=3; *(p<0.05), **(p<0.01), ***(p<0.001), ****(p<0.0001); ns (not significant).

Indeed, this effect became clearer by examining changes in [F-2,6-BP] after hypoxic exposure; the difference between cell lines was striking, with [F-2,6-BP] increasing 79(+/-11)% ($p<0.01$) in the MCF-7 cell line, with no significant change in the U87 cell line and a decrease of 48(+/-12)% ($p<0.05$) in the PC3 cell line (Figure 4.12A). These changes were directly correlated with the relative *PFKFB3:PFKFB4* expression ratios (Figures 4.12B, 4.12C and 4.12D) under hypoxic conditions, with MCF-7 having higher *PFKFB3* expression, U87 expressing comparable levels and PC3 expressing higher *PFKFB4*. This provided evidence that PFKFB4 might be acting with high bisphosphatase activity in the three cell lines, directly countering the kinase activity of PFKFB3.

4.2.4.2: siRNA knockdown of PFKFB3 reduced [F-2,6-BP] in MCF-7 cells under normoxic and hypoxic conditions; double PFKFB3/PFKFB4 knockdown had a similar effect, whereas no change in [F-2,6-BP] was observed with PFKFB4 knockdown.

To confirm this, it was necessary to examine the effect of siRNA knockdown of both isoenzymes on [F-2,6-BP]. Initial assay data was obtained from MCF-7 cells, with single and double PFKFB3/PFKFB4 knockdown. Samples were collected at 24, 48 and 72 hours, under normoxic and hypoxic conditions (Figure 4.13). There was a trend for decreased [F-2,6-BP] in response to PFKFB3 knockdown and double PFKFB3/4 knockdown. The assay was limited by high variability, meaning these findings were only significant at the later time points. siRNA knockdown of PFKFB3 reduced [F-2,6-BP] by 69(+/-10)% ($p<0.001$) after 72 h normoxia and 76(+/-10)% ($p<0.001$) after 72 h hypoxia, whereas no significant change was observed with PFKFB4 knockdown (Figure 4.13). These results confirmed the high kinase activity of PFKFB3, clearly demonstrating it to be the more important isoenzyme in determining the overall concentration of F-2,6-BP in the MCF-7 cell line. It was noted that double PFKFB3/PFKFB4 knockdown also led to a significant reduction in F-2,6-BP levels (decrease of 64(+/-10)% ($p<0.001$) after 72 h normoxia and decrease of 51(+/-11)% ($p<0.05$)

after 72 h hypoxia), being more characteristic of the PFKFB3 knockdown effect (Figure 4.13). This could be explained by the high *PFKFB3*:*PFKFB4* expression ratio in MCF-7 cells (Figure 4.12B). It was hypothesised that if the two isoenzymes were antagonising one another, a "rescue" effect after double PFKFB3/PFKFB4 knockdown would become apparent in cell lines with higher relative PFKFB4 expression.

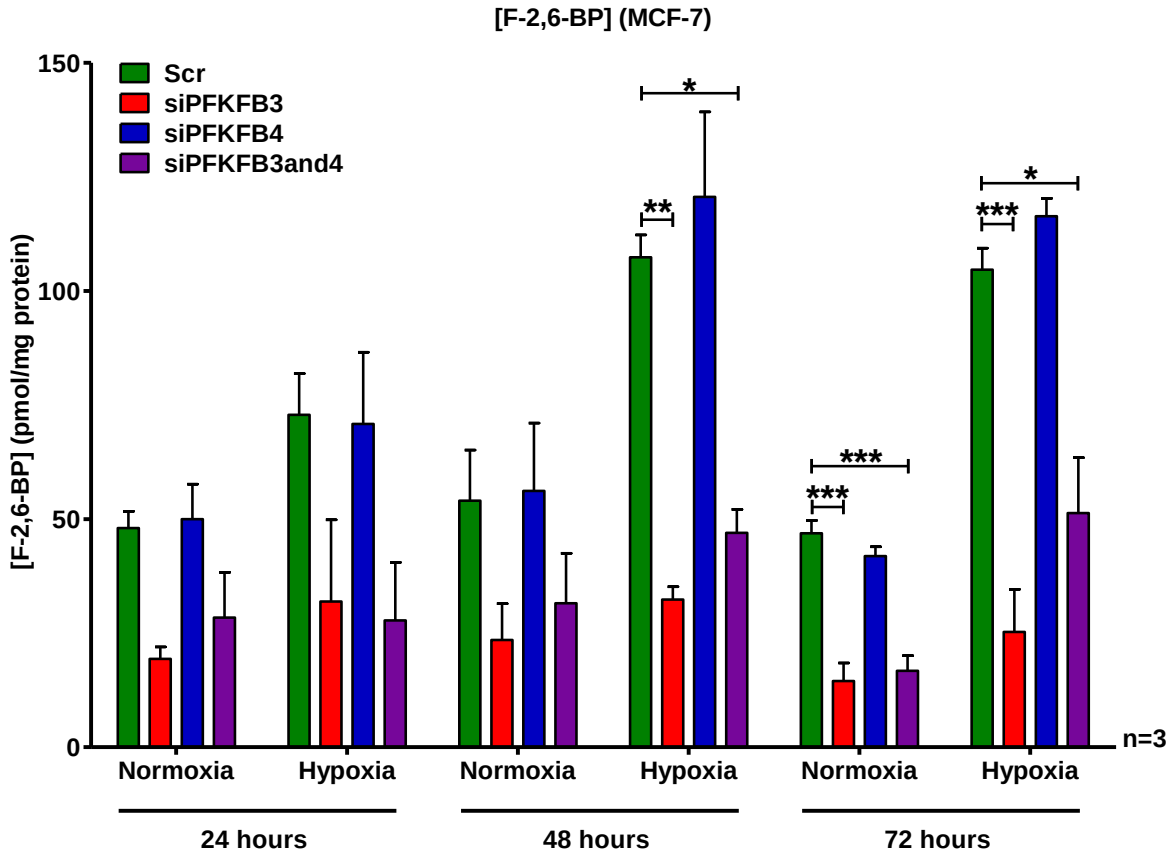

Figure 4.13: Assay of fructose-2,6-bisphosphate with single and double PFKFB3/PFKFB4 knockdown in MCF-7 cells under normoxic and hypoxic conditions. siRNA knockdown of PFKFB3 and PFKFB3and4, significantly reduced [F-2,6-BP] in MCF-7 cells at the 48 h hypoxia, 72 h normoxia and 72 h hypoxia time points. Assay samples were prepared by the author and the assay was performed by Dr Anna Manzano in Dr Ramon Bartrons' group at the University of Barcelona, Spain. Analysis and interpretation of the raw data was performed by the author. One-way ANOVA with Bonferroni post-test performed on data sets from the same time point and oxygenation status; n=3; *($p<0.05$), **($p<0.01$), ***($p<0.001$), ****($p<0.0001$).

4.2.4.3: siRNA knockdown of PFKFB3 decreased [F-2,6-BP] in U87 cells under normoxic and hypoxic conditions; double PFKFB3/PFKFB4 reduced the magnitude of this effect.

The same experiment was therefore extended to the U87 cell line, with its more balanced *PFKFB3:PFKFB4* expression ratio (Figure 4.14). There was a trend for decreased [F-2,6-BP]

with PFKFB3 knockdown, confirming high kinase activity as anticipated, but with high assay variability limiting significance to the 72 h normoxia time point only (decrease of 57(+/-10)%, $p<0.05$) (Figure 4.14). It was intriguing to note the presence of an apparent "rescue effect" on [F-2,6-BP] in response to double PFKFB3/PFKFB4 knockdown, as compared to single PFKFB3 knockdown, across different time points. This warranted further investigation to determine whether this was indeed a real effect.

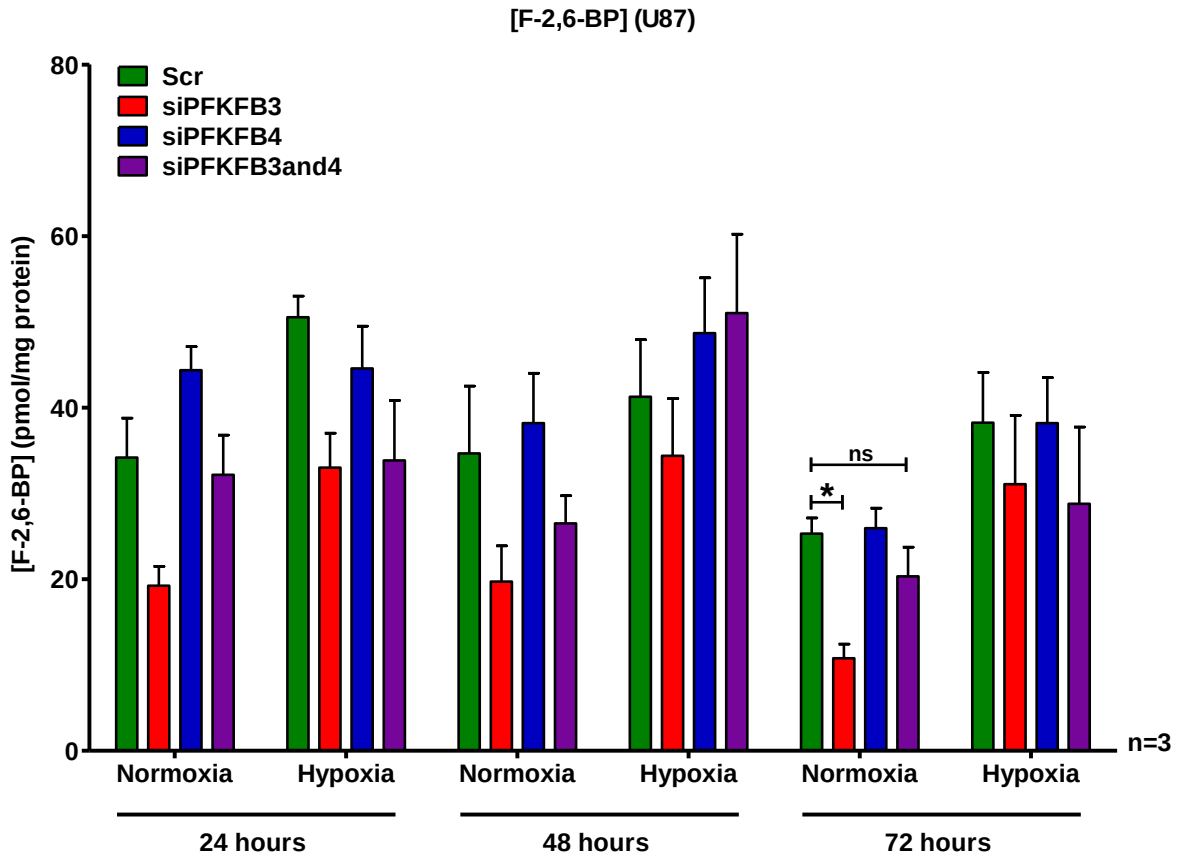

Figure 4.14: Assay of fructose-2,6-bisphosphate with single and double PFKFB3/PFKFB4 knockdown in U87 cells under normoxic and hypoxic conditions. siRNA knockdown of PFKFB3 significantly reduced [F-2,6-BP] in U87 cells at the 72 h normoxia time point. Double PFKFB3and4 knockdown at this time point resulted in no significant change in [F-2,6-BP]. Assay samples were prepared by the author and the assay was performed by Dr Anna Manzano in Dr Ramon Bartrons' group at the University of Barcelona, Spain. Analysis and interpretation of the raw data was performed by the author. n=3; One-way ANOVA with Bonferroni post-test performed on data sets from the same time point and oxygenation status; *($p<0.05$), **($p<0.01$), ***($p<0.001$), ****($p<0.0001$), ns (not significant).

An additional series of replicates were prepared at the 72 h normoxic time point and the assay results summarised in Figure 4.15B. This result confirmed that double knockdown of PFKFB3/PFKFB4 significantly increased [F-2,6-BP] relative to single PFKFB3 alone

(139(+/-33)% increase relative to siPFKFB3, p<0.05). This observation contrasted with the results from the same time point in MCF-7 cells, which exhibited no "rescue effect" with double knockdown (Figure 4.15A), which was ascribed to the differing *PFKFB3:PFKFB4* expression ratios in these cell lines, i.e. higher relative *PFKFB4* in U87.

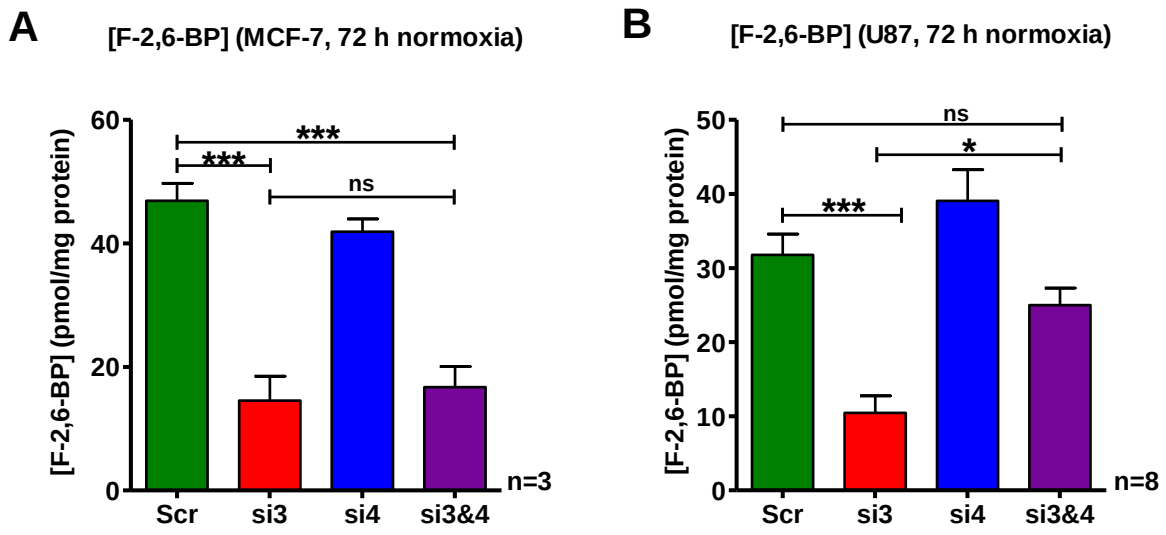

Figure 4.15: Fructose-2,6-bisphosphate assay with single and double PFKFB3 and PFKFB4 knockdown of **(A)** MCF-7 cells and **(B)** U87 cells after 72 hours in normoxia. siRNA knockdown of PFKFB3 and double PFKFB3/PFKFB4 knockdown had comparable effects in MCF-7 cells, significantly decreasing [F-2,6-BP] **(A)**. Double PFKFB3/PFKFB4 knockdown was less effective at reducing [F-2,6-BP] in U87 cells than single PFKFB3 knockdown alone **(B)**. Assay samples were prepared by the author and the assay was performed by Dr Anna Manzano in Dr Ramon Bartrons' group at the University of Barcelona, Spain. Analysis and interpretation of the raw data was performed by the author. n=3 (MCF-7), n=8 (U87); One-way ANOVA with Bonferroni post-test; *(p<0.05), **(p<0.01), ***(p<0.001), ****(p<0.0001), ns (not significant).

It should be noted that no significant increase in [F-2,6-BP] was observed in response to PFKFB4 knockdown in the U87 cell line. An increase might have been expected if PFKFB4 had high bisphosphatase activity in this cell line. This was also despite the double knockdown experiment suggesting this should be the case (Figure 4.15B). However, considering the K:B activity ratio of PFKFB3 is so unusually high, it is proposed that competing bisphosphatase activity of PFKFB4 only becomes apparent when PFKFB3 expression is reduced through siRNA knockdown. This led to the hypothesis that the bisphosphatase activity of PFKFB4 would become even more apparent in a cell line with a higher *PFKFB4:PFKFB3* expression ratio, such as PC3.

4.2.4.4: siRNA knockdown of PFKFB4 increased [F-2,6-BP] in PC3 cells, whereas double PFKFB3/PFKFB4 knockdown abolished this effect.

To test this hypothesis, the experiment and assay were repeated for a set of PC3 samples (Figure 4.16). It was immediately apparent that siRNA suppression of PFKFB4 expression resulted in a trend for increased [F-2,6-BP], which was significant at the 72 h hypoxia time point (increase of 4.4-fold, $p<0.05$), confirming high PFKFB4 bisphosphatase activity. This effect appeared to be greater under hypoxic conditions, which would be consistent with the previous finding of elevated *PFKFB4:PFKFB3* expression ratio in PC3 cells under these conditions (Table 3.2, Chapter 3). During the course of this work, a study was published which reported PFKFB4 in PC3 cells to have high bisphosphatase activity under normoxic, lipid-limited growth conditions (Ros, Santos et al. 2012). This was consistent with the findings in this Chapter.

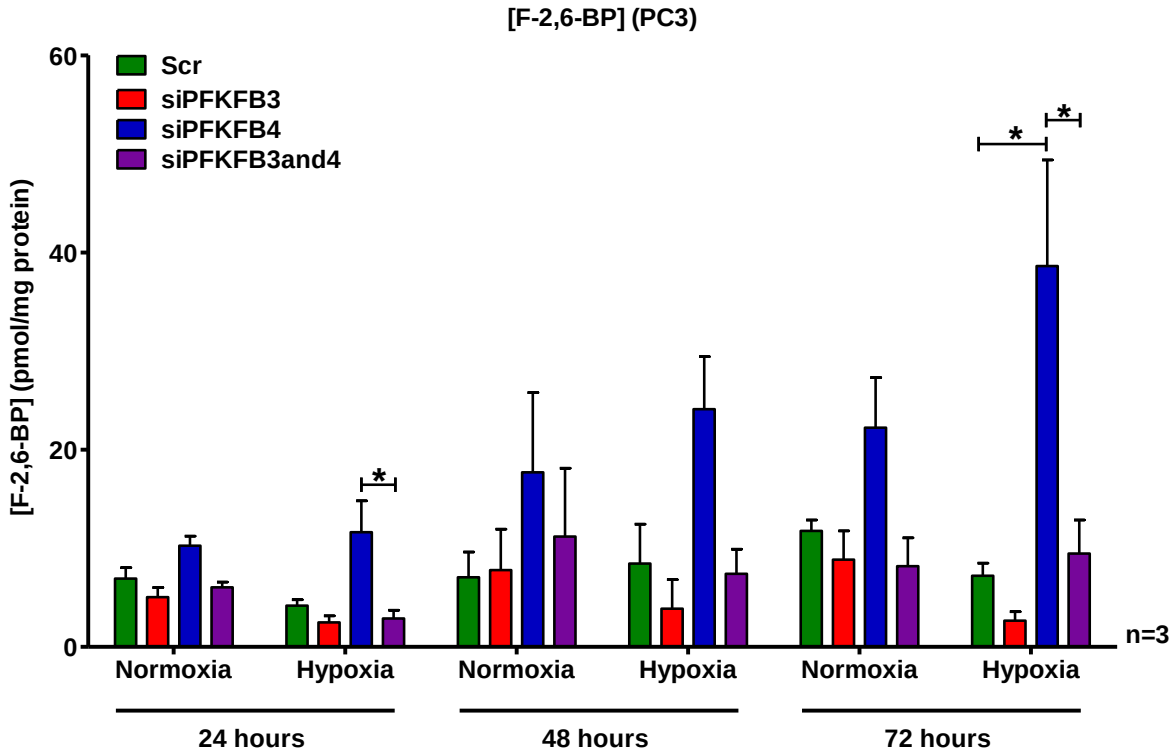

Figure 4.16: Assay of fructose-2,6-bisphosphate with single and double PFKFB3/PFKFB4 knockdown in PC3 cells under normoxic and hypoxic conditions. siRNA knockdown of PFKFB4 significantly increased [F-2,6-BP] at the 72 h hypoxia time point, whereas double PFKFB3/PFKFB4 knockdown eliminated that increase. Assay samples were prepared by the author and the assay was performed by Dr Anna Manzano in Dr Ramon Bartrons' group at the University of Barcelona, Spain. Analysis and interpretation of the raw data was performed by the author. n=3; One-way ANOVA with Bonferroni post-test performed on data sets from the same time point and oxygenation status; *($p<0.05$), **($p<0.01$), ***($p<0.001$), ****($p<0.0001$).

Basal [F-2,6-BP] was lowest in the PC3 cell line, unfortunately compounding sensitivity problems and precluding detection of any significant PFKFB3 kinase activity. Double knockdown significantly reduced [F-2,6-BP] compared to single PFKFB4 knockdown alone at the 72 hour time point under hypoxic conditions (decrease of 75(+/-29)%, $p<0.05$) (Figure 4.16).

It might be anticipated that the high *PFKFB4*:*PFKFB3* expression ratio should lead to similar effects mediated by double knockdown and PFKFB4 knockdown alone, yet this is not the case (Figure 4.16). The reason for this can likely be attributed to the relative catalytic activities, with the high kinase activity of PFKFB3 exerting a larger effect on total [F-2,6-BP].

4.2.5: Metabolic Assays

4.2.5.1: siRNA knockdown of PFKFB3 significantly increased ATP level under hypoxic conditions in MCF-7 cells; single and double siRNA knockdown of PFKFB3/PFKFB4 had minimal effect on ATP level in U87 and PC3 cells.

Having established the opposing effects of PFKFB3 and PFKFB4 on [F-2,6-BP], it was necessary to understand the wider impact of modulating levels of this metabolite on metabolic outputs. The working hypothesis at this point was that high kinase activity of PFKFB3, leading to increased [F-2,6-BP], would lead to activation of PFK-1 and an increase in flux through the glycolytic pathway (Figure 4.17A). The predominant bisphosphatase function of PFKFB4 was hypothesised to act to reduce [F-2,6-BP], leading to a decrease in PFK-1 activity and a shift in relative flux towards the alternative pentose phosphate pathway (PPP) (Figure 4.17B). As a finely balanced system, a shift in flux in either direction was hypothesised to be detrimental to the cell, which would account for knockdown of both PFKFB3 and PFKFB4 reducing cell proliferation, as previously observed (Figures 4.6-4.11).

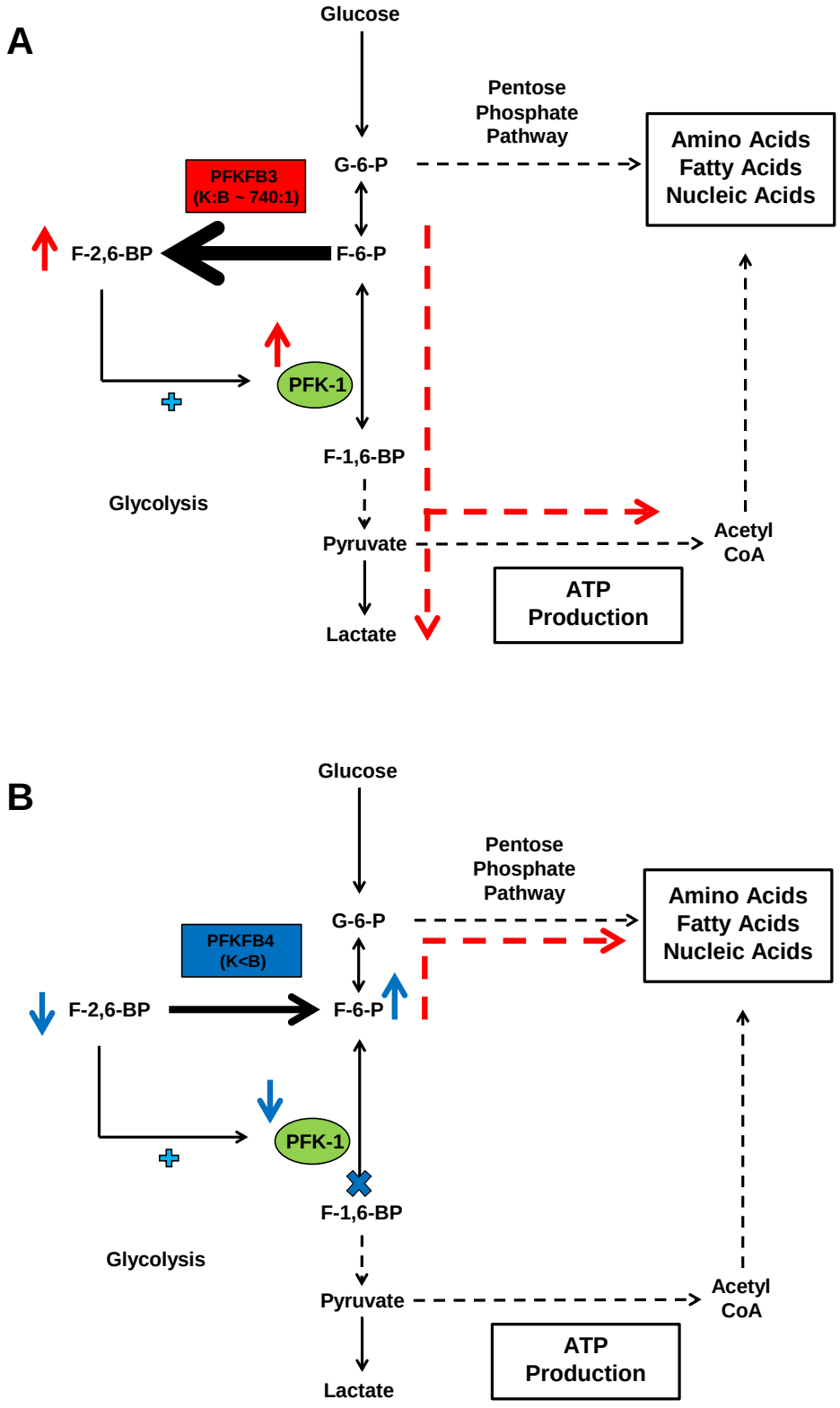

Figure 4.17: Working hypothesis of the likely effect of the opposing activities of PFKFB3 and PFKFB4 on modulating the balance between glycolysis and the PPP. The high kinase activity of PFKFB3, leading to an increase in F-2,6-BP, was hypothesised to increase glycolytic flux through a F-2,6-BP-mediated increase in PFK-1 activity. The opposing high bisphosphatase activity of PFKFB4, leading to a decrease in F-2,6-BP, was hypothesised to increase PPP flux through decreased PFK-1 activity. G-6-P (glucose-6-phosphate), F-6-P (fructose-6-phosphate), F-1,6-BP (fructose-1,6-bisphosphate), F-2,6-BP (fructose-2,6-bisphosphate), PFK-1 (6-phosphofructo-1-kinase), ATP (adenosine triphosphate), CoA (coenzyme A), K (kinase activity), B (bisphosphatase activity).

Given the relationship between [F-2,6-BP], PFK-1 activity and glycolytic activity, it was therefore of interest to measure cellular ATP content in the three cell lines of, in response to single and double PFKFB3/PFKFB4 knockdown (Figure 4.18).

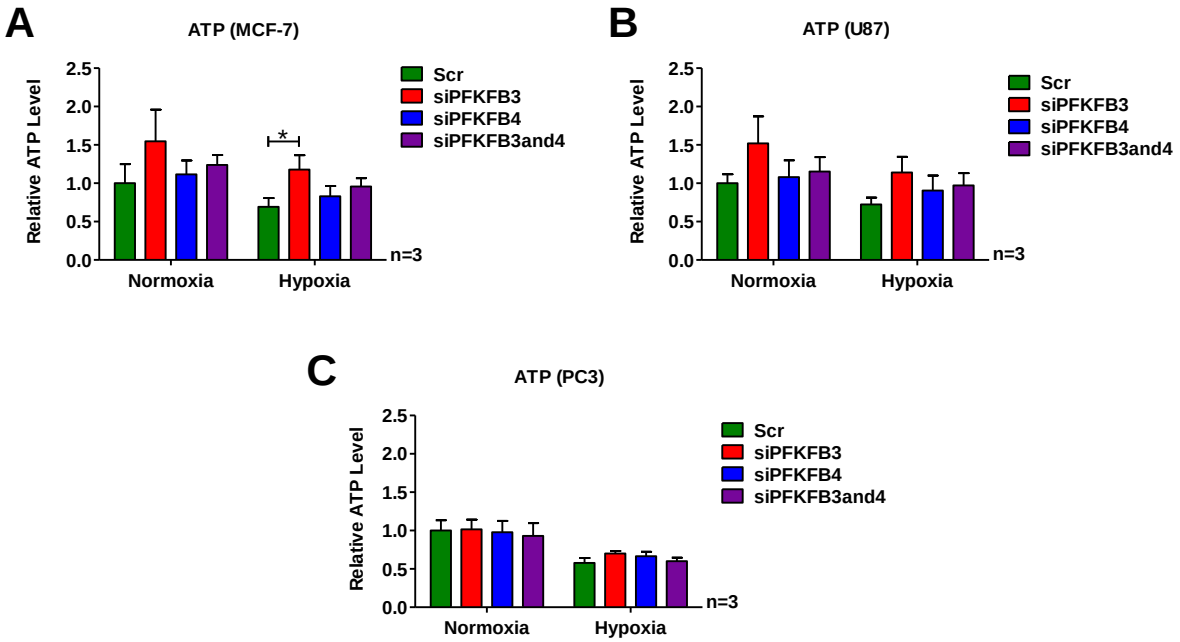

Figure 4.18: Assay of ATP levels with single and double PFKFB3/PFKFB4 knockdown in **(A)** MCF-7, **(B)** U87 and **(C)** PC3 cells under normoxic and hypoxic conditions. Single siRNA knockdown of PFKFB3 significantly increased ATP levels in **(A)** MCF-7 cells (hypoxia), but no significant effects were observed in response to single/double PFKFB3 or PFKFB4 knockdown in **(A)** MCF-7, **(B)** U87 cells or **(C)** PC3 cells after 48 h normoxia/hypoxia. n=3; One-way ANOVA analysis performed with Bonferroni correction, comparing all normoxic data sets with one another, and all hypoxic data sets with one another; *($p<0.05$), **($p<0.01$), ***($p<0.001$), ****($p<0.0001$).

At first sight, the results were unexpected as the logical expectation would be that suppression of PFKFB3 activity, leading to reduced [F-2,6-BP], would reduce activity of PFK-1, decrease glycolytic flux and therefore reduce ATP production. If PFKFB4 were to have a high bisphosphatase activity in all of the cell lines as anticipated, the converse argument and corresponding effect on ATP levels might be expected to apply. In fact, the only significant finding was an increase in ATP levels in MCF-7 cells in response to PFKFB3 knockdown under hypoxic conditions (70(+/-11)%, $p<0.05$) (Figure 4.18A).

Attempts were made to elucidate the nature of this increase in ATP production in response to PFKFB3 knockdown in MCF-7 cells with inhibitors of the three principal sources of ATP

production; oligomycin (mitochondrial respiration), 2DG (glycolysis) and etomoxir (β-oxidation). Unfortunately, no consistent effect of inhibitor treatment was observed, likely due to the small changes in ATP level involved and assay variability (data not shown).

Nevertheless, a number of literature studies have observed that inhibition of glycolysis and reduced proliferation can be associated with a corresponding increase in ATP levels (Matheson, Adams et al. 2007; Knouzy, Dubourg et al. 2010). The authors of these studies highlight the large ATP requirement of cell proliferation, suggesting reduced proliferation leads to a corresponding decrease in ATP consumption. The previous observations in this Chapter that showed knockdown of PFKFB3 was the most effective at reducing proliferation in all three cell lines (Figures 4.6-4.8) would support this explanation.

Furthermore, a reciprocal relationship between glycolysis and oxidative phosphorylation can operate (Swerdlow, E et al. 2013). Indeed, inhibition of glycolysis in PC3 cells has previously been reported to result in an up-regulation of mitochondrial respiration, to compensate (Matheson, Adams et al. 2007). ATP production via glutaminolysis is also known to increase in PC3 cells, in response to decreased glucose metabolism (Matheson, Adams et al. 2007). Mitochondrial respiration is known to contribute to ATP production in all three cell lines (Guppy, Leedman et al. 2002; Matheson, Adams et al. 2007; Zhou, Shingu et al. 2011). Therefore, modulation of its activity, as well as glutaminolysis, could promote maintenance of ATP levels and may further account for the findings in this Chapter.

4.2.5.2: siRNA knockdown of PFKFB3 and PFKFB4 had no significant effect on total lactate production in MCF-7, U87 and PC3 cells.

To further elucidate the effect of PFKFB3 and PFKFB4 on metabolic flux, lactate production was assayed in response to siRNA knockdown of these isoenzymes (Figure 4.19). Lactate production increased in the control-transfected MCF-7 and PC3 cells under hypoxic conditions, whereas no change was observed for U87 cells (Figure 4.19A). These findings were consistent with previous literature reports (Beckner, Gobbel et al. 2005; Robey, Lien et al. 2005; Higgins, Withers et al. 2009) and were also supported by the previous observation that U87 cells constitutively expressed HIF-1α in normoxia (Figure 3.8A, Chapter 3). This would likely minimise any additional increase in glycolytic flux under hypoxic conditions, which might be mediated by HIF-1α-regulated expression of glycolytic enzymes.

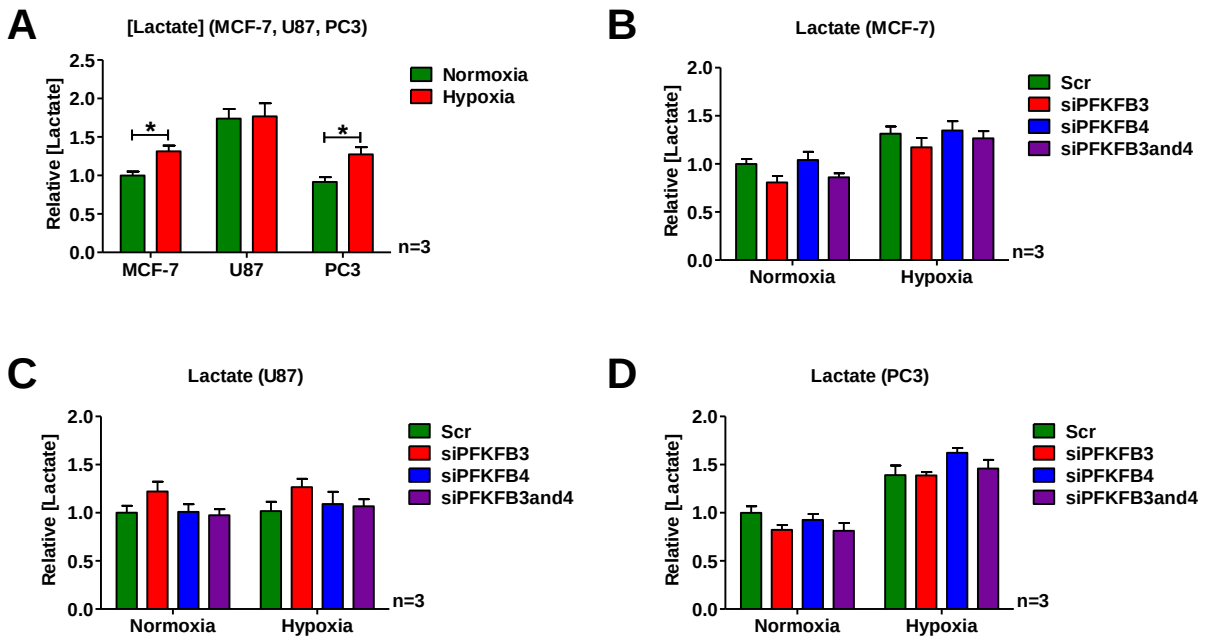

Figure 4.19: Assay of lactate levels with single and double PFKFB3/PFKFB4 knockdown in **(A)** MCF-7, **(B)** U87 and **(C)** PC3 cells under normoxic and hypoxic conditions. **(A)** Total lactate production increased in MCF-7 and PC3 cells under hypoxic conditions in Scr-control transfected cells (values normalised to MCF-7 normoxia). **(B)-(D)** No significant differences in total lactate production were observed in response to single/double siRNA knockdown of PFKFB3 and PFKFB4 (48 h normoxia/hypoxia, values normalised to scramble normoxic control). n=3; **(A)** Unpaired t-test comparing normoxic and hypoxic samples within each cell line; **(B)-(D)** One-way ANOVA analysis performed with Bonferroni correction, comparing all normoxic data sets with one another, and all hypoxic data sets with one another; *(p<0.05), **(p<0.01), ***(p<0.001), ****(p<0.0001).

There were no significant changes in total lactate observed with PFKFB3/PFKFB4 knockdown in the three cell lines (Figures 4.19B, 4.19C and 4.19D). Although not significant using the ANOVA statistical test, there was a trend for reduced lactate levels in response to PFKFB3 knockdown in MCF-7 and PC3 cells under normoxic conditions (Figures 4.19B and 4.19D, respectively). This is the pattern that had been anticipated, given the high kinase activity of PFKFB3, therefore promoting increased [F-2,6-BP], and potentially increased glycolytic flux. Nevertheless, these were relatively small differences, which was somewhat surprising given the established role of F-2,6-BP in modulating PFK-1 and glycolytic activity. However, total flux through a pathway such as glycolysis can remain constant, while proportional flux, in comparison to alternative pathways, can change.

4.2.5.3: siRNA knockdown of PFKFB3 and PFKFB4 had similar effects to one another on glycolytic efficiency in MCF-7 (increase), U87 (no change) and PC3 (decrease) cells.

Accordingly, in an attempt to further interpret these results, glucose consumption was assayed (Figure A7.1, Appendix) and the glycolytic efficiency estimated (mol lactate produced per mol glucose consumed) (Figure 4.20). The maximum glycolytic efficiency would be 2 mol lactate per mol glucose consumed, if all other glucose-utilising pathways were by-passed.

It had been anticipated that if PFKFB3 and PFKFB4 were to have opposing effects on [F-2,6-BP], they would also have opposing effects on glycolytic efficiency. In fact, reduced expression of both isoenzymes had comparable effects, markedly decreasing glycolytic efficiency in MCF-7 cells (Figure 4.20A) and having no effect in U87 cells (Figure 4.20B). PFKFB4 and PFKFB3/4 double knockdown increased efficiency in PC3 cells under normoxic conditions (Figure 4.20C).

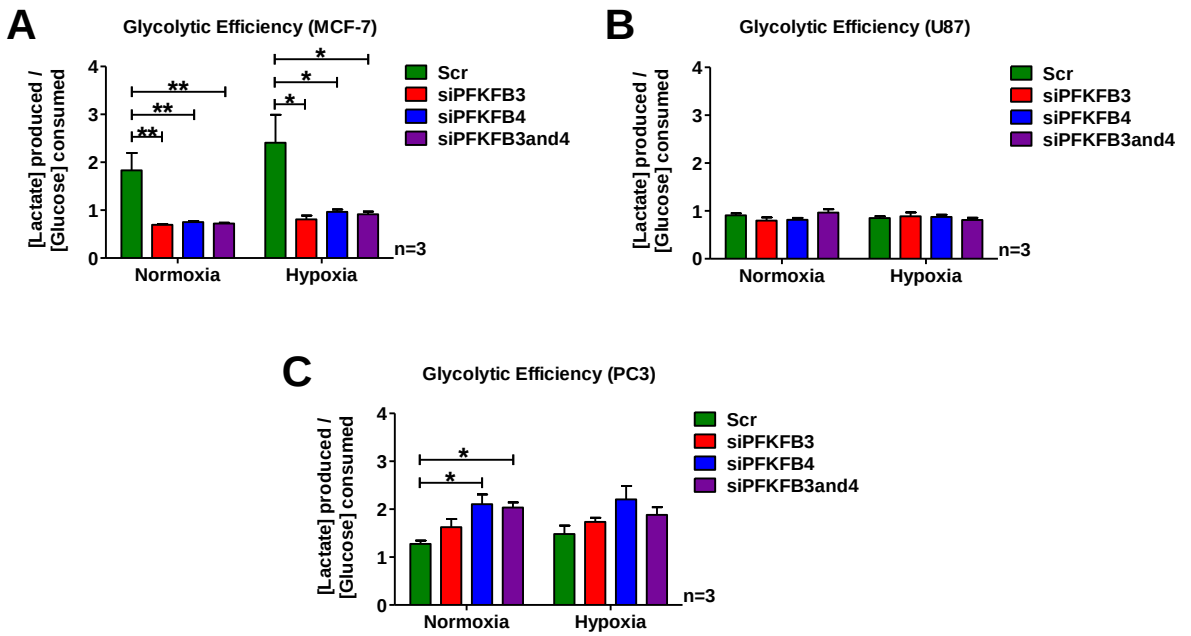

Figure 4.20: Analysis of glycolytic efficiency with single and double PFKFB3/PFKFB4 knockdown in **(A)** MCF-7, **(B)** U87 and **(C)** PC3 cells under normoxic and hypoxic conditions. Single and double siRNA knockdown of PFKFB3 and PFKFB4 significantly reduced glycolytic efficiency in **(A)** MCF-7 cells, but had no effect in **(B)** U87 cells. Single PFKFB4 knockdown and double PFKFB3/PFKFB4 knockdown significantly increased glycolytic efficiency in **(C)** PC3 cells under normoxic conditions. 48 h incubation normoxia/hypoxia. n=3; One-way ANOVA analysis performed with Bonferroni correction, comparing all normoxic data sets with one another, and all hypoxic data sets with one another; *($p<0.05$), **($p<0.01$), ***($p<0.001$), ****($p<0.0001$).

An explanation for this level of complexity was unclear, though it could be reasoned that alterations in PFKFB3 and PFKFB4 expression may elicit wider changes in gene expression linked with processes such as glucose uptake or synthesis of biosynthetic intermediates. The large changes in glycolytic efficiency appear to have comparatively little impact on ATP levels (Figure 4.18), suggesting that the changes in glucose consumption (Figure A7.1, Appendix) permit the cell to modify glucose metabolism. This would compensate for changes in glycolytic efficiency. Modification of the contribution of mitochondrial respiration to total ATP production could also occur. It would be of interest to further investigate these findings, and in particular why such changes would differ between cell lines. However, the focus of this work was to investigate the opposing effects of PFKFB3 and PFKFB4 in the context of proliferation and the [F-2,6-BP] assays, so it was more important to pursue an understanding of potential differences effected specifically on glycolytic flux.

There is a fundamental problem in the term "glycolytic efficiency" and its calculation, because although reported as an indicator of glycolytic flux, lactate production can arise from additional sources, including the pentose phosphate pathway (PPP) and glutaminolysis (Boada, Roig et al. 2000). The measurement of total lactate production had not, and indeed could not have allowed us to interpret the source of this lactate production. [F-2,6-BP] determines the activity of PFK-1, and therefore the balance between glycolysis and alternative shunting of metabolic intermediates towards the PPP. The opposing effects of PFKFB3 and PFKFB4 on [F-2,6-BP], and potentially on metabolic flux might therefore be masked by examining total lactate levels alone, which further work needed to address.

4.3: Discussion

The results demonstrated that siRNA-mediated suppression of both PFKFB3 and PFKFB4 expression reduced *in vitro* 2D growth of MCF-7, U87 and PC3 cells (Figures 4.6, 4.7 and 4.8). PFKFB3 knockdown was consistently the more effective at reducing proliferation. However, the most striking finding was that double PFKFB3/PFKFB4 knockdown was significantly less effective than PFKFB3 knockdown alone in all three cell lines under normoxic conditions (Figures 4.6A, 4.7A and 4.8A).

Both MCF-7 and U87 cell lines showed increased sensitivity to PFKFB3 and PFKFB4 inhibition under hypoxic conditions (Figures 4.6B and 4.7B, respectively), whereas the "rescue" effect was noticeably less pronounced, being significant only for the U87 cell line in hypoxia (Figure 4.7B). This would suggest a non-specific inhibitor as a hypoxia-targeted anti-cancer drug may be sufficiently effective at reducing cell growth. However, the 3D spheroid model data showed a particularly marked "rescue" effect with double knockdown in the U87 cell line (Figure 4.10). This was despite previous unpublished data from the Harris group that had shown U87 spheroids of comparable size to possess a hypoxic core. This indicated

simultaneous inhibition of total PFKFB3 and PFKFB4 enzymatic activity should be avoided as a therapy *in vivo*. If it were possible to inhibit kinase or bisphosphatase activity alone, this problem may potentially be circumvented.

The level of the "rescue" effect of double knockdown in the 2D growth studies appeared to be highest for the two cell lines (U87 (Figure 4.7) and PC3 (Figure 4.8)) with greater relative *PFKFB4*:*PFKFB3* expression ratios and higher absolute PFKFB4 expression (Table 3.2 and Figure 3.18, Chapter 3). This suggested it might be possible to predict in advance and stratify those patients likely to be most responsive to a non-specific total PFK-2/FBPase-2 inhibitor. Nevertheless, the evidence built up thus far suggested that the most effective therapy would be one that specifically targets PFKFB3. The striking effect of PFKFB3 knockdown in the PC3 spheroid model was particularly notable (Figure 4.11). It was observed that knockdown of PFKFB3 in U87 cells increased PFKFB4 protein expression (Figure 4.3B). If the isoenzymes have opposing effects, this would only serve to enhance the effect of PFKFB3-specific inhibition.

It is important to attempt to establish a mechanistic explanation for the "rescue" effect to understand the relationship between PFKFB3 and PFKFB4, but also inform future combination therapies to accentuate the effects mediated by inhibition of either of these isoenzymes on cell growth.

The [F-2,6-BP] assay results confirmed high kinase activity of PFKFB3 in MCF-7 and U87 cell lines (Figures 4.13 and 4.14). It was not possible to detect significant PFKFB3 kinase activity in the PC3 cell line, but high PFKFB4 bisphosphatase activity was observed (Figure 4.16). Double PFKFB3/PFKFB4 knockdown significantly "rescued" both the decrease in [F-2,6-BP] mediated by PFKFB3 knockdown in U87 cells (Figure 4.15B), and the increase in [F-

2,6-BP] mediated by PFKFB4 in PC3 cells (Figure 4.16). This directly implicated changes in [F-2,6-BP] as explaining the effects on proliferation of the double knockdown.

Nevertheless, knockdown of PFKFB4 in MCF-7 reduced cell proliferation, despite having no observable effect on [F-2,6-BP] (Figures 4.6 and 4.13, respectively). Furthermore, double PFKFB3/PFKFB4 knockdown had a rescue effect on cell growth in MCF-7 cell line compared to single PFKFB3 knockdown alone (Figure 4.6), despite there being no significant difference in [F-2,6-BP]. However, cell lines with low relative PFKFB4 expression, such as MCF-7 would likely be more sensitive to small changes in [F-2,6-BP], which may be beyond the detection limit of the [F-2,6-BP] assay.

ATP levels were analysed, in an attempt to explore the effects of these potentially small changes at the metabolic level (Figure 4.18), but minimal change was observed, which was initially surprising. However, the role of glycolysis in supplying biosynthetic intermediates to the cell is thought to be more important than for ATP production, which is no longer considered to be a limiting factor for cancer cell proliferation (Vander Heiden, Cantley et al. 2009). This might explain why siRNA knockdown of PFKFB3 and PFKFB4 was observed to markedly reduce cell growth, whilst having minimal effect on ATP content. Indeed it may be that the balance between glycolytic and PPP flux is crucial in meeting the ATP, biosynthetic and antioxidant requirements of the cell.

A recent study by Ros and colleagues showed an increase in ROS-mediated apoptosis in prostate cancer cells, due to PFKFB4 inhibition mediating reduced PPP and therefore a decrease in NADPH and GSH levels (Ros, Santos et al. 2012). It is therefore postulated that tipping the balance of flux in either direction (in favour of glycolysis, or in favour of the PPP)

would have a detrimental impact on the cancer cell, which may explain the growth curve results presented in this Chapter.

Initial attempts to investigate the effect of PFKFB3 and PFKFB4 on metabolic flux were met with unexpected results when glycolytic efficiency was calculated from the glucose consumption and lactate production assay data (Figure 4.20). Knockdown of the two isoenzymes had the same effect on glycolytic efficiency, albeit different effects in different cell lines. It became apparent that the "glycolytic efficiency" was an unsuitable measure to examine changes in relative glycolytic and PPP activity, due to multiple potential lactate sources. Furthermore, a distinction must be made between changes in total flux through a pathway and changes in proportional flux. Interpreting the potentially opposing effects of PFKFB3 and PFKFB4 necessitated analysis of changes in proportional flux through the glycolytic and PPP pathways, which required more detailed metabolite tracking. Further work outlined in the next Chapter sought to address this issue.

Chapter 5: Examining the Effects of Knockdown of PFKFB3 and PFKFB4 on Metabolic Pathways

5.1: Introduction and Aims

The opposing effects of PFKFB3 and PFKFB4 on intracellular [F-2,6-BP] in the cell lines investigated required further study, particularly in terms of their effects on cellular metabolism. Of particular importance was to examine any effect of these isoenzymes on the balance between glycolytic flux and flux through the pentose phosphate pathway (PPP). It was therefore necessary to gain some measure of the relative contributions of each of these pathways. A comprehensive approach was taken, involving indirect analyses (reactive oxygen species (ROS) levels and lipid droplet levels, which are directly and indirectly modulated by PPP activity, respectively) and direct analyses (quantitative mass spectrometry (MS) and nuclear magnetic resonance (NMR) analysis).

5.1.1: Reactive Oxygen Species

Reactive oxygen species (ROS), which include superoxide radicals $[O_2]^{\bullet-}$, hydroperoxyl radicals $[O_2H]^{\bullet}$ and hydroxyl radicals $[OH]^{\bullet}$, usually derive from partial reduction of oxygen as products of mitochondrial oxidative metabolism. At intermediate intracellular concentrations, they perform important signal transduction roles in cells (Sosa, Moline et al. 2013). However, excess ROS can induce oxidative stress, leading to DNA damage, inhibition of protein function and promotion of ROS-mediated apoptosis (Circu and Aw 2010; Sosa, Moline et al. 2013). Glucose metabolism via the PPP generates the by-product NADPH, which acts as a co-factor in glutathione (GSH) synthesis. GSH is one of the most ubiquitous reducing agents, and is able to scavenge ROS, thereby maintaining intracellular redox homeostasis, protecting the cell from ROS-induced oxidative stress (Vaughn and Deshmukh 2008). It was therefore anticipated that modulation of PPP activity by either PFKFB3 or

PFKFB4 should directly impact intracellular ROS levels, hence providing an indirect method for examining the effect of these isoenzymes on the two pathways. Indeed, a recent study by Ros and colleagues observed an increase in ROS levels in response to PFKFB4 knockdown in prostate cancer cells grown under lipid-limited, normoxic growth conditions (Ros, Santos et al. 2012). The authors attributed this to the high bisphosphatase activity of PFKFB4 which when depleted, caused a reduction in flux towards the PPP and a corresponding increase in glycolytic flux, via F-2,6-BP mediated activation of PFK-1. This was consistent with a previous study by Bensaad and colleagues. Those researchers observed TIGAR, which has high bisphosphatase activity, to reduce intracellular ROS, protecting cells from ROS-induced apoptosis and autophagy via diversion of glucose flux towards the PPP, thereby increasing levels of NADPH for glutathione synthesis (Bensaad, Tsuruta et al. 2006; Bensaad, Cheung et al. 2009).

5.1.2: Lipid Droplets

Lipid droplets (LDs) are dynamic intracellular organelles formed of a phospholipid and sterol monolayer which store a core of non-polar lipids, including triacylglycerides and cholesteryl esters, which can derive from both endogenous and exogenous sources (Santos and Schulze 2012). LDs have been found to be increased in cancer cells and the triacylglycerides they contain provide “building blocks” for membranes and a readily available supply of fatty acids for β-oxidation, to generate ATP (Santos and Schulze 2012; Walther and Farese 2012). This is thought to provide cancer cells with a competitive advantage when ATP supplies from other sources are low (Farese and Walther 2009).

Triacylglycerides are esters derived from glycerol-3-phosphate and three fatty acid units. Glycerol-3-phosphate can be synthesised intracellularly from glycolysis, via reduction of dihydroxyacetone phosphate, a process catalysed by the enzyme glycerol-2-phosphate

dehydrogenase (Figure 5.1). The acetyl groups for fatty acid synthesis derive principally from the TCA-cycle intermediate citrate, which is exported from the mitochondria and converted to acetyl coenzyme A (acetyl CoA) and oxaloacetate by the enzyme ATP citrate lyase (Figure 5.1). Oxaloacetate can then be converted to malate by the enzyme NAD-dependent malate dehydrogenase and the malate then undergoes conversion to pyruvate, catalysed by the enzyme NADP-dependent malate dehydrogenase. This final step generates NADPH, which is required as a reducing agent for fatty acid synthesis. Additional NADPH for this purpose is supplied by the PPP (Figure 5.1).

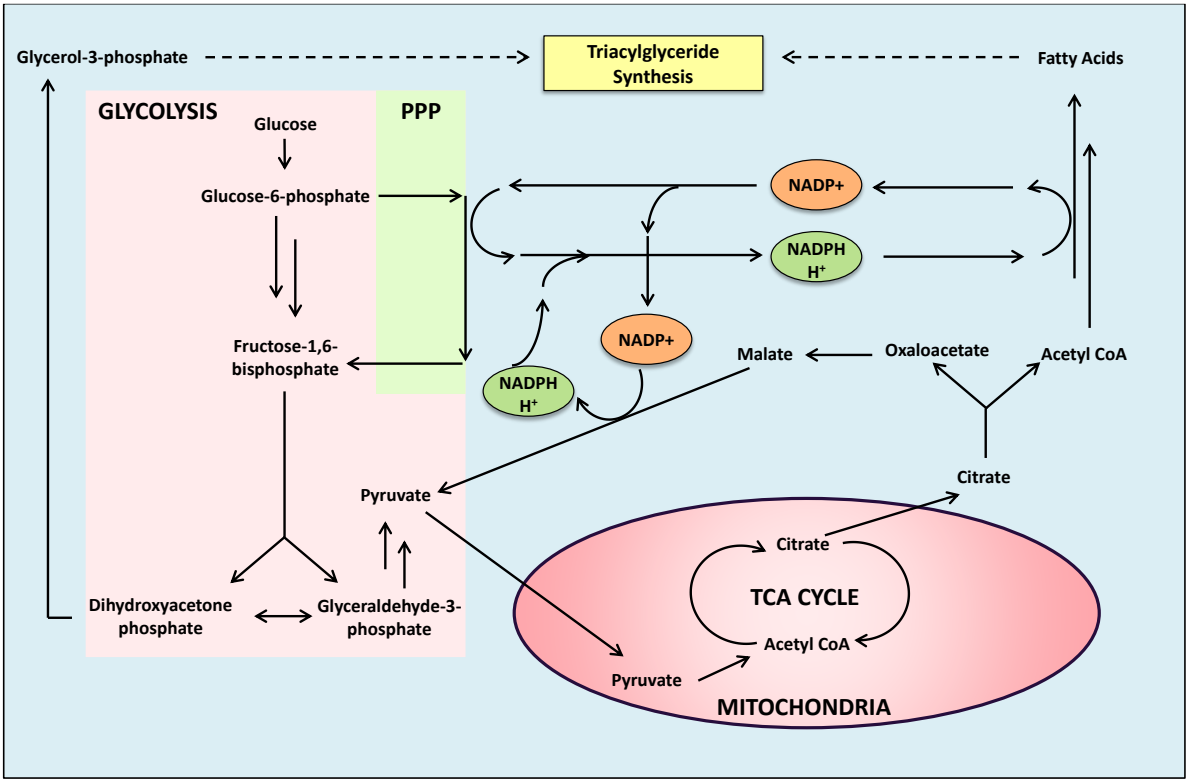

Figure 5.1: Triacylglyceride synthesis from glycerol-3-phosphate and fatty acids, derived from glucose metabolism. PPP (pentose phosphate pathway), NADPH (reduced nicotinamide adenine dinucleotide phosphate), $NADP^+$ (nicotinamide adenine dinucleotide phosphate) and TCA (tricarboxylic acid). Enzymes are excluded from Figure for simplification.

The synthesis of triacylglycerides and therefore lipid droplet levels, are thus linked to the activities of both glycolysis and the PPP. Accordingly, it was hypothesised that changes in the balance between glycolysis and the PPP potentially mediated by PFKFB3 and PFKFB4, might have a direct effect on lipid droplet levels. This would be a result of changes in lipid

synthesis mediated through modulation of the supply of biosynthetic intermediates for fatty acid and glycerol-3-phosphate synthesis via glycolysis, or modulation of the supply of NADPH via the PPP.

5.1.3: Mass Spectrometry

The use of mass spectrometry provides a highly sensitive technique to permit quantification of a large number of metabolites from a biological sample (Becker, Kortz et al. 2012). The technique offers an advantage over ^{1}H NMR due to its higher sensitivity, which means smaller amounts of sample are required for analysis. The two predominant variants employed in metabolite detection are liquid chromatography – mass spectrometry (LC-MS) and gas chromatography – mass spectrometry (GC-MS). These techniques involve chromatographic separation in the liquid or gas phases, respectively, prior to ionisation (Griffin and Kauppinen 2007). This enables separation of isomers, which is particularly important when processing cellular extracts that contain multiple metabolites with the same mass, such as glucose-6-phosphate (MW = 260 g/mol) and fructose-6-phosphate (MW = 260 g/mol) (Lei, Huhman et al. 2011).

Previous studies have employed the analysis of metabolites by LC-MS and GC-MS experiments to quantify the activity of metabolic pathways, including glycolysis, gluconeogenesis, the PPP and glutaminolysis (Huck, Struys et al. 2003; Hunnewell and Forbes 2010). The higher temperatures used in GC-MS often require chemical derivatisation of the metabolites to increase their stability, as well as their volatility. The use of LC-MS generally avoids this additional preparation step (Roessner, Wagner et al. 2000) and therefore was the preferred method for the current study.

5.1.4: Nuclear Magnetic Resonance Spectroscopy

Nuclear magnetic resonance (NMR) spectroscopy has been used extensively as a powerful tool for studying tumour metabolism (Portais, Schuster et al. 1993; Griffiths, McSheehy et al. 2002), as well as quantifying *in vitro* and *in vivo* metabolic fluxes when used in combination with ^{13}C-enriched substrates (Sibson, Mason et al. 2001; Serres, Bezancon et al. 2004; Bartnik, Sutton et al. 2005; de Graaf, Rothman et al. 2011; McIntyre, Madhu et al. 2012). The direct detection of ^{13}C-labelled metabolites by ^{13}C NMR is possible, but this technique has reduced sensitivity compared to ^{1}H NMR, meaning extended acquisition times are required. It is therefore preferable to indirectly detect the ^{13}C labels in ^{13}C-labelled metabolites by using ^{1}H NMR (Fitzpatrick, Hetherington et al. 1990; Novotny, Ogino et al. 1990). This relies on the detection of signals from protons bound to the ^{13}C atoms in the labelled metabolites, which gives rise to characteristic splitting patterns.

Although NMR has reduced sensitivity compared to mass spectrometry, it is able to provide positional enrichment information in labelling experiments. ^{13}C-labelled glucose has been widely used in NMR studies to examine *in vitro* and *in vivo* glycolytic and PPP flux, by measuring the positional enrichment of ^{13}C-labelling in the lactate derived from these pathways (Dusick, Glenn et al. 2007). This can be effectively achieved using the single tracer 2-^{13}C glucose as a substrate (Messana, Misiti et al. 1999; Delgado, Castro et al. 2004). Through mapping out the glycolytic and PPP pathways (Figures A8.1A and A8.2B, Appendix), it can be demonstrated that metabolism of 2-^{13}C glucose via glycolysis produces 2-^{13}C lactate, whereas metabolism via the PPP produces both 1,3-^{13}C lactate and 3-^{13}C lactate, as summarised in Figure 5.2. It follows then, that quantification of the ^{1}H NMR signal for 2-^{13}C lactate enables estimation of glycolytic lactate production and quantification of the combined signals for both 3-^{13}C lactate and 1,3-^{13}C lactate enables estimation of PPP lactate

production. This in turn allows an estimation of relative flux through glycolysis or the PPP to be made, after application of a correction factor.

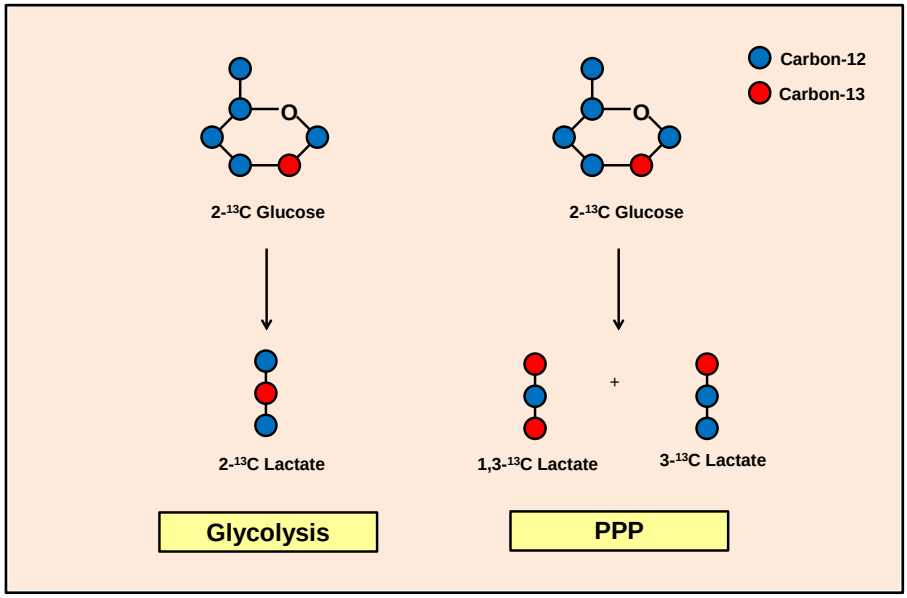

Figure 5.2: Metabolism of 2-^{13}C glucose via glycolysis and the PPP. The metabolism of 2-^{13}C glucose via glycolysis leads to production of 2-^{13}C lactate, whereas metabolism via the pentose phosphate pathway (PPP) leads to production of 1,3-^{13}C lactate and 3-^{13}C lactate. Presented equations are non-stoichiometric and unlabelled lactate production is excluded from the figure for simplification.

All metabolic studies have their limitations and the metabolism of glucose in cancer cells is naturally more complex than direct conversion to lactate through either the glycolytic or PPP pathways. The channelling of labelled pyruvate to oxidative phosphorylation will reduce the proportion of the initial ^{13}C atoms that appear in the lactate end product. Nevertheless, the loss of labelled pyruvate through oxidative phosphorylation in the mitochondria should occur in proportion to the relative amounts of the different labelled pyruvate species. The final analysis of labelled lactate ratios should therefore be unaffected. If a significant removal of ribose-5-phosphate from the "system" for nucleotide synthesis occurs, it will lead to underestimation of the contribution from the PPP (Lee, Boros et al. 1998). However, this should not preclude observation of changes in glycolytic:PPP lactate production in response to PFKFB3 or PFKFB4 siRNA knockdown.

It is possible to employ models to account for recycling of labelled fructose-6-phosphate through the PPP, in order to estimate actual fluxes through the glycolytic or PPP pathways (Wood, Katz et al. 1963; Schrader, Eskey et al. 1993). However, for our preliminary study, it was considered sufficient to restrict measurements to changes in the ratio of 2-^{13}C lactate to 1,3- and 3-^{13}C lactate, as an indicator of modification of relative flux through glycolysis or the PPP.

It was envisaged that the combination of the four assays outlined would assist in determining the effect of both PFKFB3 and PFKFB4 on metabolic flux in the cell lines of interest.

5.2: Results

5.2.1: Reactive Oxygen Species Assay

5.2.1.1: A significant increase in reactive oxygen species (ROS) levels was observed in response to PFKFB3 siRNA knockdown in MCF-7 cells under normoxic conditions; no other significant changes in ROS were observed with single or double PFKFB3 and PFKFB4 knockdown in the cell lines examined.

MCF-7, U87 and PC3 cells were reverse transfected according to the standard protocol to provide a scramble control, single PFKFB3, single PFKFB4 and double PFKFB3/PFKFB4 siRNA knockdown. After 48 hours exposure to normoxic or hypoxic conditions, the cell-permeable non-fluorescent carboxy-5(6)-carboxy-2',7'-dichlorodihydrofluorescein diacetate (carboxy-H_2DCFDA, Sigma Aldrich) was used to assay general oxidative stress in the cells. Intracellular esterases remove the acetate groups, trapping the probe in the cell, which is then oxidised to a fluorescent molecule by ROS. Propidium iodide was added to enable selection of viable cells and de-selection of dead or dying cells, which produce high levels of ROS. The mean fluorescence was measured using fluorescence activated cell sorting (FACS) (Figure 5.3).

There was a general pronounced increase in ROS levels under hypoxic conditions for both the MCF-7 and PC3 cell line (Figures 5.3A and 5.3C), which was consistent with previous literature reports (Chandel, Vander Heiden et al. 2000; Guzy and Schumacker 2006). No increase in ROS in the U87 cells under hypoxic conditions was observed (Figure 5.3B), again consistent with previous reports (Hsieh, Lee et al. 2010).

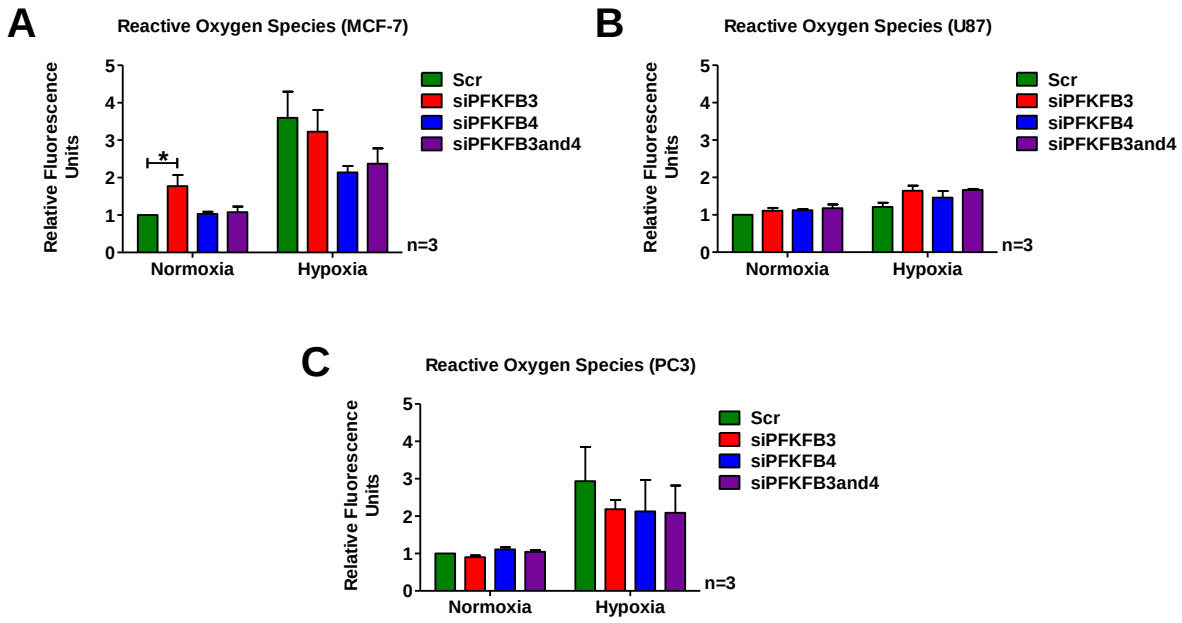

Figure 5.3: Assay of ROS levels with single and double PFKFB3/PFKFB4 knockdown in **(A)** MCF-7, **(B)** U87 and **(C)** PC3 cells under normoxic and hypoxic conditions. ROS levels were assayed using carboxy-5(6)-carboxy-2',7'-dichlorodihydrofluorescein diacetate (carboxy-H_2DCFDA) in **(A)** MCF-7, **(B)** U87 and **(C)** PC3 cells after scramble control, single PFKFB3, single PFKFB4 and double PFKFB3/PFKFB4 siRNA knockdown. The experiments were performed under both normoxic and hypoxic conditions (48 h incubation). A significant increase in ROS levels was observed in response to PFKFB3 knockdown under normoxic conditions **(A)**. ROS levels were found to increase under hypoxic conditions in the MCF-7 **(A)** and PC3 **(C)** cell lines. Mean fluorescence values of approximately 50,000 cells were normalised to scramble (normoxia) control. n=3; One-way ANOVA analysis performed with Bonferroni correction, comparing all normoxic data sets with one another, and all hypoxic data sets with one another; *($p<0.05$), **($p<0.01$), ***($p<0.001$), ****($p<0.0001$).

However, the results obtained for the PFKFB3 and PFKFB4 siRNA-treated groups were somewhat surprising (Figure 5.3). It had been anticipated that siRNA knockdown of PFKFB3 would lead to a decrease in ROS levels, by decreasing intracellular [F-2,6-BP], decreasing PFK-1 activity, decreasing glycolysis and directing glucose flux towards the PPP, thereby generating NADPH. The opposite argument was expected to apply to knockdown of PFKFB4, with its high bisphosphatase activity. In fact, the only significant finding in

response to suppression of either PFKFB3 or PFKFB4 expression was an increase in ROS levels after PFKFB3 siRNA knockdown in the MCF-7 cells under normoxic conditions (increase of 77(+/-30)%, $p<0.05$), the opposite to that originally expected (Figure 5.3A). The results suggested that PFKFB3 and PFKFB4 were able to indirectly modulate ROS levels in a manner distinct from, but potentially in addition to, a role in controlling balance between glycolytic and PPP flux.

5.2.2: Lipid Droplet and Fatty Acid Uptake Assays

The ROS assay had proved inconclusive, so another indirect method to measure potential changes in the balance between glycolysis and the PPP was employed, namely lipid droplet (LD) analysis. The fluorescent lipophilic dye LD540, based on the BODIPY fluorophore (Spandl, White et al. 2009), was used to stain lipid droplets, which were then analysed by FACS.

5.2.2.1: siRNA knockdown of PFKFB4 significantly increased lipid droplet content in MCF-7 cells under normoxic conditions; single PFKFB3 and double PFKFB3/PFKFB4 knockdown significantly increased lipid droplet content in MCF-7 cells under hypoxic conditions; no other significant changes were observed in response to single or double PFKFB3/PFKFB4 knockdown in MCF-7, U87 or PC3 cells.

The LD experiment was performed using the MCF-7, U87 and PC3 cell lines, with single and double siRNA knockdown of PFKFB3 and PFKFB4, under both normoxic and hypoxic conditions (Figure 5.4). Under hypoxic conditions, a pronounced increase in LD content for the MCF-7 cell line was observed, in addition to small increases in the U87 and PC3 cell lines (Figure 5.4). These findings were consistent with previous studies (Gordon, Barcza et al. 1977; Santos and Schulze 2012). This hypoxic increase in LD content is thought, in part, to be attributed to a reduction in mitochondrial NAD^+, leading to inhibition of β-oxidation. HIF-1 has also been shown to promote lipid droplet formation by induction of the hypoxia inducible

protein 2 (HIG-2), a protein involved in deposition of lipids in lipid droplets (Gimm, Wiese et al. 2010; Santos and Schulze 2012). Although not fully understood, it is thought that enhanced triacylglyceride storage during periods of intermittent hypoxia may provide a readily available ATP supply via β-oxidation of fatty acids following re-oxygenation (Santos and Schulze 2012).

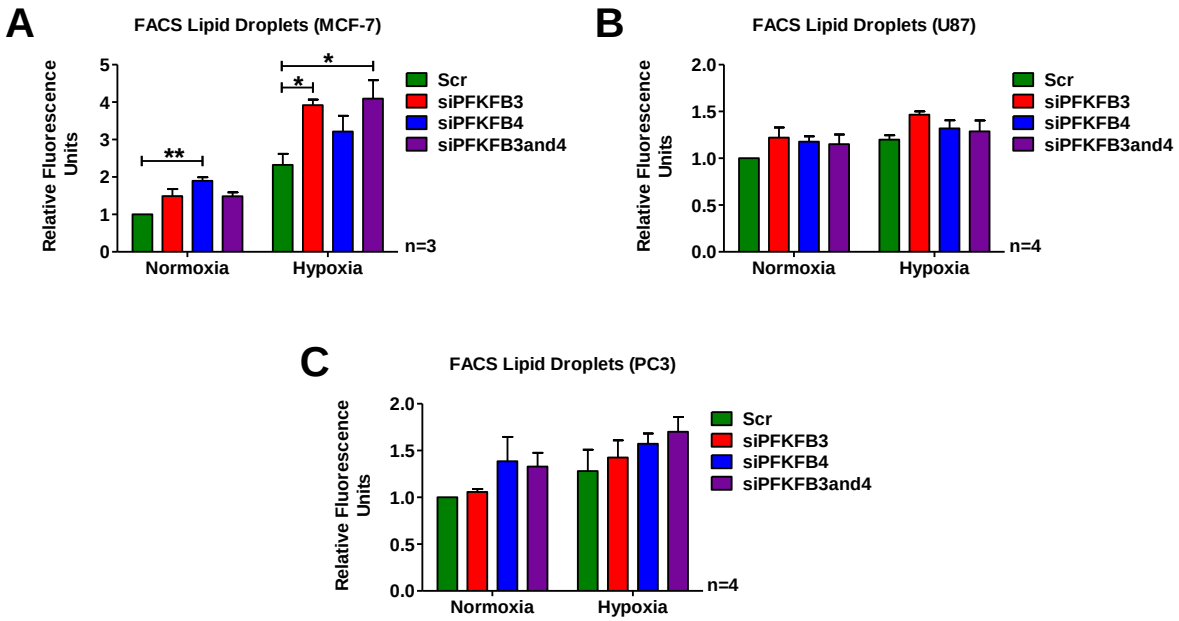

Figure 5.4: Assay of lipid droplet levels with single and double PFKFB3/PFKFB4 knockdown in **(A)** MCF-7, **(B)** U87 and **(C)** PC3 cells under normoxic and hypoxic conditions. LD540 fluorescence activated cell sorting (FACS) analysis of lipid droplet (LD) content in **(A)** MCF-7, **(B)** U87 and **(C)** PC3 cells in response to single and double siRNA knockdown of PFKFB3 and PFKFB4 expression under both normoxic and hypoxic conditions. Significant increases in lipid droplet content were observed in response to PFKFB4 knockdown (normoxia) and PFKFB3/PFKFB4 double knockdown (hypoxia) in the MCF-7 cell line **(A)**. 48 h incubation normoxia/hypoxia. n=3 (MCF-7), n=4 (U87, PC3); One-way ANOVA analysis performed with Bonferroni correction, comparing all normoxic data sets with one another, and all hypoxic data sets with one another; *($p<0.05$), **($p<0.01$), ***($p<0.001$), ****($p<0.0001$).

In the MCF-7 cells, there was a trend for increased LD content in response to both single and double PFKFB3 and PFKFB4 siRNA knockdown (Figure 5.4A). This was significant for PFKFB4 knockdown under normoxic conditions (increase of 90(+/-10)% compared to scramble (normoxic) control, $p<0.01$), as well as for both single PFKFB3 and double PFKFB3/PFKFB4 knockdown under hypoxic conditions (increases of 69(+/-14)%, $p<0.01$ and 76(+/-25)%, $p<0.01$, respectively, compared to scramble (hypoxic) control). It was noteworthy that the relative LD levels in the double PFKFB3/PFKFB4 knockdown for MCF-

7 cells were comparable to the level for single PFKFB3 knockdown (Figure 5.4A). This was consistent with MCF-7 cells having the highest *PFKFB3*:*PFKFB4* mRNA expression ratio of the three cell lines, with intracellular [F-2,6-BP] of the double knockdown mirroring that of single PFKFB3 knockdown (Figure 4.15A, Chapter 4).

There appeared to be a trend for elevated LD content in response to PFKFB3 knockdown in the U87 cell line, whereas LD content appeared higher after PFKFB4 knockdown in the PC3 cell line (Figures 5.4B and 5.4C, respectively). High inter-replicate variability would have necessitated a prohibitively high number of replicates to obtain significance for these findings. There was little evidence to suggest that PFKFB3 and PFKFB4 had opposing effects on LD levels. The results implied the activities of both isoenzymes were linked to LD levels, albeit in a cell line-specific manner. The increases in LD content observed with PFKFB4 knockdown would be consistent with an increase in glycolytic flux and supply of intermediates for triacylglyceride synthesis, so long as NADPH supply was not a limiting factor. In contrast, the simultaneous increases in LD content in response to PFKFB3 knockdown were somewhat surprising. Although knockdown of PFKFB3 would increase PPP flux, and therefore NADPH production, required for fatty acid synthesis, it seemed surprising that modulation of relative glycolytic/PPP activity in both directions could result in an increase in lipid droplet levels. Logically, one of glycerol-3-phosphate (via glycolysis) or NADPH production (via the PPP) should be a limiting factor for triacylglyceride synthesis. However, therein lay the limitation of measuring total lipid droplet content. Lipids stored in these organelles are derived from a combination of both *de novo* synthesis and uptake from the extracellular environment.

5.2.2.2: No significant changes in BODIPY-C16 uptake were observed in the MCF-7 cells in response to single or double PFKFB3/PFKFB4 knockdown, under both normoxic and hypoxic conditions.

It was supposed that the apparent siPFKFB3-mediated increase in LD levels and the siPFKFB4-mediated increase might be explained by one arising from increased fatty acid uptake by the cell and the other from increased *de novo* synthesis. This would still be consistent with the supposed opposing effects of the two isoenzymes on metabolic flux. Consequently, a fatty acid uptake experiment was performed with MCF-7 cells, chosen as these had exhibited the largest difference in LD content in response to PFKFB3/PFKFB4 knockdown (Figure 5.4A). The experiment made use of the fluorescent BODIPY palmitate analogue (BODIPY-C16) and was analysed using FACS (Figure 5.5). No significant findings were observed, though the results tentatively suggested a potential increase in fatty acid uptake in response to PFKFB3 siRNA knockdown under normoxic conditions. Nevertheless, there was certainly no evidence to suggest increased uptake in the siPFKFB3 samples under hypoxic conditions (Figure 5.5). This strongly suggested that the significant increase in lipid droplet content in response to siPFKFB3 in MCF-7 cells (Figure 5.4A), was at least in part due to increased synthesis, or reduced consumption of lipids from the LDs.

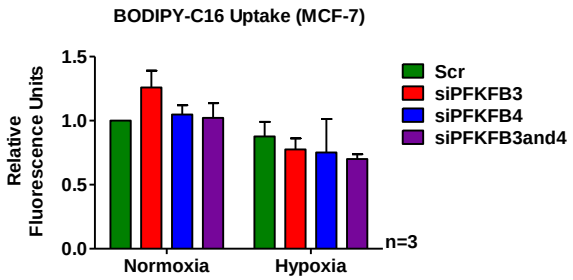

Figure 5.5: Assay of BODIPY-C16 uptake with single and double PFKFB3/PFKFB4 knockdown in MCF-7 cells under normoxic and hypoxic conditions.. The results suggested potential increased fatty acid uptake in response to PFKFB3 knockdown under normoxic conditions in MCF-7 cells. 48 h incubation (normoxia / hypoxia). n=3; One-way ANOVA analysis performed with Bonferroni correction, comparing all normoxic data sets with one another, and all hypoxic data sets with one another; *($p<0.05$), **($p<0.01$), ***($p<0.001$), ****($p<0.0001$).

Accordingly, a series of experiments with the MCF-7 cell line were also performed with deuterated media (0%, 5%, 10%), to measure incorporation of the deuterium label into fatty

acids and thus give a measure of *de novo* synthesis. The collaboration was set up with Prof. Fredrik Karpe and Dr Jennifer Collins (Karpe group). Cell-based work, sample preparation and purification were performed by the author and GC-MS was run by Dr Jennifer Collins. Unfortunately, due to unforeseen circumstances, the processed data was not returned from the collaborators and consequently could not be incorporated in this thesis.

The effects of both PFKFB3 and PFKFB4 on lipid metabolism were intriguing and it would be interesting to further investigate this in the future. The data collected implied that the role of these isoenzymes in lipid metabolism likely extends beyond regulation of glycolysis or the PPP alone. Nevertheless, these indirect measurements had not provided conclusive proof that these isoenzymes were, or were not, acting to modulate glycolysis/PPP, which was the ultimate goal of this work.

5.2.3: Quantitative Mass Spectrometry Studies

It had become apparent that indirect analysis of the balance between glycolysis and the PPP had provided insufficient information to further interpret the involvement of PFKFB3 and PFKFB4 in regulation of these pathways. Therefore, a more direct approach was desirable, through the use of quantitative mass spectrometry. It is important to note that quantification of individual metabolites does not directly indicate flux through a given pathway. Nevertheless, it can provide an indication of pathway activity. An internal collaboration was set up to develop an in-house method for quantifying the amounts of key metabolites involved in the glycolytic and PPP pathways, as detailed in Figure 5.6. This was with a view to further probing the effect of PFKFB3 and PFKFB4 on these pathways. It was not possible to analyse F-2,6-BP levels by mass spectrometry, due to the metabolite's high acid lability and the difficulty of obtaining a commercial F-2,6-BP standard of sufficient purity.

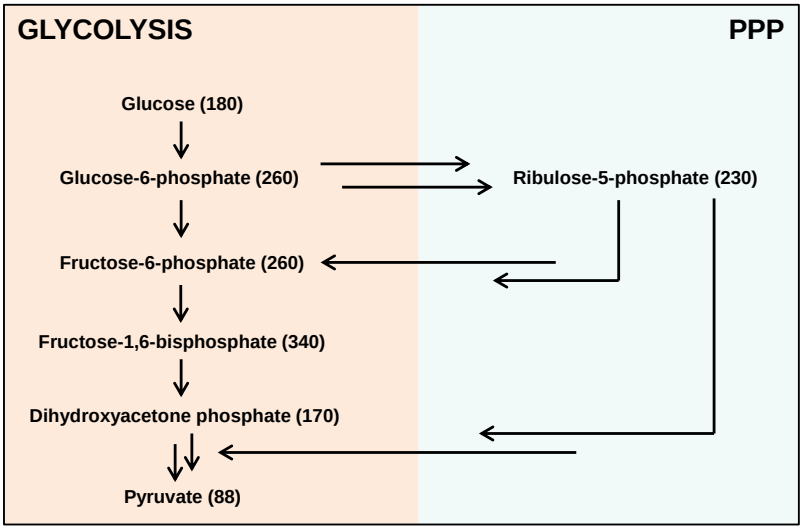

Figure 5.6: Glycolytic and PPP metabolites selected for mass spectrometry studies. A series of metabolites involved in glycolysis and the pentose phosphate pathway (PPP) were selected for liquid chromatography-mass spectrometry (LC-MS) analysis. The molecular weight of each metabolite is listed in parentheses.

The mass spectrometry experiments were designed in collaboration with Dr James McCullagh (Chemistry Research Laboratory, University of Oxford) and Khalid Al-Qahtani (McCullagh group). All cell-based experiments and cell extractions were performed by the author. The samples were then processed and run on the mass spectrometer by Khalid Al-Qahtani, whilst analysis and interpretation of the data was performed by the author.

5.2.3.1: A series of glycolytic and PPP metabolite standards were effectively separated by LC-MS and standard curves were plotted, linking peak area to metabolite concentration.

LC-MS includes an initial liquid-phase chromatographic step, which permits separation of two metabolites that have the same mass and same retention time, e.g. fructose-6-phosphate (F-6-P) and glucose-6-phosphate (G-6-P). Collaborator Khalid Al-Qahtani was able to optimise LC-MS conditions to separate all standard metabolites of interest, including F-6-P and G-6-P (Figure A9.1, Appendix).

The ionisation efficiency of different metabolites can vary considerably in mass spectrometry studies. It was therefore important to control for this by preparing a series of standard curves to correlate LC-MS peak area with the concentration of a particular metabolite. Collaborator

Khalid Al-Qahtani undertook this and demonstrated a linear relationship between peak area and metabolite concentration (Figure A10.1, Appendix). These determined standard curves were used in all subsequent concentration calculations.

5.2.3.2: Inter-sample variability precluded the use of the metabolite mass spectrometry data to make valid conclusions about relative glycolytic/PPP pathway activities.

As an initial starting point, U87 cells were reverse transfected with control scramble and sequence-specific siRNA to give a single PFKFB3, single PFKFB4 and double PFKFB3/PFKFB4 siRNA knockdown. Three plates for each condition were prepared, one for cell counting and two for analysis, from which an average would be calculated. Half of the plates were incubated under normoxic conditions for 48 hours, and the other half were incubated under hypoxic conditions for the same period of time.

The cells were then extracted by the author according to an unpublished protocol provided by the collaborators, involving the use of 80% methanol, containing 0.5 mM fumaric acid-2,3-d_2 standard. The standard was used to account for different metabolite recovery efficiencies from different biological samples. The samples were then stored on dry-ice and lyophilised as quickly as possible, to minimise potential enzymatic degradation of metabolites.

LC-MS samples were run by Khalid Al-Qahtani (McCullagh group), according to his own protocol. Effective separation of each of the metabolites of interest was achieved from the cell extracts, and the peak areas were converted to concentration values using the standard curves, before taking averages of the two readings (two samples per condition) and normalising to cell number (Figure 5.7). At first sight, it appeared that suppression of PFKFB3 expression increased the intracellular concentration of all measured metabolites in this initial study, with the exception of the PPP intermediate ribulose-5-phosphate (Figure 5.7F). However, closer inspection of the raw data prior to normalisation revealed that the concentration values for

PFKFB3 siRNA knockdown were being artificially enhanced due to the lower cell counts for this condition. It became apparent that for a number of the metabolites being examined, their concentration was outside the linear range of the standard curves previously plotted by the collaborators (Figure A10.1, Appendix). This led to the pre-normalised metabolite concentrations being erroneously reported as highly similar across the different conditions for a number of metabolites, which led to over-estimation of the PFKFB3 knockdown values, due to normalisation to a lower cell number. Furthermore, the values calculated for the two experimental sets (identical plates prepared simultaneously) before averaging, demonstrated considerable variation in absolute concentrations, despite correction for metabolite recovery efficiencies. This effect would have been exacerbated in true biological replicates, and so the assay results were unsuitable for further interpretation. The potential increase in R-5-P after PFKFB4 suppression would be interesting to investigate further (Figure 5.7F), to examine if this was representative of a real effect, particularly as a decrease in the PPP and accordingly R-5-P, would be anticipated.

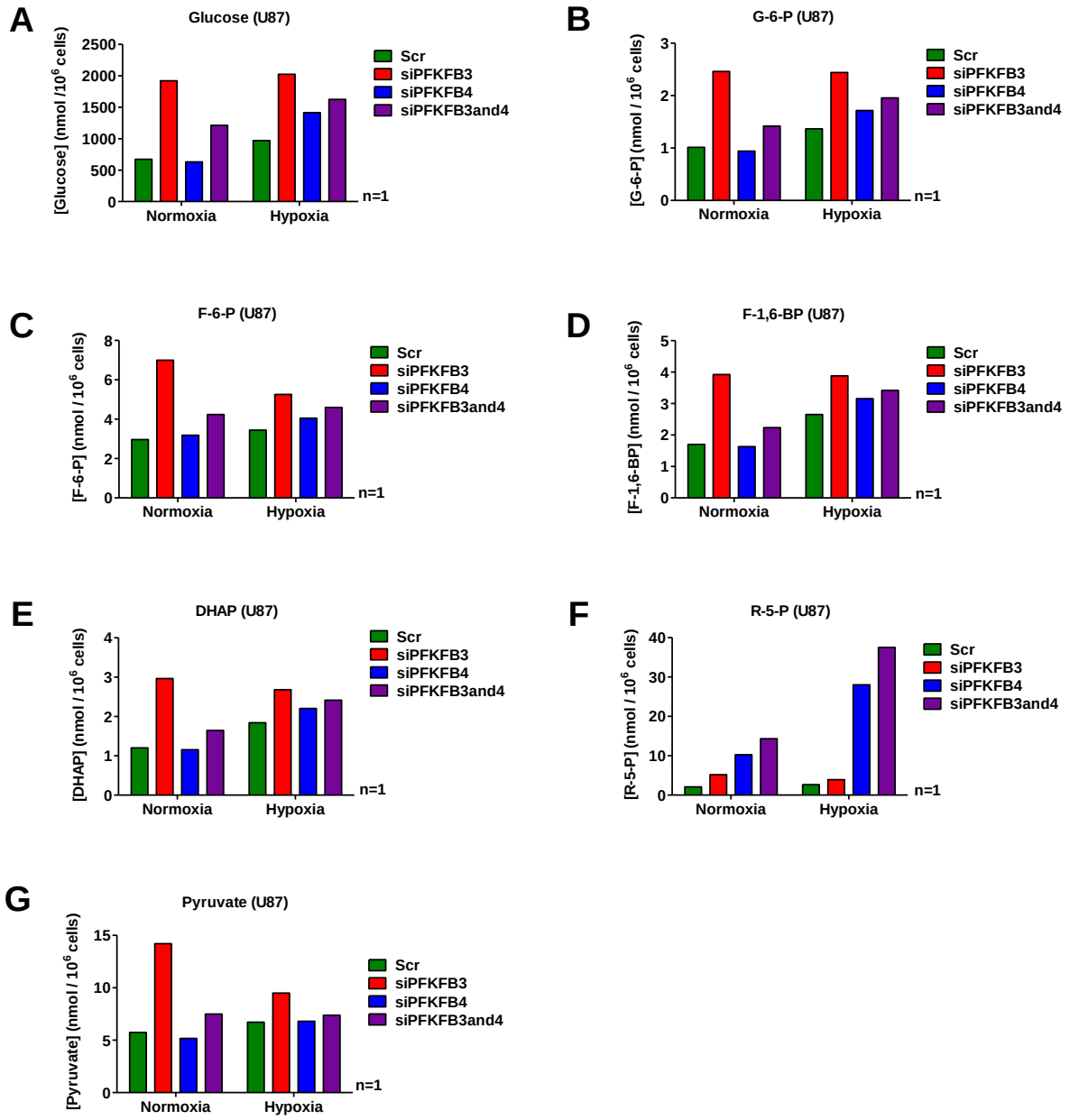

Figure 5.7: Initial quantitative liquid chromatography-mass spectrometry (LC-MS) experiment measuring changes in glycolytic/PPP metabolite concentrations in response to single and double PFKFB3 and PFKFB4 knockdown, under both normoxic and hypoxic conditions in U87 cells. Metabolites **(A)** glucose, **(B)** glucose-6-phosphate (G-6-P), **(C)** fructose-6-phosphate (F-6-P), **(D)** fructose-1,6-bisphosphate (F-1,6-BP), **(E)** dihydroxyacetone phosphate, **(F)** ribulose-5-phosphate (R-5-P) and **(G)** pyruvate. Cell-based work and extractions were performed by the author. Samples were then run on the mass spectrometer by Khalid Al-Qahtani (McCullagh group). Analysis and interpretation of the data was performed by the author.

A repeat of the experiment again demonstrated high inter-sample variability between essentially identical samples, prepared simultaneously. It was evident that further optimisation of metabolite extraction was required to reduce inter-sample variability and the potential

effects of metabolite-degradation via activity of functional enzymes in the extraction mixture. Initial attempts to reduce the time between extraction and freeze-drying were not met with success. Increasing the amount of sample was not a viable option due to the expense of transfection reagents involved. Re-calibration of the standard curves for lower metabolite concentrations was also required. The timescale of the optimisation unfortunately took it beyond the timeframe of this thesis. An alternative strategy, pending full in-house assay optimisation, would be to out-source the studies to collaborators with existing capabilities, or to commercial suppliers. In any event, the information that would be provided by this technique would only serve to supplement the more powerful flux analyses that can be provided by NMR experiments.

5.2.4: ^{1}H NMR Analysis of ^{13}C-labelled Lactate

An internal collaboration was set up to allow in-house development of the NMR assay. All cell-based experiments, purification techniques, and sample preparations were performed by the author. The NMR acquisition protocols were set by Dr Tim Claridge (Chemistry Research Laboratory, University of Oxford), who also ran the samples on the NMR spectrometer. All raw data was processed, analysed and interpreted by the author. The experiments were designed in collaboration with Dr Nicola Sibson (Gray Institute, University of Oxford), Dr Sébastien Serres (Sibson group) and Dr Tim Claridge, all of whom are gratefully acknowledged for their assistance.

5.2.4.1: Initial control samples showed high background interference in the ^{1}H NMR from media components, obscuring the signals from ^{13}C-labelled lactate.

As an initial control experiment, U87 cells were incubated with either unlabelled ^{12}C glucose-DMEM, or labelled 2-^{13}C glucose-DMEM for 24 hours, before removing the media, adding trace sodium azide as a preservative and lyophilising. ^{1}H NMR analysis confirmed

incorporation of the ^{13}C label in the lactate species, as identified by the characteristic splitting patterns, but high signal interference from other media components, particularly amino acids, made it difficult to accurately integrate the relevant ^{1}H signals from the labelled lactate species (data not shown).

5.2.4.2: Removal of amino acids from the cell media reduced background interference in the ^{1}H NMR.

It was therefore decided to reduce the background interference by repeating the experiment and passing the media through an acidified Dowex® 50W X8 acid-exchange resin under gravity filtration to remove amino acids, followed by lyophilisation. This purification method was laborious, but resulted in a much improved reduction in signal interference at the chemical shifts of interest (Figures 5.8B and 5.8C, blue curves; media from U87 cells). For ease of reference, the relevant labelled and unlabelled lactate species are depicted in Figure 5.8A.

The signal arising from the CH proton of lactate (C2 carbon) occurs from chemical shift δ = 4.44–4.16 (Figure 5.8B, blue curve). The apparent quartet at δ = 4.31 (^{3}J = 7.0 Hz) arises from coupling of the proton at C2 of unlabelled ^{12}C-lactate (H_A) with the three vicinal methyl C3 protons (H_B). The C2 protons of 3-^{13}C lactate (H_E) and 1,3-^{13}C lactate (H_G) also appear at this resonance, but additional splitting of the principal quartet by coupling to the ^{13}C atoms in these molecules was not resolved. The "satellite" peaks at δ = 4.41 and δ = 4.20 correspond to the C2 proton of 2-^{13}C lactate (H_C). This doublet of quartets arises due to coupling of the C2 proton (H_C) to the three vicinal methyl C3 protons (H_D, ^{3}J = 7.0 Hz) and additional one-bond coupling to the directly-bound 2-^{13}C atom (^{1}J = 144.0 Hz). Integration of these CH "satellite" peaks (H_C) gives the relative contribution from 2-^{13}C lactate and therefore an estimate of the contribution of lactate production via glycolysis.

The signals arising from the CH_3 protons of lactate occur from δ = 1.48– 1.20 (Figure 5.8C, blue curve). The principal multiplet at δ = 1.35– 1.32 in part results from a doublet, which arises from coupling of the three methyl C3 protons of unlabelled ^{12}C-lactate (H_B) to the vicinal C2 proton (H_A, ^3J = 7.0 Hz). A further multiplet (doublet of doublets) at the same chemical shift arises from the 2-^{13}C lactate species, due to coupling of the three methyl C3 protons (H_D) to the vicinal C2 proton (H_C, ^3J = 7.0 Hz), with additional geminal two-bond coupling to the 2-^{13}C atom itself (^2J = 4.8 Hz). The "satellite" peaks at δ = 1.44-1.41 and δ = 1.26-1.23 result from the three methyl C3 protons of both 3-^{13}C lactate (H_F) and 1,3-^{13}C lactate (H_H). The principal doublet of doublets splitting pattern arises in both species due to coupling of the three methyl C3 protons (H_F and H_H) to the vicinal C2 protons (H_E and H_G, respectively, ^3J = 7.0 Hz) and one-bond coupling to the directly-bound 3-^{13}C atom (^1J = 129.0 Hz). This doublet of doublets is further split to give a doublet of doublet of doublets for the 1,3-^{13}C lactate species due to additional vicinal three-bond coupling of H_H with the ^{13}C at the C1 position (^3J = 4.5 Hz). Integration of these CH_3 "satellite" peaks (H_F and H_H) gives the relative contribution from both 3-^{13}C lactate and 1,3-^{13}C lactate, which when corrected for proton number, gives an estimate of the contribution of lactate production via the pentose phosphate pathway (PPP).

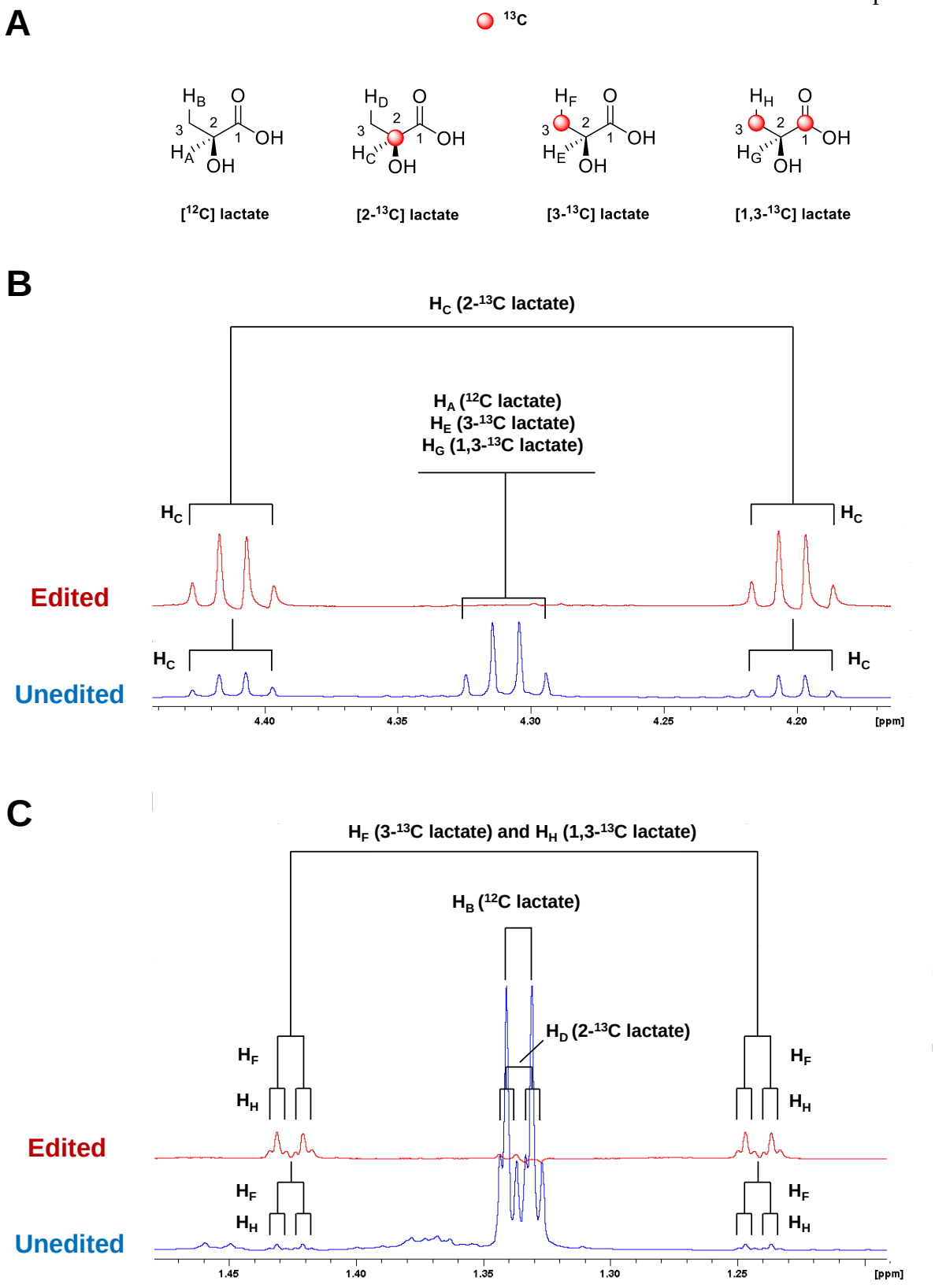

Figure 5.8: Unedited and edited NMR spectra showing ^{13}C-labelled lactate species arising from metabolism of 2-^{13}C glucose via glycolysis and the PPP. The relevant unlabelled and labelled lactate species are depicted in **(A)**. The spectra are of media samples from U87 cells after 24 h incubation with 2-^{13}C glucose showing regions of the spectrum with signals arising from **(B)** CH (carbon-2) and **(C)** CH_3 (carbon-3) protons of the lactate species. Satellite peaks (doublet of quartets) in **(B)** at δ = 4.41 and δ = 4.20 correspond to the CH proton from 2-^{13}C lactate (H_C), which is produced via glycolysis. Satellite peaks in **(C)** at δ = 1.44-1.41 and δ = 1.26-1.23 arise from the CH_3 protons of 3-^{13}C lactate (H_F) and 1,3-^{13}C lactate (H_H), which are both produced via the pentose phosphate pathway. The cells and NMR samples were prepared by the author, the NMR spectra were run by Dr Tim Claridge (Chemistry Research Laboratory) and the raw data was processed, analysed and interpreted by the author. Blue curves: unedited ^{1}H NMR, red curves: proton observed carbon edited (POCE) NMR.

5.2.4.3: POCE NMR reduced background interference but calculated standard 2-^{13}C lactate: 3-^{13}C lactate ratios did not directly correlate with those calculated from ^{1}H NMR.

In an effort to further reduce signal interference from other media components and improve signal-to-noise ratio, proton-observed carbon-editing (POCE) NMR was utilised. POCE is an NMR technique used to select only those signals in the ^{1}H NMR resulting from direct binding of protons to ^{13}C atoms. It combines the high-sensitivity of ^{1}H NMR with improvements in resolution (Fitzpatrick, Hetherington et al. 1990; Novotny, Ogino et al. 1990). This technique was applied to the same U87 control samples and the results (red curves) are shown super-imposed in Figures 5.8B and 5.8C. The technique selected only the "satellite" peaks of the signals arising from the CH protons (Figure 5.8B) and the CH_3 protons (Figure 5.8C), producing a simplified spectrum and allowing for ease of integration.

However, although the use of POCE reduces background interference, it can also introduce error, due to differences in editing efficiency between the "satellite" peaks arising from the CH proton of 2-^{13}C lactate (Figure 5.8B) and the "satellite" peaks arising from the CH_3 protons of 1,3-^{13}C lactate and 3-^{13}C lactate (Figure 5.8C). In order to investigate this potential issue, a series of standard aqueous lactate solutions were prepared, containing different proportions of 2-^{13}C lactate and 3-^{13}C lactate. A direct comparison was then made between the ratio of the 2-^{13}C lactate "satellite peaks" to the 3-^{13}C lactate "satellite peaks" calculated from standard ^{1}H NMR (unedited, ratio of H_A to H_D, Figure 5.9A, A1-4) and the ratio obtained with the POCE technique (edited, ratio of H_A to H_D, Figure 5.9B, B1-4), on the same samples. These values were corrected for proton number and are displayed in Table 5.1. Unfortunately, in this small scale study it became apparent that there was a large discrepancy between the values obtained for the two techniques (Table 5.1C, > 12% for all four samples). Furthermore, the different magnitude of that discrepancy at each concentration meant application of a correction-factor would not be possible. It was anticipated that siRNA

knockdown of PFKFB3 and PFKFB4 might induce relatively changes in relative flux through glycolysis and the PPP. It was therefore necessary to be able to detect small changes in the ratios of labelled lactate products, hence the POCE technique was found to be unsuitable for this purpose.

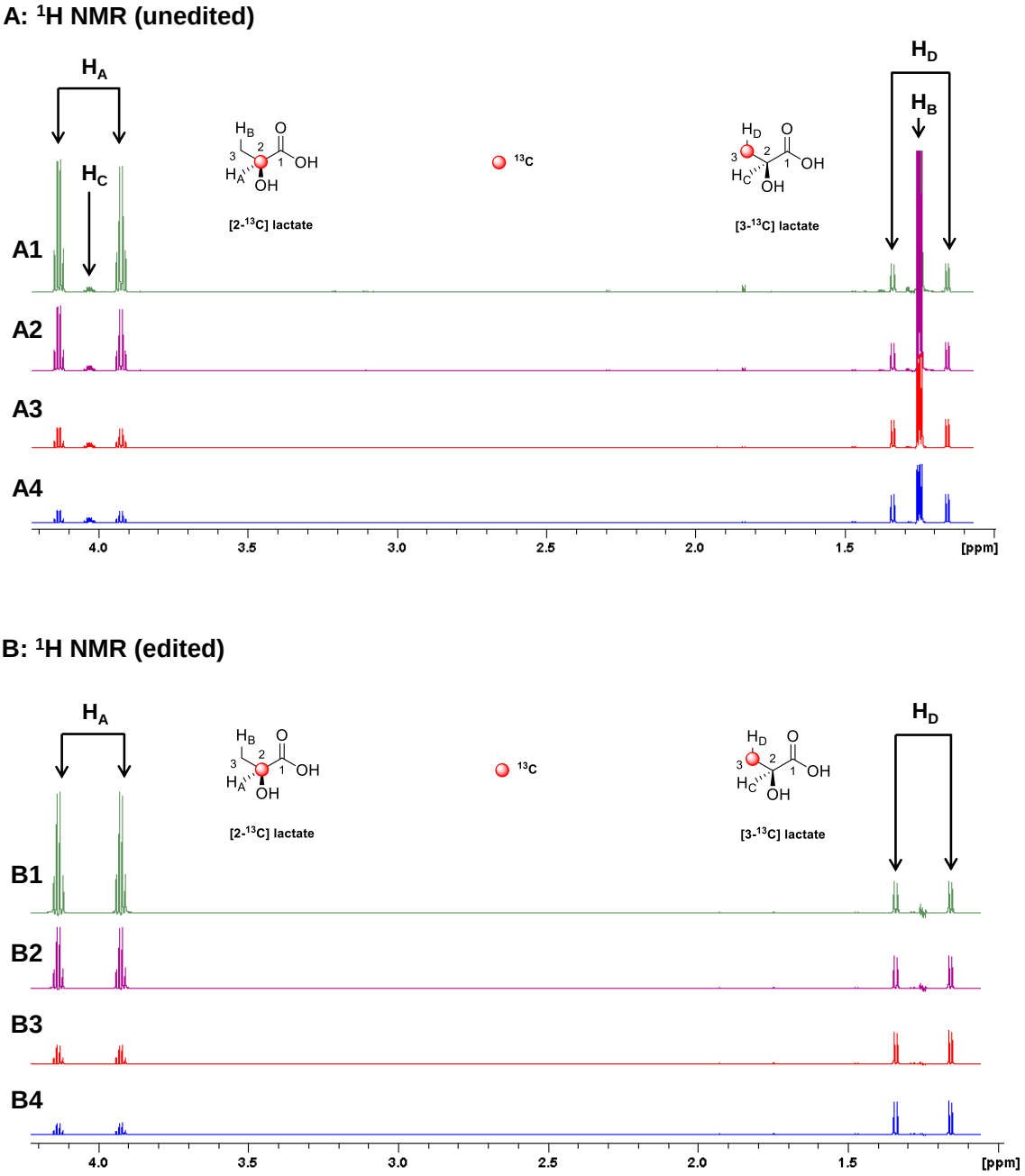

Figure 5.9: Comparison of **(A)** unedited ^{1}H NMR and **(B)** proton-observed carbon edited NMR spectra for a series of control 2-^{13}C and 3-^{13}C lactate samples. The "satellite" peaks labelled H_A arise from the CH proton (carbon-2) of 2-^{13}C lactate and the "satellite" peaks labelled H_D arise from the CH_3 protons (carbon-3) of 3-^{13}C lactate. Samples were at differing relative concentrations and spectra are normalised to the signal arising from H_D. The NMR samples were prepared by the author, the NMR spectra were run by Dr Tim Claridge (Chemistry Research Laboratory) and the raw data was processed, analysed and interpreted by the author.

	Calculated 2-^{13}C Lactate : 3-^{13}C Lactate Ratio		
	A: ^{1}H NMR (Unedited)	**B: ^{1}H NMR (Edited)**	**Variation between Ratios A and B**
1	5.16 : 1	4.36 : 1	16%
2	2.70 : 1	2.37 : 1	12%
3	0.93 : 1	0.77 : 1	17%
4	0.59 : 1	0.48 : 1	19%

Table 5.1: Comparison of 2-^{13}C lactate:3-^{13}C lactate ratios in standard samples using ^{1}H NMR and POCE. The integration data from Figure 5.9 was corrected for proton number. The calculated relative 2-^{13}C lactate:3-^{13}C lactate ratios demonstrate discrepancies between the unedited (^{1}H NMR) and edited (POCE) NMR techniques. The percentage variation between the ratios calculated using the two methods was not consistent, precluding use of a correction factor. The NMR samples were prepared by the author, the NMR spectra were run by Dr Tim Claridge (Chemistry Research Laboratory) and the raw data was processed, analysed and interpreted by the author.

No significant changes in 2-^{13}C lactate: 1,3- and 3-^{13}C lactate production ratio were observed using ^{1}H NMR in response to single or double siRNA knockdown of PFKFB3 and PFKFB4 under normoxic or hypoxic conditions, indicating no change in relative glycolysis:PPP.

U87 and PC3 cells had previously been observed to have the lowest relative *PFKFB3:PFKFB4* mRNA expression ratios, i.e. greater relative contributions from *PFKFB4* than observed in the MCF-7 cell line (Table 3.2, Chapter 3). Accordingly, it was anticipated that knockdown of PFKFB4 with its high bisphosphatase activity, leading to a shift in flux from the PPP to the glycolytic pathway, would likely be most apparent in the U87 and PC3 cell lines. U87 and PC3 cells were therefore reverse transfected to afford a scramble control, PFKFB3 knockdown, PFKFB4 knockdown and double PFKFB3/PFKFB4 knockdown. After incubation under normoxic or hypoxic conditions for 24 hours, the media was changed to 2-^{13}C glucose DMEM (U87 cells) or 2-^{13}C glucose RPMI (PC3 cells). After a further 24 hours incubation under normoxic or hypoxic conditions, media samples were collected, before purifying and analysing by ^{1}H NMR (Figures 5.10A and 5.10B).

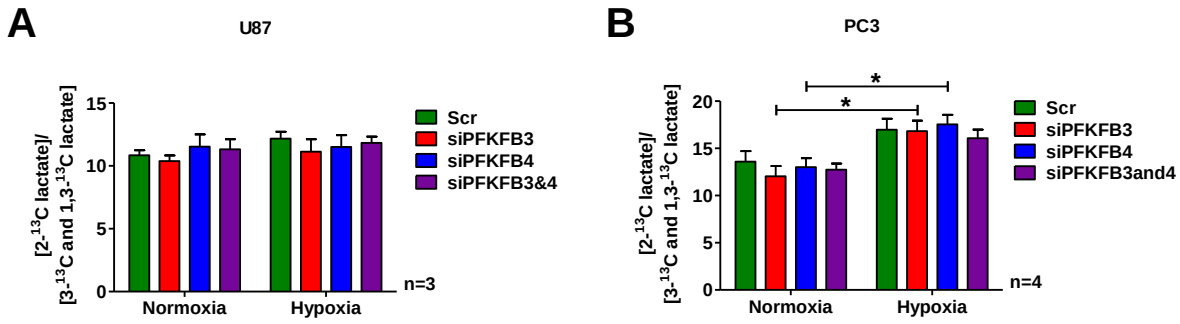

Figure 5.10: ^{1}H NMR lactate assay with single and double PFKFB3/PFKFB4 knockdown in **(A)** U87 and **(B)** PC3 cells under normoxic and hypoxic conditions. ^{1}H NMR analysis of [2-^{13}C lactate] compared to [1,3-^{13}C lactate] and [3-^{13}C lactate], corrected for proton number, was performed to indicate changes in the relative glycolytic:PPP flux ratio. No significant difference was observed in response to single or double PFKFB3 and PFKFB4 siRNA knockdown in **(A)** U87 and **(B)** PC3 cells, in both normoxia and hypoxia. n=3 (U87), n=4 (PC3); One-way ANOVA analysis performed with Bonferroni correction, comparing Scr controls to other samples with the same oxygenation status and also normoxic/hypoxic data sets for the same knockdown condition; *(p<0.05), **(p<0.01), ***(p<0.001), ****(p<0.0001). The NMR samples were prepared by the author, the NMR spectra were run by Dr Tim Claridge (Chemistry Research Laboratory) and the raw data was processed, analysed and interpreted by the author.

It had been anticipated that siRNA knockdown of PFKFB3 (high kinase activity), leading to reduced intracellular [F-2,6-BP] would lead to a reduction in flux through glycolysis and a corresponding increase in the PPP flux, i.e. a decrease in [2-^{13}C lactate]/[1,3-^{13}C lactate and 3-^{13}C lactate]. The converse argument had been anticipated to apply for siRNA knockdown of PFKFB4 (high bisphosphatase activity). In fact, no significant changes in response to single or double siRNA knockdown of PFKFB3 and PFKFB4 were detected in the labelled lactate ratio, in either cell line, under normoxic or hypoxic conditions (Figure 5.10).

There was a consistent trend for increased [2-^{13}C lactate] / [1,3-^{13}C lactate and 3-^{13}C lactate] in PC3 cells under hypoxic conditions (Figure 5.10B). This was a significant finding for siPFKFB3 (increase of 40(+/-13)%, $p<0.05$) and siPFKFB4 (increase of 35(+/-11)%, $p<0.05$) and indicated an increase in relative flux through the glycolytic pathway in PC3 cells under hypoxia. No such change was observed in the U87 cells and these results were both consistent with previous findings of a significant increase in total lactate produced by PC3 cells in hypoxia, with no change in total lactate produced by U87 cells in hypoxia (Figures 4.19C and 4.19D, Chapter 4).

Although in all cases, normoxic and hypoxic, the [2-^{13}C lactate] / [1,3-^{13}C lactate and 3-^{13}C lactate] ratio was higher for PFKFB4 than PFKFB3 (Figures 5.10A and 5.10B), these differences were small and insignificant. The low variability between replicates suggested the assay was robust and therefore if a real difference in glycolytic:PPP flux ratio did exist, it appeared this would be a small difference, which would likely require a prohibitively high number of replicates to conclusively identify.

5.3: Discussion

It was originally intended to examine potential differences in glycolytic/PPP pathway activity indirectly through the use of the ROS and lipid droplet assays (Figures 5.3 and 5.4). Analysing ROS levels for this purpose had sound basis because previous studies had shown suppression of both PFKFB4 expression and the bisphosphatase TIGAR, to increase ROS levels through a reduction in flux through the PPP and a corresponding decrease in NADPH production (Bensaad, Tsuruta et al. 2006; Ros, Santos et al. 2012).

However, the results of the assay have revealed a more complex role of both PFKFB3 and PFKFB4 than originally anticipated. The only significant finding for the ROS assay (increase in ROS with siPFKFB3 in MCF-7 cells under normoxic conditions, Figure 5.3A), did not fit with the original model of an increase in relative PPP in response to siPFKFB3, which had been anticipated to reduce ROS levels. Although the evidence presented did not necessarily preclude activity of PFKFB3 and PFKFB4 in modulating glycolytic/PPP flux, it suggested another, yet to be elucidated, role for these isoenzymes in modulating ROS levels. Indeed, knockdown of i-PFK-2/PFKFB3 expression in adipocytes has been reported to lead to increased ROS production, through promotion of elevated fatty acid oxidation (Huo, Guo et al. 2010). This report may provide a starting point for future investigation. It should be noted that no significant increase in ROS production was observed in the PC3 cell line in response

to PFKFB4 knockdown, apparently directly conflicting with the recent report from Ros and colleagues (Ros, Santos et al. 2012). However, their study was conducted under lipid-limited growth conditions, which was found to up-regulate *PFKFB4* mRNA expression. This might explain why ROS levels in cells grown under such conditions are more sensitive to PFKFB4 depletion. Indeed, the group observed higher sensitivity of growth of a panel of cancer cell lines to suppression of PFKFB4 expression when cultured in lipid-limited growth conditions, compared to culture in full media (Ros, Santos et al. 2012).

Synthesis of triacylglycerides, a principal component of LDs, generally requires intermediates from glycolysis and the TCA cycle, as well as NADPH production from the PPP. Therefore, modulation of flux through the glycolytic or PPP pathways was anticipated to have a direct impact on LD levels, depending on whether the supply of NADPH or glycolytic/PPP intermediates were limiting.

It was initially surprising then that knockdown of both PFKFB3 and PFKFB4 were able to induce an increase in LD content in the MCF-7 cell lines (Figure 5.4A). The findings were not significant for the U87 and PC3 cell lines (Figures 5.4B and 5.4C). This seemed to be partly explained by a potential increase in fatty acid uptake mediated by PFKFB3 knockdown under normoxic conditions in MCF-7 cells (Figure 5.5). Nevertheless, the increase in LD content under hypoxic conditions in response to siPFKFB3 (Figure 5.4A) occurred in the absence of increased fatty acid uptake (Figure 5.5) in MCF-7 cells. This strongly implied that reduced PFKFB3 expression was directly linked to either increased lipid synthesis, or decreased utilisation of the LD contents for ATP production (β oxidation) or membrane production. The low proliferation rates of MCF-7 cells in response to PFKFB3 knockdown (Figure 4.6, Chapter 4) would support the latter theory. Results from a collaboration to investigate changes in lipid synthesis in response to PFKFB3 or PFKFB4 knockdown are pending.

It became evident that analysis of total lipid droplet content might have masked differing functions of PFKFB3 and PFKFB4. Glucose metabolism is not the only source of intermediates for lipid synthesis. The reductive carboxylation of glutamine-derived α-ketoglutarate to generate citrate, the precursor to acetyl CoA for fatty acid synthesis, has been shown to be an important component of lipid synthesis in cancer cells (Metallo, Gameiro et al. 2012). The data suggests PFKFB3 and PFKFB4 could potentially have direct or indirect involvement in the activity of this pathway, aside from any role in regulating relative glycolytic/PPP flux, something future work should seek to investigate.

The increase in LD content for the MCF-7 cell lines in response to single and double PFKFB3/PFKFB4 knockdown appears to derive at least in part from increased *de novo* synthesis (Figures 5.4A and 5.5). This would go some way to explaining the reduction in "glycolytic efficiency", defined as mol lactate produced per mol glucose consumed, previously observed with the MCF-7 cells (Figure 4.20, Chapter 4). It seems that an increased portion of glucose is channelled away from lactate production for lipid synthesis when PFKFB3 and/or PFKFB4 expression are reduced.

The in-house mass spectrometry assay was intended to provide a highly sensitive technique for quantitatively monitoring changes in the levels of key metabolites involved in the glycolytic and PPP pathways. Although the collaboration with Dr James McCullagh and Khalid Al-Qahtani was successful in optimising LC-MS conditions to separate each of the metabolites of interest, problems with sample extraction and low metabolite concentrations prevented reliable and interpretable results from being obtained (Figure 5.7). Future work should look to overcome these in-house issues, such as altering the extraction protocol and re-establishing the standard curves in a more relevant concentration range. Alternatively, the technique should be out-sourced to an established provider.

An in-house NMR assay was set up to monitor changes in response to siRNA knockdown of PFKFB3 and PFKFB4 on the balance between glycolysis and the PPP, as measured by positional ^{13}C labelling of the lactate product. However, no significant changes in the labelled lactate product ratio (2-^{13}C lactate: 1,3-^{13}C lactate and 3-^{13}C lactate) were identified (Figure 5.10). This led to two potential explanations, the first being that the changes in glycolytic:PPP activity ratio induced by PFKFB3 or PFKFB4 knockdown were beyond the detection limit of this method. However, the assay appeared robust, with comparatively low variability between replicates, allowing confidence to be placed in the data obtained (Figure 5.10). Therefore, the second, more likely possibility was that if there were changes in glycolytic:PPP activity ratio induced by either PFKFB3 or PFKFB4 knockdown in the cell lines examined, they were only relatively small changes.

Indeed, it was considered unlikely that such small changes in relative flux could induce the large, significant changes in 2D proliferation, 3D spheroid volume and [F-2,6-BP] previously identified in response to PFKFB3 and PFKFB4 knockdown for the U87 and PC3 cell lines (Figures 4.7 and 4.8, Chapter 4; Figures 4.10 and 4.11, Chapter 4; Figures 4.14 and 4.16, Chapter 4, respectively). The wealth of evidence presented in this Chapter therefore suggested a principally non-glycolytic role for changes in F-2,6-BP induced by PFKFB3 or PFKFB4 knockdown.

It was regrettable that there was insufficient time available to explore an alternative explanation for the observed *in vitro* effects of PFKFB3 and PFKFB4 knockdown. Future work beyond the scope of this thesis must seek to address these unexpected results. One literature report has demonstrated a non-glycolytic role for PFKFB3 in regulating cell proliferation, through nuclear delivery of F-2,6-BP, leading to increased expression of cyclin-dependent kinase-1 (Yalcin, Clem et al. 2009). It is hypothesised that intracellular

compartmentalisation of F-2,6-BP may exist and it may be the location of the change in F-2,6-BP, such as at the nucleus, that is most important in mediating the observed effects on proliferation in response to PFKFB3 and PFKFB4 knockdown. A more detailed discussion in the context of existing literature reports, with suggested future studies, is provided in the final discussion (Chapter 7).

Nevertheless, the results presented in this Chapter by no means conflicted with previous findings that implicated inhibition of PFKFB3 or PFKFB4 as an attractive therapeutic strategy (2D proliferation and 3D spheroid volume studies; Figures 4.6-4.11, Chapter 4). As such, the remaining work presented in this thesis sought to build an assay-based platform from which to begin the identification and development of small molecule inhibitors.

Chapter 6: Towards the Development of PFKFB3 Inhibitors

6.1: Introduction and Aims

Whilst the exact nature of the antagonism between PFKFB3 and PFKFB4 was still unclear, the cell proliferation studies had demonstrated that isoenzyme specific PFK-2/FBPase-2 inhibition would likely be the most effective general therapeutic strategy. This was due to the apparent "rescue" effects observed with double PFKFB3/PFKFB4 knockdown, compared to single PFKFB3 knockdown alone (Figures 4.6-4.11, Chapter 4). Both PFKFB3 and PFKFB4 presented themselves as potential anti-tumour targets. High PFKFB4 mRNA expression had been correlated with poor prognosis in a literature study (Goidts, Bageritz et al. 2011) and an in-house study (Figure 3.13, Chapter 3). However, the work in this thesis had demonstrated suppression of PFKFB3 expression to be consistently more effective at reducing cell growth in MCF-7, U87 and PC3 cells, compared to PFKFB4, with a particularly marked effect under hypoxic conditions in 2D (Figures 4.6-4.8, Chapter 4). This, together with evidence from literature reports demonstrating up-regulation of PFKFB3 in tumour tissue (Atsumi, Chesney et al. 2002; Bobarykina, Minchenko et al. 2006), led to selection of PFKFB3 as the target for further study, particularly with a view to the development of a hypoxia-targeted therapeutic. It was therefore decided to focus efforts on optimising a suitable assay system to screen potential small molecule inhibitors of PFKFB3.

High throughput screening (HTS) involves assays that permit rapid detection of a single read-out, e.g. fluorescence or absorbance, enabling screening of large numbers of small molecules in order to quickly identify potential inhibitors of a given enzyme. The signal-to-noise ratio and reproducibility of the assay will determine the confidence in using it to identify such inhibitors, so it is essential to select and optimise the most suitable assay for the protein of interest.

A number of PFKFB3 assays had already been reported in the literature and used to detect inhibitory activities of small molecules. Clem and colleagues made use of a coupled enzymatic assay that inversely linked PFKFB3 kinase activity to absorbance by NADH at 340 nm (Clem, Telang et al. 2008). The assay utilised the enzymes pyruvate kinase and lactate dehydrogenase (Scheme 6.1). However, assays based on absorption typically have low sensitivity and the presence of multiple different enzymes increases the probability of observing "off-target" effects due to small molecule inhibition of these enzymes (Fan and Wood 2007).

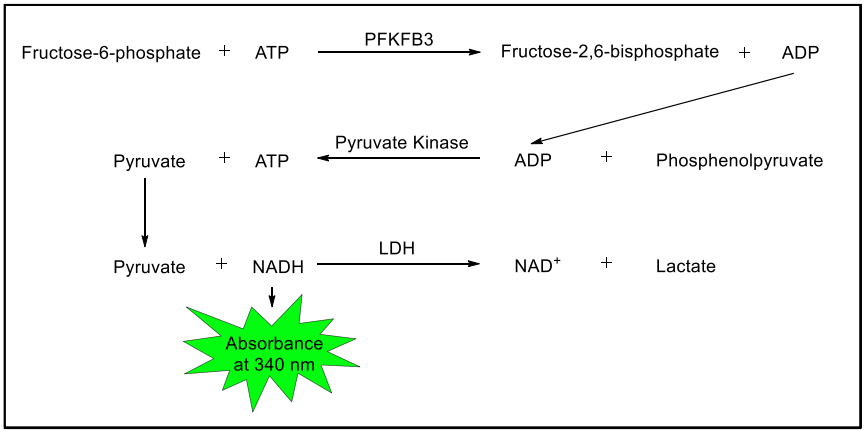

Scheme 6.1: Coupled enzymatic assay used to measure PFKFB3 activity. This method was used by Clem and colleagues (Clem, Telang et al. 2008). LDH (lactate dehydrogenase), NADH (nicotinamide adenine dinucleotide (reduced)), NAD^+ (nicotinamide adenine dinucleotide), ADP (adenosine diphosphate) and ATP (adenosine triphosphate).

Yalcin and colleagues (Yalcin, Clem et al. 2009), and Seo and colleagues (Seo, Kim et al. 2011), both employed the use of coupled enzymatic assays that involved formation of F-2,6-BP in one step, followed by purification, and assay of [F-2,6-BP] in the following step. The authors used the method of Van Schaftingen and colleagues (Van Schaftingen, Lederer et al. 1982; Van Schaftingen 1987), which was also employed for the F-2,6-BP studies in Chapter 4 (Figures 4.13-4.16). The multiple steps involved, large number of assay components, instability of [F-2,6-BP], as well as high [F-2,6-BP] assay variability observed in Chapter 4, suggested alternative strategies should be considered.

There are a plethora of different kinase assays now commercially available, with the majority utilising radioactive, fluorescent or luminescent read-outs (Jia, Quinn et al. 2008). Radioactive assays have been used to measure the transfer of ^{32}P or ^{33}P from the γ-phosphate group of ATP to the enzyme substrate. The labelled substrate is subsequently purified, usually through a single-step immobilisation, and the radioactivity quantified using scintillation counting or scintillation proximity assays (SPAs) (Gopalakrishna, Chen et al. 1992; Glickman, Schmid et al. 2008). However, the use and disposal of radioactive material involves specialist safety equipment, as well as being relatively expensive (Glickman, McGee et al. 2004). Whilst offering high sensitivity and resolution, there has now been a move towards safer and cheaper non-radioactive alternatives for HTS (Ma, Deacon et al. 2008).

There has been widespread use of fluorescent probes in kinase assays, through techniques including fluorescence intensity (FI), fluorescence polarisation (FP), fluorescence resonance energy transfer (FRET) and time-resolved fluorescence (TRF), which have been reviewed elsewhere (Ma, Deacon et al. 2008). Fluorescent assays are relatively low cost, involve no radioactivity and have high signal intensity, but suffer from high background noise and interference from fluorophores, or fluorescence-quencher molecules that may be present in a panel of test compounds (Turek-Etienne, Small et al. 2003).

Luminescent assays have lower signal intensities than fluorescent assays, as the photons are generated and emitted from the reagents themselves, rather than introduced into the system, as occurs in fluorescence-based assays. However, this also results in a better signal-noise ratio, increasing the sensitivity of assays that employ this method (Fan and Wood 2007). The use of biological molecules such as the luciferases and their photon-emitting products (oxyluciferins), permits high-efficiency photon emission. This has driven increased recent interest in the use of luminescence-based assay systems (Tanega, Shen et al. 2009).

The ideal assay would incorporate high speed and efficiency, low cost and high reproducibility. An assay must also be highly sensitive as compounds are only usually tested in duplicate due to the large number of compounds screened. These considerations must be taken into account when selecting a suitable assay.

At the initiation of this work, no human recombinant PFK-1 or PFK-2/FBPase-2 isoenzymes were commercially available. It was therefore decided to first identify and optimise an assay using the PFK-1 from *Bacillus stearothermophilus*, available from Sigma Aldrich. Amino acid sequences for the human PFK-1 isoforms and bacterial PFK-1 were obtained using UniProt (http://www.uniprot.org/). Clustal W2 was then used to compare amino acid sequences and generate a percentage homology value. The results are illustrated in Table A11.1, Appendix, with bacterial PFK-1 showing homology of 44%-45% to the 3 human PFK isoenzymes (PFKL, PFKM, PFKP). There is almost complete sequence conservation between the active sites of bacterial and human PFK-1, with 10 out of the 11 key amino acid residues being conserved (Shirakihara and Evans 1988; Ferreras, Hernandez et al. 2009). PFK-1 and PFKFB3 share the same substrate (F-6-P) so it was envisaged that the same assay would be suitable to measure kinase activity of both isoenzymes by following the same optimisation protocol. After selection and optimisation, it would be desirable to validate the assay with a known competitive inhibitor, suitable for both the PFK-1 and PFKFB3 kinase assays.

F-6-P exists as 4 forms in solution, which are the cyclic α-D-F-6-P (Scheme 6.2 (a)) and β-D-F-6-P anomers (Scheme 6.2, (b)), and the acyclic non-hydrated and hydrated keto forms. The α anomer and the predominant β anomer are able to readily interconvert in solution via a ring-opening/ring-closure mechanism (Scheme 6.2). Koerner and colleagues (Koerner, Younatha.Es et al. 1974) conducted a study of the tautomeric and anomeric specificities of PFK-1 from rabbit muscle, using 4 configurationally stable, isosteric analogues of the 4 forms

of D-F-6-P. They observed that 2,5-anhydro-D-mannitol-1-phosphate (Scheme 6.2, (d)), the β analogue, was an alternative substrate for PFK-1, whereas 2,5-anhydro-D-glucitol-6-phosphate (Scheme 6.2, (c)), the α analogue, was a competitive inhibitor of PFK-1 (K_i = 0.34 mM) (Scheme 6.2). Further studies led them to conclude that the active site of PFK possesses a tautomeric specificity for the cyclic form of D-F-6-P, whilst for phosphorylation, there is an anomeric specificity restricted to the β form (Koerner, Younatha.Es et al. 1974).

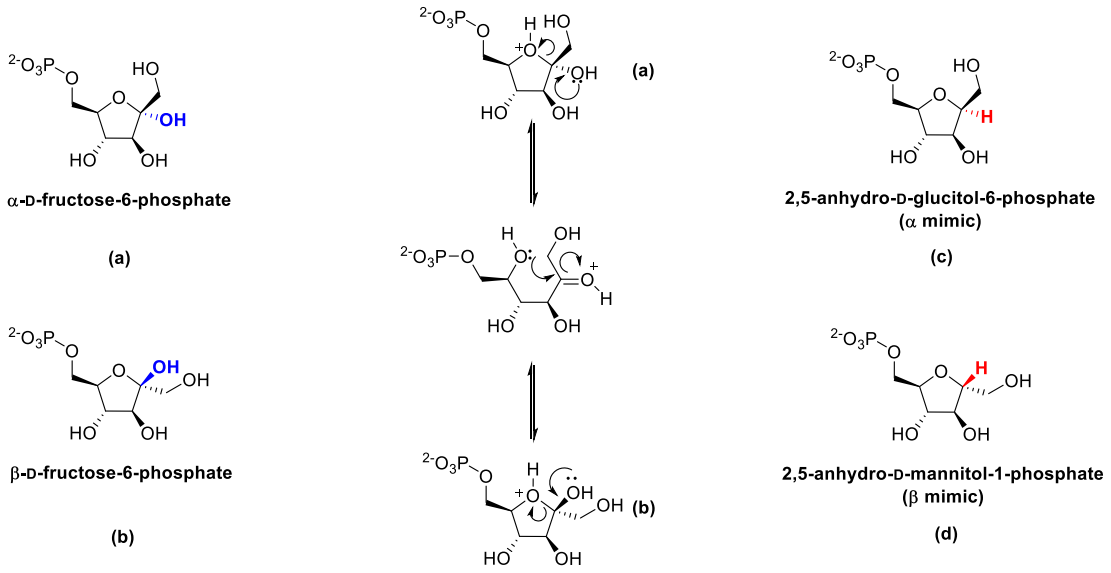

Scheme 6.2: The anomers of fructose-6-phosphate (F-6-P) and their configurationally stable analogues. F-6-P exists as two cyclic forms in solution, **(a)** α-D-F-6-P and **(b)** the predominant β-D-F-6-P, which are in equilibrium with one another via ring-opening/ring-closure. Configurationally stable analogues prevent this inter-conversion; **(c)** 2,5-anhydro-D-glucitol-6-phosphate is a mimic for the α form and **(d)** 2,5-anhydro-D-mannitol-1-phosphate is a mimic for the β form (Koerner, Younatha.Es et al. 1974).

Replacement of the anomeric hydroxyl groups (blue) with hydrogen atoms (red) (Scheme 6.2) also removes the phosphorylation site targeted by PFK-2/FBPase-2 kinase activity. Indeed, Pilkis and colleagues have shown that 2,5-anhydro-D-mannitol-1-phosphate (β-mimic) is a competitive inhibitor of PFK-2/FBPase-2 kinase activity, with K_i = 96 µM, indicating binding to the active site with an affinity approaching that of F-6-P (Pilkis, Pilkis et al. 1985). It was therefore anticipated that the α-mimic would function in a similar manner and so obtaining both F-6-P mimics for use in assay validation was desirable.

With a view to developing novel small molecule inhibitors of PFKFB3, it was necessary to obtain the leading inhibitor of this enzyme. As previously discussed, this was the compound 3PO (3-(3-pyridinyl)-1-(4-pyridinyl)-2-propen-1-one), identified through computational screening and shown to be a potent inhibitor of PFKFB3, albeit with likely cross-reactivity with the other PFK-2/FBPase-2 isoenzymes (Clem, Telang et al. 2008). A very recent report has since identified a second-generation of PFKFB3 inhibitors, based on 3PO (Clem, O'Neal et al. 2013). However, at the time this work was completed, 3PO was the leading inhibitor.

The aims of the studies contained within this Chapter were therefore to synthesise 3PO as a benchmark inhibitor, and work towards the development and validation of a suitable assay, applicable for use with PFKFB3.

6.2: Results

6.2.1: Synthesis of 3PO (3-(3-pyridinyl)-1-(4-pyridinyl)-2-propen-1-one)

At the initiation of this work, 3PO (**2**) was not commercially available, but it was important to have a supply of the compound in order to provide a benchmark against which to compare the activity of any small molecule inhibitors identified. Whilst no synthesis of 3PO had been reported in the literature, numerous reported methods had been investigated for the preparation of other chalcones (a molecule containing an aromatic ketone and an enone). These included aldol elimination (Akama, Shida et al. 1996; Otto, Bertoncin et al. 1996; Basnet, Thapa et al. 2007; Batovska, Parushev et al. 2007; Petrov, Ivanova et al. 2008), Wittig olefination (Westman 2001; Babu, Li et al. 2006), Heck coupling (Mahboobi and Wiegrebe 1988; Reetz, Drewes et al. 1989; Reichwald, Shimony et al. 2008) and Suzuki coupling (Cai, Larsen et al. 2002; Gung, Gibeau et al. 2005; Perner, Lee et al. 2005). Initial efforts focused on an aldol condensation between 3-pyridinecarboxaldehyde and 4-acetylpyridine. Treatment

of 3-pyridine carboxaldehyde and 4-acetylpyridine with NaOH (3 eq.) in MeOH led to formation of by-products **3**, **4** and **5**, alongside small quantities (< 1%) of the desired chalcone **2**, as identified by mass spectrometry and ^{1}H NMR (Scheme 6.3).

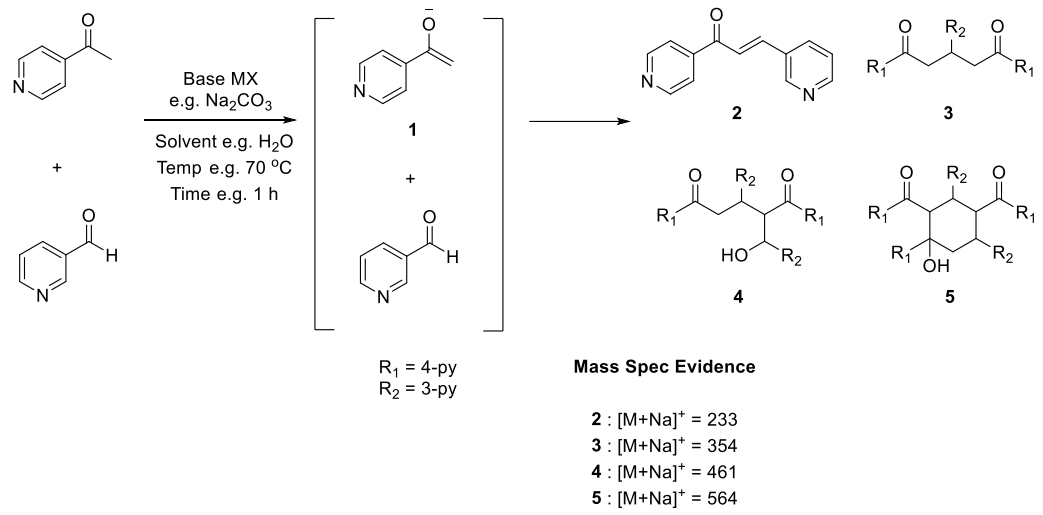

Scheme 6.3: Attempted 3PO synthesis via base-catalysed aldol reactions. The reactions led to formation of multiple by-products (**3**), (**4**) and (**5**), due to the product chalcone (**2**) being an excellent Michael acceptor, and undergoing further reaction with the enolate (**1**). py (pyridine).

By-product formation occurred as a result of Michael addition of the enolate **1** to the product chalcone **2**, which is an excellent Michael acceptor (Vatsadze, Nuriev et al. 2004). Extensive attempts were made to overcome this issue, including varying temperature, solvent, base and equivalents of reagents, but to no avail. The by-product **5** was isolated in 54% yield from the reaction using Na_2CO_3 (0.25 eq.) in H_2O, and heating at 70 °C for 1 hour (Scheme 6.3) (Akama, Shida et al. 1996; Otto, Bertoncin et al. 1996; Basnet, Thapa et al. 2007; Batovska, Parushev et al. 2007; Petrov, Ivanova et al. 2008).

In the condensation reaction of pyridine carboxaldehydes and acetyl pyridines, the Michael addition pathway has been reported to be favoured by co-ordination of a metal ion to the pyridine nitrogen (Wachter-Jurcsak, Radu et al. 1998). Indeed, use of the organic base 1,8-diazabicyclo[5.4.0]undec-7-ene (DBU) to circumvent this effect (Downs, Wolfe et al. 2005),

where metal ions were absent from the reaction mixture, afforded the 3PO derivative **6** in good yield (75%) (Scheme 6.4). However, treatment of 4-acetylpyridine with 3-pyridine carboxaldehyde under comparable conditions, resulted in low conversion (< 1%) to 3PO (**2)** (Scheme 6.4), with concomitant by-product formation, as observed previously (Scheme 6.3). An explanation for enhanced by-product formation resulting from **2** and not **6**, may potentially lie in the enhanced electrophilicity of the Michael acceptor of 3PO (**2**), which arises due to the electron-withdrawing effect of the electronegative 4-pyridinyl nitrogen atom. This may favour attack by the 4-acetylpyridine enolate.

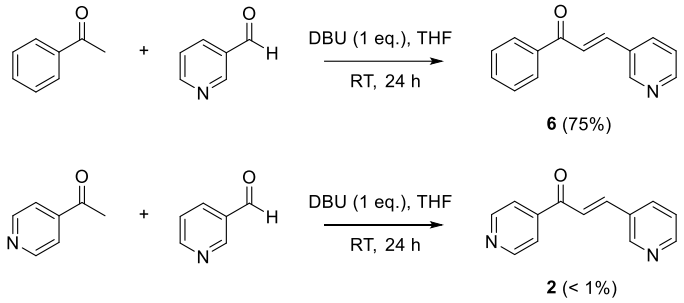

Scheme 6.4: Attempted chalcone synthesis via a DBU-mediated aldol reaction. The reaction was successful for the 3PO-derivative (**6**), but resulted in low conversion to the desired chalcone 3PO (**2**). DBU (diazabicyclo[5.4.0]undec-7-ene).

Additional methods employed, included attempted isolation of the hydrated chalcone precursor (Wei, Li et al. 2004; Downey and Johnson 2007), microwave-promoted Wittig reaction (Westman 2001; Babu, Li et al. 2006), Heck coupling (Mahboobi and Wiegrebe 1988; Reetz, Drewes et al. 1989; Reichwald, Shimony et al. 2008) and a Suzuki coupling (Cai, Larsen et al. 2002; Gung, Gibeau et al. 2005; Perner, Lee et al. 2005). However, all attempts were unsuccessful, with no evidence of desired 3PO (**2**) product formation.

An alternative route was devised, involving formation of an acyl chloride, conversion to the corresponding amide and reaction with a Grignard reagent (Scheme 6.5) (Paradies and Gorbing 1969; Furukawa, Shibutani et al. 1987; Kolly-Kovac and Renaud 2005; Sadeghian, Seyedi et al. 2008). However, where R_1=3-py (**7**) or 4-py (**8**) (3PO derivative), the alkene

protons were unexpectedly replaced by chlorine atoms, which was confirmed by reaction with *N,O*-dimethylhydroxylamine hydrochloride, affording **10** and **11** respectively, in moderate yield. The same products were observed when the reaction was repeated in the absence of light, suggesting the products were not obtained *via* a radical substitution mechanism. Under the same conditions, cinnamic acid (R_1=Ph), was converted to **12** via compound **9**, where X=H, suggesting the chlorination is dependent on the presence of the pyridine nitrogen, consistent with the reactivity of pyridines with $SOCl_2$ (Relles 1973). Suggested mechanisms for these reactions are detailed in Schemes A12.1 and A13.1 (Appendix).

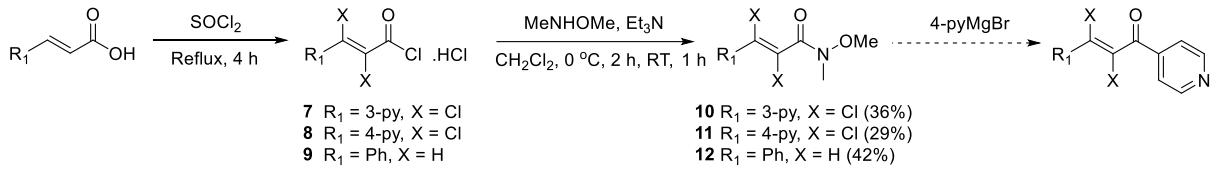

Scheme 6.5: Attempted 3PO synthesis via acyl chloride formation, conversion to amide, followed by Grignard reaction. The reaction led to unexpected chlorination products where R_1 = 3-py (**7** and **10**) and R_1 = 4-py (**8** and **11**). py (pyridine).

Synthesis of 3PO itself by this method was not possible, but the chlorinated product from this reaction could potentially be used to introduce further functionality at the vinyl chloride site and permit access to a series of 3PO derivatives in the future, such as through palladium or nickel-catalysed cross couplings (Xu, McLaughlin et al. 2009; Liu and Wang 2011).

An alternative Grignard reaction route was pursued by first synthesising the novel pentafluorophenyl ester **13**, by dropwise addition of *N,N*'-dicyclohexylcarbodiimide (DCC) to a solution of *trans*-3-(3-pyridyl)-acrylic acid and pentafluorophenol (PFP) in EtOAc, which proceeded in high yield (77%) (Brown, Bataille et al. 2002) (Scheme 6.6). Attempted reaction with 4-pyridine magnesium bromide, formed *in situ* from EtMgBr and 4-bromopyridine hydrobromide, was unsuccessful. **13** was recovered, together with a small amount of ethyl ketone **14** (< 5%).

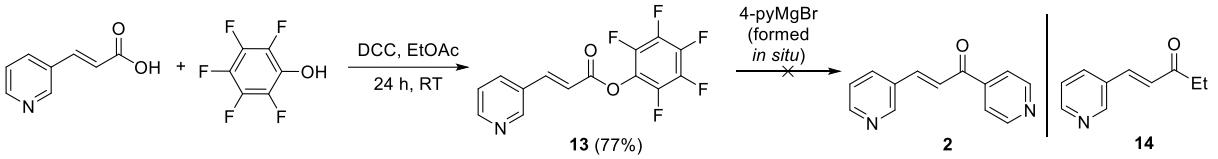

Scheme 6.6: Attempted 3PO synthesis via pentafluorophenol (PFP) ester formation and Grignard reaction. Low reactivity of the PFP ester (**13**) with the Grignard reagent precluded isolation of the desired compound 3PO (**2**). py (pyridine) and DCC (*N,N'*-dicyclohexylcarbodiimide).

In situ generation of the same Grignard reagent and reaction with benzaldehyde proved Grignard reagent formation was successful and led to the conclusion that the lack of formation of desired product **2**, was due to a lack of reactivity of the Grignard reagent with **13**.

The 4-pyridine *N*-oxide of 3PO was commercially available, and attempts to reduce the *N*-oxide with PCl_3 to **2** were successful, as evidenced by ^{1}H NMR and mass spectrometry (*m/z* = 209 ($[M-H]^-$)) (Scheme 6.7). However, it was not possible to isolate the desired product (**2**) due to the large number of apparent decomposition products.

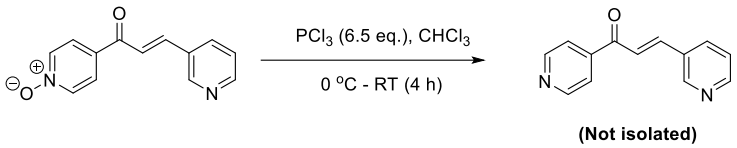

Scheme 6.7: Attempted 3PO synthesis via reduction of the 4-pyridine *N*-oxide of 3PO. Product **2** formation was confirmed by mass spectrometry but isolation was not possible due to a large number of apparent decomposition products.

3PO (**2**) was finally isolated successfully, in moderate yield (33%), from a polymer-supported Wittig reaction (Scheme 6.8). This was achieved by first forming the polymer-bound phosphorous ylide **15**, followed by reaction with 3-pyridine carboxaldehyde, to afford **2** as a single diastereoisomer. Full spectroscopic data was obtained, with characteristic ^{1}H NMR peaks at δ = 7.51 and 7.84 ppm for the two alkene protons, with a coupling constant of J = 16.0 Hz, consistent with *trans*-double bond geometry.

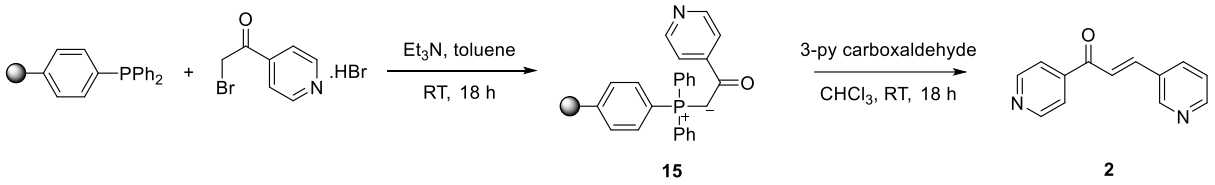

Scheme 6.8: Successful synthesis of 3PO via a polymer-supported Wittig reaction.

6.2.2: PFK-1 Assay Development

With a view to enabling high-throughput screening (HTS) of potential small molecule inhibitors of PFKFB3, it was necessary to obtain and optimise a suitably robust kinase assay. The relatively low cost, high signal-noise ratio and universal applicability (suitable for both PFK-1 and PFKFB3), led to the conclusion that the Kinase-Glo® Plus luminescence assay kit, available from Promega®, would be the most suitable to try initially. Furthermore, the presence of just one additional enzyme component (luciferase) would reduce the likelihood of off-target effects associated with many coupled enzymatic assays. The assay inversely links the PFK-1 (hereafter denoted PFK) activity to the light emitted. It enables quantification of the ATP remaining after addition of the kit, through conversion to AMP, with concomitant light emission (Scheme 6.9).

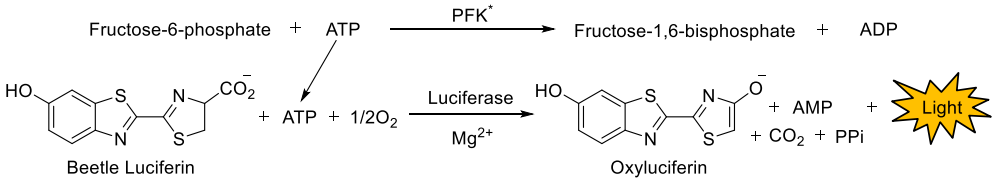

Scheme 6.9: Kinase Glo® Plus luciferase assay. The assay inversely links PFK activity with luminescence intensity (*PFK-1 from *Bacillus stearothermophilus*), PPi (pyrophosphate), AMP (adenosine monophosphate) and ATP (adenosine triphosphate).

Once selected, the assay was then optimised using a protocol developed from the "Handbook of Assay Development in Drug Discovery" (Minor 2010). As a "signal decrease" assay, it was important to ensure the assay was run under high-turnover conditions, to ensure maximum

difference of luminescence signal between the positive and negative controls, thereby increasing sensitivity (Glickman, McGee et al. 2004).

6.2.2.1: Optimisation of ATP concentration.

Linearity of [ATP] and luminescence signal was confirmed by performing the Kinase-Glo® Plus assay with serial dilutions from [ATP] = 100 µM to [ATP] = 0.10 µM, as well as a [ATP] = 0 µM control (Figure 6.1). ATP dilutions were made in HEPES buffer (500 mM) containing $MgCl_2$ (10 mM); total reaction volumes were 20 µL. 20 µL Kinase Glo® Plus kit was added to start the reaction and the luminescence signal measured after 10 min. Linear regression analysis indicated near-perfect linearity over a wide range of ATP concentrations (R^2 = 0.999) (Figure 6.1).

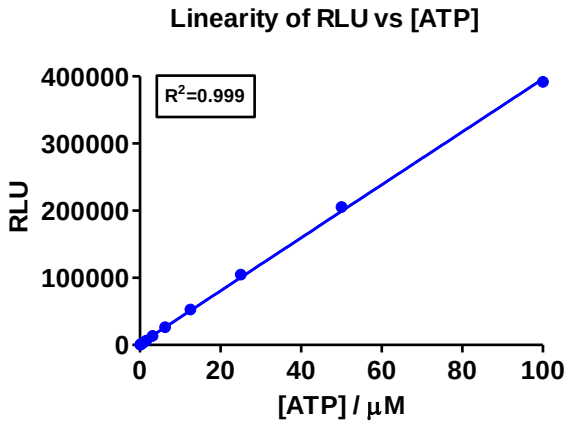

Figure 6.1: Linearity between [ATP] and luminescence signal of the Kinase Glo® Plus assay. A linear relationship between [ATP] and luminescence signal was confirmed up to [ATP] = 100 µM (R^2 = 0.999). RLU (relative luminescence units).

To optimise ATP concentration, serial ATP dilutions were prepared as above, using the maximal practical PFK concentration (100 mUnits/well) and DMSO (2%) (red curve, Figure 6.2). A series of identical dilutions were also made in the absence of PFK, as controls (blue curve, Figure 6.2). The reaction was started by the addition of F-6-P substrate (final concentration 10 µM), to give a total reaction volume of 20 µL. After incubation of the plate

for 30 min, an equal volume of Kinase Glo® Plus kit was added and incubated for a further 10 min, before measuring the luminescence signal. The optimal ATP concentration was that which gave the largest change in luminescence between the completed kinase reaction wells (red curve, Figure 6.2), and the equivalent (-)PFK control (blue curve, Figure 6.2). This was determined to be $\log_{10}([ATP]/\mu M) = 1.10$ (Figure 6.2), corresponding to [ATP] = 12.5 µM.

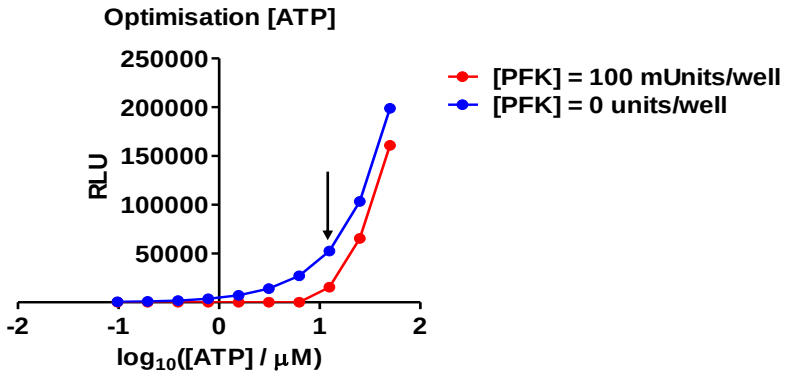

Figure 6.2: Optimisation of [ATP] in the Kinase Glo® Plus assay. Optimal [ATP] was determined to be 12.5 µM, which gave the maximal difference in luminescence signal between the (+)PFK and (-)PFK controls. RLU (relative luminescence units).

6.2.2.2: Optimisation of PFK concentration and incubation time.

The assay was repeated with serial dilutions of PFK enzyme from [PFK] = 0.1 units/well to [PFK] = 1.0 $x10^{-4}$ units/well, as well as a [PFK] = 0 units/well control. Excess [F-6-P] = 62.5 µM was used, and four sets of identical dilutions set up in duplicate. The reaction was started by the addition of optimal ATP (final concentration 12.5 µM) and a series of incubations set up (5 min, 10 min, 15 min, 30 min), before adding Kinase Glo® Plus reagent at the appropriate time point. The plates were then incubated for 10 min, before recording the luminescence signal (Figure 6.3).

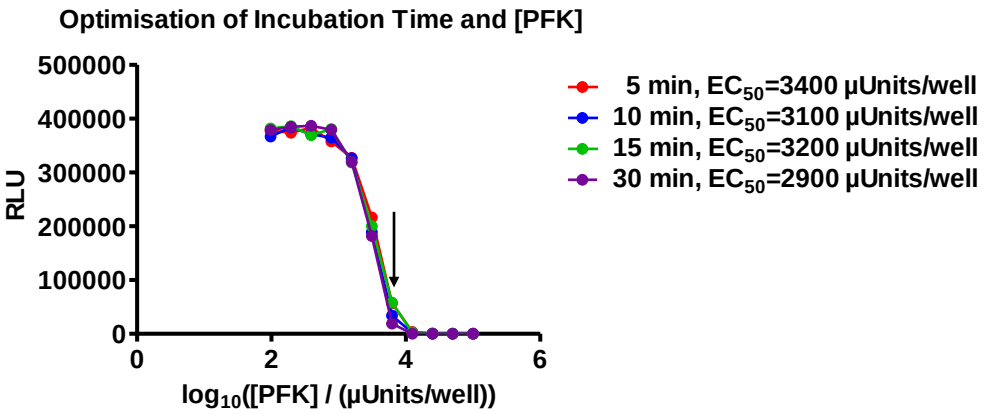

Figure 6.3: Optimisation of incubation time and [PFK] in the Kinase Glo® Plus assay. Optimal [PFK] was determined to be 6.25 mUnits/well, the minimum amount of PFK required to give the maximum difference in luminescence signal from the [PFK] = 0 mUnits/well control. Optimal reaction time was determined to be 10 min, the point after which the EC_{50} of the curves remained approximately constant. RLU (relative luminescence units).

The optimal [PFK] was the smallest amount which resulted in the maximal dynamic range between the recorded luminescence signal and that of the [PFK] = 0 units/well control (378452 relative luminescence units). This was determined to be $\log_{10}$([PFK]/(µUnits/well)) = 3.80, which translated as [PFK] = 6.25 mUnits/well (Figure 6.3). The optimal reaction time was that after which EC_{50} values remained constant. The EC_{50} values calculated (Figure 6.3) remained broadly consistent after 10 min (EC_{50} = 3100 µUnits/well), so this was chosen as the optimal incubation time.

6.2.2.3: Optimisation of F-6-P concentration.

The optimised assay conditions were run with serial dilutions of F-6-P, from [F-6-P] = 1 mM to [F-6-P] = 1 µM, as well as a [F-6-P] = 0 µM control. Two sets of duplicate dilutions were performed, one with [PFK] = 6.25 mUnits/well (red curve, Figure 6.4) and one with [PFK] = 0 mUnits/well (blue curve, Figure 6.4). The optimal [F-6-P] was the smallest amount that led to the largest dynamic range between the recorded luminescence signal (red curve, Figure 6.4) and the [PFK] = 0 mUnits/well control (blue curve, Figure 6.4). This was determined to be $\log_{10}$([F-6-P]/nM) = 5.1, which corresponded to [F-6-P] = 125 µM (Figure 6.4).

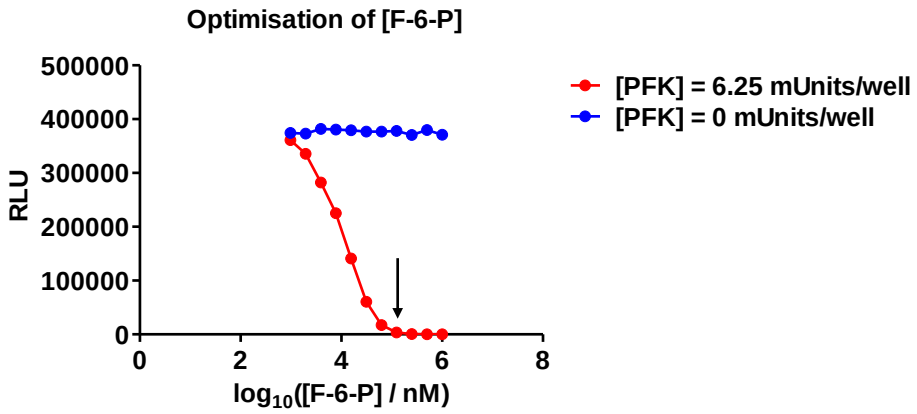

Figure 6.4: Optimisation of [F-6-P] in the Kinase Glo® Plus assay. Optimal [F-6-P] was determined to be 125 µM, the minimum amount required to give the maximum luminescence difference between the [PFK] = 6.25 mUnits/well (red curve) and [PFK] = 0 mUnits/well (blue curve) controls. RLU (relative luminescence units).

6.2.2.4: Calculation of the Z' factor for the assay.

The Z' factor is a statistical parameter that allows validation of the quality of an assay and direct comparison of the robustness of different assays, hence indicating the suitability of a particular assay for application in HTS (Zhang, Chung et al. 1999). The Z' factor is calculated using the equation in Figure 6.5A and reflects the dynamic range between the positive and negative controls (difference in means), but also the data variation of individual measurements of those controls (sum of the standard deviations). Z' can take any value from 0 to 1 and the most robust assays will be those with a large dynamic range and small standard deviations, at which point Z' would approach 1 (ideal assay). Z' ≥ 0.5 is generally considered an excellent assay (Zhang, Chung et al. 1999; Glickman, McGee et al. 2004). To calculate the Z' factor, the optimised assay was run with 48 identical samples of both the positive control ([PFK] = 6.25 mUnits/well) (red data points, Figure 6.5B) and the negative control ([PFK] = 0 mUnits/well) (blue data points, Figure 6.5B). Equation 6.5A was then used to calculate the Z' factor as Z' = 0.89 for this assay, which was considered extremely robust.

A

$$\text{Estimated Z}' \text{ factor} = 1 - \frac{3(\hat{\sigma}_p + \hat{\sigma}_n)}{|\hat{\mu}_p - \hat{\mu}_n|}$$

$\hat{\sigma}_p$ and $\hat{\sigma}_n$: sample standard deviation ($\hat{\sigma}$) and mean ($\hat{\mu}$) for the positive (p) and negative (n) controls

B

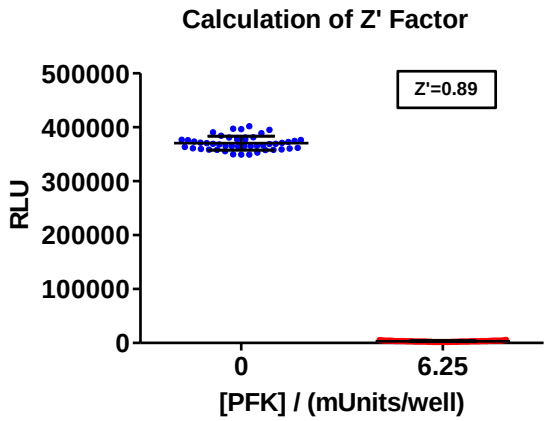

Figure 6.5: Z' factor calculation for the optimised PFK Kinase Glo® Plus assay. **(A)** Z' factor equation, calculated from the difference between the means of the positive and negative controls, and the sum of the standard deviations of the positive and negative controls. **(B)** Z' factor for the assay was calculated from 48 samples each of the positive and negative controls, as Z'=0.89. This indicated a high dynamic range between the controls and small standard deviation between replicates of each control. RLU (relative luminescence units).

6.2.2.5: Luminescence stability over time.

With a view to employing the optimised assay in HTS, it was necessary to check signal stability over time, in order to ensure batch processing of plates could be performed. The optimised assay was run in the presence (red bars, Figure 6.6) and absence (blue bars, Figure 6.6) of PFK (six replicates of each) and the luminescence signal recorded after 10 minutes incubation with Kinase Glo® Plus (t = 0 h) and every hour afterwards for a total of 6 hours (Figure 6.6). The luminescence signal for the [PFK] = 0 mUnits/well control was highly stable with a half-life > 6 hours (39% reduction in signal), suggesting batch processing would certainly be feasible. The [PFK] = 6.25 mUnits/well control signal appeared to degrade more rapidly, though this can likely be attributed to the luminescence signal from this control being

very low initially. Signal stability tests with a selection of "hits" from the initial screens would confirm extended luminescence half-life at higher RLUs. It is fully anticipated that this will be the case.

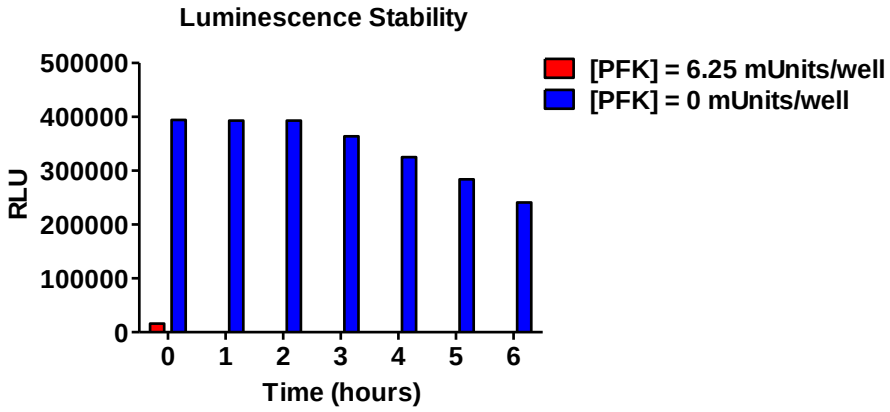

Figure 6.6: Luminescence signal stability of the Kinase Glo® Plus assay. Luminescence half-life for the [PFK] = 0 mUnits/well was > 6 hours, indicating high signal stability and suitability for batch processing. RLU (relative luminescence units).

6.2.3: Towards PFK Assay Validation

Having confirmed that the assay was suitably robust, it was desirable to establish that the inhibitory activity of known PFK inhibitors could be determined. The inhibitory activity of the allosteric inhibitor phosphoenolpyruvate (PEP) was detected by the Kinase-Glo® assay. However, it was preferable to confirm detection ability of the optimised assay using a known competitive inhibitor of the substrate (F-6-P) for both PFK and PFKFB3 (for future use). This was with a view to ultimately identifying novel F-6-P-competitive inhibitors of PFKFB3. Competitive inhibition with an enzyme's substrate provides strong evidence for binding of the inhibitor at the active site (Blat 2010). It would be desirable to develop inhibitors targeted to this site, as the ATP-binding site is highly conserved among the kinome family (Bamborough 2012), which would make PFK-2/FBPase-2 specific targeting difficult, let alone isoenzyme-specific PFKFB3 targeting.

6.2.4: Towards the Synthesis of 2,5-Anhydro-D-glucitol-6-phosphate and 2,5-Anhydro-D-mannitol-1-phosphate

2,5-Anhydro-D-glucitol-6-phosphate had been reported as a competitive inhibitor of PFK-1 (Koerner, Younatha.Es et al. 1974) and 2,5-anhydro-D-mannitol-1-phosphate (Pilkis, Pilkis et al. 1985) had been reported to be a competitive inhibitor of PFK-2/FBPase-2. It was therefore of interest to obtain these molecules to validate the assay. At the time this work was conducted, both were prohibitively expensive, so it was decided to attempt to synthesise these molecules in-house for immediate use in the assays, which would also avoid potential stability issues.

2,5-Anhydro-D-mannitol-1-phosphate was synthesised as detailed in Scheme 6.10 and references throughout the text indicate original reports of procedures utilised during the synthesis. D-Glucosamine hydrochloride **16** was allowed to reach mutorotational equilibrium by stirring in water for 20 h. Nitrous acid was formed *in situ* by addition of sodium nitrite, followed by dropwise addition of glacial acetic acid, to form the diazonium ion, which was not isolated. Ring opening, followed by diastereoselective ring closure, afforded the aldehyde **17**, which was confirmed by mass spectrometry (peak at *m/z* = 161 ($[M-H]^-$)) (Cassel, Debaig et al. 2001). **17** was reduced *in situ* by slow addition of $NaBH_4$ in water, to form polyol **18**, as evidenced by mass spectrometry (peak at *m/z* = 187 ($[M+Na]^+$)) (Cassel, Debaig et al. 2001). To aid purification, **18** was acetylated for 18 h in the presence of 1:1 pyridine:acetic anhydride, and purified by flash column chromatography, affording **19** as a colourless oil in good yield (73%) (Cassel, Debaig et al. 2001). **19** was then deacetylated with a 1M NaOMe/MeOH solution for 18 h, then neutralised by addition of Amberlite® IR-120 resin (H^+ form) to afford **18** as a colourless oil, in quantitative yield (99%). The spectroscopic data were consistent with those reported in the literature, including characteristic peaks in the ^1H NMR

for the diastereotopic CH_2 protons at δ_H = 3.62 and 3.71 ppm, and $[\alpha]_D^{25}$ +48.0 (*c* = 1.0, H_2O); lit ($[\alpha]_D^{20}$ +50.0 (*c* = 1.0, H_2O)) (Cassel, Debaig et al. 2001).

Phosphorylation of **18** was performed enzymatically using yeast hexokinase, and formation was evidenced by mass spectrometry (*m/z* = 243 ($[M-H]^-$)) (Koerner, Younatha.Es et al. 1974). The reported purification procedure involved column chromatography on a diethylaminoethyl (DEAE)-Sephadex® ion-exchange column, eluting with a H_2O:0.5 M $NaHCO_3$ gradient, followed by acidification with Dowex®-50 H^+, and neutralising with $Ba(OH)_2$, to obtain the Ba^{2+} salt (Koerner, Younatha.Es et al. 1974). However, isolation of **20** from residual salts proved problematic, with products of this type prone to phosphoryl transfer (personal communication with Dr S. Conway, Chemistry Research Laboratory, University of Oxford). An alternative isolation procedure using a Na^+ ion exchange resin was also unsuccessful.

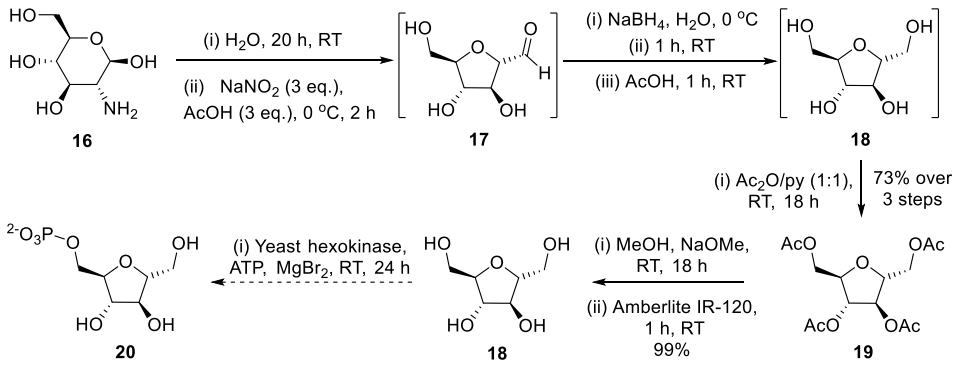

Scheme 6.10: Synthesis of 2,5-anhydro-D-mannitol-1-phosphate (**20**).

2,5-Anhydro-D-glucitol-6-phosphate was synthesised as detailed in Scheme 6.11. D-Mannitol **21** was treated sequentially with acetyl bromide for 72 h, followed by 1:1 pyridine:acetic anhydride over 18 h, **22** being isolated as a colourless, crystalline solid, in moderate yield (48%) (CrombezRobert, Benazza et al. 1997; Schmidt and Nave 2007). Reduction and elimination of **22** was achieved by heating with zinc dust and sodium acetate in glacial acetic

acid, to afford **23** as a colourless oil in 81% yield. Spectroscopic data were in full agreement with the literature and the characteristic ^{1}H NMR peaks for the diastereotopic protons at C-1 and C-6 were observed at δ_H = 5.34 and 5.29 ppm. De-acetylation of **23** to form the diol **24**, proceeded in quantitative yield (99%), through stirring with a 1M solution of NaOMe in MeOH. The literature procedure to synthesise **25** was found to be ineffective (yield < 15%), but changing solvent from toluene to a 1:1 mixture of DMF:THF, and increasing the equivalents of benzyl bromide (2.6 eq.) used, resulted in a much improved yield (72%), affording **25** as a colourless oil.

Conversion to **26** was achieved following a procedure by Donohoe and colleagues that used catalytic osmium tetroxide to effect dihydroxylation of the diene **25**, followed by acid-promoted diastereoselective oxidative cyclisation, affording the enantiomerically pure *cis* tetrahydrofuran **26** in good yield (76%) (Donohoe and Butterworth 2003). Synthesis of **27** was achieved through a modified literature procedure, by benzyl-deprotection using H_2 and Pd/C in 1:1 EtOH/THF, the product being isolated as a colourless oil in high yield (94%) (Donohoe and Butterworth 2003). The analytical data were fully consistent with the literature, including characteristic peaks in the ^{1}H NMR at δ_H = 4.12 and 3.96 ppm, corresponding to the C*H*OH protons and $[\alpha]_D^{25}$ +21.6 (*c* = 1.0, MeOH); lit ($[\alpha]_D^{20}$ +18.8 (*c* = 1.0, CH_2Cl_2)) (Donohoe and Butterworth 2003). Purification following phosphorylation of **27** to **28** using the yeast hexokinase-mediated procedure by Koerner and colleagues (Koerner, Younatha.Es et al. 1974) again proved problematic, as *per* the synthesis of **20**.

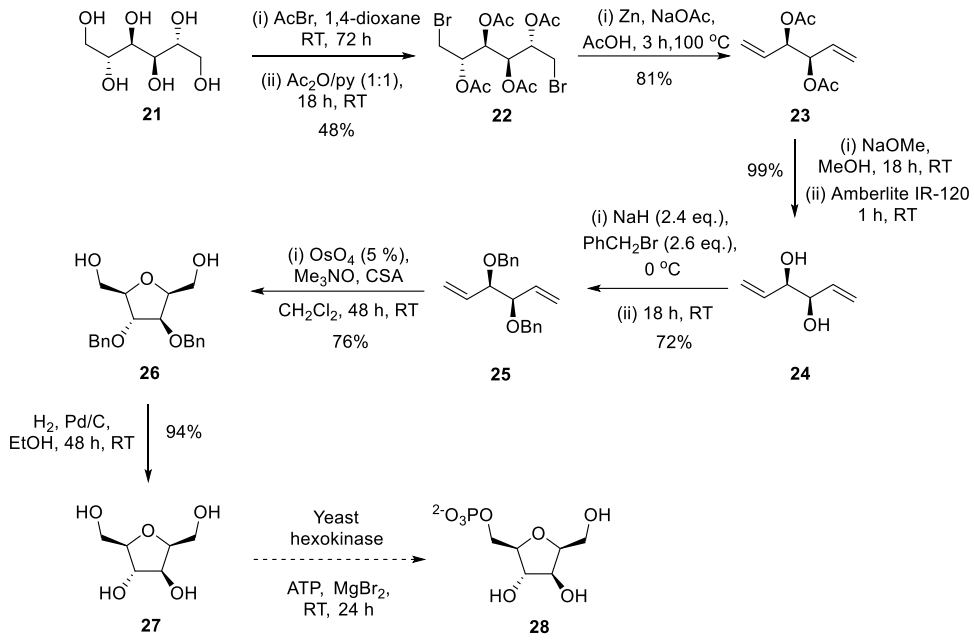

Scheme 6.11: Synthesis of 2,5-anhydro-D-glucitol-6-phosphate (**28**).

Regrettably, time constraints did not permit further investigation of purification of the phosphorylated product, or alternative sourcing. Nevertheless, the non-phosphorylated 2,5-anhydro-D-mannitol has itself been reported to inhibit PFK-1 activity *in vitro* (Riquelme, Kneer et al. 1985). It was therefore decided to test the two anhydro-sugars **18** (2,5-anhydro-D-mannitol) and **27** (2,5-anhydro-D-glucitol) in the PFK assay, to determine whether they showed any inhibitory activity. Unfortunately, neither molecule showed inhibitory activity, up to a concentration of 2 mM (Figure 6.7).

These results suggest that the previously reported inhibitory activity of 2,5-anhydro-D-mannitol *in vitro* (Riquelme, Kneer et al. 1985) was likely only due to the phosphorylated metabolites of this molecule, which result from intracellular enzymatic transformation (Riquelme, Wernette-Hammond et al. 1984). Competing project priorities unfortunately meant synthesising or sourcing known PFK competitive inhibitors was put aside, pending assay development with the PFKFB3 protein. A test of the PFKFB3 inhibitor 3PO in the PFK assay showed a small amount of inhibitory activity against bacterial PFK at high

concentration (7% inhibition, 2 mM 3PO) (Figure A14.1, Appendix). A future screen against human PFK-1 should be performed to confirm that the activity of 3PO is not due to off-target effects.

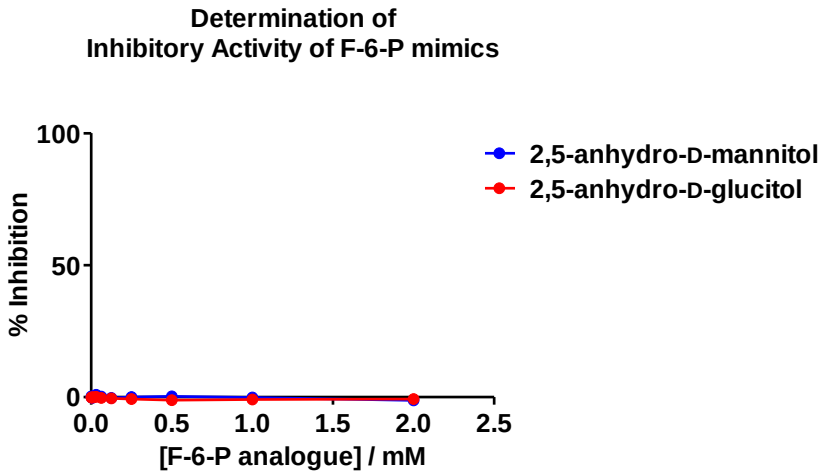

Figure 6.7: Determination of inhibitory activity of F-6-P analogues in the optimised PFK Kinase Glo® Plus assay. 2,5-anhydro-D-mannitol (**18**) and 2,5-anhydro-D-glucitol (**27**) did not exhibit inhibitory activity against bacterial PFK-1.

6.2.5: PFKFB3 Assay Development

Having determined the Kinase Glo® Plus assay to be highly robust for use with bacterial PFK-1, it was anticipated that it would be equally suitable for measuring PFKFB3 kinase activity, albeit with re-optimisation of conditions according to the same protocol. PFKFB3 became commercially available towards the end of the project (Abnova, H00005209-P01), so it was decided to attempt optimising the assay using the commercial product. Kinase activity was tested using the maximum practical concentration of enzyme (24.7 ng/well) over a range of ATP concentrations (serial dilutions from 12.5 µM to 6.1 nM, including a [ATP] = 0 µM control) (Figure 6.8).

Despite extended incubation time prior to addition of the Kinase Glo® Plus kit (90 min), no change was observed in relative luminescence units over the full range of ATP concentrations

tested. For comparison, a recent functional PFKFB3 assay reported by Clem and colleagues (Clem, O'Neal et al. 2013) used similar component concentrations (13 ng/well kinase, 10 µM ATP and 10 µM F-6-P) to that used in the present study (24.7 ng/well kinase, 12.5 µM ATP and 125 µM F-6-P). This strongly suggested that the enzyme was catalytically inactive, which may have been a result of a GST-tag at the N-terminus of the recombinant protein (site of the kinase activity). The high cost (£2740 / 100 µg) of the enzyme meant it was impractical to further investigate whether this was the case, through GST-tag removal. Again, it was regrettable that time constraints did not permit in-house purification of enzymatically active human recombinant PFKFB3. Collaboration with direct competitors was also not possible.

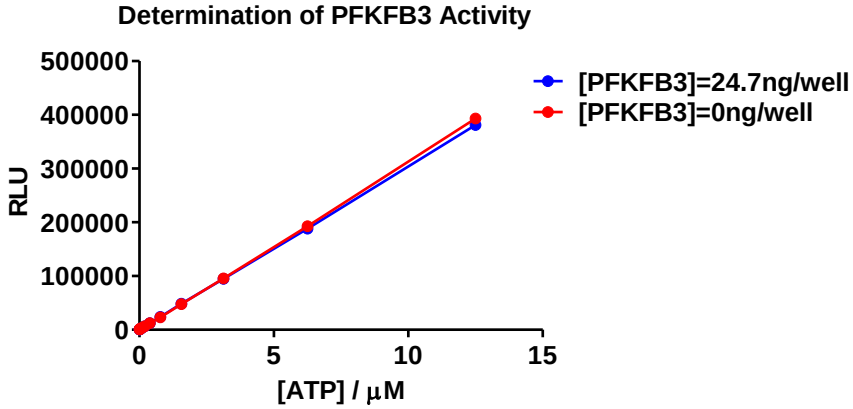

Figure 6.8: Determination of human recombinant PFKFB3 enzymatic activity. No difference in luminescence signal was observed between (+)PFKFB3 (blue) and (-)PFKFB3 (red) controls across a range of ATP concentrations, indicating human recombinant PFKFB3 (H00005209-P01) was not enzymatically active. RLU (relative luminescence units).

6.2.6: PFKFB3 Thermal Shift Assay

Whilst the commercial human recombinant PFKFB3 was not catalytically active, this would not necessarily preclude binding of potential inhibitors, including at the active site (Fedorov, Marsden et al. 2007). Therefore, it was decided to attempt using the PFKFB3 in a fluorescent thermal shift assay, with a view to potentially using this assay in the short-term to identify small molecule inhibitors of PFKFB3.

A ligand binding to a protein can stabilise the protein's native state and thereby increase its melting temperature. Use of fluorescent dyes such as SYPRO® Orange, that bind only to the unfolded state of the protein, enables a shift to be seen in the fluorescence melting curve when such a ligand is bound. This shift is proportional to the ligand concentration and binding affinity (Bullock, Debreczeni et al. 2005). A previous example from the Russell group (assay performed by Helen Storr) is shown in Figure 6.9A, which demonstrated a shift in the melting curve for PIM kinase (blue curve, DMSO control) after binding of a PIM kinase inhibitor (red curve). The same technique was applied using the maximal practical concentration of PFKFB3 protein (0.2 µM), but no difference in fluorescence signal in the presence of enzyme (red curve) could be detected (Figure 6.9B). The use of more protein would have been prohibitively expensive, so it was decided to suspend work on this assay.

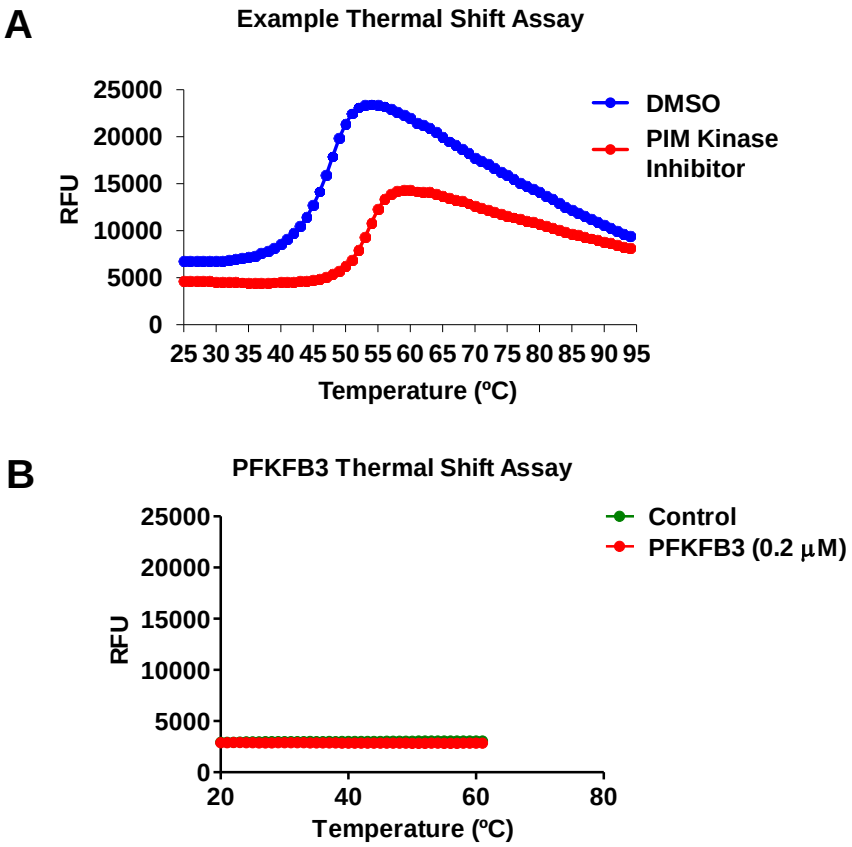

Figure 6.9: Test of human recombinant PFKFB3 in a thermal shift assay. **(A)** Sample thermal shift assay curve showing an increase in melting temperature of the PIM kinase protein in the presence of an inhibitor (assay performed by Helen Storr using an inhibitor developed in-house by Abigail Guillermo (Russell group)); **(B)** PFKFB3 thermal shift assay showed no increase in fluorescence signal with increasing temperature due to insufficient PFKFB3 protein.

6.3: Discussion

The synthesis of 3PO proved far more complex than originally anticipated, but synthesis via the polymer-supported Wittig reaction (Scheme 6.8) has provided sufficient supply to perform future enzymatic assays and *in vitro*/*in vivo* studies. The same methodology could likely be applied to the synthesis of other 3PO derivatives in order to investigate features required for inhibitory activity, which would support the design of novel inhibitors.

The studies and optimisation of the Kinase Glo® Plus assay with bacterial PFK-1 have confirmed it to be highly robust and have also established that it will likely be fully suitable for use with PFKFB3. Future work must now prioritise purifying enzymatically active human recombinant PFKFB3 in-house, followed by optimisation of the assay using the protocol applied to bacterial PFK-1. It is anticipated that the PFKFB3 assay would also have a high Z'-factor. Furthermore, high luminescence stability will enable batch processing to test large numbers of potential inhibitors from small molecule libraries.

Nevertheless, it will be important to account for possible false positives (inhibitors of luciferase itself), by screening potential "hits" against the luciferase in the absence of PFKFB3. Indeed, it would be desirable to set up an orthogonal assay to validate "hits" from the initial compound screens. For example, the ADP-Glo® assay (Promega) also utilises luciferase, but measures ADP formation. Additional screening of "hits" against this assay would identify luciferase inhibitors. The luminescence signal would decrease in both assays, whereas for true PFK/PFKFB3 inhibitors, the signal should increase in the ATP Kinase Glo® Plus assay and decrease in the ADP-Glo® assay (Glickman, McGee et al. 2004).

It was unfortunate that time constraints did not permit successful purification of the two F-6-P analogues, 2,5-anhydro-D-mannitol-1-phosphate (**20**) and 2,5-anhydro-D-glucitol-6-phosphate

(**28**). Future work must look to source these inhibitors, or investigate alternative purification procedures/synthetic methods, in order to fully validate the assay. The crude product mixtures themselves from the enzymatic phosphorylation reactions could also be tested. Nevertheless, modified versions of the established synthetic routes may be utilised to introduce additional functionality and develop a series of synthetic F-6-P analogues as potential inhibitors.

The majority of registered kinase inhibitors, e.g. imatinib and gefitinib, are directed to the ATP-binding site and act as ATP-competitive inhibitors (Fabbro, Cowan-Jacob et al. 2012). However, this site is highly conserved between different kinases, increasing the likelihood of promiscuous inhibition of multiple off-target kinases. Indeed, the vast majority of reported inhibitors are thought to target multiple protein kinases (Bamborough 2012). A move towards substrate-specific competitive inhibition would likely increase the selectivity of potential small molecule inhibitors. This is particularly important in the case of PFKFB3, given the requirement for isoenzyme-specific inhibition. The development of inhibitors that target the F-6-P binding site, shared by fewer enzymes, would likely be the most effective strategy.

It is important to be realistic about the screening capabilities in an academic environment. Industry routinely screen hundreds of thousands of compounds (Zhang, Chung et al. 1999), which is of course far beyond that which could be achieved in academia. It would be more appropriate to term the future screen that will be conducted using the Kinase Glo® Plus assay as medium-throughput. Nevertheless, intelligent construction of a screening library increases the probability of finding a "hit", whilst decreasing the required size of the screen.

Molecules that have similar 3D shapes, orientation of functionality, and electrostatics, often tend to have similar biological properties, given these features play an important role in binding of a compound at an active site (Nicholls, McGaughey et al. 2010). Accordingly, an

in-house library of approximately 25,000 small molecules has already been screened for molecules similar to 3PO, F-6-P and other PFK-2/FBPase-2 inhibitors, including the mercaptopurines (Mojena, Bosca et al. 1992). This screen was performed by Dr Raman Parkesh (Russell group) using ROCS (Rapid Overlay of Chemical Structure) software (OpenEye), and a library has been constructed from those compounds found to be most similar to the query molecules. This condensed small molecule library will form the basis of initial PFKFB3 screening in the future.

Furthermore, the crystal structure of human PFKFB3 has been reported, which will also enable docking studies to be performed, in order to identify additional potential inhibitors (Kim, Manes et al. 2006). The ability to model key interactions of inhibitors with the PFKFB3 active site will also compliment Structure-Activity Relationship studies, and identify those features that are central to the inhibitory activity of such molecules. Further derivatives would be developed to optimise and increase binding affinity with the active site residues.

Although the development of isoenzyme-specific PFKFB3 inhibitors presents a major challenge, there is literature precedent for isoenzyme-specific inhibitors of other enzymes, such as phospholipase D (PLD) (Lavieri, Scott et al. 2010) and phosphoinositide 3-kinase (PI3K) (Edgar, Wallin et al. 2010). It is intended to use the reported crystal structure of PFKFB4 (Hasemann, Istvan et al. 1996) to co-screen PFKFB3 “hits” and also identify topological features unique to the isoenzymes, to aid the development of PFKFB3-specific inhibitors. It would be important to screen potential inhibitors against PFKFB4, other PFK-2/FBPase-2 isoenzymes and proteins of the wider kinome, to test for possible cross-reactivity. Of particular concern would be PFKFB1, the principal PFK-2/FBPase-2 isoform in the liver, which supports organismal metabolic homeostasis (Ros and Schulze 2013).

Chapter 7: Final Discussion and Future Perspectives

7.1: Overview and Summary

This thesis set out with four broad aims, which are reiterated below.

- To examine the expression profiles of each of the PFK-1 and PFK-2/FBPase-2 isoenzymes in various cancer cell types and further probe their expression under hypoxic conditions, and regulation by hypoxia-inducible factors (HIFs).
- To validate PFK-2/FBPase-2 isoenzymes as anti-tumour targets and explore potential reciprocal relationships between isoenzymes.
- To investigate the requirement for isoenzyme-specific inhibition and further understanding of how individual PFK-2/FBPase-2 isoenzymes regulate metabolic flux.
- To undertake steps towards the development of an in-house assay to facilitate identification of potential PFK-2/FBPase-2 small molecule inhibitors.

The work in this thesis has expanded understanding of the relationship between the PFK-1 and PFK-2/FBPase-2 isoenzymes, as well as the bisphosphatase TIGAR. It has undertaken the first detailed comparison of relative mRNA expression levels of these enzymes under both normoxic and hypoxic conditions (Figures 3.1-3.6 and 3.14, Chapter 3). PFKFB3 and PFKFB4 were confirmed to be the most strongly induced isoenzymes in the initial three cell lines studied (MCF-7, U87, PC3). These isoenzymes were consistently expressed at comparatively high levels and regulated in a HIF-1α-dependent and HIF-2α-independent manner (Figures 3.9F-3.11F and 3.9G-3.11G, Chapter 3).

Knockdown of both PFKFB3 and PFKFB4 was shown to reduce 2D proliferation and 3D spheroid volume, in a cell dependent manner, validating them as potential anti-tumour targets (Figures 4.6-4.11, Chapter 4). It was particularly striking that the cell lines examined showed

increased sensitivity of 2D growth to PFKFB3 and PFKFB4 depletion under hypoxic conditions (Figures 4.6B-4.8B, Chapter 4). It is believed that these were the first studies to examine such effects in hypoxia, which is surprising given that both isoenzymes are strongly induced in hypoxia.

The proliferation studies revealed that double PFKFB3/PFKFB4 siRNA knockdown, which would mimic the effect of an inhibitor targeting both PFKFB3 and PFKFB4, resulted in a significant "rescue" effect, compared to the reduction in growth mediated by PFKFB3 siRNA knockdown alone (Figures 4.6-4.11, Chapter 4). These effects appeared to be directly related to opposing activities of the two isoenzymes on intracellular [F-2,6-BP], with PFKFB3 acting with a high kinase activity and PFKFB4 acting with high bisphosphatase activity (Figures 4.12-4.16, Chapter 4). This indicated an isoenzyme specific inhibitor of total PFKFB3 activity or total PFKFB4 activity would be more effective than an inhibitor targeting both isoenzymes.

It was a logical progression to pursue a metabolic explanation for the opposing effects of these isoenzymes, given the well-established role of F-2,6-BP as an allosteric activator of PFK-1 and therefore modulator of glycolytic flux (Hue and Rousseau 1993; Nissler, Petermann et al. 1995; Atsumi, Chesney et al. 2002). Furthermore, the increased sensitivity of 2D growth of MCF-7 and U87 cells to depletion of PFKFB3 and PFKFB4 in hypoxia (Figures 4.6 and 4.7, Chapter 4), compared to normoxia, led to the reasonable supposition that this was a result of the two isoenzymes being intimately involved in maintenance of the glycolytic phenotype. However, a range of assays employed to indicate changes in glycolytic/PPP flux did not fully support this hypothesis. In particular, the NMR experiments examining changes in the ^{13}C-labelled lactate species produced, suggested that if PFKFB3 or PFKFB4 suppression were effecting a change in the balance between glycolysis and the PPP, then this effect was too small to detect (Figure 5.10, Chapter 5). It was therefore considered

unlikely that this would be the predominant factor in mediating the reduction in cell proliferation induced by PFKFB3 or PFKFB4 suppression. The findings from the ROS assay (Figure 5.3, Chapter 5) and lipid droplet content assay (Figure 5.4, Chapter 5) were consistent with this assessment, given that the observations from these experiments appeared to run contrary to the predicted model of PFKFB3 and PFKFB4 activity on regulating glycolytic flux (original hypothesis: Figure 4.17, Chapter 4).

A number of questions remained about the mechanistic action of the therapeutic effects of PFKFB3 and PFKFB4 in the cell lines examined, such as a potential role for both isoenzymes in sub-cellular compartmentalisation of F-2,6-BP. However, this did not preclude progress being made towards the development of an assay system to identify potential small molecule inhibitors of PFKFB3 or PFKFB4. Both isoenzymes warrant investigation as potential anti-tumour targets. However, the present study indicated PFKFB3 inhibition would likely offer a more broadly applicable therapeutic strategy, given that the proliferation rates of the cell lines examined were consistently more sensitive to PFKFB3 inhibition than PFKFB4 inhibition (Figures 4.6-4.11, Chapter 4).

Accordingly, a robust kinase assay was trialled and optimised with bacterial PFK-1 and a synthetic route devised for the benchmark PFKFB3 inhibitor 3PO (Chapter 6). Pending purification of enzymatically active human recombinant PFKFB3 protein in-house, this assay system will provide a platform from which to begin medium throughput screening and PFKFB3 inhibitor development.

In conclusion then, this thesis has achieved its original aims and has answered in the affirmative, the original question of whether the most effective therapeutic strategy would require isoenzyme-specific inhibition of PFK-2/FBPase-2. In doing so, it has uncovered a

level of complexity in the PFKFB3 and PFKFB4 mediated effects on cell proliferation, which future work should seek to investigate.

7.2: Short Term Future Work

In the short term, it will be necessary to determine the mechanism by which PFKFB3 and PFKFB4 inhibition reduce proliferation. For example, whether the cells become senescent, undergo apoptosis or autophagy. Studies in the literature suggest that depletion of these isoenzymes induces apoptosis in cells (Calvo, Bartrons et al. 2006; Ros, Santos et al. 2012), but this may vary in a cell type dependent manner and should be investigated. The effective cell-killing effect of PFKFB3 or PFKFB4 knockdown, or longer term cytostatic effects, should also be assessed using clonogenic assays. Furthermore, the transient nature of siRNA-mediated mRNA suppression will require inducible knockouts of both PFKFB3 and PFKFB4 to be generated in-house, to facilitate longer term *in vitro* time course studies and progression to *in vivo* studies. Alternative deletion strategies could also be employed, such as zinc finger nuclease-mediated genome editing, which facilitates the creation of DNA double strand breaks at user-specified locations. The recent emergence of clustered regularly interspaced short palindromic repeats (CRISPR) technology, which utilises a RNA-guided CRISPR-associated (Cas9) nuclease to target complimentary DNA sequences for cleavage, could also be explored (Chang, Sun et al. 2013).

The use of siRNA studies provides an excellent model to examine the effect of suppression of a particular protein. This mimics the effect of a specific inhibitor of total enzyme activity, but there is an important distinction, in that siRNA studies reduce the expression of a protein, whereas an inhibitor reduces the activity of a protein whilst the protein remains physically intact. In the vast majority of cases the phenotypes induced by small molecule inhibition of a target and siRNA suppression align. However, it is possible that they would be inconsistent if

PFKFB3 or PFKFB4 were to engage in protein-protein interactions aside from their role in regulating intracellular [F-2,6-BP]. In order to exclude this possibility, it would be prudent to express catalytically inactive PFKFB3 and PFKFB4 *in vitro* to ensure it is the inhibition of their catalytic activity that accounts for the therapeutically beneficial effect of reduced expression.

This thesis has demonstrated that the most effective PFK-2/FBPase-2 therapy will be one that is isoenzyme specific. However, it is important to consider the bifunctional catalytic activity of the PFK-2/FBPase-2 isoenzymes. The siRNA studies have only permitted overall isoenzyme activity (net effect of kinase and bisphosphatase activities) to be investigated. It may be that development of a kinase-specific inhibitor, even if it exhibits cross-reactivity with a number of PFK-2/FBPase-2 isoenzymes, might be viable. It would be sensible to assess this in the short term by expressing a mutant PFKFB4 in cells, exhibiting pure kinase activity and lacking bisphosphatase activity. If simultaneous suppression of PFKFB3 and mutant PFKFB4 expression has no effect, or a synergistic effect on cell growth, compared to suppression of PFKFB3 knockdown alone, this will validate the possibility of using a non-specific PFK-2/FBPase-2 kinase inhibitor. That said, there may be difficulties in designing such an inhibitor to ensure it does not also inhibit the bisphosphatase activity of PFKFB4, through induced conformational changes. In that case, it would be necessary to revert to developing a PFKFB3-specific kinase inhibitor.

Enzymatically active human recombinant PFKFB3 must be prepared in-house, to provide sufficient supply for screening, and the assay optimised using the protocol outlined in this thesis (Chapter 6). The virtual screen of an in-house library has identified small molecules similar in shape and electrostatics to known non-specific PFKFB3 inhibitors and should form the basis of initial assay testing (screen performed by Dr Raman Parkesh, former member of

the Russell group). After confirmation of the inhibitory activity of any "hits", a series of structurally diverse active compounds should be selected for further study. Synthetic chemistry should then be utilised to examine structure-activity relationships, with a view to improving potency and gaining a deeper understanding of the features of these molecules that are central to their inhibitory activity.

If a decision is made to develop an isoenzyme-specific PFKFB3 kinase inhibitor, it will be necessary to utilise the existing crystal structures of both PFKFB3 and PFKFB4, to aid incorporation of specificity in molecular design. Human recombinant PFKFB1, PFKFB2 and PFKFB4 protein should be obtained to test for cross-reactivity. Longer term, the importance of testing potential therapeutic agents across a wider panel of kinases, to identify potential off-target effects, cannot be understated.

Aside from PFKFB3 inhibitor development, it would also be interesting to undertake a study to profile the effects of all PFK-2/FBPase-2 isoenzymes on regulation of metabolic flux, using over-expression and siRNA knockdown studies. PFKFB3 and PFKFB4 were chosen as the most important isoenzymes for study against a backdrop of supportive literature and results from the current study, demonstrating high expression levels and hypoxia-inducibility (Figures 3.1-3.6 and 3.8, Chapter 3). Whilst these isoenzymes are undoubtedly important in cancer cell survival, modulation of cytoplasmic F-2,6-BP by either PFKFB1 or PFKFB2 may unexpectedly be central to regulation of glycolytic flux.

The low expression level of PFKFB1 at the mRNA level in the cell lines examined (Figures 3.1-3.3, Chapter 3) suggests PFKFB2 might fill this role. Indeed, PFKFB2 kinase activity has been reported to be increased under hypoxic conditions by AMPK-mediated phosphorylation (Marsin, Bertrand et al. 2000). Its importance may therefore be masked to some extent by

examining expression level alone. This is a limitation of the present study that future work should seek to investigate further.

7.3: Examining the Role of PFKFB3 and PFKFB4

This study originally selected PFKFB3 and PFKFB4 for investigation as a way of exploring targets to modulate aerobic glycolysis. The work has indeed validated these isoenzymes as potential targets for further investigation and a role for PFKFB3 and/or PFKFB4 in regulating glycolytic/PPP flux in the cell lines examined cannot be completely excluded. However, it seems likely that future study of their predominant functional effects will diverge from the original target pathways. The development of PFKFB3-specific inhibitors should continue, but it will be desirable to select appropriate combination therapies to improve the effectiveness of such inhibitors in the future. In order to achieve this, it will be necessary to gain a deeper understanding of the mechanisms by which not only PFKFB3, but also PFKFB4, inhibit cancer cell proliferation.

The work contained within this thesis in no way disputes the role of F-2,6-BP as an allosteric activator of PFK-1 and therefore promoter of glycolytic flux. It fully supports the function of PFKFB3 and PFKFB4 in modulating levels of F-2,6-BP (Figures 4.12-4.16, Chapter 4). However, the results obtained add to the increasing controversy that is emerging in the literature about whether the activity of PFKFB3, and indeed PFKFB4, is only linked to glycolytic flux.

PFKFB3 has been widely held to be the predominant regulator of intracellular [F-2,6-BP] and therefore glycolytic activity in transformed cells because of its high relative expression and unusually high kinase activity (Chesney 2006). However, a number of reports suggest that different splice variants of PFKFB3 may have distinct intracellular functions. Of particular

interest is the study by Yalcin and colleagues, which demonstrated nuclear localisation of PFKFB3 splice variant 5 (UBI2K5) in HeLa cells (Yalcin, Clem et al. 2009). The study found over-expression of UBI2K5 had no effect on glucose metabolism, but increased proliferation. The authors attributed this to nuclear delivery of F-2,6-BP, with corresponding activation of cell cycle proteins, including cyclin-dependent kinase-1 (Cdk-1), potentially through a direct allosteric effect.

An apparently conflicting study by Calvo and colleagues observed UBI2K5 silencing, also in HeLa cells, to decrease intracellular [F-2,6-BP], leading to a corresponding decrease in lactate production and ATP production, apparently demonstrating a glycolytic role for this splice variant (Calvo, Bartrons et al. 2006). The picture is further complicated by the report from Zscharnack and colleagues, which observed over-expression of the PFKFB3 splice variant UBI2K4 to increase F-2,6-BP production, without eliciting a change in lactate production (Zscharnack, Kessler et al. 2009). These studies and the work in this thesis support both a pro-proliferative and pro-glycolytic role for PFKFB3.

Yalcin and colleagues have proposed the possibility of intracellular compartmentalisation of F-2,6-BP (Yalcin, Clem et al. 2009). The results presented in this thesis showing high kinase activity of PFKFB3, particularly in MCF-7 and U87 cells (Figures 4.13-4.15, Chapter 4), but minimal effect on glycolytic flux (Figure 4.19, Chapter 4 and Figure 5.10, Chapter 5) would support this notion. It seems apparent that changes in the total intracellular concentration of F-2,6-BP may be comparatively less important than the location of that change within the cell.

It would be reasonable to suggest that the conflicting reports of PFKFB3 activity may be due to the expression and sub-cellular localisation of PFKFB3 splice variants varying in a cell-type and context dependent manner, which is not as yet understood. No studies have

examined how the intracellular localisation of PFK-1 and the other PFK-2/FBPase-2 isoenzymes and splice variants might change in response to siRNA knockdown of PFKFB3 or PFKFB4. Furthermore, there have been no studies examining how the intracellular localisation of PFKFB3 and PFKFB4 splice variants might change after exposure to hypoxia. In seeking an explanation for the *in vitro* effects mediated by modulation of expression of these isoenzymes, and particularly their opposing activities, examining such factors will likely be of critical importance.

PFKFB4 has been reported to be located in the cytoplasm, i.e. the site of glycolysis (Yalcin, Clem et al. 2009). If the reduction in proliferation mediated by PFKFB3 knockdown in the three cell lines examined (Figures 4.6-4.11, Chapter 4) is principally due to a reduction in nuclear delivery of F-2,6-BP, the "rescue effect" mediated by simultaneous PFKFB4 knockdown is even more intriguing. It might imply that if PFKFB4 acts to reduce [F-2,6-BP] in the cytoplasm, with its high bisphosphatase activity, knockdown of PFKFB4 by siRNA would lead to an increase in cytoplasmic F-2,6-BP. This might then be "shuttled" to the nucleus, to counteract the effect of the PFKFB3 knockdown mediated reduction in nuclear F-2,6-BP. It is also possible that the same effect could be mediated by a change in intracellular localisation of the PFKFB4 protein itself.

Monitoring the intracellular localisation of F-2,6-BP itself isn't feasible, due to stability issues and likely leaching of the metabolite from the nuclear fraction during extraction. However, the localisation and enzymatic activities of the PFK-2/FBPase-2 isoenzymes can be examined in the nuclear and cytoplasmic fractions of cell extracts, in the manner described by Yalcin and colleagues (Yalcin, Clem et al. 2009).

This thesis has focussed purely on total PFKFB3 expression and total PFKFB4 expression, rather than specific splice variants, because the ultimate goal of this and future work is to develop a PFK-2/FBPase-2 inhibitor. The development of a PFKFB3 isoenzyme-specific inhibitor will likely bring enormous challenges, but the development of a splice variant specific inhibitor is currently considered unfeasible. For that reason, the assessment of either PFKFB3 or PFKFB4 as a suitable anti-cancer target in this thesis has not considered individual splice variants, but future mechanistic study will clearly need to examine them. It should be noted however, that aside from small molecule inhibition, alternative strategies to modify the splice variant expression profile in cells could potentially be explored. The use of modified oligonucleotides complementary to specific sequences in the pre-mRNA has been shown to repress or even enhance the expression of individual splice variants (Eperon 2012). Such oligonucleotides have been used to hide particular exons in the pre-mRNA from the splicing machinery, leading to their absence from the mature mRNA (Aartsma-Rus, Houlleberghs et al. 2010). This technology could feasibly be applied to PFKFB3 or PFKFB4 in the future.

Through the work presented in this thesis and previous reports in the literature, it has become apparent that the total intracellular concentration of F-2,6-BP does not always correlate with glycolytic flux via PFK-1 activity. In light of these findings, it would be interesting to revisit some of the literature studies. For example, that by Seo and colleagues, who demonstrated non-specific PFKFB3 inhibitors to reduce intracellular [F-2,6-BP] and reduce glycolytic flux (Seo, Kim et al. 2011). Also, the original report from Clem and colleagues of 3PO, which was found to inhibit PFKFB3 activity, reduce intracellular [F-2,6-BP] and suppress glycolytic flux, without testing PFK-2/FBPase-2 isoenzyme specificity (Clem, Telang et al. 2008). The question that now presents itself is whether the suppression of glycolytic flux in these studies is directly linked only to the suppression of full-length PFKFB3 activity, or whether it could

be due to non-specific inhibition of one of the other PFK-2/FBPase-2 isoenzymes, such as PFKFB2. It would be intriguing to examine whether the majority of the reduction in [F-2,6-BP] might be ascribed to reduced PFKFB3 expression, but that the effects on glycolytic flux might be due to smaller, more localised (cytoplasmic) changes in [F-2,6-BP], mediated by non-specific inhibition of one of the other isoenzymes.

Literature reports suggest that the relative kinase:bisphosphatase activity of PFKFB4 is highly variable, for example having been reported to exhibit kinase activity in the untransformed RWEP1 cell line and yet high bisphosphatase activity in prostate cancer cell lines (Ros, Santos et al. 2012). This thesis has demonstrated apparent high PFKFB4 bisphosphatase activity in the cell lines examined, which was particularly evident in the PC3 cell line (Figure 4.16, Chapter 4). A mechanistic understanding of these differing activities is still not fully established and possible post-translational modifications could offer a potential explanation, warranting further investigation.

To assist in interpreting some of the unanticipated results in terms of ATP production (Figure 4.18, Chapter 4), ROS levels (Figure 5.3, Chapter 5) and lipid droplet content (Figure 5.4, Chapter 5), it would be helpful to expand on the ^{13}C-labelled ^{1}H NMR metabolite tracking. A more extensive metabolic flux analysis could be conducted, including examination of the TCA cycle and glutaminolysis. Furthermore, work by other members of the Harris laboratory is already under way to quantitatively determine the levels of a far wider range of metabolites and other intermediates involved in metabolic pathways by mass spectrometry. This will aid interpretation of the effects mediated by these complex PFK-2/FBPase-2 isoenzymes.

For example, in the MCF-7 cells under normoxic conditions, PFKFB3 knockdown mediated an apparent reduction in lactate production (Figure 4.19B, Chapter 4) and an increase in ROS

production (Figure 5.3A, Chapter 5). A potential explanation for this would be a downstream effect mediating an increase in pyruvate channelling to the mitochondria, leading to increased oxidative phosphorylation. Such effects may not operate at a general level across cell types, but this should be explored, initially through oxygen consumption experiments, to further understand the function of PFKFB3.

The studies in this thesis have served to highlight the importance of examining a specific target across different cell lines. The markedly different responses of the three principal cell lines to PFKFB3 and PFKFB4 knockdown in terms of glucose consumption (Figure A7.1, Appendix), "glycolytic efficiency" (Figure 4.20, Chapter 4) and lipid droplet content (Figure 5.4, Chapter 5), serve to emphasise this point. Many studies employ just one or two cell lines, whereas a more rigorous approach with multiple cell lines is evidently preferable.

7.4: Towards a Hypoxia-Targeted PFKFB3-Specific Inhibitor.

The results have demonstrated the growth of MCF-7, U87 and PC3 cell lines to be sensitive to PFKFB3 depletion, with this effect accentuated under hypoxic conditions (Figures 4.6-4.8, Chapter 4). There is evidence in the literature that PFKFB3 is increased in tumour tissue (Atsumi, Chesney et al. 2002; Minchenko, Ochiai et al. 2005; Bobarykina, Minchenko et al. 2006), potentially increasing the sensitivity of cancer cells to the effects of PFKFB3-mediated inhibition. A Phase I clinical trial with a novel PFKFB3 inhibitor has recently been announced and the results are eagerly awaited in this respect (Clem, O'Neal et al. 2013). It will be essential to examine potential toxicity of normal tissue to PFKFB3-mediated inhibition, given the role of this isoenzyme in regulating glycolysis and/or cell proliferation.

A more effective strategy than systemic administration of a PFKFB3-specific inhibitor would be to harness the increased sensitivity of hypoxic cells to PFKFB3-depletion. The hypoxic

sub-fraction of solid tumours exhibits increased resistance to both radiotherapy and chemotherapy. The resistance to chemotherapy in part derives from the irregular vasculature and increased diffusion distances, impeding effective drug delivery. It seems likely that effective targeting of cells in the hypoxic region of the tumour would require high PFKFB3 inhibitor concentrations *in vivo*, significantly increasing the risk of toxicity to normal tissue. However, if the active inhibitor were to be delivered to the hypoxic fraction alone, it would circumvent this problem.

In recent years, there has been increasing interest in the use of hypoxia-activated prodrugs. These pharmacologically inactive compounds are converted to the active therapeutic agent via enzymatic reduction under hypoxic conditions (Wilson and Hay 2011). Hypoxia-selectivity is most frequently achieved via a transient one-electron product that can be oxidised back to the pro-drug in the presence of oxygen, or persist to mediate a pharmacological effect under hypoxic conditions (Denny 2000). The pro-drugs generally contain one of the five chemical moieties which can be reduced under hypoxic conditions, namely nitro groups, aromatic *N*-oxides, aliphatic *N*-oxides, quinones and transition metal ions (Wilson and Hay 2011).

Traditionally, chemical derivatives containing these moieties have been developed as pro-drugs of DNA-reactive cytotoxins in their own right, being activated under hypoxic conditions. The aromatic *N*-oxide tirapazamine (TPZ) typifies such a compound. TPZ is reduced by intracellular reductases to a cytotoxic radical that is oxidised back to TPZ in the presence of oxygen, but persists under hypoxic conditions, where it is able to induce direct DNA damage (Brown 1993; Siim, van Zijl et al. 1996).

However, the majority of these pro-drugs employ general DNA-damaging cytotoxic agents as the active therapeutic, limiting their use in combination with existing chemotherapies that

function via the same mechanism (Wilson and Hay 2011). An increasing number of reports have demonstrated an improved strategy of utilising the hypoxia-specific targeting of such pro-drugs to incorporate a bio-reductive "trigger" (Everett, Naylor et al. 1999). This enables delivery of a specific targeted therapeutic, such as an enzymatic inhibitor. The pro-drug is unable to bind to the protein target until release of the active compound via removal of the bio-reductive protecting group under hypoxic conditions.

For example, Granchi and colleagues have reported bio-reductively activated nitroaromatic pro-drugs targeting lysyl oxidase (LOX), which enable selective release of the active LOX inhibitor β-aminopropionitrile under hypoxic conditions (Granchi, Funaioli et al. 2009). More recently, Cazares-Korner and colleagues reported a proof-of-principle bio-reductive pro-drug as a hypoxia-specific Checkpoint kinase 1 (Chk1) and Aurora A inhibitor (Cazares-Korner, Pires et al. 2013). The group used a 4-nitrobenzyl protecting group, which was removed via nitroreductase-mediated reduction under hypoxic conditions, thereby enabling hypoxia-specific delivery of the active inhibitor (Cazares-Korner, Pires et al. 2013). The use of analogous methodology could permit hypoxia-specific delivery of PFKFB3 inhibitors to solid tumours.

It is suggested that a future project should build on the work presented in this thesis and seek to develop a PFKFB3-specific inhibitor alongside the incorporation of an appropriate bio-reductive protecting group. This would permit delivery of the active inhibitor to the hypoxic sub-fraction of the tumour (Figure 7.1). Initially, *in vitro* studies should be used to confirm hypoxia-selectivity of the bio-reductive pro-drug, before progressing to *in vivo* studies.

The effectiveness of the PFKFB3 pro-drug could be further improved by increasing the proportion of the tumour cells that are hypoxic at any one time. This could be achieved

through the use of anti-angiogenic therapies to inhibit new blood vessel formation, or vascular targeting agents that inhibit tumour blood flow (Cooney, Ortiz et al. 2005). For example, the agents bevacizumab and combrestatin A4 phosphate, respectively. There is also the possibility of harnessing the "bystander" effect (Denny 2000), where the active PFKFB3 inhibitor would be released in hypoxic cells, but would be designed to be sufficiently long-lived to enable diffusion to normoxic cells within the tumour mass (Figure 7.1).

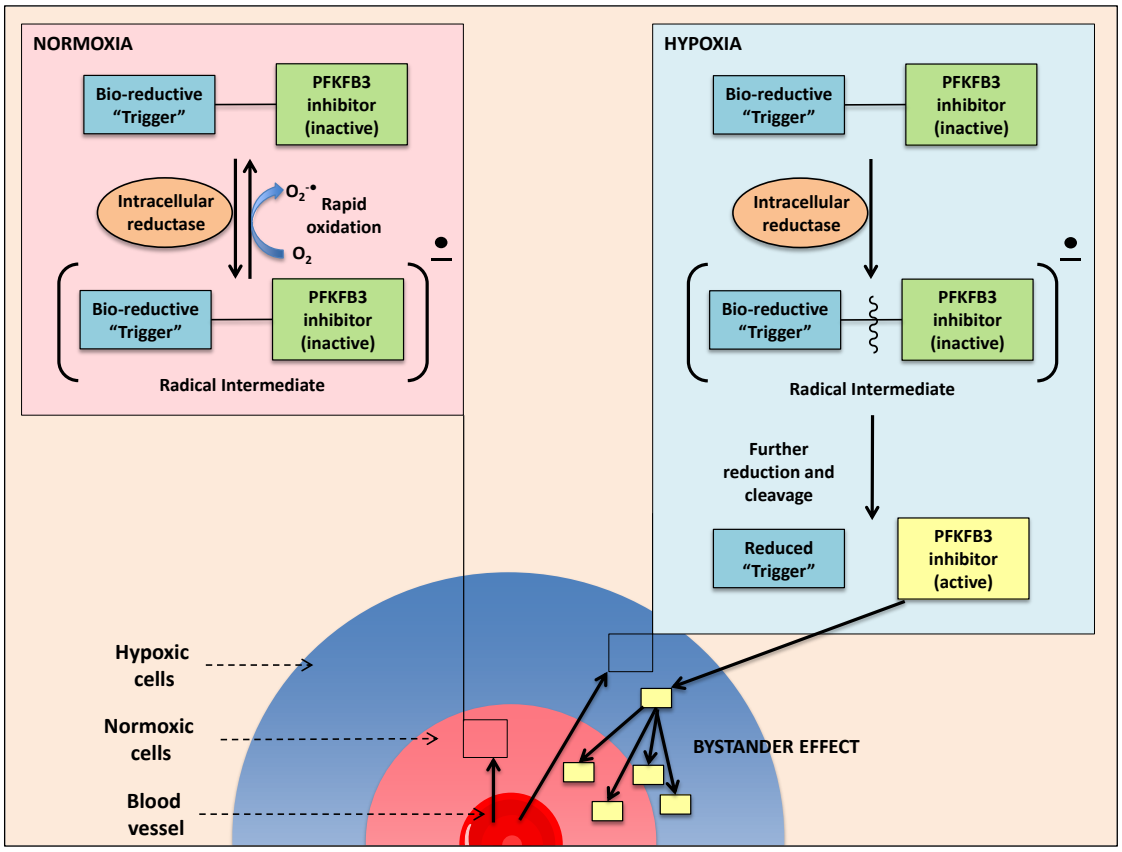

Figure 7.1: Mechanism of action of a proposed hypoxia-activated PFKFB3 inhibitor pro-drug. The bio-reductive "trigger" would be reduced by intracellular reductases to a transient radical intermediate. Under normoxic conditions, this radical would be rapidly oxidised back to the original pro-drug, with concomitant formation of superoxide. Under hypoxic conditions, the radical intermediate would undergo further reduction at the site of the bio-reductive "trigger", leading to cleavage of the "trigger", releasing the active PFKFB3 inhibitor. Appropriate physiochemical design of the inhibitor may facilitate diffusion to normoxic cells within the tumour (bystander effect).

The successful penetration of any pro-drug to the hypoxic sub-fraction of a solid tumour is extremely challenging, due to the large diffusion distances involved (Wilson and Hay 2011).

The design of such PFKFB3 inhibitor pro-drugs must therefore consider the physiochemical properties of a small molecule that are likely to enhance its stability and delivery *in vivo*.

7.5: Hypoxia-Targeted PFKFB3-Specific Inhibitors in a Clinical Setting

In addition to increasing the scope of PFKFB3 inhibitor activity, it will likely be necessary to apply a PFKFB3 inhibitor pro-drug in combination with existing radio- or chemotherapies that are able to simultaneously target the normoxic fraction of the tumour. Indeed, the use of combination therapy is particularly important to overcome the heterogeneic nature of tumours (Denison and Bae 2012). Looking at a longer term perspective, the most effective therapeutic strategy will likely be one built on a detailed understanding of the wider mechanistic action of the effects mediated by PFKFB3 inhibition, in order to utilise combination therapies that will act with complementary or even synergistic mechanisms. For example, knockdown of PFKFB3 appeared to increase oxidative stress in MCF-7 cells under normoxic conditions (Figure 5.3A, Chapter 5) and U87 cells under hypoxic conditions (Figure 5.3B, Chapter 5). This effect could be potentiated by concomitant treatment with a PPP inhibitor, to reduce NADPH production and therefore scavenging of ROS. Such a multi-targeted approach can improve efficacy and permit combination drugs to be used at lower concentrations, thereby reducing side effects (Zimmermann, Lehar et al. 2007).

7.6: Targeting Tumour Metabolism

The original brief of this thesis was to take steps towards the development of an inhibitor to target aerobic glycolysis. However, the work contained within it and undoubtedly the work that follows may well conclude that non-metabolic effects mediated by PFKFB3 and/or PFKFB4 are more important for explaining the reduction in cell proliferation in response to knockdown of these isoenzymes. Nevertheless, interest in the study of tumour metabolism

continues to increase as part of the search for druggable anti-cancer targets. Indeed, during the course of this thesis, Hanahan and Weinberg suggested that reprogramming of cellular energy metabolism should now be considered an emerging hallmark of cancer (Hanahan and Weinberg 2011). Whilst further study of PFKFB3 and PFKFB4 may reveal that the most important roles of these isoenzymes may be non-metabolic, this of course doesn't diminish the validity of leveraging the metabolic aberrations exhibited by cancer cells to identify an effective target for therapy.

The central role of PFK-1 and its potent activator F-2,6-BP, is well established and the work in this thesis does not question that relationship. It is suggested that the study of inhibitors of PFK-1 activity, either through direct PFK-1 inhibition, or through inhibition of another PFK-2/FBPase-2 isoenzyme (PFKFB1 or PFKFB2), should be a separate area of investigation, alongside the development of PFKFB3 inhibitors. The ubiquitous nature of PFK-1 expression will make this challenging, but potential targeting of PFK-1 tetramers enriched in PFK-L or PFK-P sub-units, which are known to be up-regulated in cancer and also under hypoxic conditions (Figures 3.1-3.3, Chapter 3), may afford these agents an additional level of selectivity.

7.7: The Future – Personalised Therapy and Collaborative Drug Discovery

The treatment of cancer is rapidly progressing from the one-size-fits all approach of the original chemotherapies towards targeted therapies that harness specific molecular or micro-environmental characteristics of individual tumours, treating each patient on an individual basis. The coming decades will likely see further advances in such personalised therapy, with effective stratification of patients by molecular predictors, such as the extent of tumour hypoxia (Moon, Brizel et al. 2007). This will enable identification of those patients most likely to respond to a given therapy. The development and progression of drugs from bench to

bedside continues to be a frustratingly prolonged and expensive process, with many drug candidates failing at late stage clinical trials (Hoelder, Clarke et al. 2012). However, the selection of patients for participation in clinical trials based on such molecular predictors of efficacy will likely speed up the drug approval process (Yap, Sandhu et al. 2010).

This project has been highly collaborative and multi-disciplinary in nature, linking aspects of synthetic chemistry, pharmacology and molecular biology. The future success and efficiency of drug discovery programmes, in both academia and industry, will depend on improved cross-talk between clinicians, regulators and scientists working in these disciplines. Such interdisciplinary collaboration is increasing all the time and this, together with ever closer ties between industry and academia, gives us every reason to be optimistic about the future success of cancer research programmes.

Appendix

A1: PFKFB3 and PFKFB4 antibody validation.

Supplier	Product Code	Host
Abcam	ab96699	Rabbit
Abgent	AP8145a	Rabbit
Abnova	H00005209-A01	Mouse

Table A1.1: PFKFB3 antibodies tested.

Supplier	Product Code	Host
Abcam	ab71622	Rabbit
Abgent	AP8154c	Rabbit
Epitomics	S1348	Rabbit
Santa Cruz	sc-103112	Goat

Table A1.2: PFKFB4 antibodies tested.

In our hands, the commercial PFKFB3 antibodies tested (Table A1.1) showed a lack of specificity and were unsuitable for use. However, a specific antibody targeting PFKFB3 splice variant 5 (UBI2K5) was kindly provided as a gift from Professor Salvador Moncada (University College, London), and showed high specificity. The PFKFB4 antibody from Epitomics (S1348) (Table A1.2) was found to be the most selective and was suitable for use.

A2: Selective siRNA-mediated silencing of *HIF-1α* and *HIF-2α* mRNA expression in U87, MCF-7 and PC3 cells.

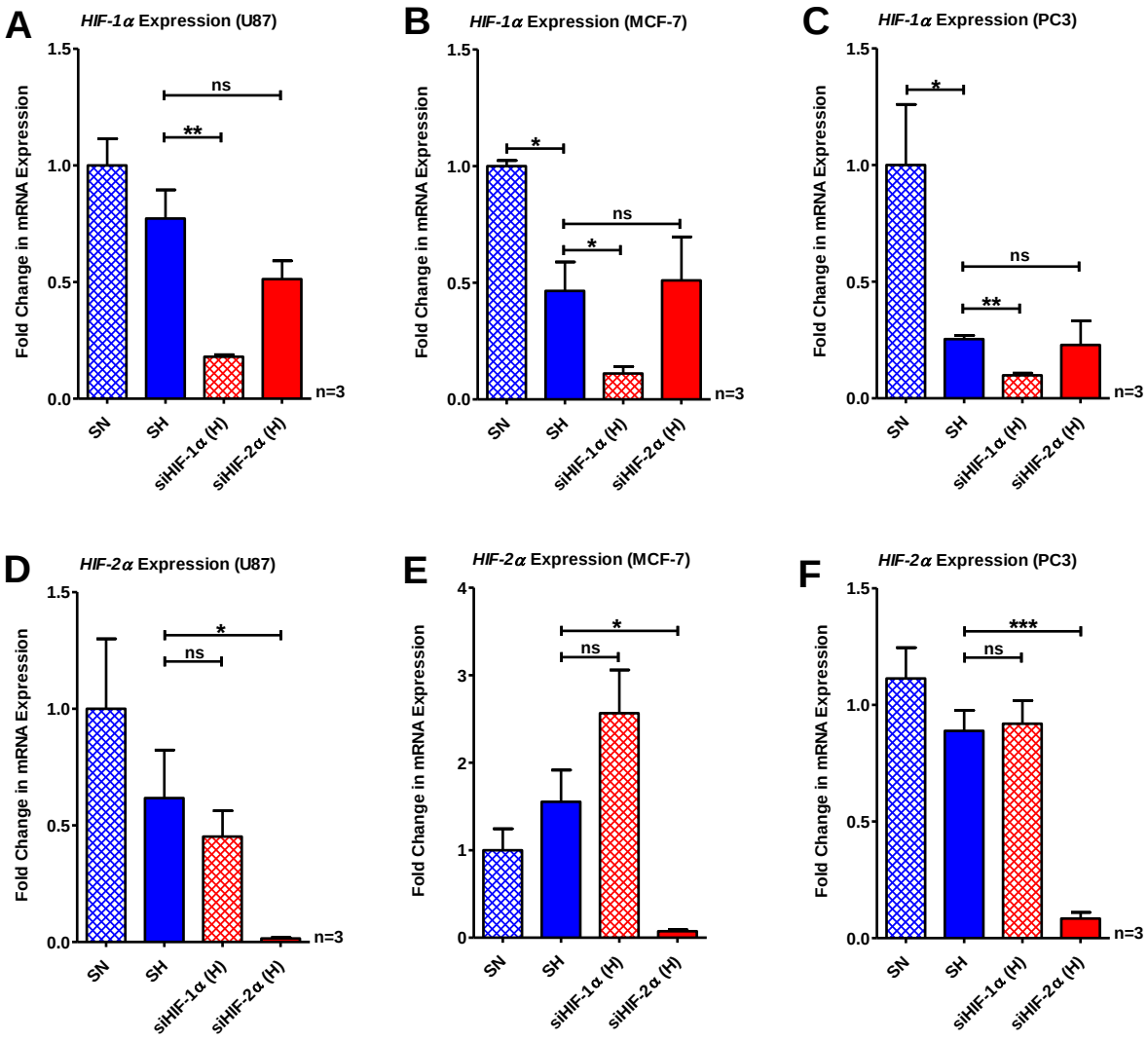

Figure A2.1: qRT-PCR validation of siRNA silencing of *HIF-1α* and *HIF-2α* mRNA in U87, MCF-7 and PC3 cells under normoxic and hypoxic conditions. Selective siRNA-mediated silencing of *HIF-1α* **(A)-(C)** and *HIF-2α* **(D)-(F)** mRNA expression was observed. Values normalised to scramble normoxia. 48 hours incubation in normoxia (N)/hypoxia (H). n=3; One-way ANOVA analysis performed with Bonferroni post-test, comparing isoenzyme mRNA expression of SH to each of the other three conditions; *($p<0.05$), **($p<0.01$), ***($p<0.001$), ****($p<0.0001$), ns (not significant). Scramble normoxia (SN), scramble hypoxia (SH).

A3: TIGAR protein expression was found to be independent of HIF-1α and HIF-2α expression.

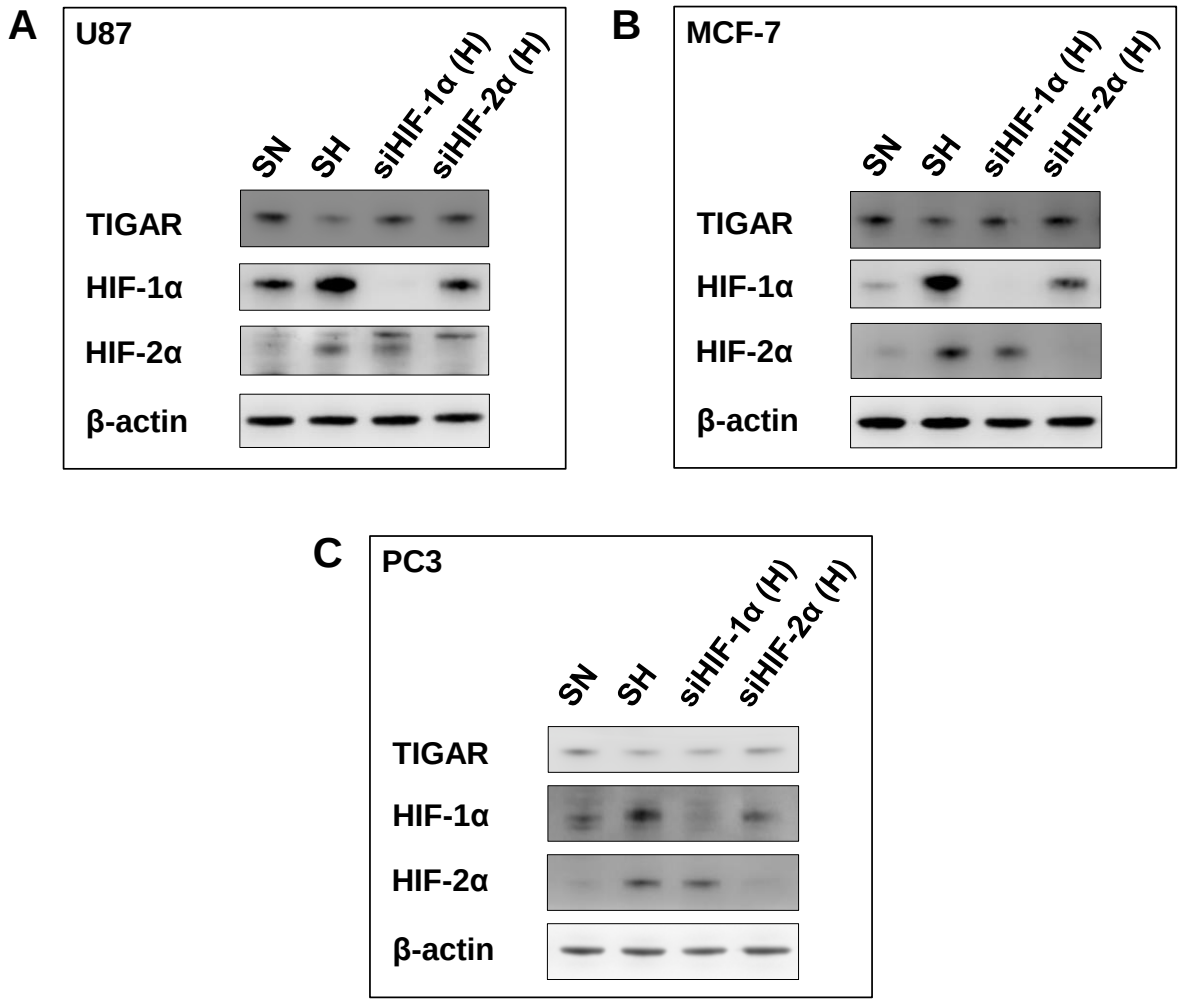

Figure A3.1: Western blot of TIGAR protein expression in response to knockdown of HIF-1α and HIF-2α expression in **(A)** U87, **(B)** MCF-7 and **(C)** PC3 cells. TIGAR protein expression was found to be independent of HIF-1α and HIF-2α expression in all three cell lines. Representative images of n≥2 independent replicates. The blots shown for **(A)** U87 and **(B)** MCF-7 are from the same gels used to probe for PFKFB3 expression in Figure 3.12, Chapter 3. SN (scramble normoxia), SH (scramble hypoxia). β-actin was used as a loading control.

A4: *PFKFB3* and *PFKFB4* mRNAs were induced under hypoxic conditions in a panel of cell lines, whereas *TIGAR* mRNA expression was unchanged.

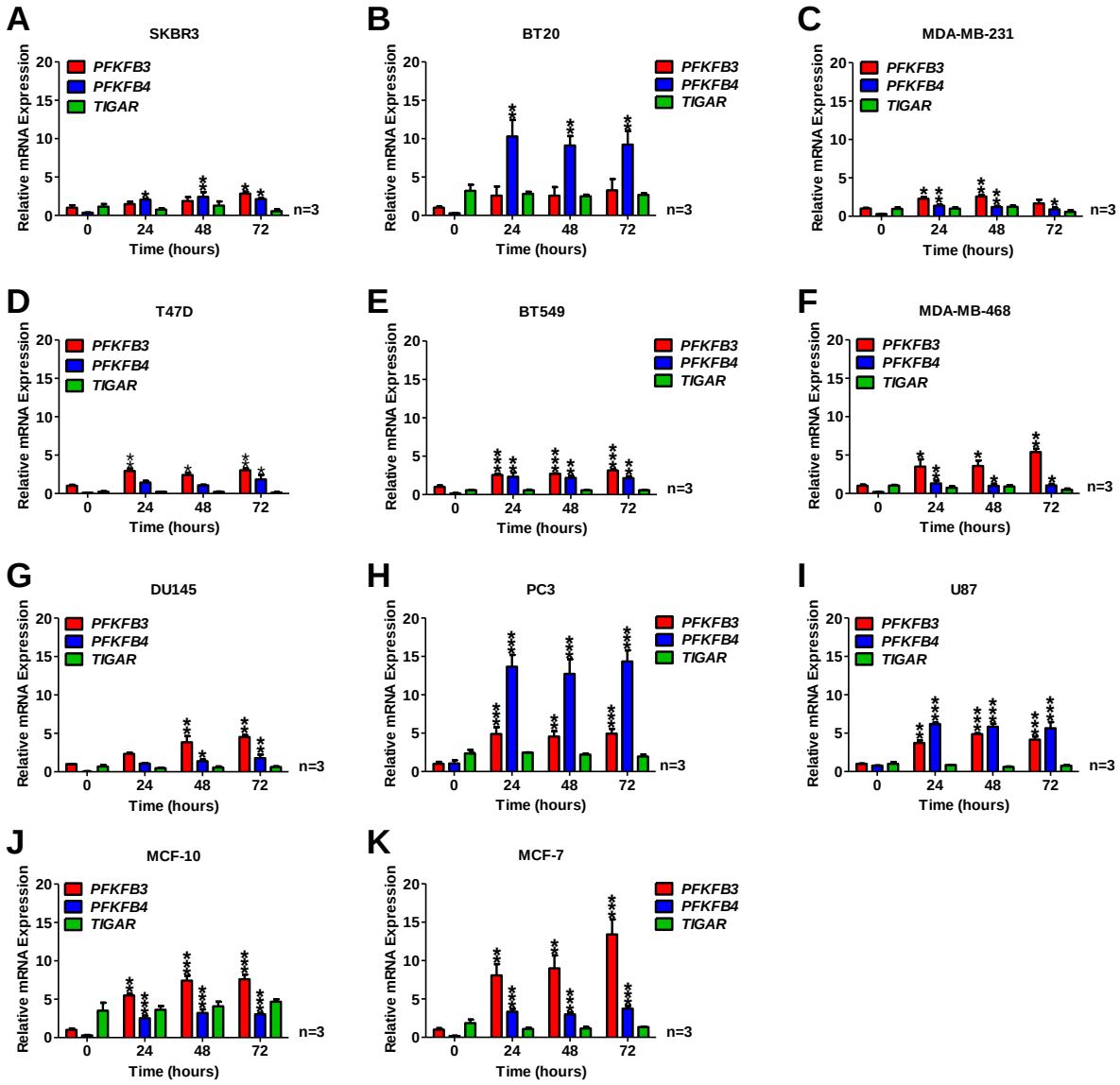

Figure A4.1: Hypoxic time course of relative *PFKFB3*, *PFKFB4* and *TIGAR* mRNA expression in a panel of cell lines. Relative expression differed markedly between cell lines. Graphs are in order **(A)-(K)** of increasing *PFKFB3* hypoxic fold change and normalised to relative *PFKFB3* expression at t = 0 h for each cell line. n=3; One-way ANOVA analysis performed with Dunnett's post-test, comparing isoenzyme mRNA expression at each time point to the corresponding expression level at t = 0 h; *(p<0.05), **(p<0.01), ***(p<0.001), ****(p<0.0001).

A5: Relative *PFKFB3, PFKFB4* and *TIGAR* mRNA expression varied markedly in a panel of cell lines under normoxic and hypoxic conditions.

Relative PFKFB3, PFKFB4 and TIGAR expression are displayed after 24 hours and 72 hours exposure to hypoxia in a panel of cell lines. The corresponding graphs for normoxia and 48 hours hypoxia are displayed in Figure 3.14, Chapter 3.

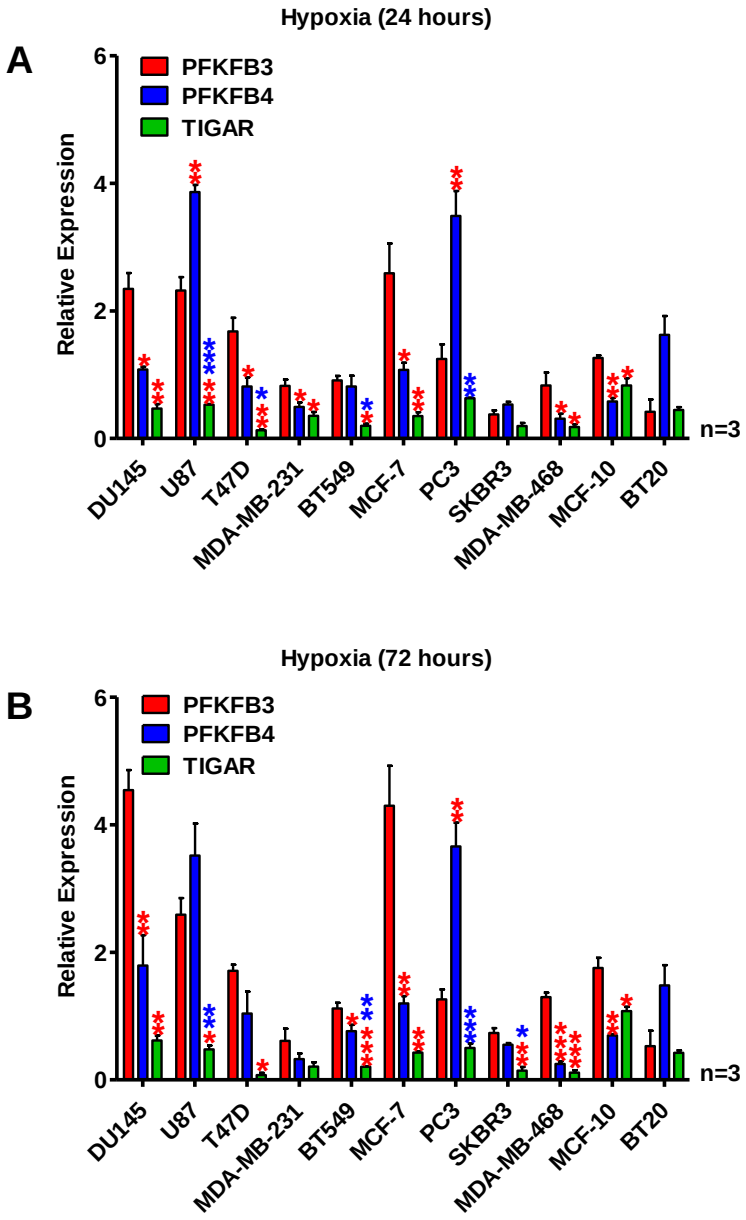

Figure A5.1: Relative *PFKFB3*, *PFKFB4* and *TIGAR* mRNA expression in a panel of cell lines after exposure to hypoxia for **(A)** 24 hours and **(B)** 72 hours. Relative expression varied markedly and was normalised to normoxic DU145 *PFKFB3* expression and cell lines ordered by decreasing normoxic *PFKFB3* expression. n=3; *(p<0.05), **(p<0.01), ***(p<0.001), ****(p<0.0001); One-way ANOVA analysis with Bonferroni correction performed within each cell line, with * denoting a significant difference from *PFKFB3* expression, and * denoting a significant difference from *PFKFB4* expression*.

A6: Selective suppression of *PFKFB3* and *PFKFB4* mRNA expression was observed with Dharmacon ON-TARGET*plus*™ PFKFB3 and PFKFB4 siRNA pools.

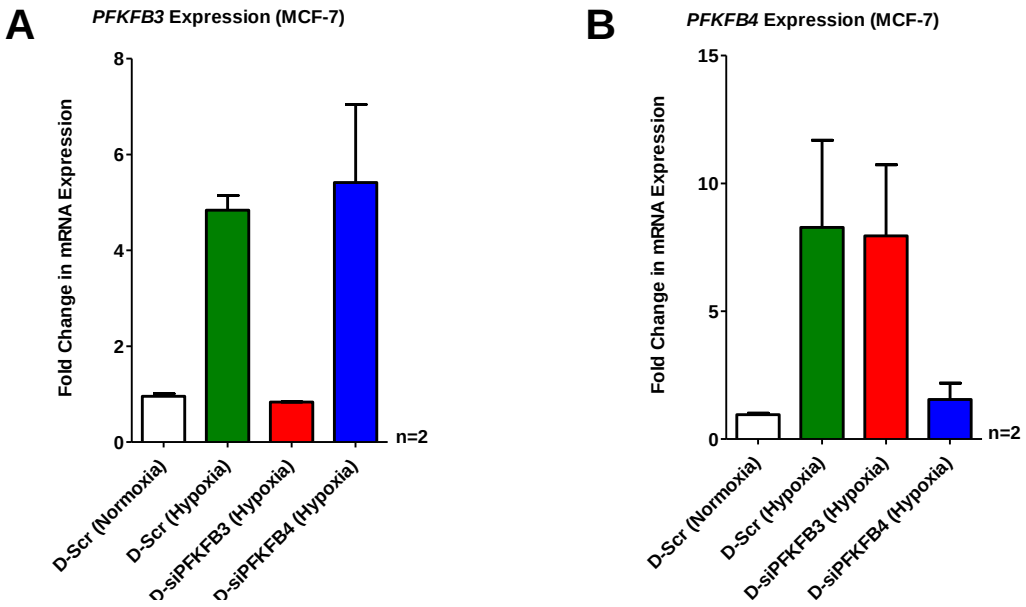

Figure A6.1: Validation of Dharmacon ON-TARGETplus™ PFKFB3 and PFKFB4 siRNA pools in MCF-7 cells. The siRNA pools were found to selectively suppress **(A)** *PFKFB3* and **(B)** *PFKFB4* mRNA expression. A Dharmacon ON-TARGET*plus*™ siRNA non-targeting pool was used as scramble (Scr) control. 48 hours normoxic/hypoxic incubation, normalised to Scr (normoxia); n=2. D (Dharmacon).

A7: Relative glucose consumption in response to single and double PFKFB3 and PFKFB4 siRNA knockdown.

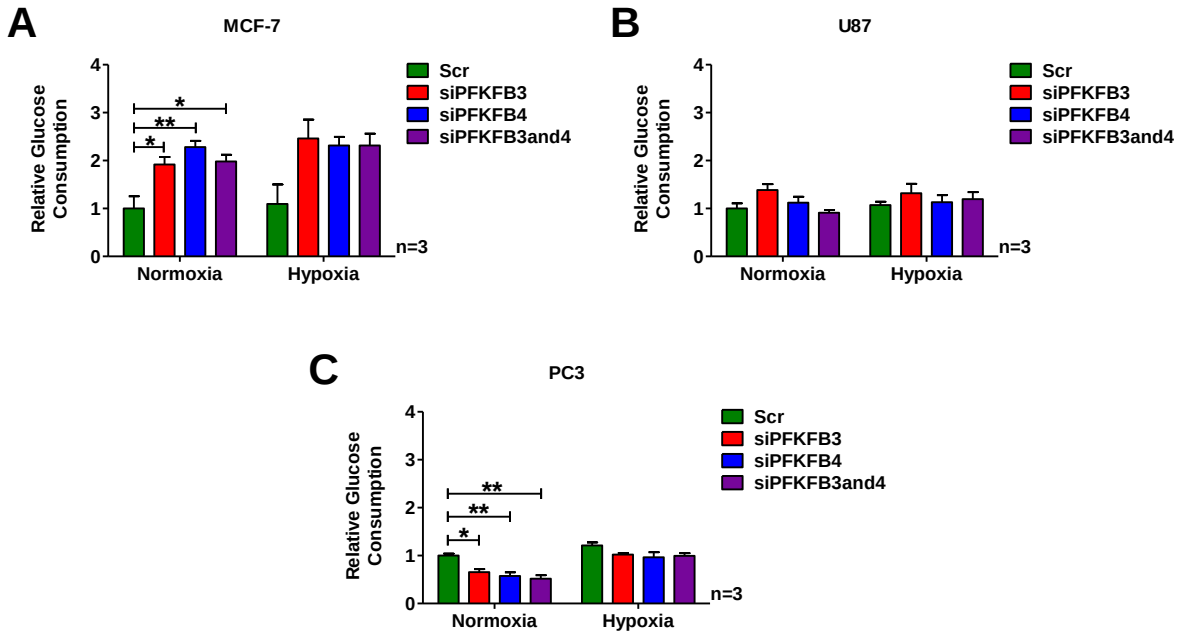

Figure A7.1: Assay of glucose consumption with single and double PFKFB3/PFKFB4 knockdown in **(A)** MCF-7, **(B)** U87 and **(C)** PC3 cells under normoxic and hypoxic conditions. Single and double PFKFB3 and PFKFB4 knockdown significantly increased glucose consumption in **(A)** MCF-7 cells under normoxic conditions, had no significant effect in **(B)** U87 cells, and significantly decreased glucose consumption in **(C)** PC3 cells. Values normalised to scramble (Scr)-control (normoxia). n=3; One-way ANOVA analysis performed with Bonferroni correction, comparing all normoxic data sets with one another, and all hypoxic data sets with one another; *($p<0.05$), **($p<0.01$), ***($p<0.001$), ****($p<0.0001$).

A8: Metabolic schemes illustrating conversion of 2-^{13}C glucose to 2-^{13}C lactate via glycolysis, but to 1,3-^{13}C lactate and 3-^{13}C lactate via the PPP.

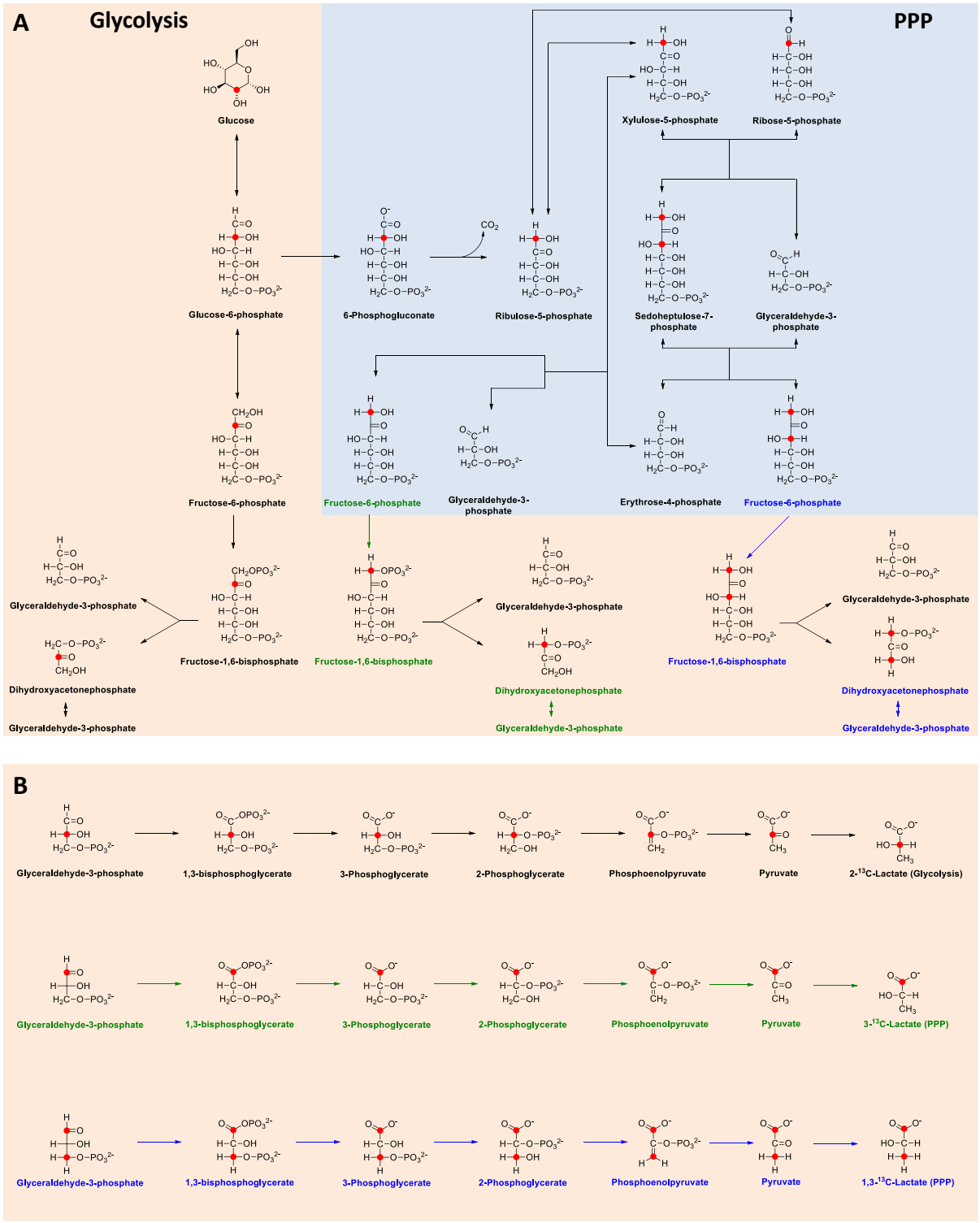

Figure A8.1: Metabolic schemes illustrating conversion of 2-^{13}C glucose to 2-^{13}C lactate via glycolysis, but to 1,3-^{13}C lactate and 3-^{13}C lactate via the PPP. **(A)** Metabolism of 2-^{13}C glucose via glycolysis produces 2-^{13}C-glyceraldehyde-3-phosphate, whereas metabolism of 2-^{13}C glucose via the PPP produces 1,3-^{13}C-glyceraldehyde-3-phosphate and 3-^{13}C-glyceraldehyde-3-phosphate. **(B)** The three ^{13}C labelled glyceraldehyde-3-phosphate species are all metabolised by the latter stages of glycolysis, to form pyruvate. Lactate dehydrogenase catalyses the final conversion of labelled pyruvate to lactate. The net effect is a conversion of 2-^{13}C glucose to 2-^{13}C lactate via glycolysis, or to 1,3-^{13}C lactate and 3-^{13}C lactate via the PPP.

A9: Successful separation and identification of the isomers glucose-6-phosphate and fructose-6-phosphate by LC-MS.

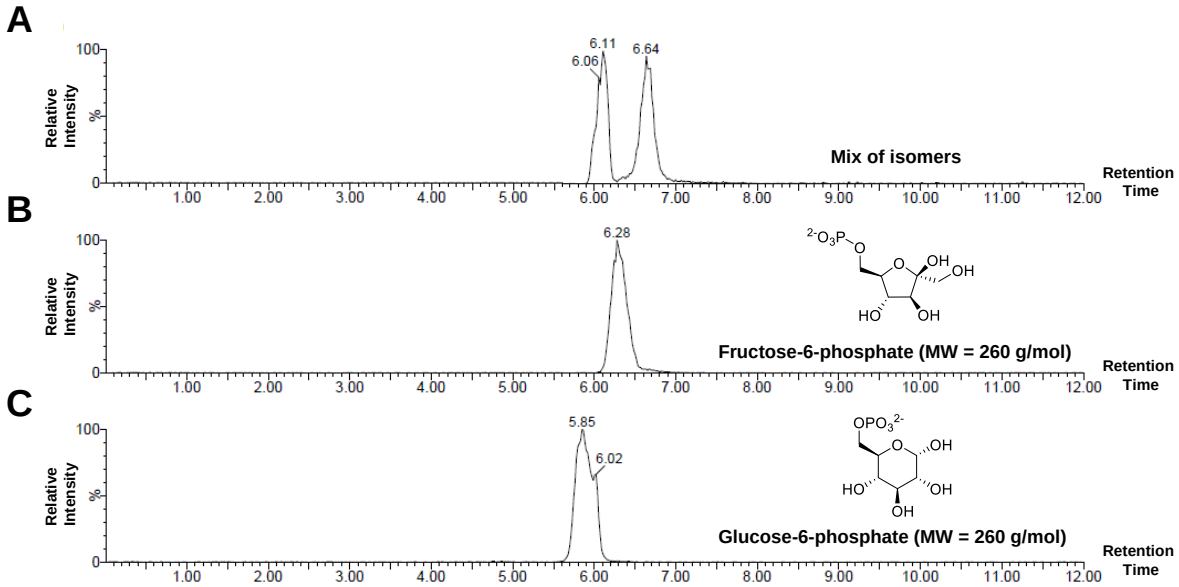

Figure A9.1: Separation of the isomers glucose-6-phosphate and fructose-6-phosphate by LC-MS. LC-MS conditions were optimised by collaborator Khalid Al-Qahtani (McCullagh group) to separate the metabolites of interest, including the isomers fructose-6-phosphate **(B)** and glucose-6-phosphate **(C)** (metabolite standards). The optimised conditions led to the two isomers having different retention times, as demonstrated in **(A)**, where both glucose-6-phosphate and fructose-6-phosphate standards were introduced simultaneously into the LC-MS system.

A10: Standard curves showed a linear relationship between metabolite concentration and relative area units in the LC-MS assay.

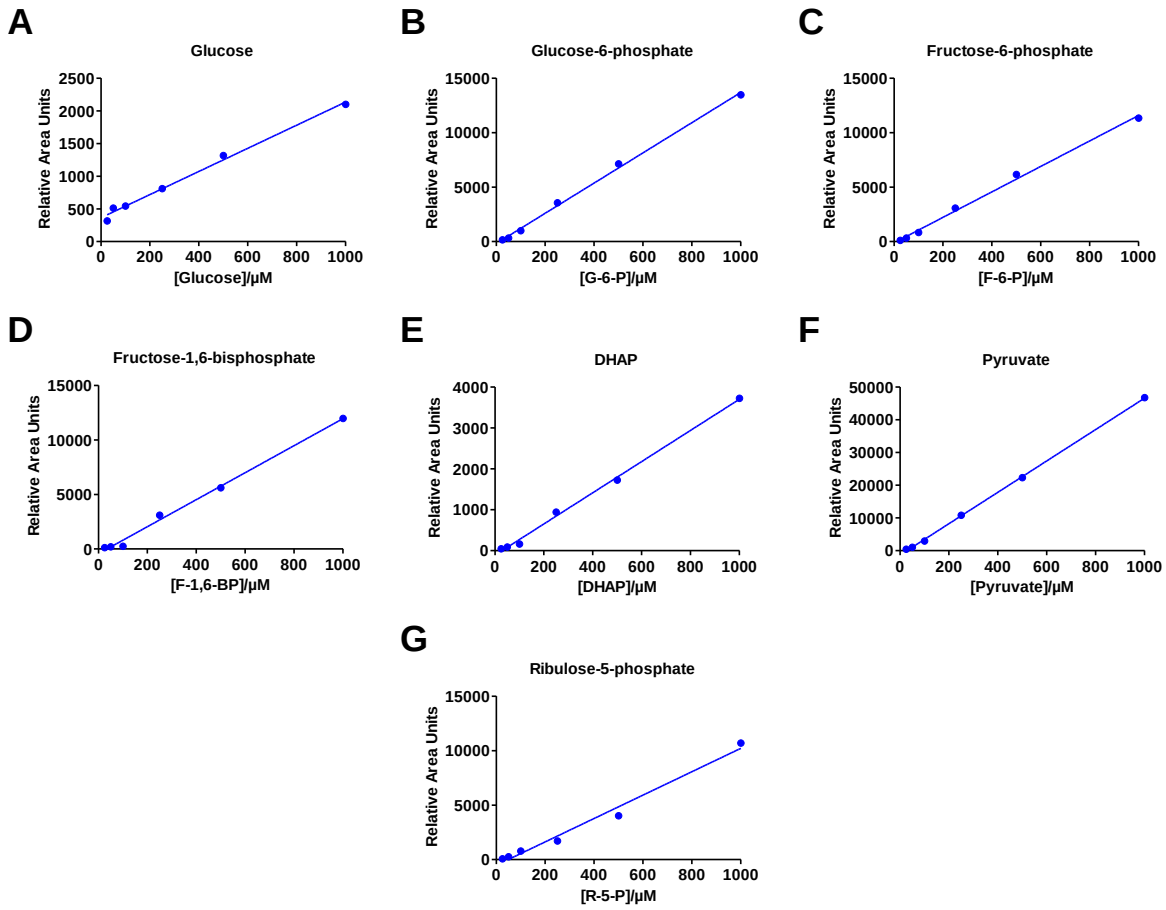

Figure A10.1: Metabolite standard curves relating metabolite concentration to relative peak area in the liquid chromatography – mass spectrometry experiments (LC-MS). Samples were prepared and analysed by collaborator Khalid Al-Qahtani (McCullagh group). Metabolites: **(A)** glucose, **(B)** glucose-6-phosphate (G-6-P), **(C)** fructose-6-phosphate (F-6-P), **(D)** fructose-1,6-bisphosphate (F-1,6-BP), **(E)** dihydroxyacetone phosphate (DHAP), **(F)** pyruvate, **(G)** ribulose-5-phosphate (R-5-P).

A11: Amino acid homology between human PFK-1 isoenzymes and PFK-1 from *Bacillus stearothermophilus*.

	Human PFK-P	Human PFK-L	Human PFK-M	PFK (*Bacillus stearothermophilus*)
Human PFK-P	100%	67%	70%	44%
Human PFK-L	67%	100%	68%	45%
Human PFK-M	70%	68%	100%	44%
PFK-1 (*Bacillus stearothermophilus*)	44%	45%	44%	100%

Table A11.1: Comparison of amino acid sequences of human PFK-1 isoenzymes and bacterial PFK-1.

A12: Suggested mechanism of chlorination (3-pyridine analogue).

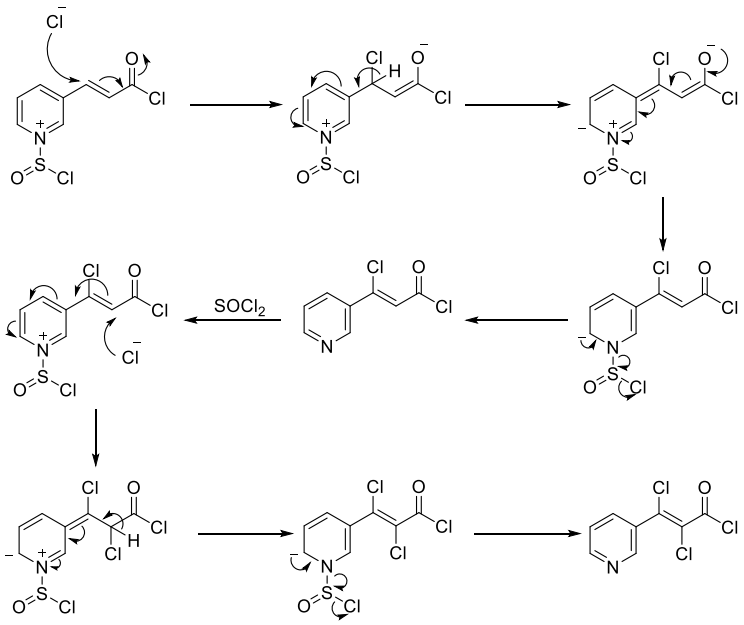

Scheme A12.1: Suggested chlorination mechanism for the 3-pyridine analogue.

A13: Suggested mechanism of chlorination (4-pyridine analogue).

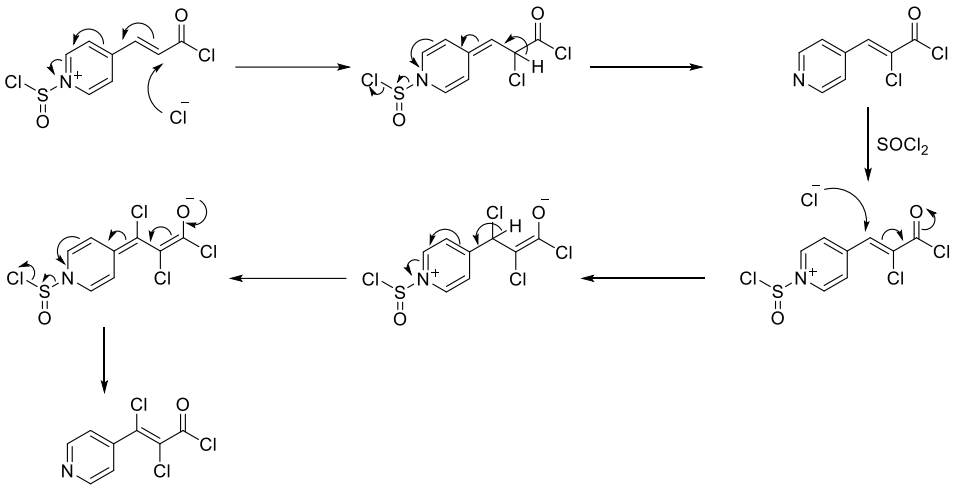

Scheme A13.1: Suggested chlorination mechanism for the 4-pyridine analogue.

A14: Determination of inhibitory activity of 3PO in the PFK-1 Kinase Glo® Plus assay.

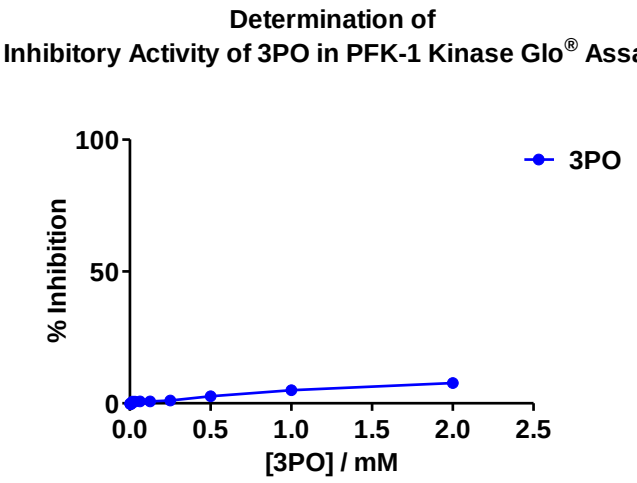

Figure A14.1: Determination of inhibitory activity of 3PO in the PFK-1 Kinase Glo® Plus assay. 3PO exhibited some inhibitory activity against the bacterial PFK-1 at high concentrations (> 1 mM).

References

Aartsma-Rus, A., H. Houlleberghs, et al. (2010). "Exonic sequences provide better targets for antisense oligonucleotides than splice site sequences in the modulation of Duchenne muscular dystrophy splicing." Oligonucleotides **20**(2): 69-77.

Akama, T., Y. Shida, et al. (1996). "Novel 5-aminoflavone derivatives as specific antitumor agents in breast cancer." Journal of Medicinal Chemistry **39**(18): 3461-3469.

Almeida, A., J. P. Bolanos, et al. (2010). "E3 ubiquitin ligase APC/C-Cdh1 accounts for the Warburg effect by linking glycolysis to cell proliferation." Proc Natl Acad Sci U S A **107**(2): 738-741.

Arany, Z., L. E. Huang, et al. (1996). "An essential role for p300/CBP in the cellular response to hypoxia." Proc Natl Acad Sci U S A **93**(23): 12969-12973.

Atsumi, T., J. Chesney, et al. (2002). "High expression of inducible 6-phosphofructo-2-kinase/fructose-2,6-bisphosphatase (iPFK-2; PFKFB3) in human cancers." Cancer Research **62**(20): 5881-5887.

Babu, K. S., X. C. Li, et al. (2006). "Synthesis, antifungal activity, and structure-activity relationships of coruscanone A analogues." Journal of Medicinal Chemistry **49**(26): 7877-7886.

Baell, J. B. and G. A. Holloway (2010). "New substructure filters for removal of pan assay interference compounds (PAINS) from screening libraries and for their exclusion in bioassays." J Med Chem **53**(7): 2719-2740.

Bailey, K. M., J. W. Wojtkowiak, et al. (2012). "Targeting the metabolic microenvironment of tumors." Adv Pharmacol **65**: 63-107.

Bamborough, P. (2012). "System-based drug discovery within the human kinome." Expert Opin Drug Discov **7**(11): 1053-1070.

Bando, H., T. Atsumi, et al. (2005). "Phosphorylation of the 6-phosphofructo-2-kinase/fructose 2,6-bisphosphatase/PFKFB3 family of glycolytic regulators in human cancer." Clin Cancer Res **11**(16): 5784-5792.

Bartnik, B. L., R. L. Sutton, et al. (2005). "Upregulation of pentose phosphate pathway and preservation of tricarboxylic acid cycle flux after experimental brain injury." J Neurotrauma **22**(10): 1052-1065.

Bartrons, R. and J. Caro (2007). "Hypoxia, glucose metabolism and the Warburg's effect." J Bioenerg Biomembr **39**(3): 223-229.

Basnet, A., P. Thapa, et al. (2007). "2,4,6-Trisubstituted pyridines: Synthesis, topoisomerase I and II inhibitory activity, cytotoxicity, and structure-activity relationship." Bioorganic & Medicinal Chemistry **15**(13): 4351-4359.

Batovska, D., S. Parushev, et al. (2007). "Study on the substituents' effects of a series of synthetic chalcones against the yeast Candida albicans." European Journal of Medicinal Chemistry **42**(1): 87-92.

Becker, S., L. Kortz, et al. (2012). "LC-MS-based metabolomics in the clinical laboratory." J Chromatogr B Analyt Technol Biomed Life Sci **883-884**: 68-75.

Beckner, M. E., G. T. Gobbel, et al. (2005). "Glycolytic glioma cells with active glycogen synthase are sensitive to PTEN and inhibitors of PI3K and gluconeogenesis." Lab Invest **85**(12): 1457-1470.

Bensaad, K., E. C. Cheung, et al. (2009). "Modulation of intracellular ROS levels by TIGAR controls autophagy." Embo Journal **28**(19): 3015-3026.

Bensaad, K., A. Tsuruta, et al. (2006). "TIGAR, a p53-inducible regulator of glycolysis and apoptosis." Cell **126**(1): 107-120.

Bertout, J. A., S. A. Patel, et al. (2008). "The impact of O2 availability on human cancer." Nat Rev Cancer **8**(12): 967-975.

Bertrand, L., D. R. Alessi, et al. (1999). "Heart 6-phosphofructo-2-kinase activation by insulin results from Ser-466 and Ser-483 phosphorylation and requires 3-phosphoinositide-dependent kinase-1, but not protein kinase B." J Biol Chem **274**(43): 30927-30933.

Bhatnagar, S., S. Sahi, et al. (2010). "Synthesis and docking studies on styryl chromones exhibiting cytotoxicity in human breast cancer cell line." Bioorg Med Chem Lett **20**(16): 4945-4950.

Bhujwalla, Z. M., D. Artemov, et al. (2002). "Combined vascular and extracellular pH imaging of solid tumors." NMR Biomed **15**(2): 114-119.

Blat, Y. (2010). "Non-competitive inhibition by active site binders." Chem Biol Drug Des **75**(6): 535-540.

Boada, J., T. Roig, et al. (2000). "Cells overexpressing fructose-2,6-bisphosphatase showed enhanced pentose phosphate pathway flux and resistance to oxidative stress." Febs Letters **480**(2-3): 261-264.

Bobarykina, A. Y., D. O. Minchenko, et al. (2006). "Hypoxic regulation of PFKFB-3 and PFKFB-4 gene expression in gastric and pancreatic cancer cell lines and expression of PFKFB genes in gastric cancers." Acta Biochim Pol **53**(4): 789-799.

Bosca, L., M. Mojena, et al. (1986). "Expression of the v-src or v-fps oncogene increases fructose-2,6-bisphosphate in chick-embryo fibroblasts - novel mechanism for the stimulation of glycolysis by retroviruses." Biochemical Journal **236**(2): 595-599.

Brizel, D. M., S. P. Scully, et al. (1996). "Tumor oxygenation predicts for the likelihood of distant metastases in human soft tissue sarcoma." Cancer Research **56**(5): 941-943.

Brown, J. M. (1993). "SR 4233 (tirapazamine): a new anticancer drug exploiting hypoxia in solid tumours." Br J Cancer **67**(6): 1163-1170.

Brown, J. M. and A. J. Giaccia (1998). "The unique physiology of solid tumors: Opportunities (and problems) for cancer therapy." Cancer Research **58**(7): 1408-1416.

Brown, J. M. and W. R. William (2004). "Exploiting tumour hypoxia in cancer treatment." Nature Reviews Cancer **4**(6): 437-447.

Brown, R. C. D., C. J. Bataille, et al. (2002). "Permanganate oxidation of 1,5,9-trienes: Stereoselective synthesis of tetrahydrofuran-containing fragments." Journal of Organic Chemistry **67**(23): 8079-8085.

Bullock, A. N., J. E. Debreczeni, et al. (2005). "Structural basis of inhibitor specificity of the human protooncogene proviral insertion site in moloney murine leukemia virus (PIM-1) kinase." J Med Chem **48**(24): 7604-7614.

Buzzai, M., R. G. Jones, et al. (2007). "Systemic treatment with the antidiabetic drug metformin selectively impairs p53-deficient tumor cell growth." Cancer Res **67**(14): 6745-6752.

Cabrera, R., A. L. B. Ambrosio, et al. (2008). "Crystallographic Structure of Phosphofructokinase-2 from Escherichia coli in Complex with Two ATP Molecules. Implications for Substrate Inhibition." Journal of Molecular Biology **383**(3): 588-602.

Cai, D., R. D. Larsen, et al. (2002). "Effective lithiation of 3-bromopyridine: synthesis of 3-pyridine boronic acid and variously 3-substituted pyridines." Tetrahedron Letters **43**(23): 4285-4287.

Calvo, M. N., R. Bartrons, et al. (2006). "PFKFB3 gene silencing decreases glycolysis, induces cell-cycle delay and inhibits anchorage-independent growth in HeLa cells." Febs Letters **580**(13): 3308-3314.

Carroll, V. A. and M. Ashcroft (2006). "Role of hypoxia-inducible factor (HIF)-1alpha versus HIF-2alpha in the regulation of HIF target genes in response to hypoxia, insulin-like growth factor-

I, or loss of von Hippel-Lindau function: implications for targeting the HIF pathway." Cancer Res **66**(12): 6264-6270.

Cassel, S., C. Debaig, et al. (2001). "Original synthesis of linear, branched and cyclic oligoglycerol standards." European Journal of Organic Chemistry **2001**(5): 875-896.

Cavalier, M. C., S. G. Kim, et al. (2012). "Molecular basis of the fructose-2,6-bisphosphatase reaction of PFKFB3: transition state and the C-terminal function." Proteins **80**(4): 1143-1153.

Cazares-Korner, C., I. M. Pires, et al. (2013). "CH-01 is a Hypoxia-Activated Prodrug That Sensitizes Cells to Hypoxia/Reoxygenation Through Inhibition of Chk1 and Aurora A." ACS Chem Biol. **8**(7): 1451-1459

Chabner, B. A. and T. G. Roberts, Jr. (2005). "Timeline: Chemotherapy and the war on cancer." Nat Rev Cancer **5**(1): 65-72.

Chandel, N. S., M. G. Vander Heiden, et al. (2000). "Redox regulation of p53 during hypoxia." Oncogene **19**(34): 3840-3848.

Chang, N., C. Sun, et al. (2013). "Genome editing with RNA-guided Cas9 nuclease in zebrafish embryos." Cell Res **23**(4): 465-472.

Chen, C. Y. and A. B. Shyu (1995). "AU-rich elements: characterization and importance in mRNA degradation." Trends Biochem Sci **20**(11): 465-470.

Chesney, J. (2006). "6-phosphofructo-2-kinase/fructose-2,6-bisphosphatase and tumor cell glycolysis." Current Opinion in Clinical Nutrition and Metabolic Care **9**(5): 535-539.

Chesney, J., R. Mitchell, et al. (1999). "An inducible gene product for 6-phosphofructo-2-kinase with an AU-rich instability element: Role in tumor cell glycolysis and the Warburg effect." Proceedings of the National Academy of Sciences of the United States of America **96**(6): 3047-3052.

Cheung, E. C., R. L. Ludwig, et al. (2012). "Mitochondrial localization of TIGAR under hypoxia stimulates HK2 and lowers ROS and cell death." Proc Natl Acad Sci U S A **109**(50): 20491-20496.

Chikri, M. and G. G. Rousseau (1995). "Rat gene coding for heart 6-phosphofructo-2-kinase/fructose-2,6-bisphosphatase: characterization of an unusual promoter region and identification of four mRNAs." Biochemistry **34**(27): 8876-8884.

Chilov, D., G. Camenisch, et al. (1999). "Induction and nuclear translocation of hypoxia-inducible factor-1 (HIF-1): heterodimerization with ARNT is not necessary for nuclear accumulation of HIF-1alpha." J Cell Sci **112** (Pt 8): 1203-1212.

Circu, M. L. and T. Y. Aw (2010). "Reactive oxygen species, cellular redox systems, and apoptosis." Free Radic Biol Med **48**(6): 749-762.

Clem, B., S. Telang, et al. (2008). "Small-molecule inhibition of 6-phosphofructo-2-kinase activity suppresses glycolytic flux and tumor growth." Molecular Cancer Therapeutics **7**(1): 110-120.

Clem, B. F., J. O'Neal, et al. (2013). "Targeting 6-Phosphofructo-2-Kinase (PFKFB3) as a Therapeutic Strategy against Cancer." Mol Cancer Ther. **12**(8): 1461-1470

Cockman, M. E., N. Masson, et al. (2000). "Hypoxia inducible factor-alpha binding and ubiquitylation by the von Hippel-Lindau tumor suppressor protein." Journal of Biological Chemistry **275**(33): 25733-25741.

Colombo, S. L., M. Palacios-Callender, et al. (2010). "Anaphase-promoting complex/cyclosome-Cdh1 coordinates glycolysis and glutaminolysis with transition to S phase in human T lymphocytes." Proc Natl Acad Sci U S A **107**(44): 18868-18873.

Cooney, M. M., J. Ortiz, et al. (2005). "Novel vascular targeting/disrupting agents: combretastatin A4 phosphate and related compounds." Curr Oncol Rep **7**(2): 90-95.

Cowan-Jacob, S. W., V. Guez, et al. (2004). "Imatinib (STI571) resistance in chronic myelogenous leukemia: molecular basis of the underlying mechanisms and potential strategies for treatment." Mini Rev Med Chem **4**(3): 285-299.

CrombezRobert, C., M. Benazza, et al. (1997). "Efficient synthesis of alpha,omega-dibromodideoxyalditols as precursors for alpha,omega-dithioalkylalditols." Carbohydrate Research **303**(3): 359-365.

Cunningham, J. T., J. T. Rodgers, et al. (2007). "mTOR controls mitochondrial oxidative function through a YY1-PGC-1alpha transcriptional complex." Nature **450**(7170): 736-740.

Currie, C. J., C. D. Poole, et al. (2012). "Mortality after incident cancer in people with and without type 2 diabetes: impact of metformin on survival." Diabetes Care **35**(2): 299-304.

Cuzick, J., I. Sestak, et al. (2013). "Selective oestrogen receptor modulators in prevention of breast cancer: an updated meta-analysis of individual participant data." Lancet **381**(9880): 1827-1834.

da-Silva, W. S., A. Gomez-Puyou, et al. (2004). "Mitochondrial bound hexokinase activity as a preventive antioxidant defense: steady-state ADP formation as a regulatory mechanism of membrane potential and reactive oxygen species generation in mitochondria." J Biol Chem **279**(38): 39846-39855.

Dang, C. V. (2012). "Cancer cell metabolism: there is no ROS for the weary." Cancer Discov **2**(4): 304-307.

Darville, M. I., I. V. Antoine, et al. (1992). "Characterization of an enhancer upstream from the muscle-type promoter of a gene encoding 6-phosphofructo-2-kinase/fructose-2,6-bisphosphatase." Nucleic Acids Res **20**(14): 3575-3583.

Darville, M. I., K. M. Crepin, et al. (1989). "5' flanking sequence and structure of a gene encoding rat 6-phosphofructo-2-kinase/fructose-2,6-bisphosphatase." Proc Natl Acad Sci U S A **86**(17): 6543-6547.

de Graaf, R. A., D. L. Rothman, et al. (2011). "State of the art direct 13C and indirect 1H-[13C] NMR spectroscopy in vivo. A practical guide." NMR Biomed **24**(8): 958-972.

DeBerardinis, R. J., A. Mancuso, et al. (2007). "Beyond aerobic glycolysis: transformed cells can engage in glutamine metabolism that exceeds the requirement for protein and nucleotide synthesis." Proc Natl Acad Sci U S A **104**(49): 19345-19350.

Delgado, T. C., M. M. Castro, et al. (2004). "Quantitation of erythrocyte pentose pathway flux with [2-13C]glucose and 1H NMR analysis of the lactate methyl signal." Magn Reson Med **51**(6): 1283-1286.

Denison, T. A. and Y. H. Bae (2012). "Tumor heterogeneity and its implication for drug delivery." J Control Release **164**(2): 187-191.

Denny, W. A. (2000). "The role of hypoxia-activated prodrugs in cancer therapy." Lancet Oncol **1**(1): 25-29.

Deprez, J., D. Vertommen, et al. (1997). "Phosphorylation and activation of heart 6-phosphofructo-2-kinase by protein kinase B and other protein kinases of the insulin signaling cascades." J Biol Chem **272**(28): 17269-17275.

Dewhirst, M. W. (1998). "Concepts of oxygen transport at the microcirculatory level." Seminars in Radiation Oncology **8**(3): 143-150.

Donohoe, T. J. and S. Butterworth (2003). "A general oxidative cyclization of 1,5-dienes using catalytic osmium tetroxide." Angewandte Chemie-International Edition **42**(8): 948-951.

Dowling, R. J., P. J. Goodwin, et al. (2011). "Understanding the benefit of metformin use in cancer treatment." BMC Med **9**: 33.

Downey, C. W. and M. W. Johnson (2007). "A tandem enol silane formation-Mukaiyama aldol reaction mediated by TMSOTf." Tetrahedron Letters **48**(20): 3559-3562.

Downs, L. E., D. M. Wolfe, et al. (2005). "Organic base-mediated condensation of pyridinecarboxaldehydes to azachalcones." Advanced Synthesis & Catalysis **347**(2-3): 235-238.

Downward, J. (2003). "Targeting RAS signalling pathways in cancer therapy." Nat Rev Cancer **3**(1): 11-22.

Druker, B. J., C. L. Sawyers, et al. (2001). "Activity of a specific inhibitor of the BCR-ABL tyrosine kinase in the blast crisis of chronic myeloid leukemia and acute lymphoblastic leukemia with the Philadelphia chromosome." N Engl J Med **344**(14): 1038-1042.

Druker, B. J., S. Tamura, et al. (1996). "Effects of a selective inhibitor of the Abl tyrosine kinase on the growth of Bcr-Abl positive cells." Nat Med **2**(5): 561-566.

Dummer, R. and K. T. Flaherty (2012). "Resistance patterns with tyrosine kinase inhibitors in melanoma: new insights." Curr Opin Oncol **24**(2): 150-154.

Dupriez, V. J., M. I. Darville, et al. (1993). "Characterization of a hepatoma mRNA transcribed from a third promoter of a 6-phosphofructo-2-kinase/fructose-2,6-bisphosphatase-encoding gene and controlled by ets oncogene-related products." Proc Natl Acad Sci U S A **90**(17): 8224-8228.

Dusick, J. R., T. C. Glenn, et al. (2007). "Increased pentose phosphate pathway flux after clinical traumatic brain injury: a [1,2-13C2]glucose labeling study in humans." J Cereb Blood Flow Metab **27**(9): 1593-1602.

Edgar, K. A., J. J. Wallin, et al. (2010). "Isoform-specific phosphoinositide 3-kinase inhibitors exert distinct effects in solid tumors." Cancer Res **70**(3): 1164-1172.

Edwards, A. M. and J. B. Howell (2000). "The chromones: history, chemistry and clinical development. A tribute to the work of Dr R. E. C. Altounyan." Clin Exp Allergy **30**(6): 756-774.

el-Maghrabi, M. R., T. H. Claus, et al. (1982). "Regulation of 6-phosphofructo-2-kinase activity by cyclic AMP-dependent phosphorylation." Proc Natl Acad Sci U S A **79**(2): 315-319.

Elbashir, S. M., J. Harborth, et al. (2001). "Duplexes of 21-nucleotide RNAs mediate RNA interference in cultured mammalian cells." Nature **411**(6836): 494-498.

Elbashir, S. M., W. Lendeckel, et al. (2001). "RNA interference is mediated by 21- and 22-nucleotide RNAs." Genes Dev **15**(2): 188-200.

Elstrom, R. L., D. E. Bauer, et al. (2004). "Akt stimulates aerobic glycolysis in cancer cells." Cancer Res **64**(11): 3892-3899.

Ema, M., S. Taya, et al. (1997). "A novel bHLH-PAS factor with close sequence similarity to hypoxia-inducible factor 1alpha regulates the VEGF expression and is potentially involved in lung and vascular development." Proc Natl Acad Sci U S A **94**(9): 4273-4278.

Eperon, I. (2012). "Antisense therapeutics: New ways to nudge splicing." Nat Chem Biol **8**(6): 507-508.

Everett, S. A., M. A. Naylor, et al. (1999). "Bioreductively-activated prodrugs for targeting hypoxic tissues: elimination of aspirin from 2-nitroimidazole derivatives." Bioorg Med Chem Lett **9**(9): 1267-1272.

Fabbro, D., S. W. Cowan-Jacob, et al. (2012). "Targeting cancer with small-molecular-weight kinase inhibitors." Methods Mol Biol **795**: 1-34.

Fan, F. and K. V. Wood (2007). "Bioluminescent assays for high-throughput screening." Assay Drug Dev Technol **5**(1): 127-136.

Farber, S., E. C. Cutler, et al. (1947). "The Action of Pteroylglutamic Conjugates on Man." Science **106**(2764): 619-621.

Farber, S. and L. K. Diamond (1948). "Temporary remissions in acute leukemia in children produced by folic acid antagonist, 4-aminopteroyl-glutamic acid." N Engl J Med **238**(23): 787-793.

Farese, R. V., Jr. and T. C. Walther (2009). "Lipid droplets finally get a little R-E-S-P-E-C-T." Cell **139**(5): 855-860.

Fedorov, O., B. Marsden, et al. (2007). "A systematic interaction map of validated kinase inhibitors with Ser/Thr kinases." Proc Natl Acad Sci U S A **104**(51): 20523-20528.

Ferreras, C., E. D. Hernandez, et al. (2009). "Subunit Interactions and Composition of the Fructose 6-Phosphate Catalytic Site and the Fructose 2,6-Bisphosphate Allosteric Site of Mammalian Phosphofructokinase." Journal of Biological Chemistry **284**(14): 9124-9131.

Fischer, K., P. Hoffmann, et al. (2007). "Inhibitory effect of tumor cell-derived lactic acid on human T cells." Blood **109**(9): 3812-3819.

Fitzpatrick, S. M., H. P. Hetherington, et al. (1990). "The flux from glucose to glutamate in the rat brain in vivo as determined by 1H-observed, 13C-edited NMR spectroscopy." J Cereb Blood Flow Metab **10**(2): 170-179.

Fleischer, M., R. Kessler, et al. (2011). "LOH on 10p14-p15 targets the PFKFB3 gene locus in human glioblastomas." Genes Chromosomes Cancer **50**(12): 1010-1020.

Frame, F. M. and N. J. Maitland (2011). "Cancer stem cells, models of study and implications of therapy resistance mechanisms." Adv Exp Med Biol **720**: 105-118.

Frank, N. Y., T. Schatton, et al. (2010). "The therapeutic promise of the cancer stem cell concept." J Clin Invest **120**(1): 41-50.

Furukawa, N., T. Shibutani, et al. (1987). "Preparation of pyridyl grignard-reagents and cross coupling reactions with sulfoxides bearing azaheterocycles." Tetrahedron Letters **28**(47): 5845-5848.

Garcia-Cao, I., M. S. Song, et al. (2012). "Systemic elevation of PTEN induces a tumor-suppressive metabolic state." Cell **149**(1): 49-62.

Garrett, C. R., H. M. Hassabo, et al. (2012). "Survival advantage observed with the use of metformin in patients with type II diabetes and colorectal cancer." Br J Cancer **106**(8): 1374-1378.

Gatenby, R. A. and R. J. Gillies (2004). "Why do cancers have high aerobic glycolysis?" Nature Reviews Cancer **4**(11): 891-899.

Gerlinger, M., A. J. Rowan, et al. (2012). "Intratumor heterogeneity and branched evolution revealed by multiregion sequencing." N Engl J Med **366**(10): 883-892.

Gillies, R. J. and R. A. Gatenby (2007). "Adaptive landscapes and emergent phenotypes: why do cancers have high glycolysis?" J Bioenerg Biomembr **39**(3): 251-257.

Gillies, R. J., I. Robey, et al. (2008). "Causes and consequences of increased glucose metabolism of cancers." J Nucl Med **49 Suppl 2**: 24S-42S.

Gillies, R. J., D. Verduzco, et al. (2012). "Evolutionary dynamics of carcinogenesis and why targeted therapy does not work." Nat Rev Cancer **12**(7): 487-493.

Gilman, A. and F. S. Philips (1946). "The Biological Actions and Therapeutic Applications of the B-Chloroethyl Amines and Sulfides." Science **103**(2675): 409-436.

Gimm, T., M. Wiese, et al. (2010). "Hypoxia-inducible protein 2 is a novel lipid droplet protein and a specific target gene of hypoxia-inducible factor-1." FASEB J **24**(11): 4443-4458.

Giroux, S. (2013). "Overcoming acquired resistance to kinase inhibition: the cases of EGFR, ALK and BRAF." Bioorg Med Chem Lett **23**(2): 394-401.

Glickman, J. F., J. McGee, et al. (2004). "Assay Development for Protein Kinase Enzymes."

Glickman, J. F., A. Schmid, et al. (2008). "Scintillation proximity assays in high-throughput screening." Assay Drug Dev Technol **6**(3): 433-455.

Goidts, V., J. Bageritz, et al. (2012). "RNAi screening in glioma stem-like cells identifies PFKFB4 as a key molecule important for cancer cell survival." Oncogene **31**(27): 3235-3243.

Gomez, M., A. Manzano, et al. (2012). "Sertoli-secreted FGF-2 induces PFKFB4 isozyme expression in mouse spermatogenic cells by activation of the MEK/ERK/CREB pathway." Am J Physiol Endocrinol Metab **303**(6): E695-707.

Gomez, M., A. Navarro-Sabate, et al. (2009). "Switches in 6-phosphofructo-2-kinase isoenzyme expression during rat sperm maturation." Biochem Biophys Res Commun **387**(2): 330-335.

Goodman, L. S., M. M. Wintrobe, et al. (1946). "Nitrogen mustard therapy; use of methyl-bis (beta-chloroethyl) amine hydrochloride and tris (beta-chloroethyl) amine hydrochloride for Hodgkin's disease, lymphosarcoma, leukemia and certain allied and miscellaneous disorders." J Am Med Assoc **132**: 126-132.

Gopalakrishna, R., Z. H. Chen, et al. (1992). "Rapid filtration assays for protein kinase C activity and phorbol ester binding using multiwell plates with fitted filtration discs." Anal Biochem **206**(1): 24-35.

Gordon, G. B., M. A. Barcza, et al. (1977). "Lipid accumulation of hypoxic tissue culture cells." Am J Pathol **88**(3): 663-678.

Goren, N., A. Manzano, et al. (2000). "6-Phosphofructo-2-kinase/fructose-2,6-bisphosphatase expression in rat brain during development." Brain Res Mol Brain Res **75**(1): 138-142.

Graeber, T. G., C. Osmanian, et al. (1996). "Hypoxia-mediated selection of cells with diminished apoptotic potential in solid tumours." Nature **379**(6560): 88-91.

Granchi, C., T. Funaioli, et al. (2009). "Bioreductively activated lysyl oxidase inhibitors against hypoxic tumours." Chemmedchem **4**(10): 1590-1594.

Gray-Schopfer, V., C. Wellbrock, et al. (2007). "Melanoma biology and new targeted therapy." Nature **445**(7130): 851-857.

Gray, L. H., A. D. Conger, et al. (1953). "The concentration of oxygen dissolved in tissues at the time of irradiation as a factor in radiotherapy." British Journal of Radiology **26**(312): 638-648.

Green, D. R. and J. E. Chipuk (2006). "p53 and metabolism: Inside the TIGAR." Cell **126**(1): 30-32.

Griffin, J. L. and R. A. Kauppinen (2007). "Tumour metabolomics in animal models of human cancer." J Proteome Res **6**(2): 498-505.

Griffiths, J. R., P. M. McSheehy, et al. (2002). "Metabolic changes detected by in vivo magnetic resonance studies of HEPA-1 wild-type tumors and tumors deficient in hypoxia-inducible factor-1beta (HIF-1beta): evidence of an anabolic role for the HIF-1 pathway." Cancer Res **62**(3): 688-695.

Gu, Y. Z., S. M. Moran, et al. (1998). "Molecular characterization and chromosomal localization of a third alpha-class hypoxia inducible factor subunit, HIF3alpha." Gene Expr **7**(3): 205-213.

Gung, B. W., C. Gibeau, et al. (2005). "Total synthesis of two novel brominated acetylenic diols (+)-diplyne C and E: stereoselective construction of the (E)-1-bromo-1-alkene." Tetrahedron-Asymmetry **16**(18): 3107-3114.

Guppy, M., P. Leedman, et al. (2002). "Contribution by different fuels and metabolic pathways to the total ATP turnover of proliferating MCF-7 breast cancer cells." Biochem J **364**(Pt 1): 309-315.

Guzy, R. D. and P. T. Schumacker (2006). "Oxygen sensing by mitochondria at complex III: the paradox of increased reactive oxygen species during hypoxia." Exp Physiol **91**(5): 807-819.

Hambley, T. W. (2008). "Physiological targeting to improve anticancer drug selectivity." Australian Journal of Chemistry **61**(9): 647-653.

Hamilton, J. A., M. J. Callaghan, et al. (1997). "Identification of PRG1, a novel progestin-responsive gene with sequence homology to 6-phosphofructo-2-kinase/fructose-2,6-bisphosphatase." Mol Endocrinol **11**(4): 490-502.

Hanahan, D. and R. A. Weinberg (2000). "The hallmarks of cancer." Cell **100**(1): 57-70.

Hanahan, D. and R. A. Weinberg (2011). "Hallmarks of cancer: the next generation." Cell **144**(5): 646-674.

Hannemann, A., B. Jandrig, et al. (2005). "Characterization of the human P-type 6-phosphofructo-1-kinase gene promoter in neural cell lines." Gene **345**(2): 237-247.

Hara, S., J. Hamada, et al. (2001). "Expression and characterization of hypoxia-inducible factor (HIF)-3alpha in human kidney: suppression of HIF-mediated gene expression by HIF-3alpha." Biochem Biophys Res Commun **287**(4): 808-813.

Harris, A. L. (2002). "Hypoxia - A key regulatory factor in tumour growth." Nature Reviews Cancer **2**(1): 38-47.

Hasemann, C. A., E. S. Istvan, et al. (1996). "The crystal structure of the bifunctional enzyme 6-phosphofructo-2-kinase/fructose-2,6-bisphosphatase reveals distinct domain homologies." Structure **4**(9): 1017-1029.

Heine-Suner, D., M. A. Diaz-Guillen, et al. (1998). "Sequence and structure of the human 6-phosphofructo-2-kinase/fructose-2,6-bisphosphatase heart isoform gene (PFKFB2)." Eur J Biochem **254**(1): 103-110.

Helmlinger, G., F. Yuan, et al. (1997). "Interstitial pH and pO2 gradients in solid tumors in vivo: high-resolution measurements reveal a lack of correlation." Nat Med **3**(2): 177-182.

Hennipman, A., J. Smits, et al. (1987). "Glycolytic enzymes in breast cancer, benign breast disease and normal breast tissue." Tumour Biol **8**(5): 251-263.

Hennipman, A., B. A. van Oirschot, et al. (1988). "Glycolytic enzyme activities in breast cancer metastases." Tumour Biol **9**(5): 241-248.

Herrero-Mendez, A., A. Almeida, et al. (2009). "The bioenergetic and antioxidant status of neurons is controlled by continuous degradation of a key glycolytic enzyme by APC/C-Cdh1." Nat Cell Biol **11**(6): 747-752.

Higgins, L. H., H. G. Withers, et al. (2009). "Hypoxia and the metabolic phenotype of prostate cancer cells." Biochim Biophys Acta **1787**(12): 1433-1443.

Hilliker, C. E., M. I. Darville, et al. (1991). "Human and rat chromosomal localization of two genes for 6-phosphofructo-2-kinase/fructose-2,6-bisphosphatase by analysis of somatic cell hybrids and in situ hybridization." Genomics **10**(4): 867-873.

Hirata, T., M. Kato, et al. (1998). "Expression of human placental-type 6-phosphofructo-2-kinase/fructose 2,6-bisphosphatase in various cells and cell lines." Biochem Biophys Res Commun **242**(3): 680-684.

Hirata, T., M. Watanabe, et al. (2000). "Inhibition of tumor cell growth by a specific 6-phosphofructo-2-kinase inhibitor, N-bromoacetylethanolamine phosphate, and its analogues." Biosci Biotechnol Biochem **64**(10): 2047-2052.

Hoelder, S., P. A. Clarke, et al. (2012). "Discovery of small molecule cancer drugs: successes, challenges and opportunities." Mol Oncol **6**(2): 155-176.

Howell, A. and D. G. Evans (2013). "Breast cancer prevention: SERMs come of age." Lancet **381**(9880): 1795-1797.

Hsieh, C. H., C. H. Lee, et al. (2010). "Cycling hypoxia increases U87 glioma cell radioresistance via ROS induced higher and long-term HIF-1 signal transduction activity." Oncol Rep **24**(6): 1629-1636.

Hu, C. J., L. Y. Wang, et al. (2003). "Differential roles of hypoxia-inducible factor 1alpha (HIF-1alpha) and HIF-2alpha in hypoxic gene regulation." Mol Cell Biol **23**(24): 9361-9374.

Huang, L. E., Z. Arany, et al. (1996). "Activation of hypoxia-inducible transcription factor depends primarily upon redox-sensitive stabilization of its alpha subunit." J Biol Chem **271**(50): 32253-32259.

Huang, L. E., J. Gu, et al. (1998). "Regulation of hypoxia-inducible factor 1 alpha is mediated by an O-2-dependent degradation domain via the ubiquitin-proteasome pathway." Proceedings of the National Academy of Sciences of the United States of America **95**(14): 7987-7992.

Huck, J. H., E. A. Struys, et al. (2003). "Profiling of pentose phosphate pathway intermediates in blood spots by tandem mass spectrometry: application to transaldolase deficiency." Clin Chem **49**(8): 1375-1380.

Hue, L., C. Beauloye, et al. (2002). "Insulin and ischemia stimulate glycolysis by acting on the same targets through different and opposing signaling pathways." J Mol Cell Cardiol **34**(9): 1091-1097.

Hue, L. and G. G. Rousseau (1993). "Fructose 2,6-bisphosphate and the control of glycolysis by growth factors, tumor promoters and oncogenes." Adv Enzyme Regul **33**: 97-110.

Hunnewell, M. G. and N. S. Forbes (2010). "Active and Inactive Metabolic Pathways in Tumor Spheroids: Determination by GC-MS." Biotechnology Progress **26**(3): 789-796.

Huo, Y., X. Guo, et al. (2010). "Disruption of inducible 6-phosphofructo-2-kinase ameliorates diet-induced adiposity but exacerbates systemic insulin resistance and adipose tissue inflammatory response." J Biol Chem **285**(6): 3713-3721.

Israelsen, W. J. and M. G. Vander Heiden (2010). "ATP consumption promotes cancer metabolism." Cell **143**(5): 669-671.

Ivan, M., K. Kondo, et al. (2001). "HIFalpha targeted for VHL-mediated destruction by proline hydroxylation: implications for O2 sensing." Science **292**(5516): 464-468.

Ivascu, A. and M. Kubbies (2007). "Diversity of cell-mediated adhesions in breast cancer spheroids." Int J Oncol **31**(6): 1403-1413.

Iwai, K., K. Yamanaka, et al. (1999). "Identification of the von Hippel-lindau tumor-suppressor protein as part of an active E3 ubiquitin ligase complex." Proc Natl Acad Sci U S A **96**(22): 12436-12441.

Jaakkola, P., D. R. Mole, et al. (2001). "Targeting of HIF-alpha to the von Hippel-Lindau ubiquitylation complex by O2-regulated prolyl hydroxylation." Science **292**(5516): 468-472.

Jaffe, N., E. Frei, 3rd, et al. (1974). "Adjuvant methotrexate and citrovorum-factor treatment of osteogenic sarcoma." N Engl J Med **291**(19): 994-997.

Jain, R. K. (2005). "Normalization of tumor vasculature: an emerging concept in antiangiogenic therapy." Science **307**(5706): 58-62.

Jeon, Y. K., S. Y. Jang, et al. (2011). "Sulforaphane induces apoptosis in human hepatic cancer cells through inhibition of 6-phosphofructo-2-kinase/fructose-2,6-biphosphatase4, mediated by hypoxia inducible factor-1-dependent pathway." Biochim Biophys Acta **1814**(10):1340-1348.

Jia, Y., C. M. Quinn, et al. (2008). "Current in vitro kinase assay technologies: the quest for a universal format." Curr Drug Discov Technol **5**(1): 59-69.

Jones, D. T. and A. L. Harris (2006). "Identification of novel small-molecule inhibitors of hypoxia-inducible factor-1 transactivation and DNA binding." Molecular Cancer Therapeutics **5**(9): 2193-2202.

Jordan, V. C. (2007). "Chemoprevention of breast cancer with selective oestrogen-receptor modulators." Nat Rev Cancer **7**(1): 46-53.

Kaadige, M. R., M. G. Elgort, et al. (2010). "Coordination of glucose and glutamine utilization by an expanded Myc network." Transcription **1**(1): 36-40.

Ke, Q. and M. Costa (2006). "Hypoxia-inducible factor-1 (HIF-1)." Mol Pharmacol **70**(5): 1469-1480.

Keith, B., R. S. Johnson, et al. (2012). "HIF1alpha and HIF2alpha: sibling rivalry in hypoxic tumour growth and progression." Nat Rev Cancer **12**(1): 9-22.

Kelly, P. N., A. Dakic, et al. (2007). "Tumor growth need not be driven by rare cancer stem cells." Science **317**(5836): 337.

Kessler, R., F. Bleichert, et al. (2008). "6-Phosphofructo-2-kinase/fructose-2,6-bisphosphatase (PFKFB3) is up-regulated in high-grade astrocytomas." J Neurooncol **86**(3): 257-264.

Kessler, R. and K. Eschrich (2001). "Splice isoforms of ubiquitous 6-phosphofructo-2-kinase/fructose-2,6-bisphosphatase in human brain." Brain Res Mol Brain Res **87**(2): 190-195.

Kim, I. S., J. S. Oh, et al. (2007). "Synthesis and conformational analysis of 3-hydroxypipecolic acid analogs via CSI-mediated stereoselective amination." Tetrahedron **63**: 2622-2633.

Kim, J. W., I. Tchernyshyov, et al. (2006). "HIF-1-mediated expression of pyruvate dehydrogenase kinase: a metabolic switch required for cellular adaptation to hypoxia." Cell Metab **3**(3): 177-185.

Kim, S. G., M. Cavalier, et al. (2007). "A direct substrate-substrate interaction found in the kinase domain of the bifunctional enzyme, 6-phosphofructo-2-kinase/fructose-2,6-bisphosphatase." J Mol Biol **370**(1): 14-26.

Kim, S. G., N. P. Manes, et al. (2006). "Crystal structure of the hypoxia-inducible form of 6-phosphofructo-2-kinase/fructose-2,6-bisphosphatase (PFKFB3) - A possible new target for cancer therapy." Journal of Biological Chemistry **281**(5): 2939-2944.

Kimata, M., S. Matoba, et al. (2010). "p53 and TIGAR regulate cardiac myocyte energy homeostasis under hypoxic stress." Am J Physiol Heart Circ Physiol **299**(6): H1908-1916.

Kitamura, K., K. Uyeda, et al. (1989). "Catalytic site of rat liver and bovine heart fructose-6-phosphate,2-kinase:fructose-2,6-bisphosphatase. Identification of fructose 6-phosphate binding site." J Biol Chem **264**(11): 6344-6348.

Knouzy, B., L. Dubourg, et al. (2010). "Ifosfamide metabolite chloroacetaldehyde inhibits cell proliferation and glucose metabolism without decreasing cellular ATP content in human breast cancer cells MCF-7." J Appl Toxicol **30**(3): 204-211.

Koerner, T. A. W., Younatha.Es, et al. (1974). "Fructose-6-phosphate site of Phosphofructokinase. I. Tautomeric and anomeric specificity." Journal of Biological Chemistry **249**(18): 5749-5754.

Kole, H. K., R. J. Resnick, et al. (1991). "Regulation of 6-phosphofructo-1-kinase activity in ras-transformed RAT-1 fibroblasts." Archives of Biochemistry and Biophysics **286**(2): 586-590.

Kolly-Kovac, T. and P. Renaud (2005). "Radical-mediated synthesis of racemic deoxypodophyllotoxin and related lignans." Synthesis-Stuttgart(9): 1459-1466.

Krishna, R. and L. D. Mayer (2000). "Multidrug resistance (MDR) in cancer. Mechanisms, reversal using modulators of MDR and the role of MDR modulators in influencing the pharmacokinetics of anticancer drugs." Eur J Pharm Sci **11**(4): 265-283.

Kroemer, G. and J. Pouyssegur (2008). "Tumor cell metabolism: cancer's Achilles' heel." Cancer Cell **13**(6): 472-482.

Kufner, U. and R. R. Schmidt (1985). "Novo-synthesis of carbohydrates and related natural-products. 19. A short synthesis of D,L-exo-brevicomin from divinylglycol." Synthesis-Stuttgart(11): 1060-1062.

Kuwai, T., Y. Kitadai, et al. (2003). "Expression of hypoxia-inducible factor-l alpha is associated with tumor vascularization in human colorectal carcinoma." International Journal of Cancer **105**(2): 176-181.

Lau, F. T. K. and A. R. Fersht (1989). "Dissection of the effector-binding site and complementation studies of escherichia-coli phosphofructokinase using site-directed mutagenesis." Biochemistry **28**(17): 6841-6847.

Lavieri, R. R., S. A. Scott, et al. (2010). "Design, synthesis, and biological evaluation of halogenated N-(2-(4-oxo-1-phenyl-1,3,8-triazaspiro[4.5]decan-8-yl)ethyl)benzamides: discovery of an isoform-selective small molecule phospholipase D2 inhibitor." J Med Chem **53**(18): 6706-6719.

Lee, W. N., L. G. Boros, et al. (1998). "Mass isotopomer study of the nonoxidative pathways of the pentose cycle with [1,2-13C2]glucose." Am J Physiol **274**(5 Pt 1): E843-851.

Lee, Y. H., Y. Li, et al. (2003). "Tissue-specific structure/function differentiation of the liver isoform of 6-phosphofructo-2-kinase/fructose-2,6-bisphosphatase." J Biol Chem **278**(1): 523-530.

Lei, Z., D. V. Huhman, et al. (2011). "Mass spectrometry strategies in metabolomics." J Biol Chem **286**(29): 25435-25442.

Leite, T. C., D. Da Silva, et al. (2007). "Lactate favours the dissociation of skeletal muscle 6-phosphofructo-1-kinase tetramers down-regulating the enzyme and muscle glycolysis." Biochemical Journal **408**: 123-130.

Lewis, L. D. (2006). "Cancer pharmacotherapy: 21st century 'magic bullets' and changing paradigms." Br J Clin Pharmacol **62**(1): 1-4.

Li, B., K. Takeda, et al. (2012). "Coordinated expression of 6-phosphofructo-2-kinase/fructose-2,6-bisphosphatase 4 and heme oxygenase 2: evidence for a regulatory link between glycolysis and heme catabolism." Tohoku J Exp Med **228**(1): 27-41.

Li, F., Y. Wang, et al. (2005). "Myc stimulates nuclearly encoded mitochondrial genes and mitochondrial biogenesis." Mol Cell Biol **25**(14): 6225-6234.

Li, H. and G. Jogl (2009). "Structural and Biochemical Studies of TIGAR (TP53-induced Glycolysis and Apoptosis Regulator)." Journal of Biological Chemistry **284**(3): 1748-1754.

Li, T., N. Kon, et al. (2012). "Tumor suppression in the absence of p53-mediated cell-cycle arrest, apoptosis, and senescence." Cell **149**(6): 1269-1283.

Liu, N. and Z. X. Wang (2011). "Kumada Coupling of Aryl, Heteroaryl, and Vinyl Chlorides Catalyzed by Amido Pincer Nickel Complexes." Journal of Organic Chemistry **76**(24): 10031-10038.

Lunt, S. Y. and M. G. Vander Heiden (2011). "Aerobic glycolysis: meeting the metabolic requirements of cell proliferation." Annu Rev Cell Dev Biol **27**: 441-464.

Ma, H., S. Deacon, et al. (2008). "The challenge of selecting protein kinase assays for lead discovery optimization." Expert Opin Drug Discov **3**(6): 607-621.

Madan, E., R. Gogna, et al. (2011). "Regulation of glucose metabolism by p53: emerging new roles for the tumor suppressor." Oncotarget **2**(12): 948-957.

Madan, E., R. Gogna, et al. (2012). "TIGAR induces p53-mediated cell-cycle arrest by regulation of RB-E2F1 complex." Br J Cancer **107**(3): 516-526.

Mahboobi, S. and W. Wiegrebe (1988). "Enantioselective synthesis of some nicotiana alkaloids." Archiv Der Pharmazie **321**(3): 175-177.

Makino, Y., R. Cao, et al. (2001). "Inhibitory PAS domain protein is a negative regulator of hypoxia-inducible gene expression." Nature **414**(6863): 550-554.

Makino, Y., R. Uenishi, et al. (2007). "Transcriptional up-regulation of inhibitory PAS domain protein gene expression by hypoxia-inducible factor 1 (HIF-1): a negative feedback regulatory circuit in HIF-1-mediated signaling in hypoxic cells." J Biol Chem **282**(19): 14073-14082.

Manzano, A., J. X. Perez, et al. (1999). "Cloning, expression and chromosomal localization of a human testis 6-phosphofructo-2-kinase/fructose-2,6-bisphosphatase gene." Gene **229**(1-2): 83-89.

Manzano, A., J. L. Rosa, et al. (1998). "Molecular cloning, expression, and chromosomal localization of a ubiquitously expressed human 6-phosphofructo-2-kinase/fructose-2,6-bisphosphatase gene (PFKFB3)." Cytogenetics and Cell Genetics **83**(3-4): 214-217.

Mardis, E. R., L. Ding, et al. (2009). "Recurring mutations found by sequencing an acute myeloid leukemia genome." N Engl J Med **361**(11): 1058-1066.

Marsin, A. S., L. Bertrand, et al. (2000). "Phosphorylation and activation of heart PFK-2 by AMPK has a role in the stimulation of glycolysis during ischaemia." Curr Biol **10**(20): 1247-1255.

Marsin, A. S., C. Bouzin, et al. (2002). "The stimulation of glycolysis by hypoxia in activated monocytes is mediated by AMP-activated protein kinase and inducible 6-phosphofructo-2-kinase." J Biol Chem **277**(34): 30778-30783.

Marunych, R. Y., D. M. Minchenko, et al. (2011). "Effect of hypoxia and ischemia on the expression of phosphofructokinase-1 and lactate dehydrogenase genes in glioma U87 cells with ERN1 knockdown " Фізика живого, **19**(1): 52-60.

Maschek, G., N. Savaraj, et al. (2004). "2-deoxy-D-glucose increases the efficacy of adriamycin and paclitaxel in human osteosarcoma and non-small cell lung cancers in vivo." Cancer Res **64**(1): 31-34.

Masson, N., C. Willam, et al. (2001). "Independent function of two destruction domains in hypoxia-inducible factor-alpha chains activated by prolyl hydroxylation." EMBO J **20**(18): 5197-5206.

Masui, K., B. Gini, et al. (2013). "A tale of two approaches: complementary mechanisms of cytotoxic and targeted therapy resistance may inform next-generation cancer treatments." Carcinogenesis **34**(4): 725-738.

Matheson, B. K., J. L. Adams, et al. (2007). "Effect of metabolic inhibitors on ATP and citrate content in PC3 prostate cancer cells." Prostate **67**(11): 1211-1218.

Matoba, S., J. G. Kang, et al. (2006). "p53 regulates mitochondrial respiration." Science **312**(5780): 1650-1653.

Mattes, W. B., J. A. Hartley, et al. (1986). "DNA sequence selectivity of guanine-N7 alkylation by nitrogen mustards." Nucleic Acids Res **14**(7): 2971-2987.

Maxwell, P. H., M. S. Wiesener, et al. (1999). "The tumour suppressor protein VHL targets hypoxia-inducible factors for oxygen-dependent proteolysis." Nature **399**(6733): 271-275.

Maynard, M. A., H. Qi, et al. (2003). "Multiple splice variants of the human HIF-3 alpha locus are targets of the von Hippel-Lindau E3 ubiquitin ligase complex." J Biol Chem **278**(13): 11032-11040.

McIntyre, D. J., B. Madhu, et al. (2012). "Magnetic resonance spectroscopy of cancer metabolism and response to therapy." Radiat Res **177**(4): 398-435.

Melillo, G. (2006). "Inhibiting hypoxia-inducible factor 1 for cancer therapy." Molecular Cancer Research **4**(9): 601-605.

Mendoza, E. E., M. G. Pocceschi, et al. (2012). "Control of Glycolytic Flux by AMP-Activated Protein Kinase in Tumor Cells Adapted to Low pH." Transl Oncol **5**(3): 208-216.

Messana, I., F. Misiti, et al. (1999). "Quantitative determination of the main glucose metabolic fluxes in human erythrocytes by 13C- and 1H-MR spectroscopy." J Biochem Biophys Methods **39**(1-2): 63-84.

Metallo, C. M., P. A. Gameiro, et al. (2012). "Reductive glutamine metabolism by IDH1 mediates lipogenesis under hypoxia." Nature **481**(7381): 380-384.

Michelakis, E. D., L. Webster, et al. (2008). "Dichloroacetate (DCA) as a potential metabolic-targeting therapy for cancer." Br J Cancer **99**(7): 989-994.

Minchenko, A., I. Leshchinsky, et al. (2002). "Hypoxia-inducible factor-1-mediated expression of the 6-phosphofructo-2-kinase/fructose-2,6-bisphosphatase-3 (PFKFB3) gene. Its possible role in the Warburg effect." J Biol Chem **277**(8): 6183-6187.

Minchenko, O., I. Opentanova, et al. (2003). "Hypoxic regulation of the 6-phosphofructo-2-kinase/fructose-2,6-bisphosphatase gene family (PFKFB-1-4) expression in vivo." FEBS Lett **554**(3): 264-270.

Minchenko, O., I. Opentanova, et al. (2004). "Hypoxia induces transcription of 6-phosphofructo-2-kinase/fructose-2,6-biphosphatase-4 gene via hypoxia-inducible factor-1alpha activation." FEBS Lett **576**(1-2): 14-20.

Minchenko, O. H., A. Ochiai, et al. (2005). "Overexpression of 6-phosphofructo-2-kinase/fructose-2,6-bisphosphatase-4 in the human breast and colon malignant tumors." Biochimie **87**(11): 1005-1010.

Minchenko, O. H., T. Ogura, et al. (2005). "Splice isoform of 6-phosphofructo-2-kinase/fructose-2,6-bisphosphatase-4: expression and hypoxic regulation." Mol Cell Biochem **280**(1-2): 227-234.

Minchenko, O. H., T. Ogura, et al. (2005). "6-Phosphofructo-2-kinase/fructose-2,6-bisphosphatase gene family overexpression in human lung tumor." Ukr Biokhim Zh **77**(6): 46-50.

Minchenko, O. H., I. L. Opentanova, et al. (2005). "Expression and hypoxia-responsiveness of 6-phosphofructo-2-kinase/fructose-2,6-bisphosphatase 4 in mammary gland malignant cell lines." Acta Biochim Pol **52**(4): 881-888.

Minor, L. (2010). Handbook of Assay Development in Drug Discovery, Taylor and Francis Group

Mojena, M., L. Bosca, et al. (1992). "Inhibition of 6-phosphofructo-2-kinase activity by mercaptopurines." Biochemical Pharmacology **43**(4): 671-678.

Moncada, S., E. A. Higgs, et al. (2012). "Fulfilling the metabolic requirements for cell proliferation." Biochem J **446**(1): 1-7.

Moon, E. J., D. M. Brizel, et al. (2007). "The potential role of intrinsic hypoxia markers as prognostic variables in cancer." Antioxid Redox Signal **9**(8): 1237-1294.

Moon, J. S., W. J. Jin, et al. (2011). "Androgen stimulates glycolysis for de novo lipid synthesis by increasing the activities of hexokinase 2 and 6-phosphofructo-2-kinase/fructose-2,6-bisphosphatase 2 in prostate cancer cells." Biochem J **433**(1): 225-233.

Moreno-Sanchez, R., S. Rodriguez-Enriquez, et al. (2007). "Energy metabolism in tumor cells." FEBS J **274**(6): 1393-1418.

Morrison, W. B. (2010). "Cancer chemotherapy: an annotated history." J Vet Intern Med **24**(6): 1249-1262.

Murray, K. J., M. R. El-Maghrabi, et al. (1984). "Amino acid sequence of the phosphorylation site of rat liver 6-phosphofructo-2-kinase/fructose-2,6-bisphosphatase." J Biol Chem **259**(12): 7673-7681.

Nicholl, J., J. A. Hamilton, et al. (1997). "The third human isoform of 6-phosphofructo-2-kinase/fructose-2,6-bisphosphatase (PFKFB3) map position 10p14-p15." Chromosome Res **5**(2): 150.

Nicholls, A., G. B. McGaughey, et al. (2010). "Molecular shape and medicinal chemistry: a perspective." J Med Chem **53**(10): 3862-3886.

Nissler, K., H. Petermann, et al. (1995). "Fructose 2,6-bisphosphate metabolism in Ehrlich ascites tumour cells." J Cancer Res Clin Oncol **121**(12): 739-745.

Niu, T., W. M. Zhang, et al. (2009). "A Powerful Reagent for Synthesis of Weinreb Amides Directly from Carboxylic Acids." Organic Letters **11**(19): 4474-4477.

Novellasdemunt, L., L. Bultot, et al. (2013). "PFKFB3 activation in cancer cells by the p38/MK2 pathway in response to stress stimuli." Biochem J **452**(3): 531-543.

Novellasdemunt, L., M. Obach, et al. (2012). "Progestins activate 6-phosphofructo-2-kinase/fructose-2,6-bisphosphatase 3 (PFKFB3) in breast cancer cells." Biochem J **442**(2): 345-356.

Novotny, E. J., Jr., T. Ogino, et al. (1990). "Direct carbon versus proton heteronuclear editing of 2-13C ethanol in rabbit brain in vivo: a sensitivity comparison." Magn Reson Med **16**(3): 431-443.

O'Hare, T., D. K. Walters, et al. (2005). "In vitro activity of Bcr-Abl inhibitors AMN107 and BMS-354825 against clinically relevant imatinib-resistant Abl kinase domain mutants." Cancer Res **65**(11): 4500-4505.

Obach, M., A. Navarro-Sabate, et al. (2004). "6-Phosphofructo-2-kinase (pfkfb3) gene promoter contains hypoxia-inducible factor-1 binding sites necessary for transactivation in response to hypoxia." J Biol Chem **279**(51): 53562-53570.

Oda, T., C. Heaney, et al. (1994). "Crkl is the major tyrosine-phosphorylated protein in neutrophils from patients with chronic myelogenous leukemia." J Biol Chem **269**(37): 22925-22928.

Ohh, M., C. W. Park, et al. (2000). "Ubiquitination of hypoxia-inducible factor requires direct binding to the beta-domain of the von Hippel-Lindau protein." Nat Cell Biol **2**(7): 423-427.

Okamura, N. and R. Sakakibara (1998). "A common phosphorylation site for cyclic AMP-dependent protein kinase and protein kinase C in human placental 6-phosphofructo-2-kinase/fructose-2,6-bisphosphatase." Biosci Biotechnol Biochem **62**(10): 2039-2042.

Okar, D. O., A. Manzano, et al. (2001). "PFK-2/FBPase-2: maker and breaker of the essential biofactor fructose-2, 6-bisphosphate." Trends in Biochemical Sciences **26**(1): 30-35.

Olson, S., K. Uyeda, et al. (1989). "Localization of fructose 6-P,2-kinase: fructose 2,6-bisphosphatase to human chromosome X." Somat Cell Mol Genet **15**(6): 617-621.

Osborn, M. J., M. Freeman, et al. (1958). "Inhibition of dihydrofolic reductase by aminopterin and amethopterin." Proc Soc Exp Biol Med **97**(2): 429-431.

Otto, S., F. Bertoncin, et al. (1996). "Lewis acid catalysis of a Diels-Alder reaction in water." Journal of the American Chemical Society **118**(33): 7702-7707.

Overgaard, J. and M. R. Horsman (1996). "Modification of hypoxia-induced radioresistance in tumors by the use of oxygen and sensitizers." Seminars in Radiation Oncology **6**(1): 10-21.

Pape, M. R., C. Prokop, et al. (1996). "Localization of the Pfkfb 2 gene on rat chromosome 13." Mamm Genome **7**(7): 559.

Paradies, H. H. and M. Gorbing (1969). "A new method for preparation of organomagnesium compounds of pyridine." Angewandte Chemie-International Edition **8**(4): 279.

Paradise, R. K., D. A. Lauffenburger, et al. (2011). "Acidic extracellular pH promotes activation of integrin alpha(v)beta(3)." PLoS One **6**(1): e15746.

Park, K. H., S. E. Choi, et al. (2005). "Downregulation of the anaphase-promoting complex (APC)7 in invasive ductal carcinomas of the breast and its clinicopathologic relationships." Breast Cancer Res **7**(2): R238-247.

Patiar, S. and A. L. Harris (2006). "Role of hypoxia-inducible factor-1 alpha as a cancer therapy target." Endocrine-Related Cancer **13**: S61-S75.

Pegoraro, C., F. Maczkowiak, et al. (2013). "Pfkfb (6-phosphofructo-2-kinase/fructose-2,6-bisphosphatase) isoforms display a tissue-specific and dynamic expression during Xenopus laevis development." Gene Expr Patterns **13**(7): 203-211.

Pelicano, H., D. S. Martin, et al. (2006). "Glycolysis inhibition for anticancer treatment." Oncogene **25**(34): 4633-4646.

Perner, R. J., C. H. Lee, et al. (2005). "Synthesis and biological evaluation of 6,7-disubstituted 4-aminopyrido[2,3-d]pyrimidines as adenosine kinase inhibitors." Bioorganic & Medicinal Chemistry Letters **15**(11): 2803-2807.

Petrov, O., Y. Ivanova, et al. (2008). "SOCl2/EtOH: Catalytic system for synthesis of chalcones." Catalysis Communications **9**(2): 315-316.

Pfaffl, M. W. (2001). "A new mathematical model for relative quantification in real-time RT-PCR." Nucleic Acids Res **29**(9): e45.

Pierotti, M. A., F. Berrino, et al. (2013). "Targeting metabolism for cancer treatment and prevention: metformin, an old drug with multi-faceted effects." Oncogene **32**(12): 1475-1487.

Pilkis, S. J., J. Pilkis, et al. (1985). "The sugar phosphate specificity of rat hepatic 6-phosphofructo-2-kinase/fructose-2,6-bisphosphatase." J Biol Chem **260**(12): 7551-7556.

Porporato, P. E., S. Dhup, et al. (2011). "Anticancer targets in the glycolytic metabolism of tumors: a comprehensive review." Front Pharmacol **2**: 49.

Portais, J. C., R. Schuster, et al. (1993). "Metabolic flux determination in C6 glioma cells using carbon-13 distribution upon [1-13C]glucose incubation." Eur J Biochem **217**(1): 457-468.

Rankin, E. B. and A. J. Giaccia (2008). "The role of hypoxia-inducible factors in tumorigenesis." Cell Death Differ **15**(4): 678-685.

Reetz, M. T., M. W. Drewes, et al. (1989). "A simple synthetic route to statine and statine analogs." Journal of the Chemical Society-Chemical Communications(19): 1474-1475.

Reichert, M., D. Saur, et al. (2007). "Phosphoinositide-3-kinase signaling controls S-phase kinase-associated protein 2 transcription via E2F1 in pancreatic ductal adenocarcinoma cells." Cancer Res **67**(9): 4149-4156.

Reichwald, C., O. Shimony, et al. (2008). "A new Heck reaction modification using ketone Mannich bases as enone precursors: Parallel synthesis of anti-leishmanial chalcones." Bioorganic & Medicinal Chemistry Letters **18**(6): 1985-1989.

Relles, H. M. (1973). "Thionyl chloride-pyridine chemistry. 2. Synthesis and reactions of *N*-alpha-styrylpyridinium salts." Journal of Organic Chemistry **38**(8): 1570-1574.

Reynolds, T. Y., S. Rockwell, et al. (1996). "Genetic instability induced by the tumor microenvironment." Cancer Research **56**(24): 5754-5757.

Rider, M. H., L. Bertrand, et al. (2004). "6-phosphofructo-2-kinase/fructose-2,6-bisphosphatase: Head-to-head with a bifunctional enzyme that controls glycolysis." Biochemical Journal **381**: 561-579.

Rider, M. H. and L. Hue (1984). "Activation of rat heart phosphofructokinase-2 by insulin in vivo." FEBS Lett **176**(2): 484-488.

Rider, M. H., J. van Damme, et al. (1992). "Evidence for new phosphorylation sites for protein kinase C and cyclic AMP-dependent protein kinase in bovine heart 6-phosphofructo-2-kinase/fructose-2,6-bisphosphatase." FEBS Lett **310**(2): 139-142.

Rider, M. H., J. Vandamme, et al. (1992). "The two forms of bovine heart 6-phosphofructo-2-kinase/fructose-2,6-bisphosphatase result from alternative splicing." Biochem J **285 (Pt 2)**: 405-411.

Riera, L., A. Manzano, et al. (2002). "Insulin induces PFKFB3 gene expression in HT29 human colon adenocarcinoma cells." Biochim Biophys Acta **1589**(2): 89-92.

Riquelme, P. T., N. M. Kneer, et al. (1985). "Inhibition by 2,5-anhydromannitol of glycolysis in isolated rat hepatocytes and in Ehrlich ascites cells." Proc Natl Acad Sci U S A **82**(1): 78-82.

Riquelme, P. T., M. E. Wernette-Hammond, et al. (1984). "Mechanism of action of 2,5-anhydro-D-mannitol in hepatocytes. Effects of phosphorylated metabolites on enzymes of carbohydrate metabolism." J Biol Chem **259**(8): 5115-5123.

Robey, I. F., A. D. Lien, et al. (2005). "Hypoxia-inducible factor-1alpha and the glycolytic phenotype in tumors." Neoplasia **7**(4): 324-330.

Robey, R. B. and N. Hay (2009). "Is Akt the "Warburg kinase"?-Akt-energy metabolism interactions and oncogenesis." Semin Cancer Biol **19**(1): 25-31.

Rodriguez-Rodriguez, P., E. Fernandez, et al. (2012). "Excitotoxic stimulus stabilizes PFKFB3 causing pentose-phosphate pathway to glycolysis switch and neurodegeneration." Cell Death Differ **19**(10): 1582-1589.

Roessner, U., C. Wagner, et al. (2000). "Technical advance: simultaneous analysis of metabolites in potato tuber by gas chromatography-mass spectrometry." Plant J **23**(1): 131-142.

Rofstad, E. K., B. Mathiesen, et al. (2006). "Acidic extracellular pH promotes experimental metastasis of human melanoma cells in athymic nude mice." Cancer Res **66**(13): 6699-6707.

Ros, S., C. R. Santos, et al. (2012). "Functional metabolic screen identifies 6-phosphofructo-2-kinase/fructose-2,6-biphosphatase 4 as an important regulator of prostate cancer cell survival." Cancer Discov **2**(4): 328-343.

Ros, S. and A. Schulze (2013). "Balancing glycolytic flux: the role of 6-phosphofructo-2-kinase/fructose 2,6-bisphosphatases in cancer metabolism." Cancer & Metabolism **1**(8): 1-10.

Sablina, A. A., A. V. Budanov, et al. (2005). "The antioxidant function of the p53 tumor suppressor." Nat Med **11**(12): 1306-1313.

Sadeghian, H., S. M. Seyedi, et al. (2008). "Design and synthesis of eugenol derivatives, as potent 15-lipoxygenase inhibitors." Bioorganic & Medicinal Chemistry **16**(2): 890-901.

Saed, G. M., N. M. Fletcher, et al. (2011). "Dichloroacetate induces apoptosis of epithelial ovarian cancer cells through a mechanism involving modulation of oxidative stress." Reprod Sci **18**(12): 1253-1261.

Saggar, J. K., M. Yu, et al. (2013). "The tumor microenvironment and strategies to improve drug distribution." Front Oncol **3**: 154.

Sakai, A., M. Kato, et al. (1996). "Cloning of cDNA encoding for a novel isozyme of fructose 6-phosphate, 2-kinase/fructose 2,6-bisphosphatase from human placenta." J Biochem **119**(3): 506-511.

Sakakibara, R., M. Kato, et al. (1997). "Characterization of a human placental fructose-6-phosphate 2-kinase fructose-2,6-bisphosphatase." Journal of Biochemistry **122**(1): 122-128.

Sakata, J., Y. Abe, et al. (1991). "Molecular cloning of the DNA and expression and characterization of rat testes fructose-6-phosphate,2-kinase:fructose-2,6-bisphosphatase." J Biol Chem **266**(24): 15764-15770.

Sanchez-Martinez, C. and J. J. Aragon (1997). "Analysis of phosphofructokinase subunits and isozymes in ascites tumor cells and its original tissue, murine mammary gland." FEBS Lett **409**(1): 86-90.

Sanchez, W. Y., S. L. McGee, et al. (2013). "Dichloroacetate inhibits aerobic glycolysis in multiple myeloma cells and increases sensitivity to bortezomib." Br J Cancer **108**(8): 1624-1633.

Santos, C. R. and A. Schulze (2012). "Lipid metabolism in cancer." FEBS J **279**(15): 2610-2623.

Sasieni, P. D., J. Shelton, et al. (2011). "What is the lifetime risk of developing cancer?: the effect of adjusting for multiple primaries." Br J Cancer **105**(3): 460-465.

Sawyers, C. (2004). "Targeted cancer therapy." Nature **432**(7015): 294-297.

Schmidt, B. and S. Nave (2007). "Synthesis of dihydrofurans and dihydropyrans with unsaturated side chains based on ring size-selective ring-closing metathesis." Advanced Synthesis & Catalysis **349**(1-2): 215-230.

Schofield, C. J. and P. J. Ratcliffe (2004). "Oxygen sensing by HIF hydroxylases." Nat Rev Mol Cell Biol **5**(5): 343-354.

Scholnick, P., D. Lang, et al. (1973). "Regulatory mechanisms in carbohydrate metabolism. IX. Stimulation of aerobic glycolysis by energy-linked ion transport and inhibition by dextran sulfate." J Biol Chem **248**(14): 5175.

Schrader, M. C., C. J. Eskey, et al. (1993). "A carbon-13 nuclear magnetic resonance investigation of the metabolic fluxes associated with glucose metabolism in human erythrocytes." Biochim Biophys Acta **1182**(2): 162-178.

Schulze, A. and A. L. Harris (2012). "How cancer metabolism is tuned for proliferation and vulnerable to disruption." Nature **491**(7424): 364-373.

Semenza, G. L. (2007). "Evaluation of HIF-1 inhibitors as anticancer agents." Drug Discovery Today **12**: 853-859.

Semenza, G. L., F. Agani, et al. (1997). "Structural and functional analysis of hypoxia-inducible factor 1." Kidney Int **51**(2): 553-555.

Semenza, G. L., P. H. Roth, et al. (1994). "Transcriptional regulation of genes encoding glycolytic enzymes by hypoxia-inducible factor 1." J Biol Chem **269**(38): 23757-23763.

Semenza, G. L. and G. L. Wang (1992). "A nuclear factor induced by hypoxia via de novo protein synthesis binds to the human erythropoietin gene enhancer at a site required for transcriptional activation." Mol Cell Biol **12**(12): 5447-5454.

Seo, M., J. D. Kim, et al. (2011). "Structure-Based Development of Small Molecule PFKFB3 Inhibitors: A Framework for Potential Cancer Therapeutic Agents Targeting the Warburg Effect." PLoS One **6**(9): e24179.

Serres, S., E. Bezancon, et al. (2004). "Ex vivo analysis of lactate and glucose metabolism in the rat brain under different states of depressed activity." J Biol Chem **279**(46): 47881-47889.

Shannon, A. M., D. J. Bouchier-Hayes, et al. (2003). "Tumour hypoxia, chemotherapeutic resistance and hypoxia-related therapies." Cancer Treatment Reviews **29**(4): 297-307.

Shirakihara, Y. and P. R. Evans (1988). "Crystal-structure of the complex of phosphofructokinase from escherichia-coli with its reaction-products." Journal of Molecular Biology **204**(4): 973-994.

Sibson, N. R., G. F. Mason, et al. (2001). "In vivo (13)C NMR measurement of neurotransmitter glutamate cycling, anaplerosis and TCA cycle flux in rat brain during." J Neurochem **76**(4): 975-989.

Siim, B. G., P. L. van Zijl, et al. (1996). "Tirapazamine-induced DNA damage measured using the comet assay correlates with cytotoxicity towards hypoxic tumour cells in vitro." Br J Cancer **73**(8): 952-960.

Skovsgaard, T. (1977). "Transport and binding of daunorubicin, adriamycin, and rubidazone in ehrlich ascites tumor-cells." Biochemical Pharmacology **26**(3): 215-222.

Smallbone, K., D. J. Gavaghan, et al. (2005). "The role of acidity in solid tumour growth and invasion." J Theor Biol **235**(4): 476-484.

Sosa, V., T. Moline, et al. (2013). "Oxidative stress and cancer: an overview." Ageing Res Rev **12**(1): 376-390.

Spandl, J., D. J. White, et al. (2009). "Live cell multicolor imaging of lipid droplets with a new dye, LD540." Traffic **10**(11): 1579-1584.

Spitz, G. A., C. M. Furtado, et al. (2009). "Acetylsalicylic acid and salicylic acid decrease tumor cell viability and glucose metabolism modulating 6-phosphofructo-1-kinase structure and activity." Biochemical Pharmacology **77**(1): 46-53.

Staal, G. E., A. Kalff, et al. (1987). "Subunit composition, regulatory properties, and phosphorylation of phosphofructokinase from human gliomas." Cancer Res **47**(19): 5047-5051.

Stubbs, M. and J. R. Griffiths (2010). "The altered metabolism of tumors: HIF-1 and its role in the Warburg effect." Adv Enzyme Regul **50**(1): 44-55.

Subarsky, P. and R. P. Hill (2003). "The hypoxic tumour microenvironment and metastatic progression." Clinical & Experimental Metastasis **20**(3): 237-250.

Sullivan, R. J. and K. T. Flaherty (2013). "Resistance to BRAF-targeted therapy in melanoma." Eur J Cancer **49**(6): 1297-1304.

Swanton, C. (2012). "Intratumor heterogeneity: evolution through space and time." Cancer Res **72**(19): 4875-4882.

Swerdlow, R. H., L. E, et al. (2013). "Glycolysis-respiration relationships in a neuroblastoma cell line." Biochim Biophys Acta **1830**(4): 2891-2898.

Swietach, P., R. D. Vaughan-Jones, et al. (2007). "Regulation of tumor pH and the role of carbonic anhydrase 9." Cancer Metastasis Rev **26**(2): 299-310.

Tanega, C., M. Shen, et al. (2009). "Comparison of bioluminescent kinase assays using substrate depletion and product formation." Assay Drug Dev Technol **7**(6): 606-614.

Tanimoto, K., Y. Makino, et al. (2000). "Mechanism of regulation of the hypoxia-inducible factor-1 alpha by the von Hippel-Lindau tumor suppressor protein." EMBO J **19**(16): 4298-4309.

Telang, S., A. Yalcin, et al. (2006). "Ras transformation requires metabolic control by 6-phosphofructo-2-kinase." Oncogene **25**(55): 7225-7234.

Tennant, D. A., R. V. Duran, et al. (2010). "Targeting metabolic transformation for cancer therapy." Nat Rev Cancer **10**(4): 267-277.

Thompson, C. B. (2009). "Attacking cancer at its root." Cell **138**(6): 1051-1054.

Turek-Etienne, T. C., E. C. Small, et al. (2003). "Evaluation of fluorescent compound interference in 4 fluorescence polarization assays: 2 kinases, 1 protease, and 1 phosphatase." J Biomol Screen **8**(2): 176-184.

Udagawa, T. and M. Wood (2010). "Tumor-stromal cell interactions and opportunities for therapeutic intervention." Curr Opin Pharmacol **10**(4): 369-374.

Van Schaftingen, E. (1987). "Fructose 2,6-bisphosphate." Adv Enzymol Relat Areas Mol Biol **59**: 315-395.

Van Schaftingen, E. and H. G. Hers (1981). "Inhibition of fructose-1,6-bisphosphatase by fructose 2,6-biphosphate." Proc Natl Acad Sci U S A **78**(5): 2861-2863.

Van Schaftingen, E., L. Hue, et al. (1980). "Control of the fructose-6-phosphate/fructose 1,6-bisphosphate cycle in isolated hepatocytes by glucose and glucagon. Role of a low-molecular-weight stimulator of phosphofructokinase." Biochem J **192**(3): 887-895.

Van Schaftingen, E., L. Hue, et al. (1980). "Fructose 2,6-bisphosphate, the probably structure of the glucose- and glucagon-sensitive stimulator of phosphofructokinase." Biochem J **192**(3): 897-901.

Van Schaftingen, E., B. Lederer, et al. (1982). "A kinetic study of pyrophosphate: fructose-6-phosphate phosphotransferase from potato tubers. Application to a microassay of fructose 2,6-bisphosphate." Eur J Biochem **129**(1): 191-195.

Vander Heiden, M. G. (2011). "Targeting cancer metabolism: a therapeutic window opens." Nat Rev Drug Discov **10**(9): 671-684.

Vander Heiden, M. G., L. C. Cantley, et al. (2009). "Understanding the Warburg effect: the metabolic requirements of cell proliferation." Science **324**(5930): 1029-1033.

Vatsadze, S. Z., V. N. Nuriev, et al. (2004). "New aspects of the aldol condensation of acetylpyridines with aromatic aldehydes." Russian Chemical Bulletin **53**(4): 911-915.

Vaughn, A. E. and M. Deshmukh (2008). "Glucose metabolism inhibits apoptosis in neurons and cancer cells by redox inactivation of cytochrome c." Nat Cell Biol **10**(12): 1477-1483.

Ventura, F., S. Ambrosio, et al. (1995). "Cloning and expression of a catalytic core bovine brain 6-phosphofructo-2-kinase/fructose-2,6-bisphosphatase." Biochem Biophys Res Commun **209**(3): 1140-1148.

Vidal, H., K. M. Crepin, et al. (1993). "Cloning and expression of novel isoforms of 6-phosphofructo-2-kinase/fructose-2,6-bisphosphatase from bovine heart." FEBS Lett **330**(3): 329-333.

Vivanco, I. and C. L. Sawyers (2002). "The phosphatidylinositol 3-Kinase AKT pathway in human cancer." Nat Rev Cancer **2**(7): 489-501.

Vogelstein, B., D. Lane, et al. (2000). "Surfing the p53 network." Nature **408**(6810): 307-310.

Vora, S., J. P. Halper, et al. (1985). "Alterations in the activity and isozymic profile of human phosphofructokinase during malignant transformation invivo and invitro - transformation-linked and progression-linked discriminants of malignancy." Cancer Research **45**(7): 2993-3001.

Wachter-Jurcsak, N., C. Radu, et al. (1998). "Addressing the unusual reactivity of 2-pyridinecarboxaldehyde and 2-quinolinecarboxaldehyde in base-catalyzed aldol reactions with acetophenone." Tetrahedron Letters **39**(23): 3903-3906.

Walther, T. C. and R. V. Farese, Jr. (2012). "Lipid droplets and cellular lipid metabolism." Annu Rev Biochem **81**: 687-714.

Wang, G. L., B. H. Jiang, et al. (1995). "Hypoxia-inducible factor-1 is a basic-helix-loop-helix-PAS heterodimer regulated by cellular O-2 tension." Proceedings of the National Academy of Sciences of the United States of America **92**(12): 5510-5514.

Wang, Q., C. Moyret-Lalle, et al. (2003). "Alterations of anaphase-promoting complex genes in human colon cancer cells." Oncogene **22**(10): 1486-1490.

Wang, T., C. Marquardt, et al. (1976). "Aerobic glycolysis during lymphocyte proliferation." Nature **261**(5562): 702-705.

Wanka, C., J. P. Steinbach, et al. (2012). "Tp53-induced glycolysis and apoptosis regulator (TIGAR) protects glioma cells from starvation-induced cell death by up-regulating respiration and improving cellular redox homeostasis." J Biol Chem **287**(40): 33436-33446.

Warburg, O. (1956). "Origin of Cancer Cells." Science **123**(3191): 309-314.

Ward, P. S. and C. B. Thompson (2012). "Metabolic reprogramming: a cancer hallmark even warburg did not anticipate." Cancer Cell **21**(3): 297-308.

Wartenberg, M., F. C. Ling, et al. (2003). "Regulation of the multidrug resistance transporter P-glycoprotein in multicellular tumor spheroids by hypoxiainducible factor-1 and reactive oxygen species." Faseb Journal **17**(1): 503-505.

Weber, G. (1977). "Enzymology of Cancer Cells.2." New England Journal of Medicine **296**(10): 541-551.

Wei, H. X., K. Y. Li, et al. (2004). "Versatile one-step one-pot direct aldol condensation promoted by MgI2." Helvetica Chimica Acta **87**(9): 2354-2358.

Weinhouse, S. (1976). "The Warburg hypothesis fifty years later." Z Krebsforsch Klin Onkol Cancer Res Clin Oncol **87**(2): 115-126.

Westman, J. (2001). "An efficient combination of microwave dielectric heating and the use of solid-supported triphenylphosphine for Wittig reactions." Organic Letters **3**(23): 3745-3747.

Wick, A. N., D. R. Drury, et al. (1957). "Localization of the primary metabolic block produced by 2-deoxyglucose." J Biol Chem **224**(2): 963-969.

Wiesener, M. S., J. S. Jurgensen, et al. (2003). "Widespread hypoxia-inducible expression of HIF-2alpha in distinct cell populations of different organs." FASEB J **17**(2): 271-273.

Williams, A. C., T. J. Collard, et al. (1999). "An acidic environment leads to p53 dependent induction of apoptosis in human adenoma and carcinoma cell lines: implications for clonal selection during colorectal carcinogenesis." Oncogene **18**(21): 3199-3204.

Williams, K. J., B. A. Telfer, et al. (2005). "Enhanced response to radiotherapy in tumours deficient in the function of hypoxia-inducible factor-1." Radiotherapy and Oncology **75**(1): 89-98.

Wilson, W. R. and M. P. Hay (2011). "Targeting hypoxia in cancer therapy." Nat Rev Cancer **11**(6): 393-410.

Wood, H. G., J. Katz, et al. (1963). "Estimation of pathways of carbohydrate metabolism." Biochem Z **338**: 809-847.

Wouters, A., B. Pauwels, et al. (2007). "Review: Implications of in vitro research on the effect of radiotherapy and chemotherapy under hypoxic conditions." Oncologist **12**(6): 690-712.

Xu, Y., M. McLaughlin, et al. (2009). "A General Method for the Synthesis of 3,5-Diarylcyclopentenones via Friedel-Crafts Acylation of Vinyl Chlorides." Journal of Organic Chemistry **74**(14): 5100-5103.

Yalcin, A., B. F. Clem, et al. (2009). "Nuclear Targeting of 6-Phosphofructo-2-kinase (PFKFB3) Increases Proliferation via Cyclin-dependent Kinases." Journal of Biological Chemistry **284**(36): 24223-24232.

Yalcin, A., S. Telang, et al. (2009). "Regulation of glucose metabolism by 6-phosphofructo-2-kinase/fructose-2,6-bisphosphatases in cancer." Experimental and Molecular Pathology **86**(3): 174-179.

Yap, T. A., M. Gerlinger, et al. (2012). "Intratumor heterogeneity: seeing the wood for the trees." Sci Transl Med **4**(127): 127ps110.

Yap, T. A., S. K. Sandhu, et al. (2010). "Envisioning the future of early anticancer drug development." Nat Rev Cancer **10**(7): 514-523.

Yu, D., C. H. Chen, et al. (2004). "Anti-AIDS agents. 60. Substituted 3'R,4'R-di-O-(-)-camphanoyl-2',2'-dimethyldihydropyrano[2,3-f]chromone (DCP) analogues as potent anti-HIV agents." J Med Chem **47**(16): 4072-4082.

Yu, F., S. B. White, et al. (2001). "HIF-1alpha binding to VHL is regulated by stimulus-sensitive proline hydroxylation." Proc Natl Acad Sci U S A **98**(17): 9630-9635.

Yun, S. J., S. W. Jo, et al. (2011). "PFKFB4 as a prognostic marker in non-muscle-invasive bladder cancer." Urol Oncol **30**(6): 893-899.

Zancan, P., M. M. Marinho-Carvalho, et al. (2008). "ATP and fructose-2,6-bisphosphate regulate skeletal muscle 6-phosphofructo-1-kinase by altering its quaternary structure." Iubmb Life **60**(8): 526-533.

Zancan, P., A. O. Rosas, et al. (2007). "Clotrimazole inhibits and modulates heterologous association of the key glycolytic enzyme 6-phosphofructo-1-kinase." Biochemical Pharmacology **73**(10): 1520-1527.

Zancan, P., M. Sola-Penna, et al. (2010). "Differential expression of phosphofructokinase-1 isoforms correlates with the glycolytic efficiency of breast cancer cells." Mol Genet Metab **100**(4): 372-378.

Zhang, J. H., T. D. Chung, et al. (1999). "A Simple Statistical Parameter for Use in Evaluation and Validation of High Throughput Screening Assays." J Biomol Screen **4**(2): 67-73.

Zhang, Z., Y. W. Dong, et al. (2003). "Efficient and clean aldol condensation catalyzed by sodium carbonate in water." Chemistry Letters **32**(10): 966-967.

Zhao, Y., E. B. Butler, et al. (2013). "Targeting cellular metabolism to improve cancer therapeutics." Cell Death Dis **4**: e532.

Zhong, H., A. M. De Marzo, et al. (1999). "Overexpression of hypoxia-inducible factor 1 alpha in common human cancers and their metastases." Cancer Research **59**(22): 5830-5835.

Zhou, B. B., H. Zhang, et al. (2009). "Tumour-initiating cells: challenges and opportunities for anticancer drug discovery." Nat Rev Drug Discov **8**(10): 806-823.

Zhou, Y., T. Shingu, et al. (2011). "Metabolic alterations in highly tumorigenic glioblastoma cells: preference for hypoxia and high dependency on glycolysis." J Biol Chem **286**(37): 32843-32853.

Zimmermann, G. R., J. Lehar, et al. (2007). "Multi-target therapeutics: when the whole is greater than the sum of the parts." Drug Discov Today **12**(1-2): 34-42.

Zscharnack, K., R. Kessler, et al. (2009). "The PFKFB3 splice variant UBI2K4 is downregulated in high-grade astrocytomas and impedes the growth of U87 glioblastoma cells." Neuropathol Appl Neurobiol **35**(6): 566-578.

Zu, X. L. and M. Guppy (2004). "Cancer metabolism: facts, fantasy, and fiction." Biochem Biophys Res Commun **313**(3): 459-465.

Zuckerman, V., K. Wolyniec, et al. (2009). "Tumour suppression by p53: the importance of apoptosis and cellular senescence." J Pathol **219**(1): 3-15.